Dissertation zur Erlangung des Doktorgrades der Naturwissenschaften

vorgelegt beim Fachbereich Biochemie, Chemie und Pharmazie

der

Goethe-Universität in Frankfurt am Main

Development and Application of Optogenetic Methods to Functionally Characterize Synaptic Transmission and Neural Circuits in the Nematode *Caenorhabditis elegans*

von

Christian Schultheis

aus Offenbach am Main

Frankfurt am Main, 2011

(D30)

Vom Fachbereich Biochemie, Chemie und Pharmazie
der Goethe-Universität als Dissertation angenommen.

Dekan: Prof. Dr. Thomas Prisner

Gutachter: Prof. Dr. Alexander Gottschalk

                Prof. Dr. Bernd Ludwig

Datum der Disputation:

Eidesstattliche Erklärung

Ich erkläre hiermit an Eides Statt, dass ich die vorgelegte Dissertation mit dem Titel

„Development and Application of Optogenetic Methods to Functionally Characterize Synaptic Transmission and Neural Circuits in the Nematode *Caenorhabditis elegans*"

selbständig angefertigt und mich anderer Hilfsmittel als der in ihr angegebenen nicht bedient habe, insbesondere, dass aus Schriften Entlehnungen, soweit sie in der Dissertation nicht ausdrücklich als solche mit Angabe der betreffenden Schrift bezeichnet sind, nicht stattgefunden haben. Ich habe bisher an keiner anderen Universität ein Gesuch um Zulassung zur Promotion eingereicht oder die vorliegende oder eine andere Arbeit als Dissertation vorgelegt.

Frankfurt am Main, den

(Christian Schultheis)

1. <u>Table of contents</u>

2. Introduction

Nervous systems are complex organs that sense and integrate environmental information to elicit adequate responses. Understanding of the functionality of these processes requires knowledge of the circuitry of neural networks and the role of individual neurons therein. With respect to this, several methods were developed that facilitate the visualization or selective manipulation of neuronal activity to allow the functional characterization of neurons and synaptic proteins. With a comparably simple nervous system and a limited repertoire of behaviors, these techniques can be ideally applied to the small nematode *Caenorhabditis elegans*, making the worm a widely used model organism in neurobiology.

2.1. The nematode *Caenorhabditis elegans*

2.1.1. General introduction
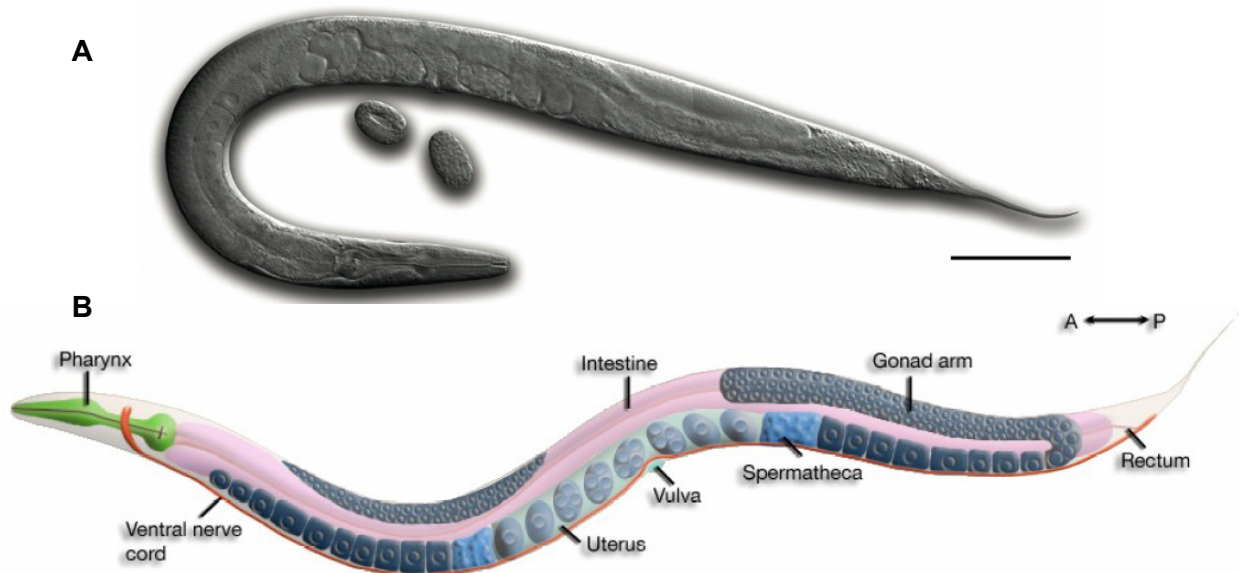
Figure 1: Anatomy of an adult *Caenorhabditis elegans* hermaphrodite
(**A**) Differential interference contrast (DIC) image and of an adult hermaphrodite; scale bar = 100 µm (**B**) Schematic drawing of an adult hermaphrodite depicting main anatomical features in simplified form; adapted from [1]

C. elegans is a nematode of about 1,2 mm in length and 80 µm in diameter that naturally lives in the soil where it subsists on microbes (**Figure 1**; [2]). For use in the lab the worms can be easily cultivated on small agar plates inoculated with bacteria (for a general overview over cultivation see [3]).

The life cycle of *C. elegans* usually endures two to three weeks but is also affected by external factors as for example the temperature (**Figure 2**; [4]). After hatching, the worms proceed through four larval stages (L1-L4) to reach adulthood and produce about 300 progeny. However, life-threatening conditions as indicated for instance by high population densities or limited food resources may induce developmental arrest after the second larval stage [5]. In this case, *C. elegans* enters the so called dauer-state which is a non-feeding form specialized for survival and dispersal [6]. Once conditions improve, worms can resume normal development.
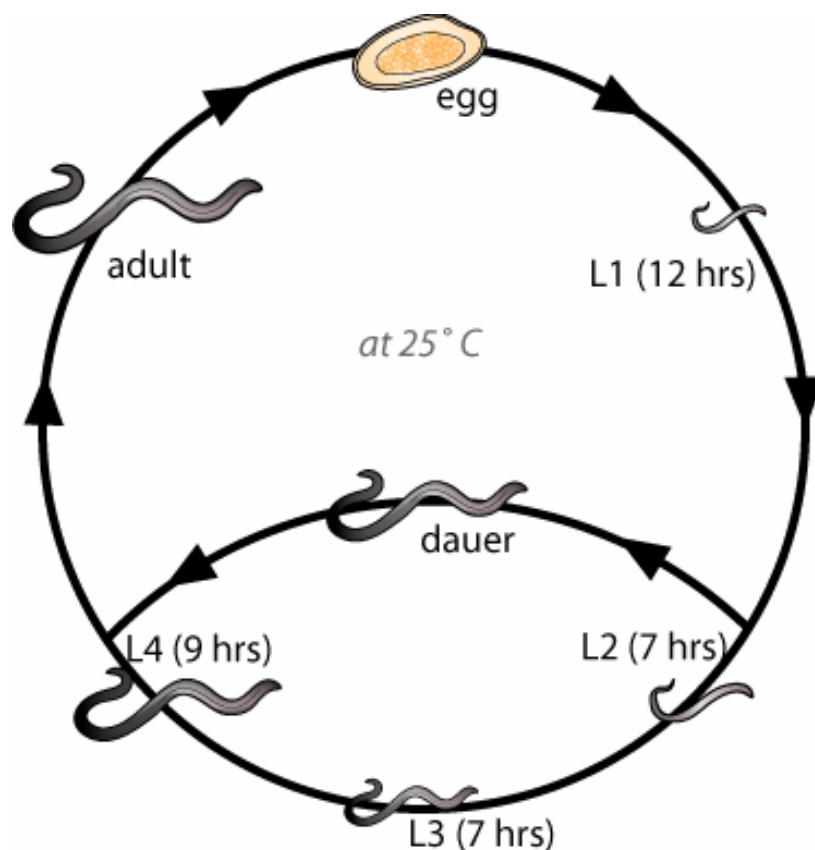
Figure 2: The life cycle of *C. elegans*
Scheme of the *C. elegans* life cycle depicting development from egg to adulthood, including the optional dauer arrest under unfavorable environmental conditions; residence times for each state at 25 °C are given in brackets; taken from [7]

On a cellular level, development in *C. elegans* is stereotypic and starts with single precursor cells in the embryo that always divide and finally differentiate equally in all animals including also stereotypic programmed cell death events [8-12]. Thus, adult worms comprise an identical number of cells at invariable positions within the body (959 somatic cells in hermaphrodites and 1031 in males). With respect to this, virtual reconstruction from thin electron-microscopic slices allowed the morphological characterization of all cells in *C. elegans* [13-15].

Similarly, the nematode is also genetically well described and was the first multi-cellular organism with a completely sequenced genome [16]. With respect to this, numerous techniques evolved that facilitate the comparably rapid and straightforward genetic manipulation of the worm. Here, random mutagenesis by UV irradiation, optionally chemically supported by mutagens like EMS (ethyl methane sulfonate) or TMP (trimethylpsoralen) [17,18], is widely used in forward genetic screens for the identification of novel proteins that suppress or induce specific phenotypes (see e.g. [19,20]). Complementary, other approaches allow the directed manipulation or suppression of gene products. For instance, transposon-dependent techniques were recently described that facilitate the specific deletion or modification of sequences within the genome [21,22]. In addition, RNA-interference (RNAi) – initially discovered in *C. elegans* [23] – was established as method for the specific knock-down of gene expression [24,25]. Here, a library of dsRNA synthesizing bacteria is commercially available that targets approximately 75 % of all *C. elegans* genes [26,27]. Furthermore, microinjection of artificial DNA into gonads allows the generation of transgenic animals for the heterologous expression of proteins [28,29]. Finally, *C. elegans* has two sexes – hermaphrodites and males – that allow the combination of genotypes from different strains by crossing.

2.1.2. Anatomy of the nervous system and sensory system

In the adult *C. elegans* hermaphrodite, the nervous system contains 302 neurons that are anatomically bundled in either the nerve ring or two nerve cords on the dorsal and ventral side (**Figure 3**). For its morphological characterization, the nervous system was completely reconstructed at the ultrastructural level [13-15]. Thus, the entire neural network could be mapped, determining the position and circuitry of individual neurons as well as the number and types of synapses formed in-between.

Hereby, it was also shown that most neurons possess a simple mono- or bipolar morphology with usually unbranched neurites.
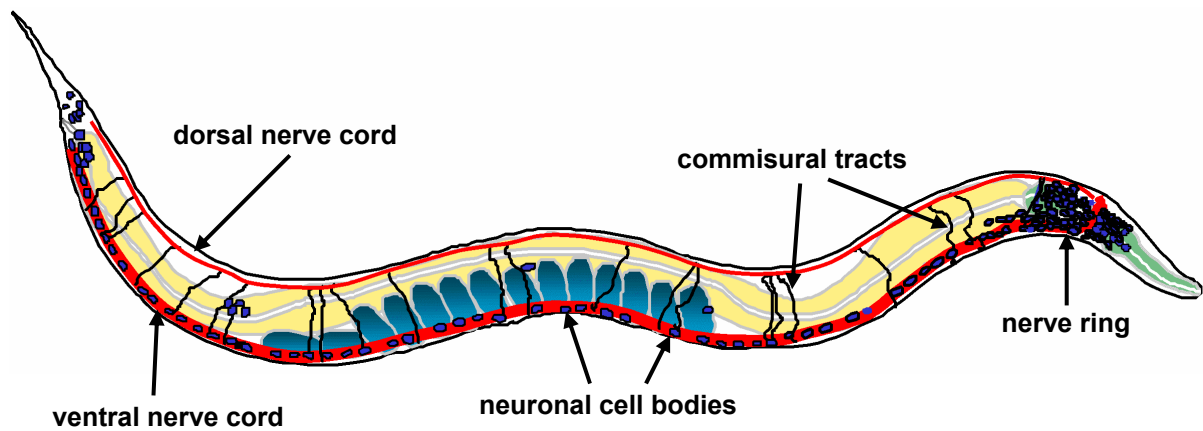
Figure 3: The nervous system of *C. elegans*
Scheme of the nervous system of *C. elegans* depicting the nerve ring in the head, and both nerve cords on the ventral and dorsal side (shown in red); intestine depicted in yellow, pharynx in green; adapted from [30]

Despite the limited number of neurons and a comparably simple architecture, the nervous system in *C. elegans* executes similar basic functions as nervous systems in vertebrates. This includes the sensation of a wide variety of external stimuli [31,32].

For instance, chemosensory neurons in *C. elegans* express approximately one thousand different G-protein coupled receptors (GPCRs) that allow the detection of numerous olfactory and gustatory attractants and repellents [33-38]. Likewise, thermosensory neurons were characterized that facilitate the search for moderate environmental temperatures but also mediate escape reflexes to noxious cold or heat [39,40], while light-sensitive neurons were identified that induce photophobic behaviors in response to near UV and blue light [41,42]. Furthermore, the nematode also detects and avoids environments with high osmotic strength [43].

In addition, *C. elegans* also possesses 32 mechanosensory neurons with extended processes that are distributed throughout the body to constitute a large receptive field [44]. Moreover, mechano-gated channels expressed in these neurons display a diverse sensitivity to allow the detection of stimuli with a broad range of intensities [45,46]. Thus, several mechanosensory neurons were characterized with respect to their responsiveness and localization within the body. For instance, AVM, ALMR, and ALML were identified as the primary neurons to sense gentle touch to the anterior

half, while PLMR and PLML have similar functions for the posterior half of the worm (**Figure 4**; [31,47]).
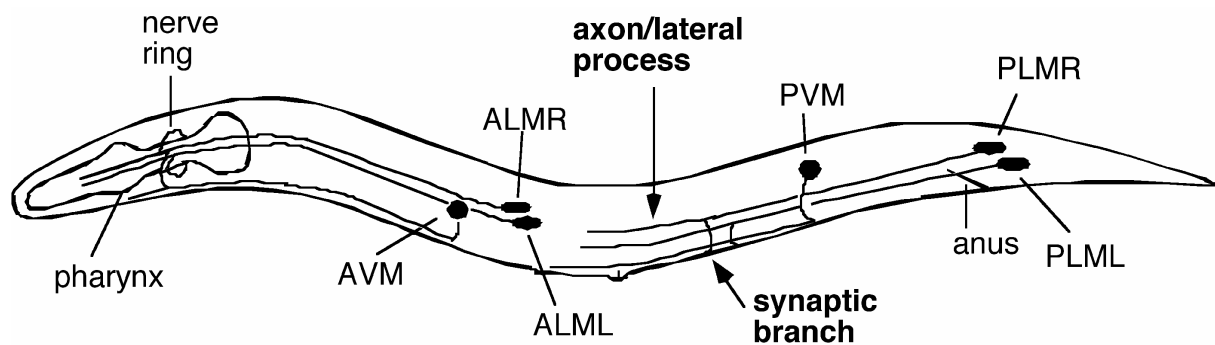
Figure 4: Organization of mechanosensory neurons in *C. elegans*
Schematic drawing of *C. elegans* displaying the morphology of anterior (ALML/R and AVM) and posterior (PLML/R and PVM) touch neurons; taken from [30]

2.1.3. The body wall muscle and motorneural circuitry

In *C. elegans*, 95 body wall muscle cells (BWMs) are arranged in two subventral and two subdorsal stripes that span the longitudinal axis of the animal (**Figures 5A** and **B**; [12,48]). Unlike vertebrate skeletal muscle cells, BWMs do not assemble into a syncytium but are electrically coupled by gap junctions to adjacent muscle cells [49-51].

Besides excitatory cholinergic motorneurons (MNs), *C. elegans* also possesses inhibitory GABAergic MNs which are exclusively stimulated by the cholinergic MNs (**Figure 5C**). Both types of motorneurons form synaptic contact to BWMs at about two thousand so-called neuromuscular junctions (NMJs) to control excitation of the muscle cells. For this, protrusions of the muscle cells break through the surrounding basal lamina and contact motorneurons at en-passant synapses (**Figure 5B**). These structures are also referred to as muscle arms. Anatomically, the connectivity pattern of motorneurons accomplishes the coordinated and antiphasic stimulation and inhibition of muscle cells on the dorsal and ventral sides, thus resulting in a bending of the worm (**Figure 5C**). With respect to this, the propagation of alternating waves of excitation and inhibition along the longitudinal axis of the animal induces a sinusoidal moving pattern [48].
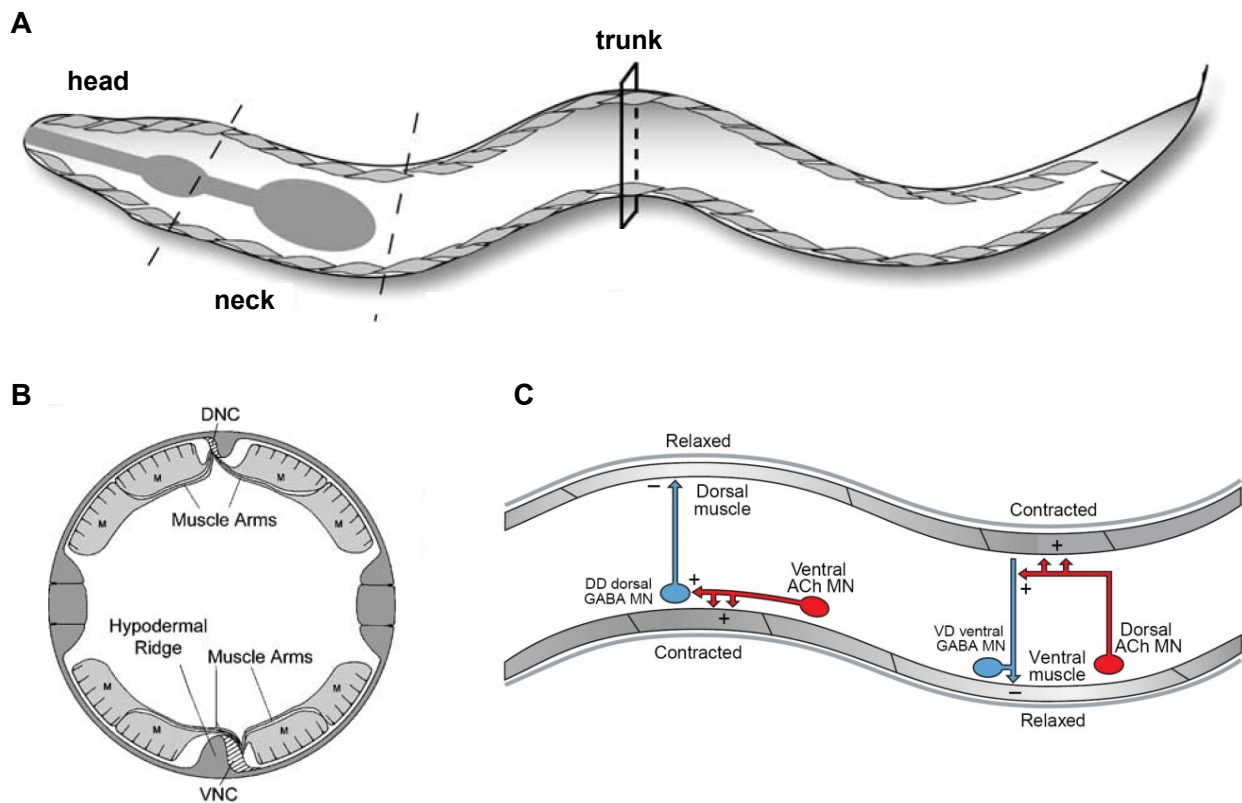
Figure 5: The body wall muscle of *C. elegans* and its innervation by excitatory and inhibitory motorneurons
(**A**) Organization of body wall muscle cells in dorsal and ventral stripes along the longitudinal axis of *C. elegans*; taken from [48] (**B**) Cross section displaying both ventral and dorsal stripes of muscle cells (*M*) with muscle arm connection to either ventral (*VNC*) or dorsal nerve cord (*DNC*) motorneurons; taken from [48] (**C**) Model of motorneuron (MN) connectivity for excitation and inhibition of muscle cells by cholinergic (ACh) as well as GABAergic motorneurons on the dorsal (DD) and ventral (VD) side; taken from [52]

For the perception of the respective neurotransmitter (**Figure 6**), muscle cells express a single ionotropic GABA$_A$ receptor, encoded by UNC-49 [53,54], and two nicotinic acetylcholine receptors (AChRs) that can be distinguished by their sensitivity towards the cholinergic agonists levamisole (L-AChR) and nicotine (N-AChR) [55-62]. Furthermore, acetylcholine and GABA also exert negative feedback in cholinergic MNs via the metabotropic receptors GAR-2 (for ACh) and GBB-1/2 (for GABA). Here it was shown that GAR-2 reduces synaptic efficacy through activation of the Gα$_o$ pathway (**Figure 8**; [63-65]), while the mechanism of GBB-1/2 mediated feedback was recently unclear and subject to investigation within this work.
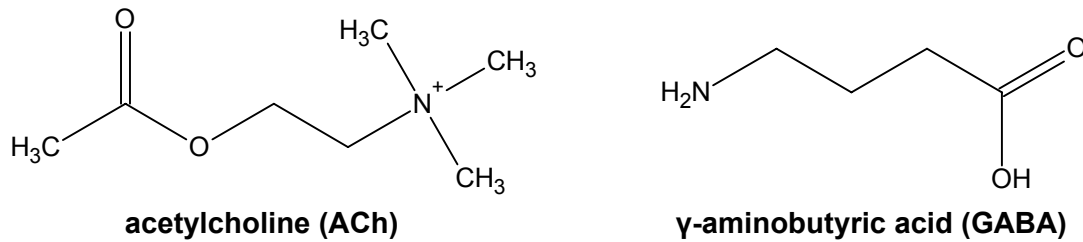
Figure 6: Neurotransmitters at the neuromuscular junction
Chemical structure of the neurotransmitters acetylcholine (ACh) and γ-aminobutyric acid (GABA)

The temporally precise control over muscle cell excitation also requires instant clearance of the neurotransmitters from the synaptic cleft. For this, acetylcholine is hydrolyzed by three different acetylcholine esterases (ACE-1/2/3; [66-70]), while choline is subsequently transported into cholinergic MNs by CHO-1 [71-73]. Likewise, GABA is removed from the NMJ by re-uptake through SNF-11, the *C. elegans* homologue of the vertebrate GAT-1 transporter [74,75]. However, requirement of GABA re-uptake for recycling of the neurotransmitter in GABAergic MNs is currently controversial [74-76].

2.1.4. Synaptic transmission

As *C. elegans* does not possess voltage-gated sodium channels, neurons probably forward signals passively [77,78]. With respect to this, the small size of these cells most likely circumvents the need for an active or even saltatory propagation. Still, earlier studies demonstrated that pharyngeal and body wall muscle cells depolarize in an all-or-none fashion employing voltage-gated calcium channels [79,80]. Similarly, calcium driven action potentials are also considered – though highly controversial – to be elicited in individual neurons of the nematode [81-83].

For the propagation of signals between neurons, *C. elegans* uses chemical and electrical synaptic transmission. In latter case, neurons are coupled by gap junctions to form an electric continuum, allowing the direct transfer of signals between adjacent cells [50,51,84]. During chemical synaptic transmission, on the other hand, electric information is temporarily translated into chemical signals. More precisely, stimulation

of the presynaptic terminal induces release of neurotransmitter which then binds to specific receptors on the postsynaptic side to induce direct or indirect changes of the membrane potential.

2.1.4.1. Synaptic vesicle organization

Presynaptically, neurotransmitters are stored in synaptic vesicles (SVs) which are specialized compartments of about 30 nm in diameter ([85]; this work). With respect to this, studies in diverse model organisms like fly, frog, mouse, and squid revealed a basically similar organization of SVs in presynaptic terminals, where the vesicles can be assigned to three distinct pools according to electrophysiological, morphological and biochemical criteria (for review see [86]). Here, the readily-releasable pool (RRP) of SVs is found in close proximity to the active zone and contains fusion competent SVs that immediately exocytose upon calcium-influx [87,88]. The recycling pool on the other hand is not necessarily found in direct vicinity of the active zone and mainly donates synaptic vesicles to refill the RRP [89,90]. During low or normal firing frequencies of neurons, solely these two pools provide SVs for fusion. Finally, the reserve pool (RP) in the periphery of synaptic boutons harbors the largest number of SVs that are presumably allocated during sustained hyperstimulation of neurons [91,92].

In *C. elegans*, SVs in motorneurons similarly localize to distinct regions within the presynaptic terminal. However, a clear assignment to three pools as described above is not common here. In fact, for most experiments a pool of docked and primed vesicles is defined and analyzed, encompassing SVs that exocytose immediately during acute stimulation [93,94]. Comparable to findings in other organisms, this pool is also referred to as readily releasable pool.

2.1.4.2. Synaptic vesicle exocytosis

The recruitment of SVs from the periphery to the RRP is accompanied by docking and priming of the vesicles (see **Figure 7** for overview of the SV cycle). As shown for *C. elegans*, localization of SVs close to the active zone requires the proteins UNC-18 [95], RAB-3 and its interacting partner RIM (encoded in *C. elegans* by UNC-10; [93,96-98]) in a process only partially understood so far. During priming, SVs are then made fusion competent through loose association of the SNARE complex (<u>s</u>oluble <u>n</u>-ethyl-maleimide sensitive factor <u>a</u>ttachment <u>r</u>eceptor) which consists of the

vesicular SNARE protein synaptobrevin (SNB-1) and two target SNARE proteins SNAP25 (RIC-4) and syntaxin (UNC-64) [99-103]. With respect to this, the priming factor UNC-13 stabilizes the open conformation of syntaxin and hence promotes assembly of the SNARE complex [102-105]. Finally, depolarization of the presynaptic terminal results in a calcium influx through voltage-gated calcium-channels to induce fusion of primed SVs [106-109]. Here, synaptotagmin putatively detects increased calcium levels and promotes the tight association of the SNARE complex to result in synaptic vesicle exocytosis and hence neurotransmitter release [108,110,111].
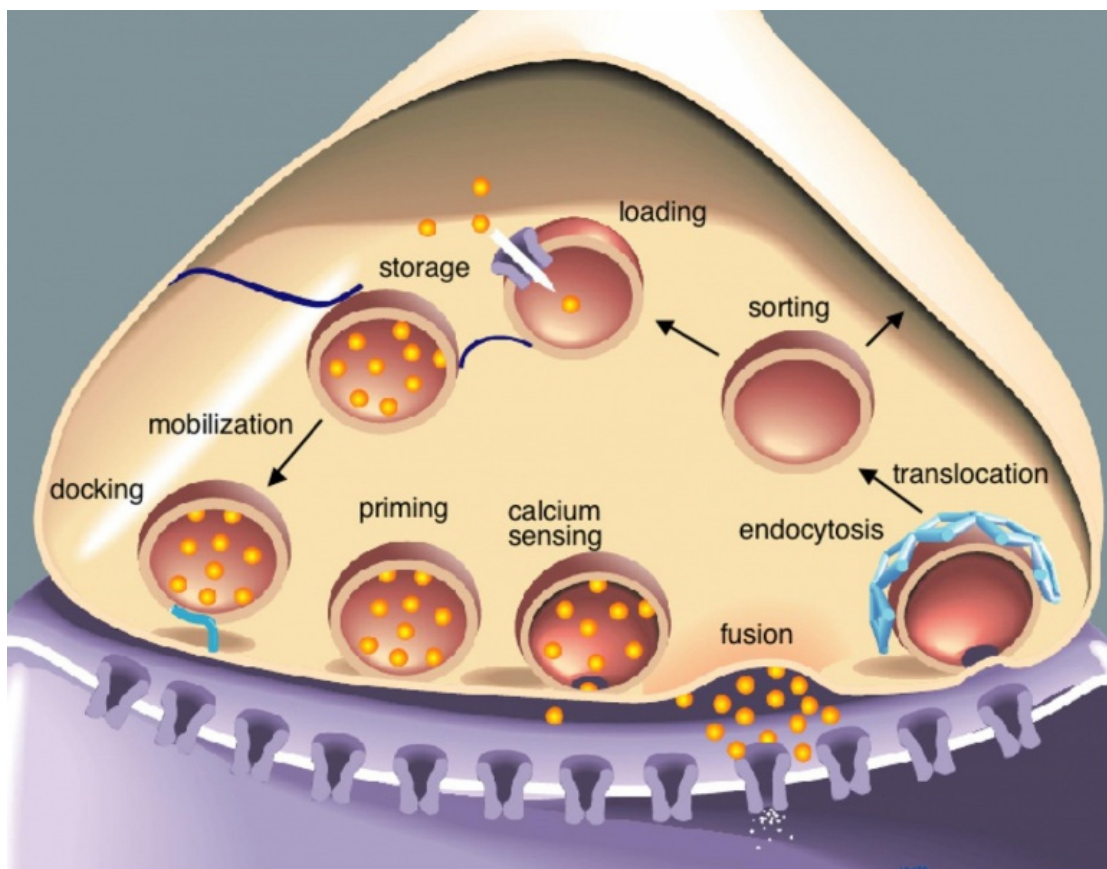
Figure 7: The synaptic vesicle cycle
Schematic presentation of the synaptic vesicle cycle; for explanation see text; taken from [112]

2.1.4.3. Synaptic vesicle recycling

Maintenance of synaptic functionality during ongoing transmission requires the rapid replenishment of SVs after exocytosis. With respect to this, the major pathway to retrieve SVs is considered to be the clathrin-dependent endocytosis, which was also characterized in *C. elegans*. Initially, the adaptor proteins AP180 (UNC-11) and the

AP2 complex recruit the endocytotic machinery and SV proteins to the plasma membrane [113-118], while clathrin and presumably endophilin-A (UNC-57) then facilitate bending of the membrane to initiate the invagination and budding of SVs [119-123]. Subsequently, dynamin (DYN-1) assembles around the neck of the invaginated vesicles to accomplish the fission [124-129]. Finally, the clathrin coat is removed in a process requiring synaptojanin (UNC-26) which hydrolyses phosphate groups from various phosphoinositides and thus probably reduces the binding affinity of coat proteins for synaptic vesicles [130,131]. Furthermore, electron microscopic studies of UNC-26 mutant worms also revealed phenotypes reminiscent of an additional role of synaptojanin in early steps of endocytosis [122,132,133].

Besides the clathrin-dependent pathway, additional mechanisms of SV recycling were described in other organisms. During *kiss-and-run*, SVs only partly fuse with the presynaptic terminal to open a small pore for neurotransmitter release [134-136]. Instead of completing exocytosis, semi-fused vesicles then bud off again and are prepared for another round in the SV cycle. However, only a small fraction of SVs is considered to be recycled by *kiss-and-run* [137-139]. Another mechanism, named *bulk phase* endocytosis, is almost exclusively observed during continuous stimulation of presynaptic terminals and thus is possibly employed only when the capacity of SV recycling via clathrin-dependent endocytosis and *kiss-and-run* is saturated [140]. *Bulk phase* endocytosis starts with the invagination of large vesicular structures from the plasma membrane of presynaptic terminals [141]. Subsequently, SVs are supposed to regenerate from these structures by mechanisms similar to the direct endocytosis from the plasma membrane. The existence of *kiss-and-run* and *bulk phase* endocytosis in *C. elegans* was not confirmed so far, probably due to the difficulties to apply standard methods for neuronal stimulation like high extracellular KCl or electrical stimuli, as well as for imaging neuronal ultrastructure by electron microscopy in these animals.

Finally, endocytosed vesicles are prepared for another round of fusion and neurotransmitter release. For this, vesicular ATPases acidify SVs while specific neurotransmitter transporters use the pH and optionally also the potential across the membrane to load the vesicles [142-144]. In *C. elegans*, UNC-17 [145] and UNC-47 [146] were identified as vesicular transporters for acetylcholine and GABA, respectively.

2.1.4.4. Regulation of neurotransmitter release by intracellular signaling cascades
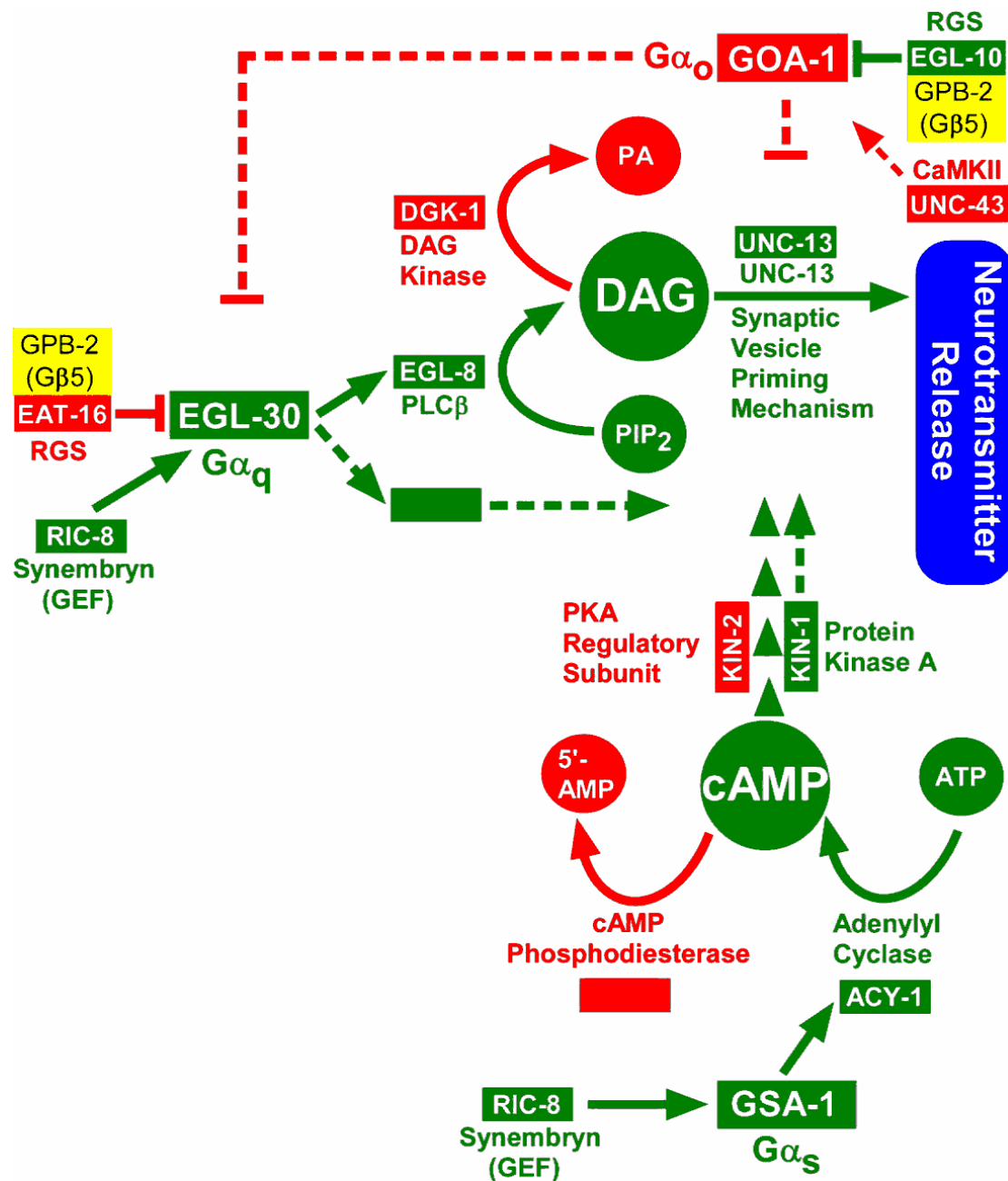
Figure 8: Regulation of neurotransmitter release by intracellular signaling cascades
Scheme of intracellular signaling cascades that regulate neurotransmitter release in neurons; relevant substances are depicted in circles, proteins in boxes (where known, names of *C. elegans* proteins are given within solid boxes); proteins, substances, and interactions colored in red or green, respectively, inhibit and promote SV release; solid lines depict confirmed interactions, dashed lines indicate assumed interactions; AMP = adenosine monophosphate, ATP = adenosine triphosphate, CaMKII = calmodulin-dependent protein kinase II, cAMP = cyclic adenosine monophosphate, DAG = diacylglycerol, GEF = guanine nucleotide exchange factor, PKA = protein kinase A, PA = phosphatidic acid, PIP_2 = phosphatidylinositol-4,5-bisphosphate, PLCβ = phospholipase Cβ, RGS = regulator of G-protein signaling; adapted from [147]

As shown for C. elegans and other organisms, the synaptic efficacy and plasticity are also subject to modulation through intracellular signaling cascades (**Figure 8**). For instance, the $G\alpha_q$ pathway activates diacylglycerol (DAG) synthesis to enhance SV priming and release. More precisely, DAG binds to the C1 domain of UNC-13 and by this recruits this protein to the synapse to promote SV fusion [104,148-151]. Opposing this, $G\alpha_o$ signaling is inhibiting neurotransmitter release, conceivably by destruction of DAG [152-155].

Furthermore, various aspects of basic neuronal activity are also regulated by the $G\alpha_s$ pathway that mainly exerts its effects via synthesis of the second messenger cAMP (**Figure 18A**). Here, elaborate studies in *Drosophila* demonstrated that cAMP-driven protein kinase A (PKA) increases recruitment of SVs from the reserve pool to the RRP [156] and also alters transcription of different proteins via the cAMP response element (CRE) [157-160]. In line with this, mutant flies with deficient cAMP synthesis display defects in short-term plasticity, e.g. lacking post-tetanic potentiation (PTP) after NMJ hyperstimulation [161]. In *C. elegans*, $G\alpha_s$ regulates synaptic efficacy by similar mechanisms. Here it is assumed, that cAMP affects the mobilization of a certain pool of SVs [162] to impact on the strength of synaptic transmission [147,149] while a regulatory function of $G\alpha_s$ on cell surface expression of distinct receptors was also demonstrated [163,164].

2.1.4.5. Perception of neurotransmitters

On the postsynaptic side of chemical synapses, neurotransmitters bind to specific receptors that re-translate chemical signals into changes of the membrane potential. Here, metabotropic G-protein coupled receptors (GPCRs) mostly activate intracellular signaling cascades for the modulation of synaptic efficacy (see **Figure 8**; [165,166]). In line with a regulatory function, metabotropic receptors are similarly found on pre- and extrasynaptic sides to mediate positive or negative feedback. Furthermore, neurotransmitters also activate ionotropic receptors to induce direct changes of the membrane potential. Depending on the selectivity and conductivity of their ion channels, these receptors may induce a depolarization or hyperpolarization of post-synaptic terminals.

With respect to this, several regulatory mechanisms were investigated that control receptor activity on the cell surface. In *C. elegans*, these processes are best understood for the nicotinic AChRs of the body wall muscle cells. These receptors

belong to the highly conserved *cys-loop* class of ligand-gated ion channels (LGICs) that is found in all animals and encompasses ionotropic receptors with ligand-binding sites for glycine, serotonin, and GABA [167-169]. Independent from ligand specificity, *cys-loop* receptors are usually composed of five subunits that share a similar structure and common motifs. Thus it was shown that each subunit comprises a large extracellular amino-terminal domain that is mainly composed of β-strands and contains the characteristic *cys-loop*, four membrane spanning helices (M1-M4), and a short C-terminus (**Figure 9**; [170-173]).
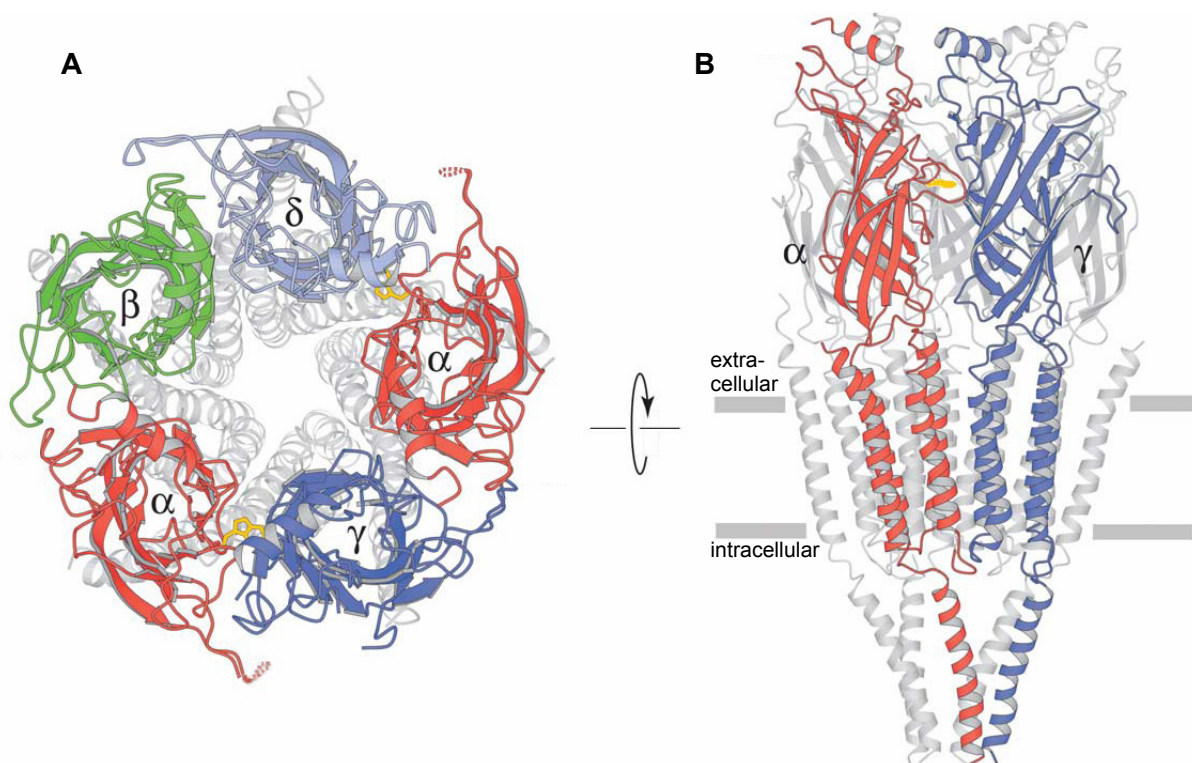
Figure 9: Structure of the *Torpedo* acetylcholine receptor
Ribbon diagrams of the acetylcholine receptor from *Torpedo* (PDB 2BG9; [170]) displaying arrangement of α- (red), β- (green), γ- (blue), and δ-subunits (light blue) in the receptor as viewed from the synaptic cleft (**A**) or perpendicular to the membrane plane (**B**); a conserved Trp (position 149 in the α-subunits) is depicted in yellow, the dashed lines indicate the position of the *C-loop* in α-subunits (in **A**); taken from [170]

Subunits of the nAChRs are further subdivided into α- and non-α, with former ones containing the *C-loop* motif formed by a disulfide bond of two cysteines in the extracellular domain (**Figure 9A**; [172]). Here it was shown that the *C-loop* plays a role in receptor assembly [174] and gating [175]. Furthermore, as this motif is important for ligand binding, the number of α-subunits in the pentameric LGIC also

equals the number of ligand binding sites [176,177]. In *C. elegans*, the levamisole-sensitive AChR is composed of three α and two non-α subunits while the nicotine-sensitive AChR comprises five identical α-subunits [57,60].

During assembly of the AChRs in the ER, distinct dimeric intermediates form and finally re-arrange into pentameric receptors [178]. Along this way, the subunits interact with chaperones like BIP, calcineurin, ERp57, and calreticulin that retain single subunits in ER and prevent ER-associated degradation (ERAD; [179-184]). However, as about 70 % of all synthesized subunits are degraded this way, ERAD seems to be an important mechanism for quality control of receptor assembly [180,185].

Adding to this, subunits also contain specific ER retention motifs that are only masked in the pentameric receptors to prevent ER exit of single subunits and intermediate polymers [186]. However, once a mature receptor formed, the protein 14-3-3η binds to a specific motif in the large intracellular loop between M3 and M4 and promotes transport of the AChR to the Golgi apparatus [187,188]. This process is regulated by the Gα$_s$ signaling cascade as binding of 14-3-3η requires preceding phosphorylation of the motif by PKA [163]. Likewise, the gene of 14-3-3η also comprises a CRE-motif (*cAMP response element*) that promotes expression through the transcription factor CREB (*cAMP response element binding*) [164]. Furthermore, another protein was recently identified in *C. elegans* – RIC-3 – that expedites assembly or ER exit of ionotropic AChRs [189].

In the Golgi apparatus, receptors are prone to be targeted for lysosomal degradation and require positive regulators for further transport to the cell surface. In case of the L-AChR it was shown, that UNC-50 interacts with soluble guanine nucleotide exchange factors (GEFs) of Arf – a Golgi resident GTPase that organizes COP-I dependent transport from the Golgi apparatus – to promote cell surface expression of this receptor [190].

Finally, receptors are clustered on the cell surface of the postsynaptic side. In vertebrates, agrin is secreted presynaptically and activates the receptor tyrosine kinase MuSK [191,192] which in turn organizes the post-synaptic scaffold to localize receptor clusters opposite to the active zone [193-195]. In *C. elegans*, clustering of the levamisole-sensitive AChR in BWMs requires the formation of a complex including the transmembrane protein LEV-10 and the two secreted proteins LEV-9 and OIG-4 [196,197]. Besides tight regulation of surface expression, receptors are

also modulated on a functional level by selective phosphorylation and dephosphorylation [198] which requires the phosphatase calcineurin [199,200].

2.2. Neurobiological techniques

While structure and anatomic assembly of most nervous systems are well-characterized today, less is known about how neural networks perceive and integrate information for the generation of adequate responses. With respect to this, *C. elegans* provides several advantages for the investigation of related mechanisms, making the nematode a favorable model organism in neurobiology. For instance, *C. elegans* exhibits a limited repertoire of behaviors that are regulated by a comparably simple nervous system with known morphology [13-15]. Furthermore, the susceptibility for genetic manipulation [16-18,21,22,24-29] is accompanied by the viability of most mutants [201,202] to afford the functional analysis of gene products.

Based on these attributes, several methods were established for *C. elegans* that aim at the functional characterization of its nervous system. For example, different techniques evolved that allow the analysis of neuronal and muscle cell activity. Here, electrophysiological recordings can be applied to measure post-synaptic currents in pharyngeal or body wall muscle cells [55,203]. This technique is often combined with pharmacological or electrical stimulation to characterize synaptic transmission at the neuromuscular junction [55]. However, electrophysiological methods require invasive surgery on fixed worms, thus eliminating the possibility of behavioral analysis. Furthermore, patch-clamp recording of individual neurons is very difficult in *C. elegans* and was thus successfully performed only seldom [204,205]. With respect to this, genetically encoded calcium indicators (GECIs) were established in the last decade that visualize changes of intracellular calcium concentrations by means of fluorescence [206-209]. Thus, targeted expression of GECIs allows to correlate neuronal activity with specific phenotypes or behaviors [209]. This approach was already employed in freely moving *C. elegans* to map a neural circuit that integrates chemosensory information for an adequate regulation of locomotory behavior [210].

Techniques that report neuronal activity are ideally complemented by methods that facilitate the directed manipulation of neuronal processes to highlight associated phenotypes. Here, laser irradiation [211] or transgenic expression of caspases [212-214] are commonly applied for the selective ablation of neurons. However, the high

intensity of laser light potentially harms surrounding cells whereas genetic ablation requires suitable promoters for the cell-specific expression of the caspases. Furthermore, ablation of neurons occurs early during development, and thus possibly induces compensatory re-wiring of the nervous system.

On the other hand, pharmacological treatment allows the reversible manipulation of the intact nervous system in live animals. Therefore, physiologically active substances are supplemented to the surrounding medium to allow penetration through the cuticula of *C. elegans*. However, as this process is rather inefficient for most pharmaceuticals, high concentrations need to be applied, making estimation of effective concentrations inside the body difficult.
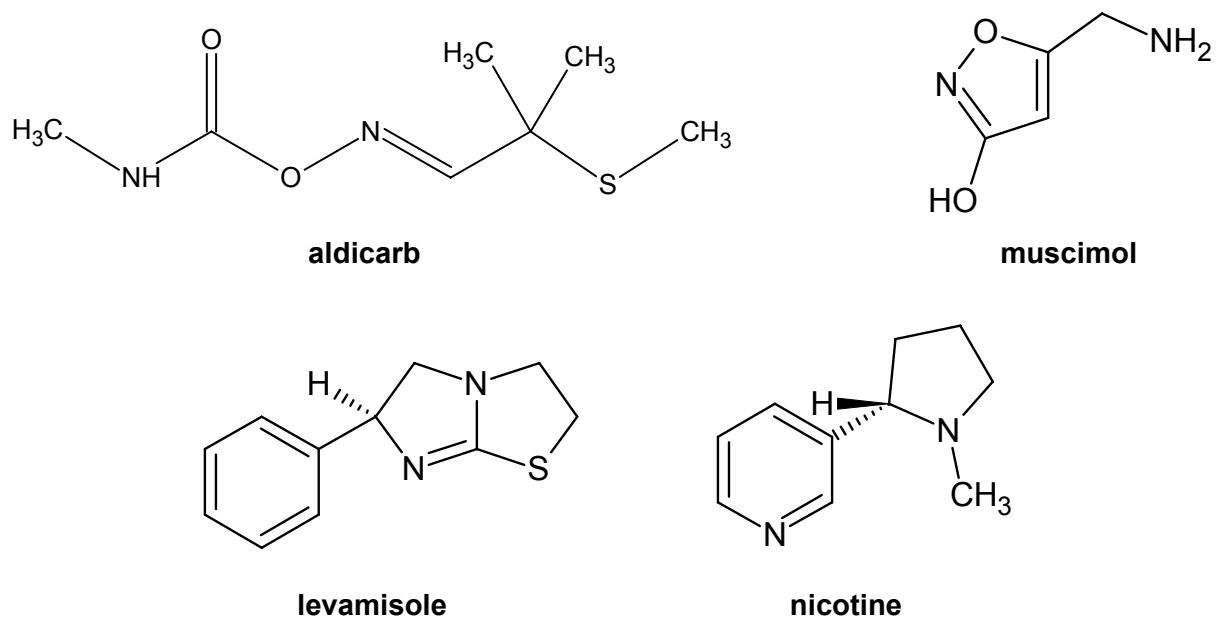
Figure 10: Pharmacological substances to stimulate the *C. elegans* NMJ
Chemical structures of aldicarb (inhibitor of acetylcholine esterase), muscimol (agonist of GABA receptors), levamisole, and nicotine (both agonists of acetylcholine receptors)

Still, pharmacological intervention is commonly used for the investigation of synaptic transmission at the neuromuscular junction of *C. elegans*. Here, different substances are employed to specifically enhance excitation or inhibition of muscle cells (**Figure 10**). For instance, the potent acetylcholine esterase inhibitor aldicarb induces an accumulation of acetylcholine in the synaptic cleft to activate both the L- and N-AChR [215]. More specifically, application of either levamisole or nicotine allows the selective activation of the respective AChR [55,216]. As a consequence, all three

substances effectively stimulate muscle cells to induce tetanic paralysis in the long-term. In contrast, treatment of worms with the GABA agonist muscimol stimulates the GABA$_A$ receptor and hence evokes ongoing relaxation [54]. In all cases, analysis of resulting peculiarities of locomotory impairment potentially reveals defects of synaptic transmission. This approach can also be combined with the genetic manipulation of animals in forward and reverse screens for the detection and functional characterization of proteins within this process.

However, pharmacological approaches only provide poor temporal and spatial specificity. To bypass these limitations, light-controlled techniques were developed that take advantage of the high precision of optical set-ups to facilitate the acute and targeted manipulation of neuronal activity. These methods are ideally applied to transparent organisms like *C. elegans* that allow the non-invasive illumination in live animals.

Initially, biologically inactive caged compounds that release neurotransmitter upon illumination were successfully employed for the stimulation of neurons in living brain slices from rat [217]. Still, for repeated or long-term applications, this approach requires the replenishment of caged compounds to compensate for diffusion and consumption. As to this, invasive delivery processes limit the applicability in live animals. In another approach, Szobota and colleagues engineered a light-driven kainate type glutamate receptor for a direct excitation of neurons [218]. Therefore, the receptor was coupled to the ligand glutamate via a photo-switchable azobenzene linker. While two different colors of light separately triggered photoisomerization of the linker and the reverse reaction, the glutamate was selectively brought close to or removed from the receptor binding pocket, respectively, to control channel gating. This approach was proven and tested in mammalian cultured neurons and even zebrafish [218].

Thus, while light-controlled techniques ideally provide temporal and spatial specificity, application of recent approaches in live animals is still hampered by the demanding delivery of exogenous cofactors and the inefficient expression of used tools. These drawbacks can be bypassed using light-driven microbial rhodopsins for the direct manipulation of the membrane potential and thus of neuronal activity. For this, the cation channel Channelrhodopsin-2 (ChR2) was demonstrated to facilitate the depolarization of excitable cells [219,220], while the chloride pump Halorhodopsin (NpHR) affords the hyperpolarization by light [221]. Notably, the essential cofactor of

all rhodopsins, the chromophore retinal (**Figure 12**), is readily available in all vertebrate tissues [222] or can be easily supplemented by nutrition in case of *C. elegans* and *Drosophila melanogaster* [219,223].

2.3. Optogenetics

2.3.1. Channelrhodopsin-2

Channelrhodopsin-2 (ChR2; GenBank-No. AF461397) is a blue light driven cation channel that was originally isolated from the green alga *Chlamydomonas reinhardtii* [224,225]. Here, ChR2 is enriched in the so-called eyespot and mediates phototactic responses together with a second rhodopsin, ChR1 [226,227].
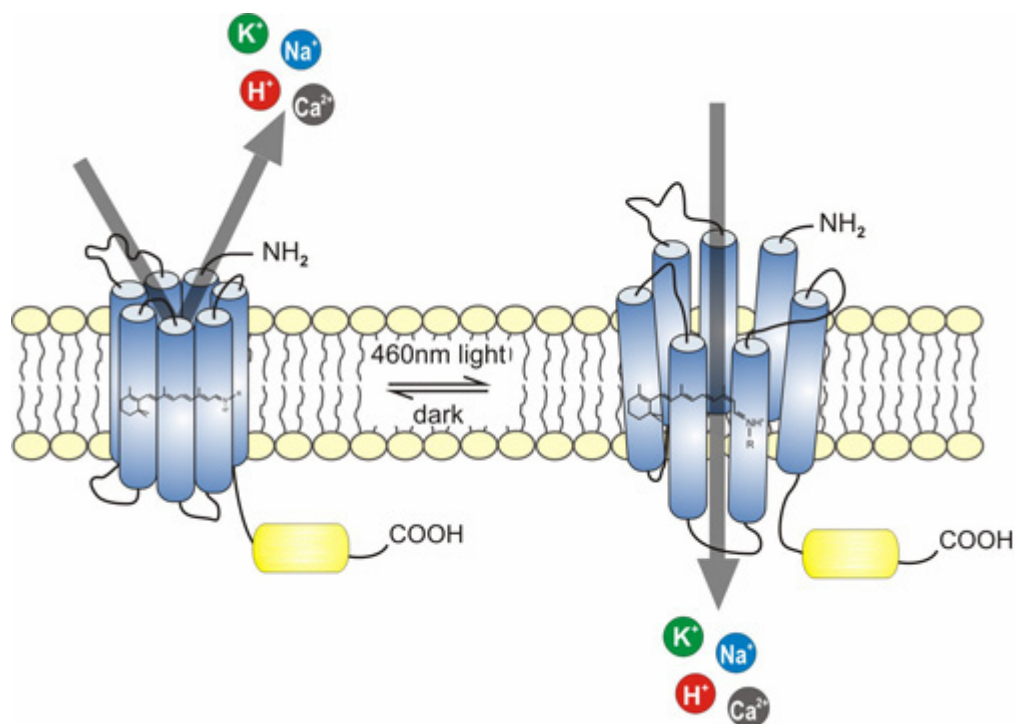
Figure 11: Topology and light-response of ChR2
Topology of ChR2 including the heptahelical transmembrane domain (blue) and the large cytosolic domain (yellow); photoactivation with blue light induces formation of a cation channel with permeability for protons, Na^+, K^+, and Ca^{2+}; adapted from [228]

The ChR2 primary structure contains 737 amino acids that can be roughly divided into an amino-terminal domain comprising seven transmembrane helices (amino acids 1-315) and a large intracellular carboxy-terminal moiety (amino acids 316-737)

(**Figure 11**). The ion channel and its functional properties are solely determined by the amino terminal domain [229] which also covalently binds the essential cofactor retinal via a Schiff base to a lysine in the seventh transmembrane helix (Lys257; **Figure 12**; [230]). However, while a clear function of the large cytosolic terminus could not be demonstrated yet, it is assumed that this part is involved in intracellular signaling pathways [224,227].
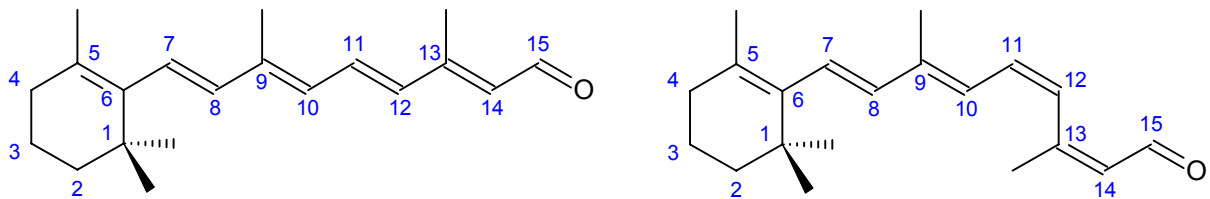
Figure 12: Different isomers of retinal
Chemical structure of retinal in the all-*trans* (left) and 13-*cis* (right) conformation

The action spectrum of ChR2 displays a maximum at about 460 nm (**Figure 15**; [224]). Starting from the dark-adapted ground state (D480; the number indicates the absorbance maximum of the respective photointermediate), photoactivation of ChR2 induces isomerization of all-*trans* retinal to 13-*cis* retinal in less than 50 ns (**Figures 12** and **13**; [231-234]). This is accompanied by deprotonation of the Schiff base (P390; 25 µs) and subsequent reprotonation (P520; 1,5 ms) [235]. In addition, major conformational changes occur in P520 that induce formation of a channel with a diameter of approximately 6 Å [224]. The lining and geometry of the pore endows the channel with a slight inward-rectifying permeability for monovalent cations such as protons, Na^+, and K^+ as well as small divalent cations like Ca^{2+} [224]. Here, the single channel conductance for sodium was determined to be circa 40 fS [236]. Following P520, the channel closes after circa 10 ms and ChR2 progresses to the non-responsive P480 state. As ChR2 only recovers after about six seconds from this intermediate, P480 is also referred to as desensitized state [233,237]. As a consequence of this, only a minor population of ChR2 proteins is light-responsive during sustained photoactivation, resulting in a reduced steady-state current of about 30 % of the initial peak value (see **Figure 16**; [224,238]). Notably, P480 can be bypassed when green or yellow light is presented to the open channel in the P520 state [235]. Furthermore, hydrolysis of the Schiff base in P480 results in formation of

the so-called *lost states* P380 and P353 [239]. Subsequently, the Schiff base reforms during thermal relaxation of the protein to D480 within several minutes [231,235,239,240]. This side reaction is very prominent for Cys128 mutants of ChR2 and triggers progressive inactivation of these variants [241].
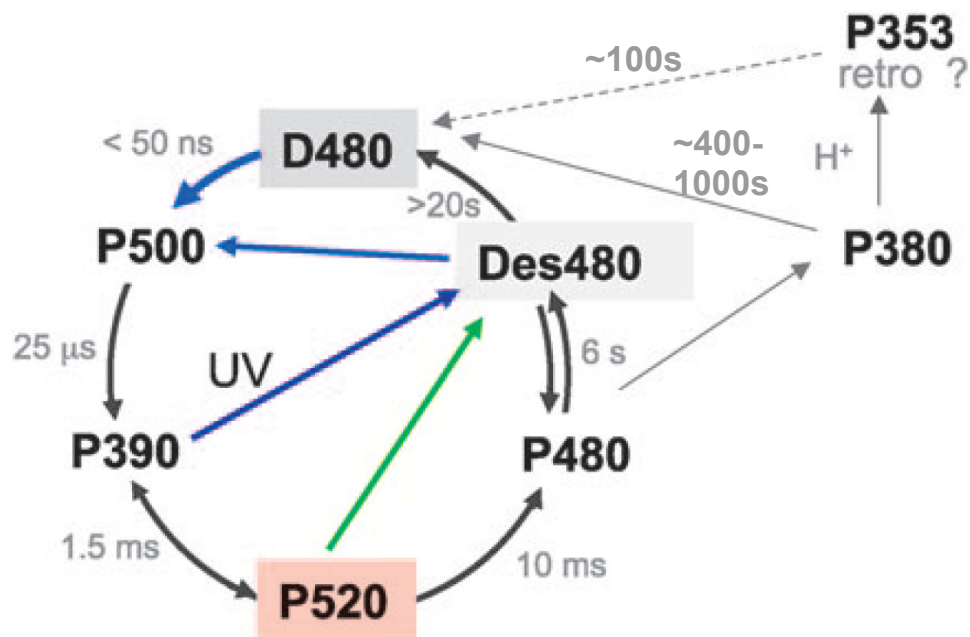
Figures 13: The photocycle of ChR2
Model of an eight-state photocycle of ChR2 including time constants and the so-called *lost states* (P380 and P353) which prominently reduce excitability of ChR2(C128X) mutants; colored arrows indicate the absorption of a photon of the respective wavelength; adapted from [231]

2.3.2. Halorhodopsin

The archaeon *Natronomonas pharaonis* was originally isolated from soda lakes in Egypt where the organism faces high salt concentrations and basic pH [242]. To withstand these harsh conditions, the halobacterium expresses the yellow light driven chloride importer halorhodopsin (NpHR; GenBank-No. AAM15777) which generates an electrochemical gradient across the cell membrane [243]. The archaeon uses this gradient to maintain the osmotic balance and for the synthesis of ATP [244,245].

The primary structure of NpHR contains 291 amino acids that form the typical heptahelical arrangement of microbial rhodopsins with the cofactor retinal bound via a Schiff base to a lysine in TM7 (Lys256; **Figure 14**; [243,246]).
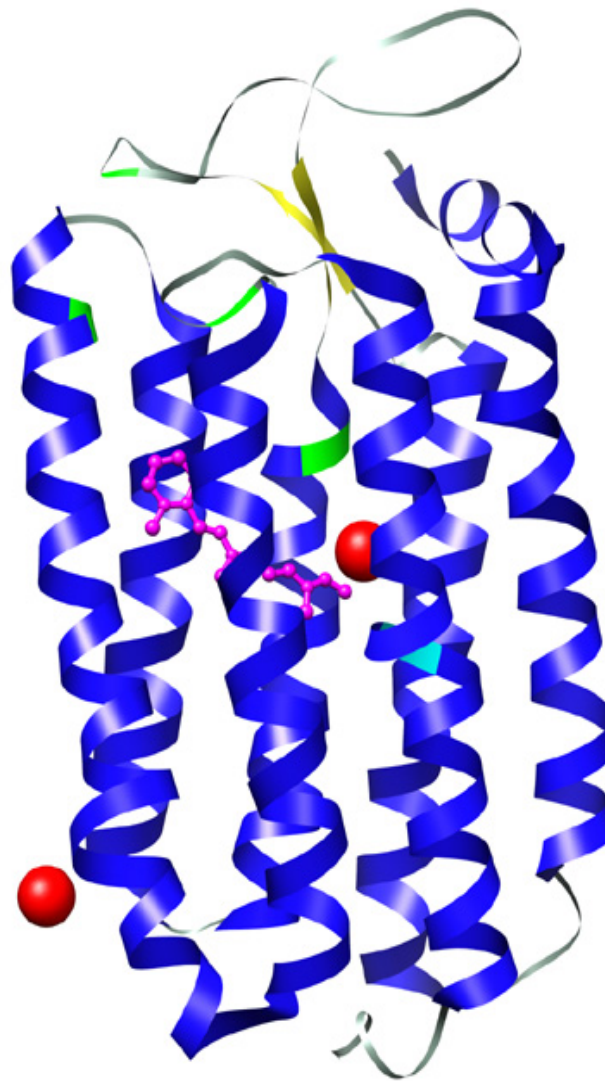
Figure 14: Structure of halorhodopsin from *Natronomonas pharaonis*
Three-dimensional structure of halorhodopsin from *Natronomonas pharaonis* (PDB 3A7K; [246]) depicting transmembrane helices (blue), the cofactor retinal (purple), the retinal binding site (Lys256; light blue), chloride anions (red), and residues that form the putative anion uptake pathway (green); generated using Chimera [247]

NpHR absorbs yellow light (absorption maximum at ~580 nm; **Figure 15**) to induce the vectorial transport of chloride ions from the extracellular site to the cytoplasm [221,248,249]. However, while only few details are known about the photocycle thus far [250,251], analysis of the crystal structure of NpHR yielded insight into structural

determinants of the chloride import (**Figure 14**; [246]). Here, four charged amino acids were identified that form the putative anion uptake pathway on the extracellular site (**Figure 14**, green residues), validating earlier studies on mutant variants of NpHR [252]. Furthermore, an amphipathic helix at the amino-terminus combines with the loop between TM2 and TM3 to constitute an extracellular cap structure. Conceivably, this hydrophobic cover prevents the arbitrary exchange of chloride between the extracellular medium and the anion binding site. On the cytoplasmic site of NpHR, hydrophobic residues form an energetic barrier that prevents direct release of chloride into the cytoplasm. Thus it is assumed that a proton/HCl antiport mechanism applies here, which is similarly considered for halorhodopsin from *Halobacterium salinarium* [246].
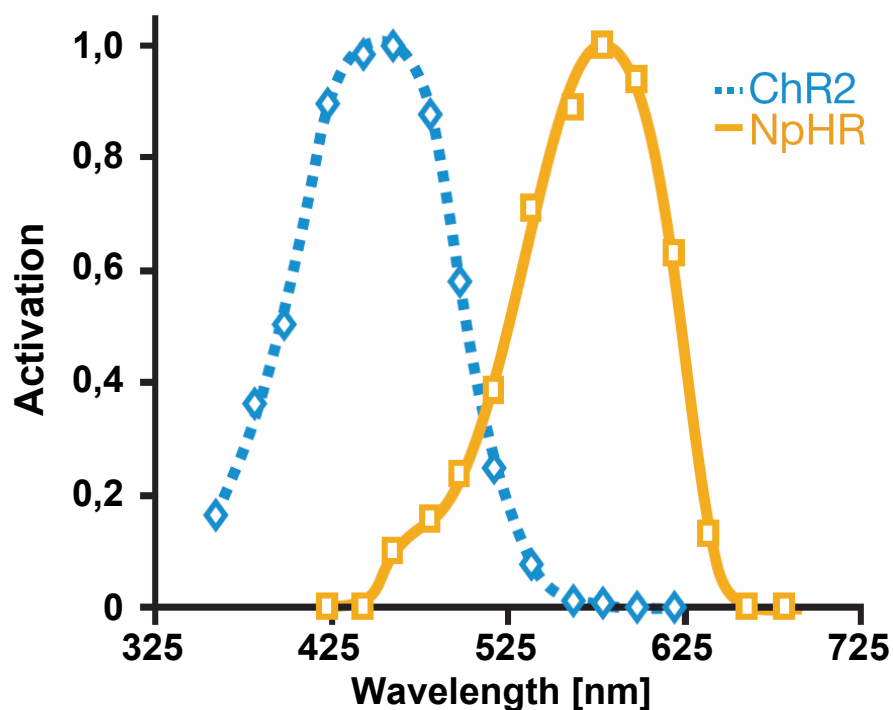
Figure 15: Action spectra of ChR2 and NpHR
Action spectra of ChR2 (blue) and NpHR (yellow) normalized to the maximum activity; adapted from [221]

2.3.3. Optogenetics

2.3.3.1. Optogenetic application of Channelrhodopsin-2 and Halorhodopsin

Soon after their biophysical characterization, heterologous expression of microbial rhodopsins in various organisms was investigated for its potential to allow manipulation of the membrane potential by light. Thus it was shown that photoactivation of Channelrhodopsin-2 (ChR2) affords the depolarization of neurons and muscle cells (**Figure 16A**; [219,220]) whereas Halorhodopsin (NpHR) facilitates the hyperpolarization (**Figure 16B**; [221]). As the action spectra of both rhodopsins are fairly separated (**Figure 15**), two different colors of light can be presented for the bidirectional control of the membrane potential in cells expressing the two opsins. Also, as both rhodopsins operate in the millisecond time range, this approach ideally allows the temporally precise control of intervention. Thus, the combination of optics – allowing fast and relatively non-invasive stimulation of microbial rhodopsins – and genetics to provide promoter-dependent cellular specificity gave rise to a new discipline in the neurosciences, namely optogenetics.
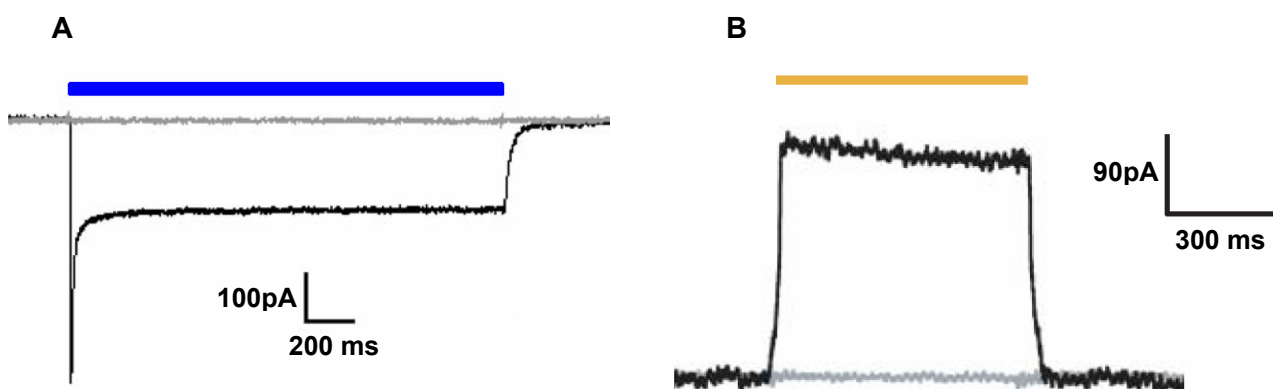
Figure 16: Voltage-clamp measurements of *C. elegans* muscle cells expressing optogenetic tools
Whole-cell voltage-clamp measurements of *C. elegans* body wall muscle cells expressing ChR2(H134R) (**A**; adapted from [219]) or NpHR (**B**; adapted from [221]) while being photostimulated with blue and yellow light, respectively, as indicated by the colored bars; animals were raised either in presence (black graphs) or absence (grey) of all-*trans* retinal

Thus far, optogenetic techniques were applied to various organisms ranging from the nematode *C. elegans* [229] to primates like the macaque [253]. Here it was demonstrated that heterologous expression of most optogenetic proteins is generally

well-tolerated and non-toxic. Furthermore, the cofactor retinal (**Figure 12**) was found to be available in all vertebrate tissues [222] or could be easily supplemented by nutrition where required [219,223], thus avoiding invasive delivery processes.

2.3.3.2. Improvement of optogenetic techniques

Since the initial characterization of both rhodopsins, much effort has been put into modification of these proteins to improve their utility for optogenetic applications. Here, surface expression of ChR2 and NpHR in mammalian neurons was enhanced by codon optimization [254,255] and addition of motifs that promote the transport to the plasma membrane [255,256].

Furthermore, molecular engineering of ChR2 yielded variants with altered ion selectivity, ion conductance, spectral properties, or photocycle kinetics. With an impact on the functionality of ChR2, mutated amino acids are hence often found in close proximity of the putative channel or near the retinal binding pocket of the rhodopsin (**Figure 17**). Ideally, the diverse characteristics of these mutant variants often allow the application for specific optogenetic purposes. For instance, mutation of the proton acceptor His134 to Arg doubled the mean open time of the channel and thus also increased the steady state currents of ChR2 from 30 to 60 % during sustained photoactivation (**Figure 16A**; [219]). Conversely, mutation of Glu123 to Ala significantly shortened closing kinetics, allowing spike firing with more than 200 Hz in neurons capable to elicit such high firing frequencies [257]. Thus, this mutant can be employed to mimic activity of neurons with high-frequency firing rates as e.g. parvalbumin expressing neurons [258]. Furthermore, other ChR2 mutants were described that selectively increase current amplitudes up to 10-fold (Thr159Cys; [259]) or exhibit enhanced calcium conductance (Leu132Cys; [260]). Finally, ChR2 was also engineered to allow long-term depolarizations under minimal light-invasive conditions for photoactivation. With respect to this, mutation of Cys128 to Ser was described to decelerate channel closing to several minutes [261]. Ideally, an initial short light stimulus suffices to evoke prolonged depolarizations using this mutant.
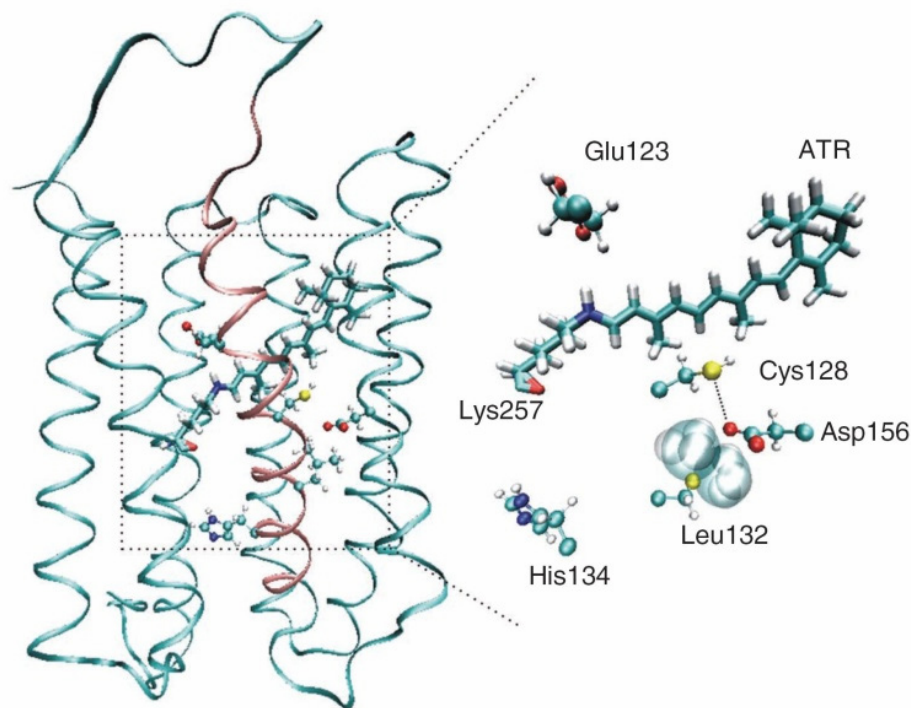
Figure 17: Homology model of ChR2 with relevant residues for functionality
Homology model of ChR2 based on the structure of sensory rhodopsin II from *Natronomonas pharaonis* (PDB 1H2S; [262]) depicting the position of relevant residues that determine functional properties; the inset shows the putative arrangement of several residues with respect to retinal; taken from [260]

2.3.4. Other optogenetic tools

2.3.4.1. Rhodopsins

Besides ChR2 and NpHR, several other light-driven proteins were identified in various organisms that are potentially useful for optogenetic applications. For instance, the blue light driven proton pump Mac from the fungus *Leptosphaeria maculans* [263] efficiently hyperpolarizes excitable cells, thus constituting a spectral alternative to the yellow light driven NpHR [264,265]. Similarly, various channelrhodopsins were discovered in other organisms like *Volvox carteri* [266,267] and the flagellate *Mesostigma viride* [268]. These rhodopsins partly exhibit red-shifted action spectra compared to ChR2, but are less efficient for the depolarization of excitable cells. However, chimeric rhodopsins of ChR1 from *Volvox carteri* and ChR1 from *Chlamydomonas reinhardtii* were successfully employed to stimulate excitable cells in mice and *C. elegans* in response to red light (K. Erbguth,

A. Gottschalk, personal communication; [269,270]). Likewise, chimeras of ChR1 and ChR2 from *Chlamydomonas reinhardtii* exhibit reduced desensitization and allow excitation by green light [238,271]. A red-shifted action spectrum is particularly of benefit for stimulation in mammalian brain tissue, where blue light tissue penetration suffers from higher scattering and absorption effects [272].

2.3.4.2. *Photoactivated adenylyl cyclase*

While microbial rhodopsins provide means for the light-driven manipulation of the membrane potential, another class of proteins was characterized that facilitates the photo-stimulated synthesis of the second messenger cAMP (**Figure 18A**). In *Euglena gracilis*, the p*hotoactivated adenylyl cyclase* (PAC) was identified as a major component of the autofluorescent paraxonemal body (PAB) which is the photosensory organ of this freshwater flagellate [273,274]. Here, photoactivation of PAC by blue light contributes to the cAMP mediated phototaxis and step-up photophobicity [274,275]. Further characterization revealed that PAC is a tetramer consisting of two α and two β subunits, each of which contains two cyclase and two BLUF domains that bind FAD non-covalently as essential cofactor (**Figure 18B**).
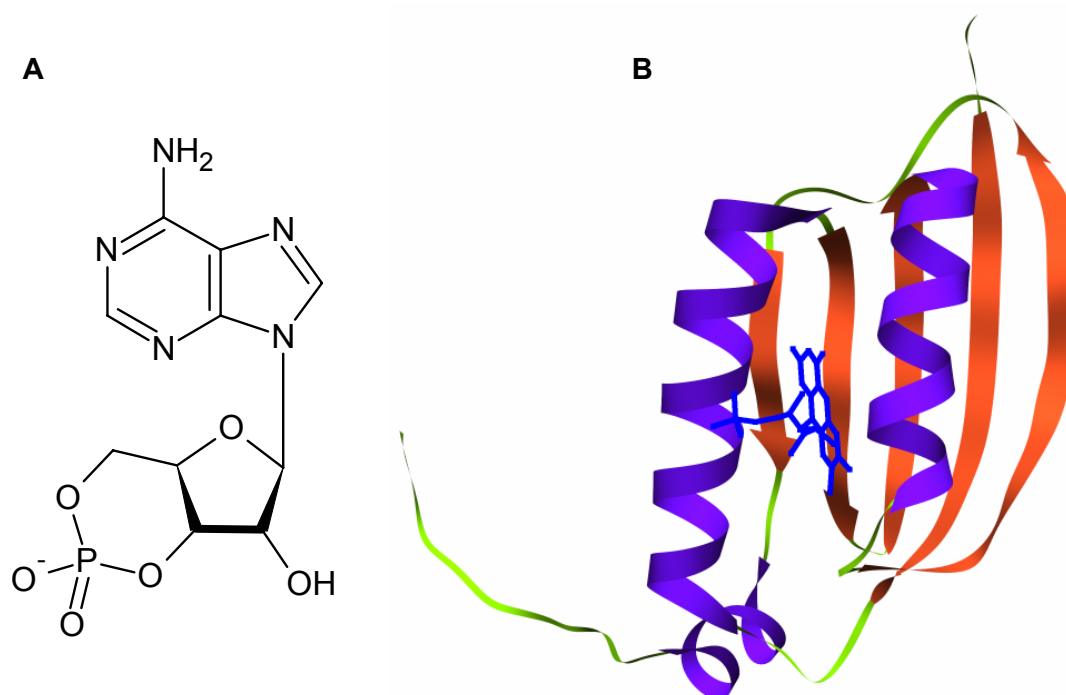
Figure 18: Structure of cAMP and the BLUF domain
(**A**) The chemical structure of cyclic adenosine monophosphate (cAMP) (**B**) Three-dimensional structure of the BLUF domain of AppA from *R. sphaeroides* (PDB 1YRX; [276]) consisting of a five-stranded β-sheet (red), two α-helices (purple), and the cofactor flavin mononucleotide (FMN; blue); generated using Chimera [247]

As shown by crystal structures, BLUF domains contain a ferredoxin like fold, consisting of a five-stranded ß-sheet and two α-helices (**Figure 18B**; [276]). Here, absorption of a photon induces conformational changes that are accompanied by electron transfer from the protein moiety to the flavin in a radical-pair mechanism. Thereby, transient anionic and neutral flavin radicals are generated that are finally oxidized to form the long-lived signaling state [277].

Thus, heterologous expression of subunits of PAC ideally complements the optogenetics toolbox for the light-driven synthesis of cAMP to investigate related biological processes. This was already shown for *Drosophila* and *Aplysia*, where photoactivation of PACα increased cAMP levels to alter synaptic efficacy and as a consequence also behavior [278,279].

3. <u>Objectives</u>

Ideally, optogenetics allow the directed manipulation of neuronal activity by light and with high temporal precision. To tap the full potential of this technique, the aim of this work was to develop and to optimize optogenetics-based methods for the nematode *C. elegans* that facilitate the functional characterization of synaptic transmission and of neural networks, for example of those involved in generating behavior.

Due to its high abundance and the experimental accessibility, the neuromuscular junction is commonly used to investigate molecular mechanisms of chemical synaptic transmission in *C. elegans*. Here, the proteins NRA-2 and NRA-4 were recently co-purified with the levamisole-sensitive acetylcholine receptor from body wall muscle cells [184]. For their functional characterization, pharmacological and electrophysiological techniques were to be applied to analyze the role of both proteins for synaptic transmission. Furthermore, these experiments also aimed to unravel a potential interaction of NRA-2 and NRA-4 with Nodal signaling as demonstrated for the vertebrate homologues of both proteins [280,281].

However, characterization of synaptic transmission could be improved by more precise stimulation techniques. Potentially, this could be achieved using optogenetics for the selective photoactivation of GABAergic and cholinergic motorneurons to evoke the acute release of the respective neurotransmitter. To test this, ChR2 was to be expressed and photoactivated selectively in both types of motorneurons which could allow to analyze muscle cell excitation by electrophysiological recordings and behavioral assays. Applied to mutant animals, this approach could also be probed for the characterization of proteins with a role in synaptic transmission. For instance, this method was then to be used to unravel the mechanism of negative feedback mediated by the metabotropic GABA$_B$ receptor in cholinergic motorneurons. Therefore, peculiarities of contraction effects evoked by the photostimulation of cholinergic motorneurons were to be analyzed in dependence of the GABA$_B$ receptor.

Ideally, the non-invasive optogenetic stimulation could also be combined with high-pressure freeze electron microscopy to study presynaptic terminals of hyperstimulated neurons in intact *C. elegans*. This approach was to be applied for the investigation of dynamics of synaptic vesicle exo- and endocytosis as a function of

neuronal activity. Furthermore, these studies also aimed to analyze mechanisms of SV recycling and the functional role of synaptic proteins herein.

The optogenetic manipulation of neuronal activity is likewise expedient to dissect the functional role of individual neurons in a neural network. However, this approach requires the cell-specific application of optogenetic techniques and hence is often limited by the expression pattern of promoters used. Thus, methods that improve the specificity of optogenetic intervention would be desirable. To this end, a recombinase-based approach [282-284] was to be adapted for optogenetic proteins that limits transcription to the intersection of expression patterns of two different promoters. Likewise, an automated tracking system was to be developed that facilitates the real-time evaluation of positional data. Ideally, this information would allow targeting of light-stimuli to defined areas in the moving animal, thus restricting the photoactivation of light-responsive cells to this region.

Finally, application of optogenetic techniques was thus far restricted to the short-term manipulation of the membrane potential as extensive light requirements prevented the use for prolonged intervention. Concerning this, selective mutagenesis recently yielded ChR2 mutants with delayed closing of the open channel [261] that ideally allow to induce prolonged depolarizations in neurons under minimal light-invasive conditions. To evaluate the utility for *C. elegans*, these variants were to be expressed in different excitable cells in order to analyze their light demands and the aptitude to affect neuronal activity in the long-term.

Furthermore, the recently described *photoactivated adenylyl-cyclase* (PAC)α [274,275,278,279,285] was to be established as optogenetic tool that facilitates the light-induced synthesis of the second messenger cAMP in *C. elegans*. This approach would be especially of benefit for neurobiological research in the nematode as common pharmacological techniques to manipulate cAMP levels are inefficient in this organism [149].

4. Summary

In the following section, the results of publications implicated in this work are summarized. These publications are attached in print form to the appendix of this work and can also be found on the enclosed CD-ROM (including supplementary information).

4.1. Analyses of synaptic transmission at chemical synapses

4.1.1. Functional characterization of the L-AChR associated proteins NRA-2 and NRA-4

In a recent study, the proteins NRA-2 and NRA-4 – the *C. elegans* homologues of nicalin (nicastrin-like) and NOMO (nodal modulator) – were co-purified with the levamisole-sensitive acetylcholine receptor (L-AChR) [184], indicating a putative role in synaptic transmission at the neuromuscular junction. In vertebrates, however, nicalin and NOMO were described as inhibitors of Nodal signaling with impact on embryogenesis of the animals [280].

Thus, to investigate the function of NRA-2 and NRA-4 in *C. elegans*, pharmacological and electrophysiological techniques were applied for the analyses of animals with mutant alleles of either gene. The two mutant alleles of *nra-2* used here – *ok1731* and *tm1453* – delete large parts of the gene and also produce premature stop codons that truncate the protein C-terminal. In the *nra-4* allele *hd127*, 183 nucleotides of the promoter including a leader sequence and the entire first exon are deleted. Still, confirmed by RT-PCR, a transcript lacking the first exon is produced by the worms as the second exon starts with an ATG start codon. However, as *nra-4(hd127)* mutant animals displayed clear effects in experiments described hereafter, it is supposed that functionality of NRA-4 is impaired in these worms.

Initially it was found that mutants of NRA-2 and NRA-4 displayed resistance towards the ACh esterase inhibitor aldicarb (**supp. Figure 8** in publication I) but also towards the two cholinergic agonists levamisole and nicotine (**Figures 1C** and **1D** in publication I). This is in line with reduced post-synaptic currents evoked by both agonists as determined in whole cell patch clamp recordings from muscle cells (**Figure 4B** in publication I). However, responses to the GABA agonist muscimol

were not altered in mutant worms (**Figures 1E** and **4C** in publication I), confirming an exclusive impact of NRA-2/4 on the two nicotinic AChRs in *C. elegans* BWMs. With respect to this, effects of single mutants were not additive for NRA-2; NRA-4 double mutants, supporting a concerted mechanism of both proteins.

To assign NRA-2/4 mediated alterations of pharmacological properties to the respective nicotinic AChR, electrophysiological currents were then analyzed in muscle cells of animals that only expressed one of the two receptors. Here, mutant animals lacking the N-AChR displayed reduced whole-cell patch clamp currents evoked by levamisole in absence of NRA-2 (**Figure 4D** in publication I). This is in line with a decrease of open frequencies and open durations of the L-AChR as detected by single-channel recordings (**Figure 6** in publication I). Likewise, sustained optogenetic stimulation of cholinergic MNs revealed a rapid desensitization of this receptor towards acetylcholine, which is consistent with prolonged closed times and reduced open frequencies (**Figures 5** and **6** in publication I). Similar experiments in mutant animals lacking the L-AChR displayed a slight increase of sensitivity of the N-AChR towards acetylcholine in NRA-2 mutant animals, while effects of nicotine were largely unaffected by NRA-2/4 (**Figure 4D** in publication I).

For the visualization of the cellular and intracellular expression of NRA-2 and NRA-4, fluorescent reporter constructs were generated. Hence it was shown that both proteins were ubiquitously expressed in the nervous system and muscle cells of *C. elegans* (**supp. Figure 11** in publication I). Within the BWMs, both proteins localized to the ER where a direct interaction could be demonstrated, further indicating a conjoint function (**Figures 2C** and **2D** in publication I). Likewise, NRA-2 also co-localized with the L-AChR subunit UNC-29 in the ER but not at the plasma membrane (**Figure 3** in publication I), supporting a role of NRA-2/4 for the maturation of the receptors.

For a more detailed analysis, the surface expression of labeled L-AChR subunits was investigated in dependence of NRA-2/4. Here it was found that surface expression of the α-subunit UNC-38 was reduced in mutants of NRA-2 while simultaneously appearance of the α-subunit ACR-8 at the plasma membrane increased (**Figure 8** in publication I). In line with these findings, mutation of ACR-8 also suppressed reduced sensitivity of NRA-2 mutants towards cholinergic agonists (**Figure 7C** in publication I).

Taken together, these data support a role of NRA-2/4 in the ER of muscle cells for the regulation of subunit composition and hence pharmacological properties of both nicotinic AChRs at the cell surface. Conceivably, NRA-2/4 affect assembly of the receptors within the ER, e.g. by excluding or promoting the integration of distinct subunits. Alternatively, both proteins could also selectively bias ER exit or degradation of receptors with specific subunit compositions.

With respect to this, available mutants of known *C. elegans* TGFβ receptors and ligands did not phenocopy NRA-2/4 mediated effects, indicating that both proteins exert their function on AChRs independent of Nodal signaling (**suppl. Figure 10** in publication I). Still, while this work focussed on receptor maturation, a less prominent function of NRA-2/4 within Nodal signaling in other cells or during embryogenesis can not be clearly ruled out.

4.1.2. Optogenetic analysis of synaptic function in *C. elegans*

In *C. elegans*, pharmacological intervention and electrical stimulation are applied to stimulate synaptic transmission at the neuromuscular junction for the visualization of defects within this process. Still, the pharmacological approach is hampered by its poor spatial and temporal resolution that prevents a more detailed characterization of synaptic proteins, whereas the electrical stimulation only exhibits a restricted applicability in live animals.

To bypass these limitations, ChR2(H134R) was selectively expressed in either cholinergic or GABAergic motorneurons (MNs) to facilitate the precise stimulation of these cells in live animals by light. Basically, photostimulation of either type of motorneuron elicited the acute release of the respective neurotransmitter to evoke concomitant excitation (through ACh; animals containing the *zxIs6*-transgene) or inhibition (through GABA; animals containing the *zxIs3*-transgene) of muscle cells. On the behavioral level, this induced changes in the relative body length of the animals. Here, continuous stimulation of cholinergic MNs evoked persistent contractions of about 10 %. In contrast, ChR2 mediated release of GABA induced lengthening of circa 5 % (**Figure 1** and **suppl. Video 2** in publication II). However, due to the desensitization of the ionotropic GABA$_A$ receptor in muscle cells, relaxation effects decayed after a few seconds during sustained illumination.

In electrophysiological recordings, photostimulation of cholinergic and GABAergic MNs evoked peak currents in muscle cells of about 1300 pA and 800 pA, respectively (**Figure 2** in publication II). During a one second stimulus, these currents rapidly decayed to 6 % (for cholinergic MNs) and 9 % (for GABAergic MNs) of the initial amplitude due to desensitization of the post-synaptic receptors (also see **Figure 5** in publication I). This is in line with decreasing relaxation effects observed in behavioral assays for stimulation of GABAergic MNs. However, reduced currents during prolonged photo-release of ACh still seem to suffice to evoke full contraction amplitudes in the long-term. Potentially, this is achieved by temporal summation of depolarization in muscle cells. Thus, these data qualify ChR2 as light-driven tool for the acute and precise photostimulation of both types of motorneurons in live *C. elegans*. Notably, the performance of photostimulation outclasses electrical stimulation techniques which are not feasible for GABAergic MNs [287] and display reduced reliability for cholinergic MNs during repeated or prolonged stimulation.

To probe the utility of the optogenetic approach for the quantitative analysis of defective synaptic transmission, effects of photostimulation were analyzed in different mutant animals. Among those were e.g. mutants lacking synaptojanin (*unc-26(s1710)*; [130]) or synaptotagmin (*snt-1(md290)*; [111]). Synaptotagmin is a calcium sensor required for exocytosis of synaptic vesicles [111,288,289], but also recruits AP2 via its C2 domain to the plasma membrane of presynaptic terminals and thus is crucial for SV endocytosis [111,117]. Synaptojanin on the other hand is a polyphosphoinositide-phosphatase that interacts with several synaptic proteins, probably orchestrating SV recycling [130,132,290,291]. Photoactivation of cholinergic and GABAergic motorneurons in synaptotagmin- or synaptojanin-deficient animals elicited contractions and relaxations, respectively, that ceased relative to the wildtype control during sustained stimulation (**Figures 3D**, **4E**, and **4D** in publication II). In line with this, photoactivation of cholinergic and GABAergic MNs also evoked reduced peak currents in synaptotagmin mutant animals that further declined for consecutive light-pulses (**Figure 6** in publication II). However, synaptojanin deficient animals only displayed reduced post-synaptic currents for the photostimulation of cholinergic MNs while the electrophysiological measurements for photo-release of GABA were basically indistinguishable to wildtype (**Figure 6** in publication II). Conceivably, the brevity of light-pulses is not sufficient to accentuate defects induced by synaptojanin in GABAergic MNs.

Notably, in all presynaptic mutants tested, photostimulation of cholinergic motorneurons induced smaller post-synaptic currents than in wildtype (**Figures 4A** and **4B** in publication II) while contraction amplitudes were enhanced (**Figure 4C** in publication II). Here, contradictory behavioral effects could be assigned to compensatory mechanisms of the muscle cells in mutant animals (**supp. Figure 5** in publication II). Thus, while ChR2 provides useful means for stimulation of motorneurons, multiple analyses of resulting effects have to be considered for accurate characterization of synaptic transmission at the NMJ.

Taken together, it was demonstrated that photoactivation of ChR2 in cholinergic and GABAergic motorneurons of *C. elegans* facilitates the acute release of the respective neurotransmitter to elicit excitatory or inhibitory chemical synaptic transmission at the NMJ. Hereby, this approach provides means for the temporally precise and non-invasive stimulation of these cells in freely moving animals, making it superior over conventional pharmacological or electrical techniques, e.g. to allow the investigation of synaptic transmission.

4.1.3. Optogenetic analysis of GABA$_B$ receptor signaling in *C. elegans* motorneurons

In mammals, GABA$_B$ receptors couple to Gα_i and Gα_o signaling cascades to mediate negative feedback on both the pre- and postsynaptic sides (reviewed by [292]). More precisely, modification of ion channel properties induces an acute suppression of neuronal activity [293,294] whereas inhibition of cAMP synthesis modulates synaptic plasticity in the long-term [295-297]. *C. elegans* similarly expresses a GABA$_B$ receptor which is composed of GBB-1 and GBB-2, the homologues of the mammalian GABA$_B$ receptor subunits GABA$_{B1}$ and GABA$_{B2}$ [65,298]. In the worm, GBB-1 and GBB-2 form a putative heterodimeric complex (GBB-1/2) that inhibits cholinergic motorneurons in response to extrasynaptic GABA [65]. As GABAergic motorneurons are exclusively stimulated by cholinergic motorneurons (**Figure 9** in publication III), this is probably a mechanism of negative heterosynaptic feedback to regulate the activity of cholinergic motorneurons. Conceivably, GBB-1/2 may mediate their effects via signaling cascades to induce lasting depression of cholinergic MNs similar the role of the GABA$_B$ receptor in mammals. Alternatively, the receptor could also exert an immediate and temporary inhibition of cholinergic MNs in dependence

of extracellular GABA concentrations. To unravel the mechanism of feedback, optogenetic techniques were applied for the selective stimulation of motorneurons while resulting behavioral effects were analyzed in dependence of GBB-1/2.

To demonstrate a physiological role of GBB-1/2 for the stimulation of muscle cells at the NMJ, GABAergic MNs were photoactivated to evoke the acute release of the inhibitory neurotransmitter GABA. Here it was shown, that both the ionotropic $GABA_A$ receptor (encoded by UNC-49; [54]) as well as GBB-1/2 contributed to the resulting relaxation effects (**Figures 1** and **2** and **suppl. Videos 1** and **2** in). In this respect, selective expression of GBB-2 in cholinergic but not GABAergic motorneurons largely rescued GBB-1/2 mediated relaxations in GBB-2 mutant animals.

Furthermore, GBB-2 mutants also displayed higher crawling velocity and reduced body thrashing frequencies in liquid environment (**Figures 1C** and **4** in publication III). Again, specific rescue in cholinergic MNs restored body thrashing frequencies of mutant animals. In addition, a new analysis tool was developed that allowed the measurement of bending angles of moving worms. More precisely, custom scripts for ImageJ [299] and Gnu R [300] were written that facilitate the recognition of worm shapes in extracted frames of recorded videos and that determine the median of these shapes. The medians are then further divided into nine segments of equal length while angles are calculated between adjacent segments in a clockwise manner. Using this tool it was found, that GBB-2 mutant animals also displayed increased bending angles compared to wildtype during photoactivation of GABAergic motorneurons (**Figure 4D** in publication III). Taken together, these results are in line with previous reports [65], suggesting that GBB-1/2 mediate negative feedback selectively in cholinergic MNs and by this also affect diverse locomotory behaviors.

To directly assess the inhibitory effects of GBB-1/2, cholinergic MNs were photostimulated for 30 seconds while resulting contraction effects were analyzed in dependence of the metabotropic $GABA_B$ receptor. Conceivably, the accompanying excitation of GABAergic MNs through cholinergic synapses suffices to induce heterosynaptic GABA feedback in cholinergic MNs. For this, different light intensities were presented either continuously or in pulsed fashion with the aim to accentuate effects of GBB-1/2 (**Figures 5** and **6C** in publication III). However, only for pulsed stimulation protocols minor dynamic effects were observed in dependence of the $GABA_B$ receptor. More precisely, GBB-2 mutant animals displayed slightly stronger

contractions between 3 and 14 seconds of photostimulation using high light intensities and between 14 and 24 seconds for low intensities.

To further enhance GABA mediated feedback effects, cholinergic and GABAergic MNs were then photoactivated concomitantly (**Figure 8** in publication III). Applying various illumination protocols, a small dynamic decrease of contractions was observed for GBB-2 mutant animals relative to wildtype. Specifically, the mutants displayed stronger contractions in the initial six seconds of either continuous or pulsed stimulation with low intensity, while wildtype animals contracted stronger to the end of pulsed photostimulations.

Similarly, contractions were also analyzed in mutant animals lacking the GABA transporter SNF-11. Ideally, these mutants fail to remove GABA from the synaptic cleft [74], thus potentially also pronouncing negative feedback effects mediated by GBB-1/2. However, SNF-11 deficient worms displayed stronger contractions than wildtype during prolonged photostimulation of cholinergic MNs (**Figure 7** in publication III), supporting a role of SNF-11 in recycling of GABA rather than in clearance from the synapse, as suggested by Jiang and Colleagues [75]. Moreover, contractions in double mutants of GBB-2 and SNF-11 were further enhanced, however, not displaying a dynamic component.

In summary, these results demonstrate that negative feedback mediated by GBB-1/2 is of physiological relevance for distinct locomotory behaviors in *C. elegans*. With respect to this, GBB-1/2 induce the acute and direct inhibition of cholinergic MNs and thus possibly affect the balanced excitation and inhibition of muscle cells on the dorsal and ventral sides. However, marginal dynamics of GBB-1/2 mediated effects indicate that the metabotropic receptor only induces minor short- or long-term alterations of synaptic efficacy.

4.2. Analyses of neural circuits and the generation of behavior

4.2.1. Real-time multimodal optical control of neurons and muscles in freely behaving *C. elegans*

Ideally, optogenetic techniques allow the functional characterization of individual neurons to unravel the relation between neuronal activity and corresponding behaviors. This especially applies to small organisms like *C. elegans* that provide a

simple nervous system with well characterized anatomy and comparably small neural networks that regulate a limited repertoire of locomotory behaviors. However, this approach requires the cell-specific application of optogenetic techniques and hence is often restricted by the expression pattern of promoters used.

To address these limitations, a tracking system was developed that facilitates the real-time analysis of positional information of freely moving *C. elegans*. Therefore, animals on standard NGM agar plates were placed under an epifluorescent microscope and recorded by a digital camera coupled to this device (**Figure 1A** in publication IV[301]). Immediate computational analysis of the video data extracted the current position of the animal that was used to track the moving worm by controlling an x-y translational stage. Subsequent analysis of these data also yielded various locomotory parameters, e.g. velocity, trajectory, or bending along the longitudinal axis.

Furthermore, the positional information was also used to project defined illumination patterns onto animals by an integrated video projector. This projector was equipped with three distinct filters to facilitate simultaneous photoactivation of different optogenetic tools with fairly separated action spectra (**Figure 1B** in publication IV). Ideally, the targeted illumination allows selected photoactivation of cells expressing optogenetic tools within defined regions of the animal. This was demonstrated projecting various illumination patterns onto neuronally paralyzed worms expressing ChR2(H134R) in BWMs to induce different body postures of the animals (**Figure 1C** and **suppl. Video 2** in publication IV).

Gentle touches in *C. elegans* are detected by anterior (ALML/R and AVM) and posterior (PLML/R) sensory neurons (**Figure 4** and **Figure 1D** in publication IV) that induce an escape response of the animal in the direction opposite to where the stimulus was experienced [31,302]. For an optogenetic analysis of this system, ChR2(H134R) was expressed in all of these touch neurons as specific promoters for expression in either anterior or posterior neurons were not available. Initially, blue light was presented as a 20 μm wide bar migrating constantly from the tail to the nose of freely moving worms to investigate responses to local stimulation. In line with previous studies [31,302], animals displayed a slight acceleration in forward direction while the light bar was still in the posterior half of the animal. However, a reversal was induced as soon as the cell bodies of the anterior touch cells (which have only anterior extensions) were illuminated (**Figures 1E**, **1F**, and **2** and **suppl. Video 3** in

publication IV). Furthermore, the extent of behavioral responses also varied with the intensity of blue light, indicating that sophisticated illumination protocols allow mimicking mechanostimuli as perceived by the animal with precise localization and strength (**Figure 3** in publication IV).

With respect to this, photostimulation of anterior touch neurons required higher light intensities to induce backing responses when posterior touch neurons were activated concomitantly (**Figure 4** and **suppl. Videos 6** and **7** in publication IV). Conceivably, sensory information from both sets of touch neurons is integrated to evoke an adequate behavioral response. To test this hypothesis, anterior touch neurons were photostimulated by blue light illumination of the second quarter of the worm that harbors cell bodies of these cells. In addition, the proton pump MAC was expressed in command interneurons to allow inhibition of these cells through green light illumination targeted to the anterior-most quarter of the worm (**Figure 5A** in publication IV). Here, sustained photoactivation of the anterior touch cells evoked prolonged reversals that, however, were terminated with the onset of inhibition of command interneurons (**Figure 5** and **suppl. Video 8** in publication IV), indicating these cells are required to facilitate escape responses after stimulation of mechanosensory neurons.

Taken together, a tracking system was developed that facilitates the selective illumination of defined areas in moving worms and by this potentially improves cellular specificity of optogenetic intervention. In addition, various locomotory parameters can be extracted for an adequate analysis of phenotypes induced by the optogenetic manipulation of neuronal activity. Thus, this system ideally improves the application of optogenetic techniques for the functional characterization of neurons and neural networks, as exemplary demonstrated for the analysis of mechanosensation in *C. elegans*.

4.3. Implementation of additional optogenetic tools

4.3.1. Optogenetic long-term manipulation of behavior and development in *C. elegans*

The most commonly used ChR2 variant, ChR2(H134R), exhibits fast closing kinetics that allow the stimulation of excitable cells with millisecond precision [219]. However, elicitation of prolonged depolarizations with ChR2(H134R) requires accompanying

photoactivation with high intensities of blue light. Resulting phototoxic and – especially in *C. elegans* [41,42] – phototactic effects thus prevent the applicability for long-term stimulations. With respect to this, several mutations of the ChR2 residue Cys128 were recently described to decelerate channel closing in the range of seconds to several minutes [261]. Ideally, these mutants complement the optogenetics toolbox in *C. elegans* to allow elicitation of long-term depolarizations under minimal light-invasive conditions.

To test this, body wall muscle cells expressing either ChR2(C128A), (C128S), (C128T), or (H134R) were photoactivated for one second while the resulting contractions were analyzed (**Figures 1A** and **1B** in publication V). Here, all ChR2 variants basically evoked similar reductions in body length. However, in the case of ChR2(H134R) contractions instantly ceased after termination of illumination, while Cys128 mutants induced prolonged effects lasting from few seconds in case of ChR2(C128T) to more than five minutes for ChR2(C128S). Similarly, a one second photostimulus applied to ChR2(C128S) expressed in either GABAergic or cholinergic MNs evoked prolonged stimulation of these neurons as deduced from the resulting contraction and relaxation effects, respectively (**Figure 2** and **supp. Figure 3** in publication V). Moreover, as a consequence of the decelerated closing kinetics, temporal accumulation of the open channel also effectively rendered ChR2(C128S) more light sensitive than ChR2(H134R), requiring approximately 10-fold less light to evoke effects of comparable amplitude (**Figures 1D**, **2C**, **2D** and **supp. Figures 1B** and **1C** in publication V). In line with previous reports [235,261], it could further be shown that yellow light efficiently closed the channel of ChR2(C128S) prematurely, allowing the separate inactivation with a second color of light (**Figures 1E** and **2B** and **suppl. Videos 1** and **2** in publication V).

Next, ChR2(C128S) was expressed in command interneurons to probe its feasibility to induce prolonged depolarizations in neurons of *C. elegans*. Naturally, concerted excitation and mutual inhibition of forward and backward command interneurons forms a bi-stable switch that determines the direction of locomotion (**Figure 3A** in publication V, [212]). However, concomitant photostimulation of both types of command interneurons by ChR2(C128S) sustainably disturbed this balance and induced pronounced backward locomotion that could be reliably terminated by yellow light (**Figure 3B** and **suppl. Video 3** in publication V).

Ideally, repeated stimulation of ChR2(C128S) further facilitates the long-term depolarization over several hours. This was tested in muscle cells by application of different stimulation protocols (**Figure 1F** in publication V). Here, contractions were reduced to about 20 % of the initial value after 120 minutes – however – now remaining at a steady-state for more than 24 hours. Recent studies indicate that the Schiff base connecting the retinal to the apoenzyme hydrolyzes in P480 of C128 mutants and thus accounts for the increasing inactivation of the protein [239]. Albeit ceasing in the long-term, ChR2(C128S) mediated depolarizations conceivably also suffice to stimulate neurons for several days, e.g. to manipulate development of *C. elegans*. With respect to this, environmental stimuli determine if the nematode develops to adulthood or enters and arrests in the dauer state that is resistant to harsh conditions (**Figure 4A** in publication V; [5,6,303]). Here, ASJ sensory neurons are stimulated by favorable cues in a process involving activation of the soluble guanylyl cyclase DAF-11 and subsequent depolarization of the neurons through cGMP gated (CNG) ion channels [304,305]. Downstream signaling via insulin and TGFβ pathways then induces reproductive development to adulthood. In line with this, mutants of DAF-11 mostly arrest in the dauer-state. To bypass this dauer-constitutive (*daf-c*) phenotype, DAF-11 deficient animals expressing ChR2(C128S) selectively in ASJ sensory neurons were exposed to low intensities of blue light after hatching. After three days, only about 20 % of these worms arrested in the dauer state while approximately 80 % developed to adulthood. In contrast, only circa 20 % of DAF-11-mutant animals that did not express ChR2(C128S) in ASJ sensory neurons reached adulthood (**Figure 4B** in publication V). This indicates that ChR2(C128S) mediated long-term depolarization of ASJ substituted for the absent depolarization through CNG channels. Still, the rescue of dauer entry was not complete, indicating that development in *C. elegans* is regulated by additional neurons [306-308]. Furthermore, photoactivation of ASJ sensory neurons in dauer-arrested animals also triggered dauer exit of a large fraction of animals. Interestingly, this effect was temporally limited to the first 24 hour period (**Figure 4C** in publication V).

Taken together, ChR2(C128S) was established as an optogenetic tool for *C. elegans* that allows to induce long-term depolarizations in excitable cells under low light conditions. These properties make ChR2(C128S) highly applicable for the study of

biological processes that are based on the long-term activity of neurons, as was exemplary demonstrated for the development of *C. elegans*.

4.3.2. Light-driven synthesis of cAMP by PACα to manipulate neurotransmitter release and behavior in *C. elegans*

In response to environmental stimuli, neurons experience a dynamic adaptation of their morphology and function. In this process of neuronal plasticity, the $G\alpha_s$ signaling cascade plays a prominent role, e.g. for the mobilization of SVs from the reserve pool [156,162], regulation of protein transcription [157-160] and formation of new synaptic branches [309,310]. Thereby, $G\alpha_s$ exerts its effects mainly via synthesis of the second messenger cAMP (**Figure 18A**). For the investigation of underlying mechanisms, several techniques were developed that facilitate the manipulation of cAMP levels in neurons. However, as selective pharmacological intervention of cAMP synthesis and degradation is inefficient in *C. elegans* [149], research in the worm mostly relied on genetically modified animals with altered cAMP metabolism [147,149,162,311]. Still, genetic techniques lack both cellular and temporal specificity.

As a new approach, heterologous expression of the *photoactivated adenylyl cyclase* (PAC)α from *Euglena gracilis* was recently demonstrated to allow the acute synthesis of cAMP by light in neurons of *Drosophila* [278,285] and *Aplysia* [279]. To probe the utility of this protein as optogenetic tool in *C. elegans*, two lines with either high or low expression levels of PACα in cholinergic motorneurons were generated (**Figure 1** and **supp. Figure 1** in publication VI) while effects of photoactivation were analyzed in behavioral assays and by electrophysiology.

In liquid environment, photoactivation of PACα induced an increase of body thrashing frequencies for both lines (**Figure 2** and **suppl. Video 1** in publication VI). However, effects were more prominent for worms with high expression levels. Similarly, crawling velocities on solid medium increased by circa 40 % in response to blue light illumination (**Figure 3** in publication VI). This is also in line with enhanced velocities measured for *gain-of-function* mutants of the $G\alpha_s$ protein GSA-1 and the adenylyl cyclase ACY-1 [149], that congenitally exhibit elevated cAMP levels (**supp. Figure 2** in publication VI). Furthermore, photoactivation of PACα also suppressed long bouts

of backward movement (**Figure 5** in publication VI), indicating that enhanced cAMP levels in cholinergic neurons affect locomotory behaviors.

Conceivably, elevated cAMP concentrations enhance the synaptic efficacy of motorneurons to account for the observed behavioral effects. To test this hypothesis, miniature post-synaptic currents (mPSCs) in muscle cells were measured by electrophysiology. Here it was found that photoactivation of PACα increased the frequency of mPSCs while their amplitude was essentially unaffected, indicative of augmented synaptic transmission (**Figure 4** in publication VI).

Taken together, these results demonstrate the utility of PACα as optogenetic tool for the light-driven cAMP synthesis in *C. elegans* to allow investigation of cAMP mediated effects on neurons. Notably, some locomotory parameters as e.g. crawling velocity or body thrashing frequency were reduced in PACα expressing animals prior to photoactivation when compared to control animals (**Figures 2A** and **3A** in publication VI). As this depression was dependent on the expression level, dark activity of PACα potentially induces compensatory mechanisms to account for this. It thus seems to be critical to find suitable expression levels that balance between unwanted dark activity and sufficient cAMP synthesis during illumination.

5. <u>Discussion and outlook</u>

Nervous systems are complex organs that accomplish the cognition of environmental cues as well as the processing of this information and the subsequent elicitation of appropriate responses. With increasing complexity in higher eukaryotes, the diversity and the specificity of perceptive and executive functions of this organ are likewise enhanced. Thus, nervous systems regulate diverse processes starting from the precise stimulation of muscle cells to coordinate locomotion to the generation of complex behaviors that can be considered as characteristics of intelligence [312].

Unraveling the mechanisms underlying these functions of the nervous system is at the very heart of neurobiological research. For this, several techniques were developed that selectively interrupt distinct neuronal activities to allow the functional characterization of distinct proteins and neurons through analysis of the resulting effects. However, previous methods either lack spatial and temporal resolution or exhibit a limited applicability in live and freely moving animals. With respect to this, optogenetics were recently described as a promising new approach that facilitates the light-driven and bi-directional manipulation of the membrane potential in excitable cells with high temporal precision [219-221].

To tap the full potential of this technique for applications in the nematode *C. elegans*, several methods were developed in the work presented here that improve the cellular specificity of optogenetic intervention and that expand the spectrum of applications. Based on these advances, powerful tools for the functional characterization of synaptic transmission and for the investigation of neural networks in *C. elegans* were established.

5.1. <u>Functional characterization of chemical synaptic transmission using optogenetics</u>

5.1.1. Optogenetics-based electrophysiological and behavioral assays for the investigation of chemical synaptic transmission

Mechanisms of chemical synaptic transmission are highly conserved in all nervous systems from the nematode to mammals and utilized for both the propagation, but

also the modulation of information. For the analysis of the molecular mechanisms of this process by optogenetics-based approaches, ChR2(H134R) was selectively expressed in either cholinergic or GABAergic motorneurons of *C. elegans* [286]. Here it was shown that photoactivation triggered the acute release of the respective neurotransmitter with high temporal precision in live animals, resulting in excitatory or inhibitory chemical synaptic transmission at the neuromuscular junction, respectively. For the functional characterization of synaptic transmission, the optogenetic stimulation was combined with the analysis of behavioral effects and electrophysiological recordings of the post-synaptic currents. Compared to conventional pharmacological and electrical stimulation techniques, this optogenetics-based approach provides higher accuracy and – as a consequence – resulting effects more reliably report a role of synaptic proteins for transmission in mutant animals.

Thus, optogenetics ideally contribute to the identification novel proteins with a role in synaptic transmission. With respect to this, forward genetic screens are easily accomplished in *C. elegans*, using random mutagenesis for the generation of large libraries of mutant animals [17,18] or RNA-interference for the knock down of selected genes [24,25]. In earlier studies, these methods were already coupled to pharmacological and phenotypical analyses for the identification of proteins with a major impact on synaptic transmission [19,215,298,313]. However, to identify proteins with a less prominent role in this process, genetic techniques are ideally combined with optogenetic based methods that confer an enhanced sensitivity for the detection of impaired transmission. Concerning this, microfluidic devices were recently developed for *C. elegans* that facilitate the automated analysis of behavioral effects during optogenetic stimulation [314,315] and thus conceivably allow the high-throughput screen for so far unknown synaptic proteins. Finally, more elaborate optogenetic methods were established in this work that subsequently facilitate the precise functional characterization of candidate genes detected in these screens.

5.1.2. Optogenetics-based electron microscopy for the investigation of synaptic vesicle exo- and endocytosis

Moreover, it is conceivable to combine the accurate stimulation by optogenetics with additional methods for the analysis of different aspects of synaptic transmission. For

instance, electron microscopy (EM) is commonly used to study the morphological organization of synaptic vesicles in presynaptic terminals [130,133,316,317]. Here, this method ideally also allows investigation of the synaptic vesicle cycle in stimulated neurons. For this, EM is often combined with electrical or osmotic stimulation techniques, restricting the applicability to either cultured cells or dissected animals. Possibly, these limitations can be bypassed employing optogenetic techniques for the non-invasive stimulation of neurons in live animals.

This was tested in collaboration with M. Brauner, J. Liewald, and A. Gottschalk (Goethe-University, Frankfurt am Main) as well as J. Hegermann, M. Kittelmann, and S. Eimer from the European Neuroscience Institute (ENI, Göttingen). For this, cholinergic motorneurons in *C. elegans* were photostimulated using either ChR2(H134R) or ChR2(C128S) (performed by M. Brauner and C. Schultheis) while high-pressure freezing was applied afterwards for the conservation of animals and subsequent electron-microscopic analyses (performed by J. Hegermann and M. Kittelmann). For the investigation of dynamics of SV exo- and endocytosis in dependence of neuronal activity, the length of stimulation periods as well as the recovery time after hyperstimulation were varied. Furthermore, four distinct SV pools were defined with respect to vicinity to the plasma membrane and distance from the active zone while the number and distribution of synaptic vesicles herein was analyzed (**Figure 19**).

Following 30 seconds of hyperstimulation using ChR2(H134R), SVs from all pools were almost entirely depleted after 5 seconds recovery (**Figure 19B**) and replenishment was completed only after approximately 12 seconds recovery. Notably, pools at distant sites from the dense projections refilled first, indicating a lateral approach of SVs to the active zone (**Figure 19B**).

A

B

C

| 5 s recovery (no ATR) | 5 s recovery (plus ATR) | 10 s recovery (plus ATR) |
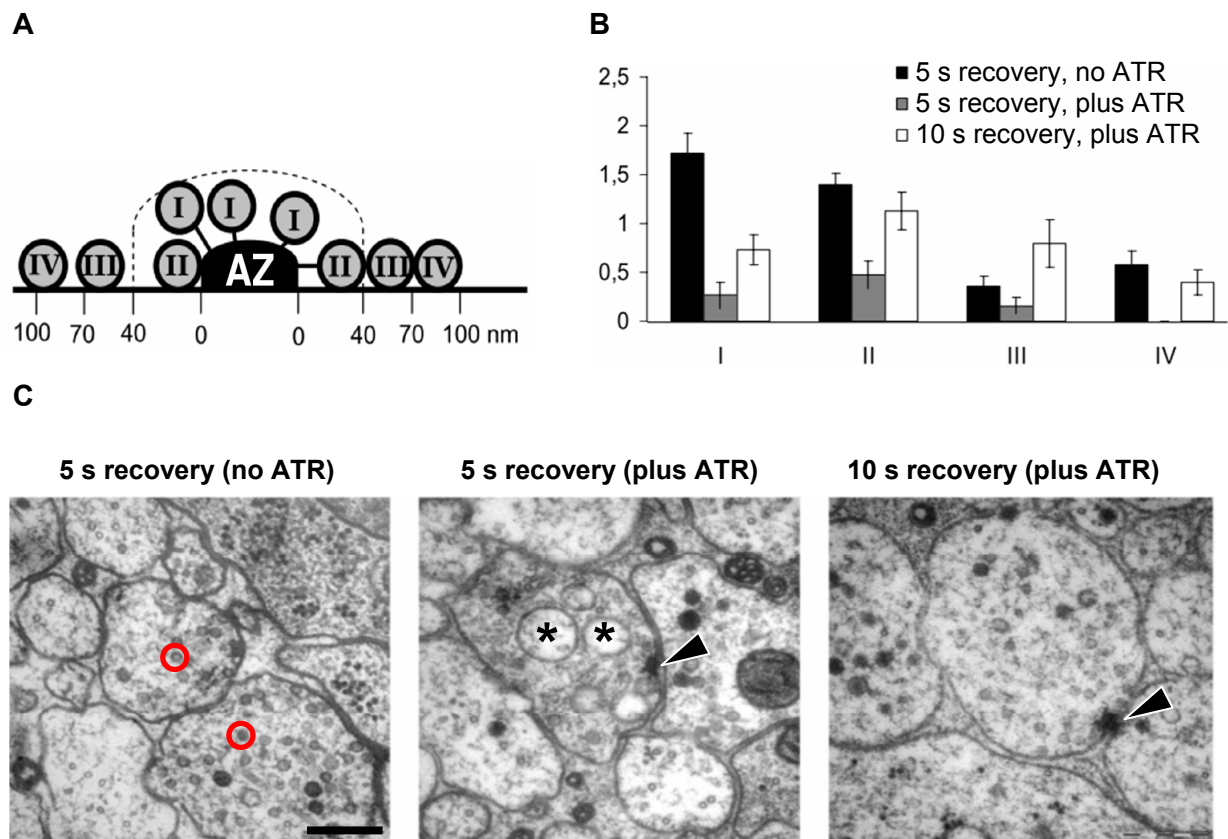
Figure 19: Recovery of SV pools after hyperstimulation
Animals expressing ChR2(H134R) in cholinergic neurons were raised in presence (plus ATR) or absence of retinal (no ATR) and photostimulated for 30 seconds (**A**) Definition of SV pools with respect to distance to the active zone (AZ) and spatial vicinity to the plasma membrane (**B**) Average number of SVs in the four defined pools after 5 or 10 seconds recovery; given are means ± s.e.m. (**C**) representative EM images after 5 or 10 seconds recovery; active zones are indicated by arrowheads, asterisks mark large vesicular structures, exemplary SVs are encircled in red; scale bar = 150 nm

To analyze the recovery of synaptic efficacy after hyperstimulation, post-synaptic peak currents in muscle cells evoked by photostimulation of motorneurons after dark periods of various lengths were measured (**Figure 20**; performed by J. Liewald). To correct these measurements for the desensitization of ChR2(H134R), values were calibrated for currents evoked directly by ChR2(H134R) in muscle cells. These data confirm results from EM studies, indicating that synapses physiologically regenerate within circa 20 seconds after hyperstimulation.

A

B
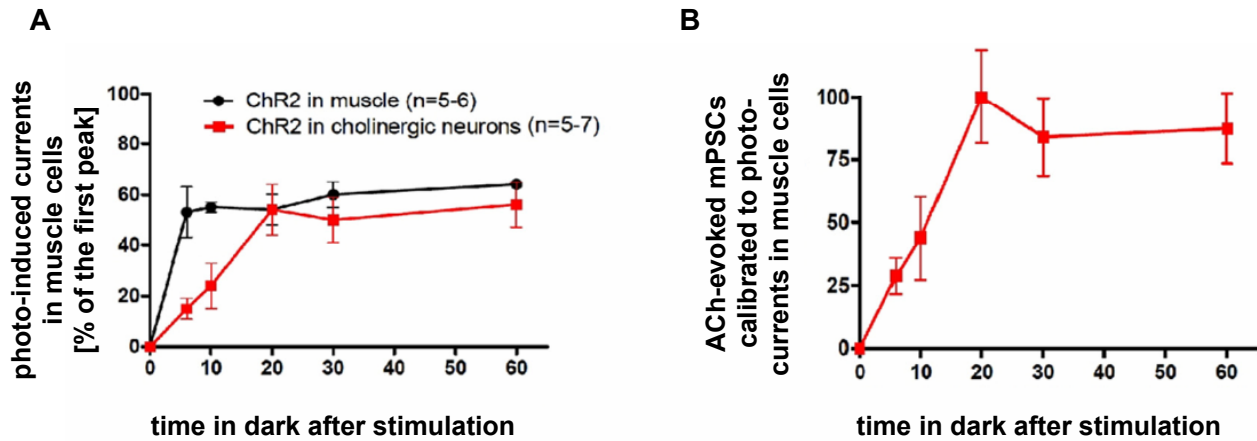
Figure 20: Recovery of photo-induced currents in muscle cells
(**A**) After 30 seconds hyperstimulation of muscle cells (black line) or cholinergic neurons (red) expressing ChR2(H134R), recovery of photo-evoked currents in muscle cells after distinct dark periods was analyzed (**B**) Currents in muscle cells (from **A**) evoked by photostimulation of cholinergic neurons calibrated to currents induced by photostimulation of muscle cells; displayed are means ± s.e.m.

Furthermore, large vesicular structures of up to 250 nm in diameter were observed (**Figures 19C and 21A**) that vanished between six and eight seconds after hyperstimulation (**Figure 21A**). Employing ChR2(C128S) for the continuous stimulation of cholinergic motorneurons during the obligatory 5 second sample preparation for HPF in absence of light, it was furthermore shown that these structures already appeared after 6 seconds of hyperstimulation. However, the amplitude of miniature post-synaptic currents (mPSCs) was effectively not altered during these periods, that means despite the presence of these structures, indicating that they presumably do not represent large neurotransmitter loaded compound vesicles (**Figure 21B**). On the other hand, these formations potentially resemble intermediates of *bulk phase* endocytosis that were similarly described to occur during hyperstimulation of neurons in other organisms [141,318,319].

In mutant animals lacking endophilin (*unc-57(e406)*) or synaptojanin (*unc-26(s1710)*), hyperstimulation of cholinergic motorneurons likewise produced large vesicular structures that – however – only disappeared approximately one minute after stimulation. This indicates a role of both proteins in clearance of the vesicular structures (**Figure 21A**). Conceivably, the mechanism of clathrin-dependent endocytosis of SVs from the plasma membrane may similarly apply to dissolve the

vesicular intermediates of *bulk phase* endocytosis, thus potentially also requiring the same set of proteins.
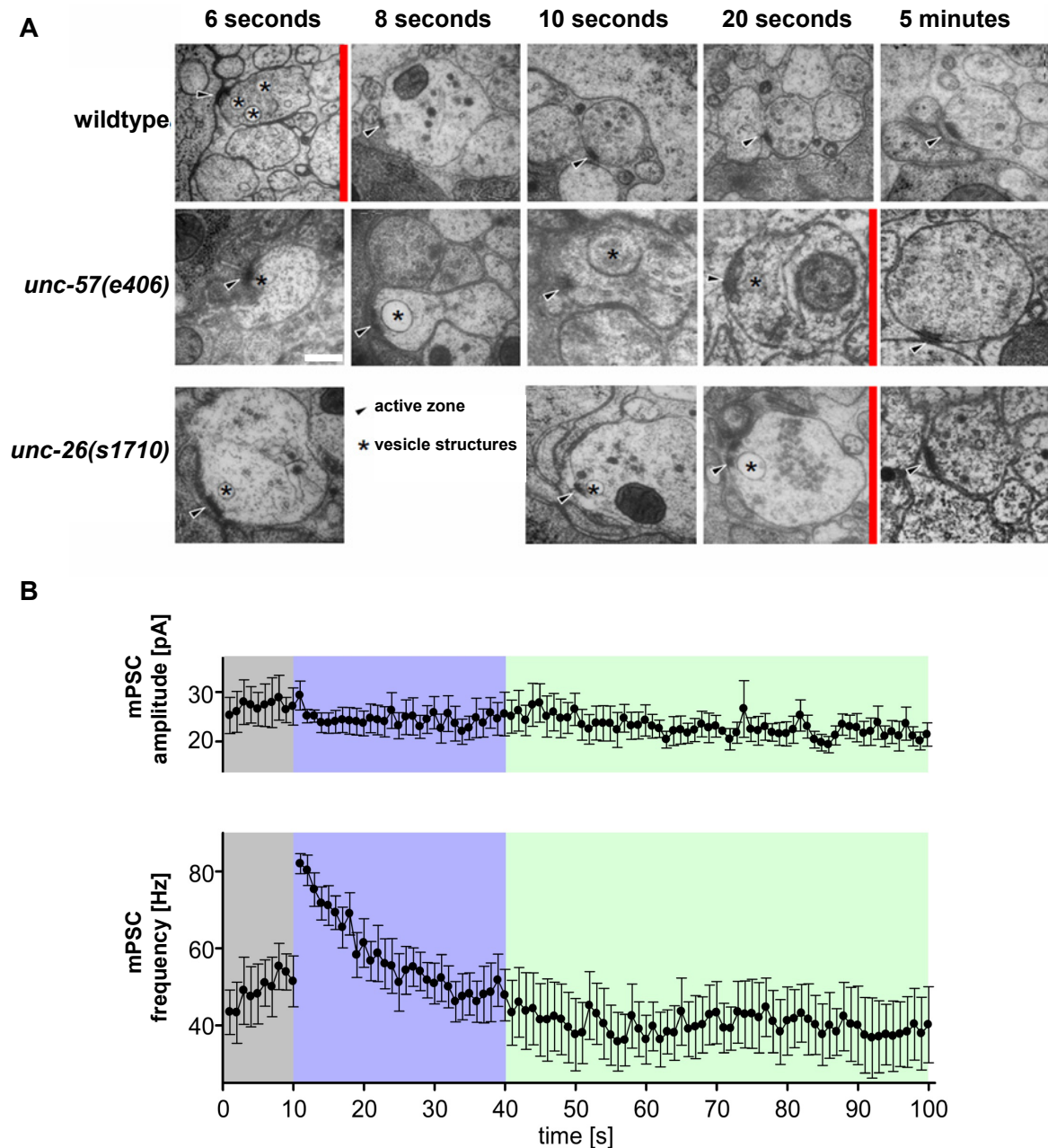
Figure 21: Clearance of large vesicular structures for different genotypes
(**A**) Wildtype, endophilin- (*unc-57(e406)*) and synaptojanin-deficient animals (*unc-26(s1710)*) expressing ChR2(H134R) in cholinergic neurons were photostimulated for 30 seconds while the vanishing of large vesicular structures (marked by stars) was analyzed after distinct recovery periods by HPF-EM; arrowheads indicate active zones; red bars indicate timepoint when large vesicular structures disappeared; scale bar = 150 nm (**B**) Analysis of the frequency and amplitude of miniature post-synaptic currents (mPSCs) in muscle cells before (shaded grey), during (blue), and after 30 seconds photostimulation of cholinergic neurons (light green)

Thus, the combined application of optogenetics and HPF-EM allowed for the first time the investigation of exo- and endocytosis of synaptic vesicles in intact animals as a function of neuronal activity in a temporally resolved manner. Furthermore, applied to mutant animals, the utility of this approach for the investigation of related molecular mechanisms was also demonstrated.

Thus, methods presented in this work will contribute in the future to complete the still enigmatic understanding of chemical synaptic transmission in *C. elegans*. As this process is highly conserved in most organisms, results obtained in the nematode will likely pave the way to similar findings in other animals as well. Finally, given the elementary role of chemical synaptic transmission for the propagation and integration of information, comprehension of this process is also a prerequisite to understand how diverse behaviors are generated by the nervous system.

5.2. Functional characterization of neural networks using optogenetics

5.2.1. Approaches to enhance cellular specificity of optogenetic intervention

Ideally, the directed manipulation of neuronal activity by light also allows the functional characterization of individual neurons in the nervous system. For this, effects of optogenetic intervention have to be analyzed, e.g. by studying the peculiarities of resulting behaviors or – more directly – by visualization of the activity of connected neurons.

5.2.1.1. Targeted photostimulation of optogenetic tools in freely moving animals

However, the accuracy of this approach can be limited by the promoters used that often do not allow an exclusive expression of optogenetic tools in the cells of interest. To facilitate the cell-specific intervention anyhow, a tracking system was developed that allows the targeted illumination of defined regions in freely moving animals, thus ideally limiting the photoactivation to distinct cells expressing the optogenetic tools [301]. The utility of this approach was demonstrated following up the integration of mechanosensory stimuli in the nervous system of *C. elegans*.

Still, the selective photostimulation of individual neurons using this approach is constrained by the spatial resolution of illumination (~14 µm) and by the temporal resolution which is limited by the image capture and processing rate to 40 ms (**suppl. Note 2** in publication IV). With respect to this, the movement of animals during updated projection patterns (up to 10 µm) has likewise to be considered. Thus, the area of illumination should be defined as wide as possible to ensure proper photoactivation of optogenetic tools. As a consequence, specific stimulation of selected neurons within a group requires the sufficient spatial separation of these cells. Complicating things, it has to be considered that neurites often expand the perceptive field of neurons for the optogenetic manipulation.

5.2.1.2. Enhancing cellular specificity of expression through genetic fragmentation of ChR2 and NpHR

Thus, optogenetic techniques would highly benefit from enhanced cellular specificity of expression. To achieve this, different approaches were probed that ideally limit functional expression of optogenetic tools to the intersected expression patterns of two different promoters (**Figure 22A**). During this work, following up on the preceding diploma thesis [320], ChR2(H134R) and NpHR were genetically fragmented to allow the separate expression of complementary N- and C-terminal halves using different promoters. Ideally, each fragment alone is inactive in terms of ion conductance and light sensation while complementary halves functionally reconstitute to render cells expressing both fragments sensitive to optogenetic intervention.

To identify suitable splitting sites with putative minor impact on functionality in reassembled proteins, primary structures of both rhodopsins were compared to those of close relatives from *Halobacterium salinarium* with resolved crystal structure – that was bacteriorhodopsin for ChR2 [321] and halorhodopsin for NpHR [322]. To monitor the assembly of co-expressed fragments, complementary halves of GFP [323] or CFP/YFP [324] were optionally attached to the sites of fragmentation (**Figures 22B and 23**). These split fluorophores regain light emitting properties after reconstitution and thus were used to visualize assembly of ChR2 and NpHR fragments where applied. Furthermore, the high affinity of GFP fragments for reconstitution ideally also served to enforce the assembly of attached rhodopsin halves [323]. Similarly, cCFP and nYFP were coupled to fragments of both rhodopsins using antiparallel strands of a leucine zipper to promote assembly [324-326]. Finally, signal sequences were

added to single fragments to avoid inverted membrane topology and to enhance surface expression at the plasma membrane (**Figure 23**; also see additional material and methods).
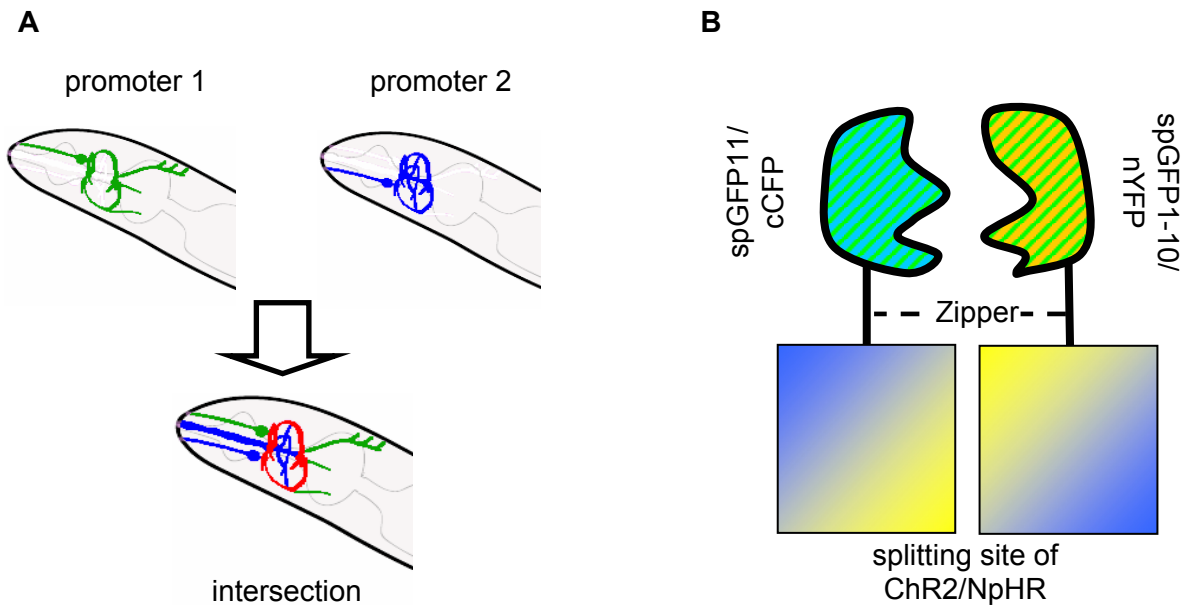
Figure 22: Enhanced cellular specificity for expression of optogenetic tools
A Schematic drawing explaining the improved cellular specificity when complementary fragments of either ChR2 or NpHR are expressed from distinct promoters (expression patterns depicted in green and blue, respectively) to result in conjoint expression and thus potentially functional reconstitution in the cellular intersection of both promoters only (indicated in red) **B** Scheme displaying the arrangement of split-fluorophores (either from the spGFP [325] or cCFP/nYFP system [326]) that were added to some fragmentation-sites of ChR2 or NpHR (protein residues depicted in blue/yellow); the fluorophore fragments cCFP and nYFP were couple to the rhodopsins via antiparallel leucine zippers [326-328]

To test this system, complementary fragments were expressed concomitantly in muscle cells while induced contraction and relaxation effects during photoactivation were analyzed (**Figure 23**). Here, compared to full-length constructs, behavioral effects were relative small or not detectable, indicating that for most splitting sites rhodopsins did not functionally reconstitute from complementary halves. Where applicable, assembly of split-fluorophores was also investigated. Essentially, fluorescence was rather weak and mostly localized to intracellular aggregates while only faint signals were detected at the plasma membrane. This is in line with behavioral assays, indicating that reconstitution of complementary fragments is rather inefficient, leading probably to misfolding and thus aggregation.

aa105/106: 0,0%; sigseq: 0,5%

aa110/111: 0,4% [322]; sigseq: 1,1% [322]

aa88/89: 0,2%

aa99/100: 0,4%; sigseq: 0,5%

aa99/100: 0,0%

N

extracellular

Channelrhodopsin-2

Halorhodopsin

intracellular

N

YFP C

eCFP C

aa74/75: 0,0%

aa142/143: n.d. [322]

aa206/207: 0,5% [322]

aa199/200: 0,3%

aa62/63: n.d.; sigseq: n.d.

aa144/144: 1,0% [322]; sigseq: 0,6% [322]

full-length ChR2: 11,3%

full-length NpHR: 4,6%
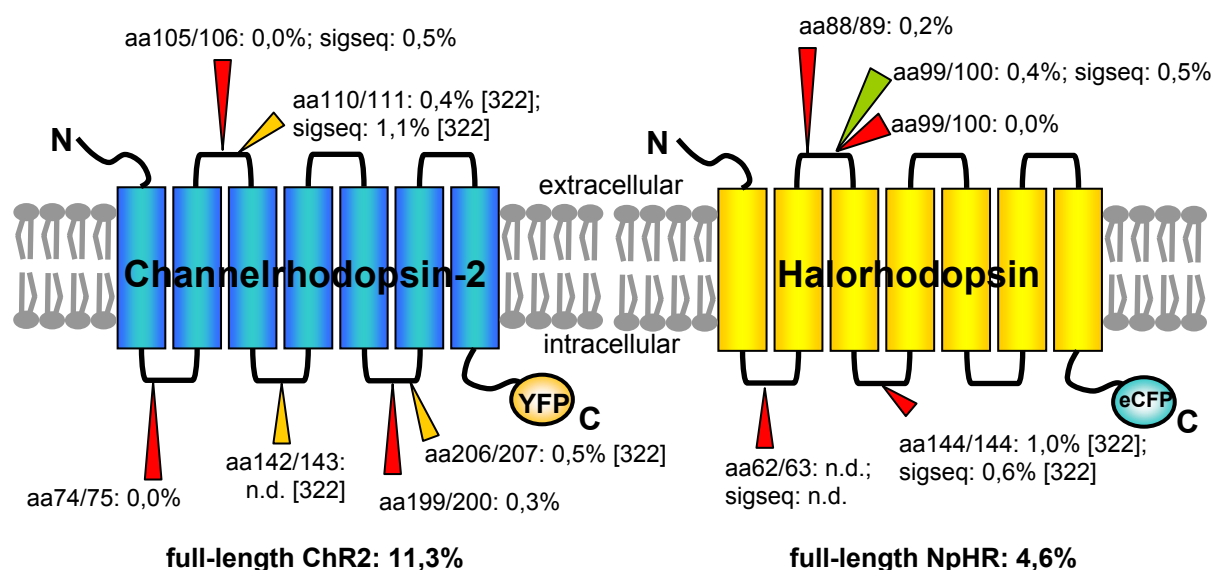
Figure 23: Splitting and reconstitution of ChR2 and NpHR
Schematic drawings of ChR2 (blue) and NpHR (yellow) depicting the heptahelical topology and sites of fragmentation as indicated by colored arrowheads; aminoacids flanking fragmentation sites are indicated together with resulting contraction (ChR2) or relaxation effects (NpHR) for co-expression and photostimulation of complementary fragments in muscle cells; optionally, either the spGFP (green arrowheads; [325]) or cCFP/nYFP system (yellow; [326]) were applied (for explanation see text and **Figure 22B**), when no split fluorophore was used (red) YFP and eCFP were added to the C-termini of ChR2 and NpHR, respectively; in some cases a putative signal sequence ("sigseq"; aa 1-27 of ChR2 or aa -19-0 of NpHR; also see additional material and methods) was added to the N- (ChR2) or C-terminal halves (NpHR) to ensure proper expression and membrane topology; notably, some constructs were already made and tested in the preceding diploma thesis [322]; n.d. = not determined; n≥9

5.2.1.3. Enhancing cellular specificity of expression employing recombinase-based methods

As to not give up the idea of employing intersecting promoter expression to achieve cell-specific photo-excitation or -inhibition, recombinase based approaches were probed for the expression of optogenetic tools as a whole [257,282-284]. In this system, the first promoter is genetically coupled to the respective rhodopsin via a so-called stop-cassette that includes transcriptional termination sites to prevent expression (**Figure 24**). However, the stop cassette is encompassed by particular recognition sites for either FLP or Cre recombinase that allow excision of this fragment and hence enable subsequent transcription of the rhodopsin. Using a second promoter for expression of the respective recombinase thus ideally also limits expression of optogenetic tools to the intersected cellular patterns of both promoters.
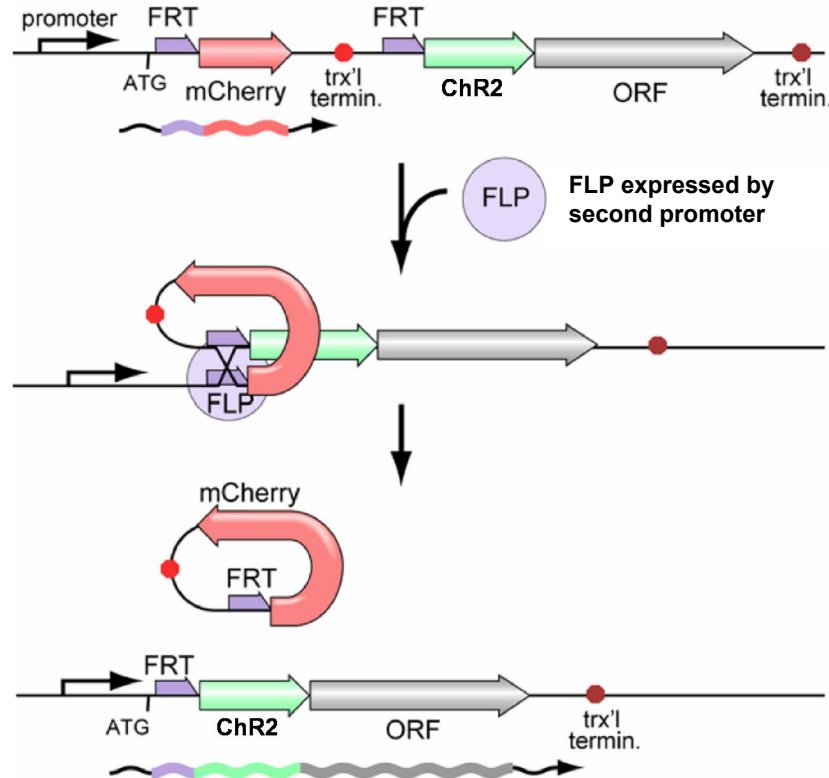
Figure 24: Cell specific expression of optogenetic tools employing recombinases
Scheme explaining cell specific expression of optogenetic tools using recombinase-based approaches, exemplary shown for ChR2 and the FLP recombinase (works analogously for Cre and other optogenetic tools); for detailed explanation see text; FLP = FLP recombinase, FRT = flippase recognition target; trx'l = transcriptional termination site; adapted from [284]

The utility of this system was tested for the cell-specific expression of ChR2(H134R), C-terminally tagged with YFP or mCherry, in AVA backward command interneurons of *C. elegans*. For this, two different promoter pairs were employed that only share AVA neurons in their expression patterns: *pgpa-14* [327] and *pglr-1* [328] as well as *prig-3* [329] and *pflp-18* [330,331]. Using FLP recombinase, the intensity of fluorescence in AVA neurons – and hence expression levels of ChR2 – varied for both promoter pairs as well as for the two respective possibilities to express FLP and ChR2. However, due to its low single channel conductance [236], high expression levels of ChR2 are required for optogenetic applications. Thus, to probe if the obtained concentrations of ChR2 allow to achieve sufficient depolarization of AVA to trigger behavioral responses, reactions of transgenic animals to blue light were analyzed. As shown in other parts of this work (see e.g. [301,332]), photoactivation of

AVA is expected to elicit backing responses in forward moving animals. With respect to this, only when *prig-3* was used for expression of FLP and *pflp-18* for expression of ChR2, a large fraction of animals displayed photo-induced reversals (~25%; **Figure 25**). Consistently, fluorescence in AVA neurons was also most intense in these animals.

Similarly, the efficiency of the Cre-based system was tested using *pgpa-14* for expression of this recombinase and *pglr-1* for expression of ChR2(H134R) (animals generated by C. Schmitt). Here, more than thirty percent of all animals reversed upon photoactivation with blue light (**Figure 25**), which is a significantly higher fraction than observed for the comparable line employing FLP recombinase. Likewise, intensity of fluorescence was also enhanced when Cre was used, indicating that this recombinase allows higher expression levels of ChR2 (C. Schmitt, personal communication).
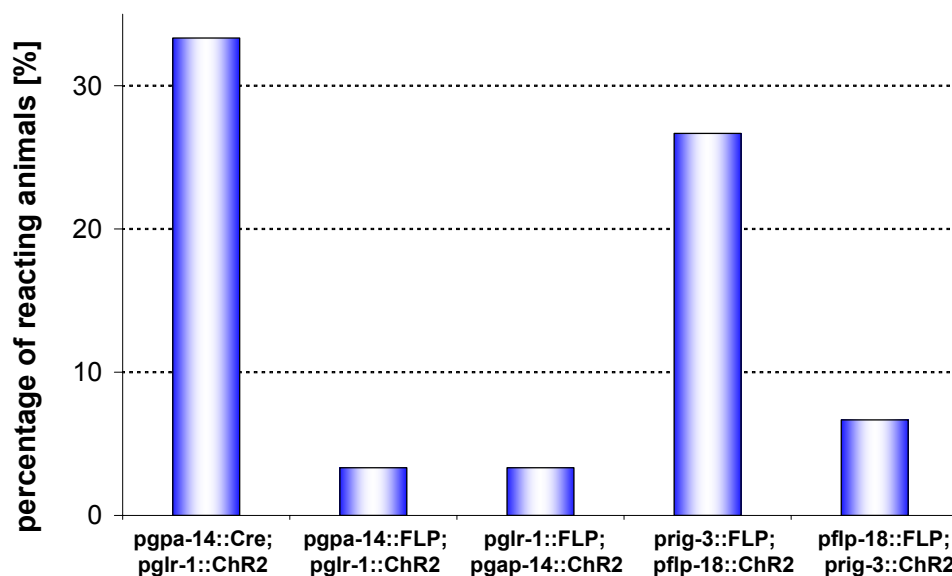
Figure 25: Selective expression and photoactivation of ChR2 in AVA
Different promoter combinations were probed for selective expression of ChR2 in AVA command interneurons using either FLP or Cre recombinase; given is the fraction of animals reversing upon blue light stimulation; n=30

Nevertheless, recombinase-based approaches – and here Cre in particular – were shown to improve cellular specificity of ChR2 expression in *C. elegans*. Still, for the maximization of expression levels the deliberate choice or promoters seems to be

crucial. Finally, this approach is likely adaptable to other optogenetic proteins and may also be combined with the targeted illumination system presented in this work [301] for further refinement of cellular specificity of optogenetic intervention.

5.2.2. Optogenetics-based approaches for the functional characterization of neural networks

In combination with adequate tools for the analysis of resulting effects, the cell-specific optogenetic manipulation of neuronal activity will be useful to study functional roles of neural networks and individual neurons herein. In favor of using such techniques, *C. elegans* possesses a comparably simple nervous system with known morphology [13-15] that regulates a limited repertoire of behaviors. Here, the relatively straightforward analysis of locomotion often suffices to study functional aspects of the nervous system. To this end, the tracking system presented in this work [301] allows the extraction of various locomotory parameters in combination with optogenetic intervention. However, other tools also facilitate the more direct analysis of neuronal activity as a consequence of optogenetic manipulation. Here, electrophysiological recordings allow the measurement of changes in the membrane potential in pharyngeal [203] and body wall muscle cells [55,286]. Still, the small size and the restricted accessibility of individual neurons limits the feasibility of electrophysiology for these cells [333]. Alternatively, genetically encoded calcium indicators (GECIs) that report calcium levels by means of fluorescence were successfully applied for the visualization of neuronal activity in *C. elegans* [209,334-337]. Furthermore, GECIs were recently also combined with optogenetics to analyze the flow of information in neural networks of freely-moving animals [210].

Finally, optogenetic techniques can also be combined with conventional genetic methods to study the function of neurons at a molecular level. For instance, mutant alleles are available for many genes or can be readily generated by standard techniques to analyze the role of individual proteins for neuronal integrity and function [17,18,21,22]. Likewise, cell-specific RNA-interference can be applied to knock-down gene expression locally [338], while heterologous expression of proteins conversely allows to enhance expression levels. Ideally, these approaches potentiate the power of optogenetic methods, for instance to identify neurotransmitters and the respective receptors used for synaptic transmission between neurons in networks.

5.3. Expansion of the optogenetics toolbox

5.3.1. Optogenetic tools for the depolarization of excitable cells

5.3.1.1. ChR2 variants for the long-term depolarization

Besides the simple hyper- and depolarization of neurons, the potential of optogenetics can conceivably be exploited for a more sophisticated manipulation of neuronal activity. With respect to this, the kinetics of ChR2 allow to induce depolarizations in neurons with millisecond precision, while the strength of this effect can be adjusted by means of the light intensity used for photoactivation. Thus, elaborate illumination protocols allow elicitation of diverse patterns of depolarization in neurons. As information in the nervous system is often encoded by the pattern of neuronal activity, optogenetics thus allow mimicking and hence investigating this code.

With respect to this, additional ChR2 variants were described recently that exhibit accelerated kinetics to induce action potentials with more than 200 Hz in neurons capable to elicit such high firing rates [257]. However, neurons in *C. elegans* most likely forward information in a graded fashion [77,78], thus omitting the need for fast ChR2 variants. On the other hand, some neurons enter lasting signaling states and hence display prolonged depolarizations, as e.g. photoreceptor cells in the mammalian eye in darkness [339,340]. Similarly, sensory neurons in *C. elegans* respond to environmental cues by tonic depolarization to impact on the development of the nematode. With respect to this, ChR2(C128S) was established as optogenetic tool that facilitates the prolonged depolarization of *C. elegans* neurons for several minutes under minimal light-invasive conditions. Still, long-term depolarizations for several hours evoked by repeated stimulations suffered from ongoing inactivation of the protein (**Figure 1F** in publication V). In further experiments, it was also shown that excitability of ChR2(C128S) largely ceased within 2-4 hours when retinal supplementation was abolished, indicating a sustained requirement of this cofactor (**Figure 26** and **supp. Figure 6** in publication V). This is particularly important for organisms that do not provide endogenous retinal such as *C. elegans* or *Drosophila*. For the worm, utility of ChR2(C128S) is hence restricted when the cofactor can not be supplemented by the food. This is the case for the non-feeding dauer animals and thus possibly explains the relatively brief time window of less than 24 hours allowing dauer-exit upon photostimulation of ASJ sensory neurons (**Figure 4C** in

publication V). Thus, these drawbacks limit applicability of ChR2(C128S) for long-term depolarization.

Interestingly, the widely used variant ChR2(H134R) maintained constant excitability over several days when retinal supplementation was abandoned, indicating a higher off-retinal stability than observed for ChR2(C128S) (**Figure 26** and **supp. Figure 6** in publication V). As earlier studies showed that properties of distinct ChR2 single mutants potentially add up in the respective double mutants [257,259], the utility of ChR2(C128S; H134R) for long-term depolarization with particular focus on off-retinal stability was analyzed. Remarkably, ChR2(C128S; H134R) exhibited an enhanced off-retinal stability similar to H134R single mutants (**Figure 26**), indicating that this attribute of H134R can be introduced into other ChR2 variants.
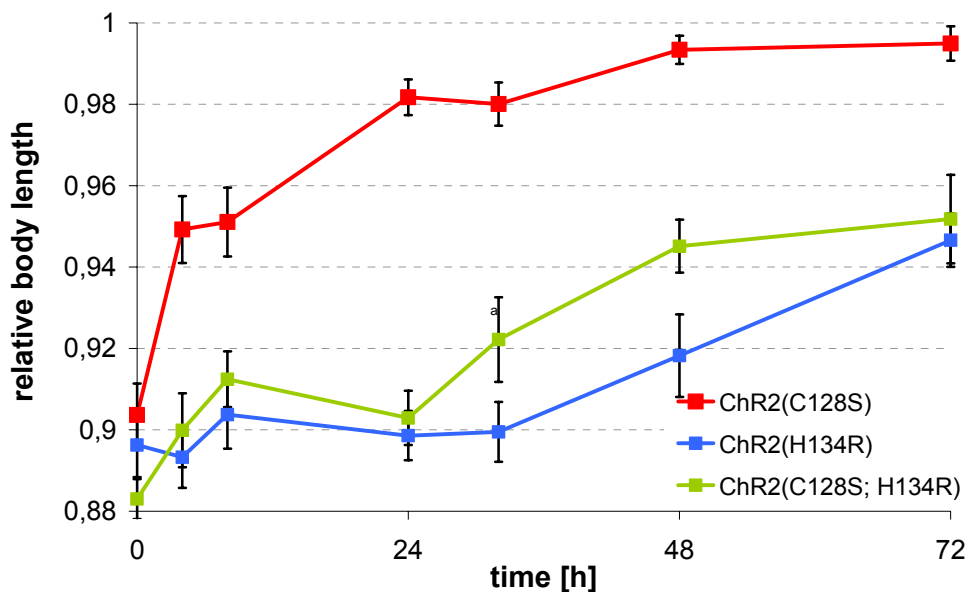
Figure 26: Off-retinal stability of different ChR2 variants
Animals expressing either ChR2(C128S), (H134R), or (C128S; H134R) in BWMs were cultivated on retinal supplemented plates. After transfer to retinal free plates contractions in response to blue light (1,4 mW/mm²) were measured at given timepoints as changes of the relative body length; n≥10, given are means ± s.e.m.

On the other hand, the double mutant also displayed essential features of C128S that are useful for the long-term depolarization of excitable cells. More precisely, ChR2(C128S; H134R) required about 10-fold less light than H134R to evoke full contraction amplitudes in muscle cells (**Figure 27**). The low light requirements help to

avoid phototoxic and – particularly in live *C. elegans* – phototactic side effects. Furthermore, contractions evoked by a single stimulus applied to ChR2(C128S; H134R) lasted even longer than for C128S, indicating that closing kinetics are further decelerated in the double mutant (**Figure 28**). With respect to this, closing of the channel in H134R single mutants is likewise decelerated for some few milliseconds compared to WT-ChR2 [238]. Conceivably, this effect also adds up in the double mutant to lengthen the duration of the open photointermediate. Finally it was also observed that repeated stimulation of ChR2(C128S; H134R) in muscle cells evoked higher contraction amplitudes than C128S, implying that this ChR2 variant recovers faster from the so-called lost states (**Figure 29**). Here, recent spectroscopic analysis suggests that the Schiff base connecting the retinal to the apoenzyme hydrolyzes in P480 of C128 mutants to induce formation of the lost states (**Figure 13** ;[239]). While this reaction is virtually absent in H134R [239], this mutant possibly prevents the temporary dissociation of the cofactor. Conceivably, this also accounts for the enhanced off-retinal stability observed for the double mutant.
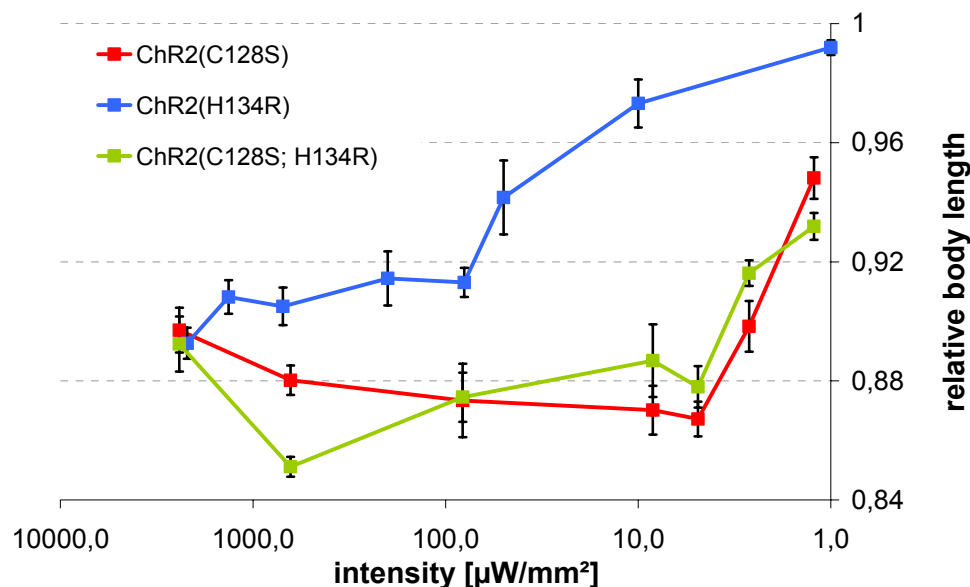
Figure 27: Effective light-sensitivity of different ChR2 variants
Animals expressing either ChR2(C128S), (H134R), or (C128S; H134R) in BWMs were photoactivated with light-intensities from 0,001 to 2,4 mW/mm² while resulting contractions were measured as changes of the relative body length; n≥10, given are means ± s.e.m.
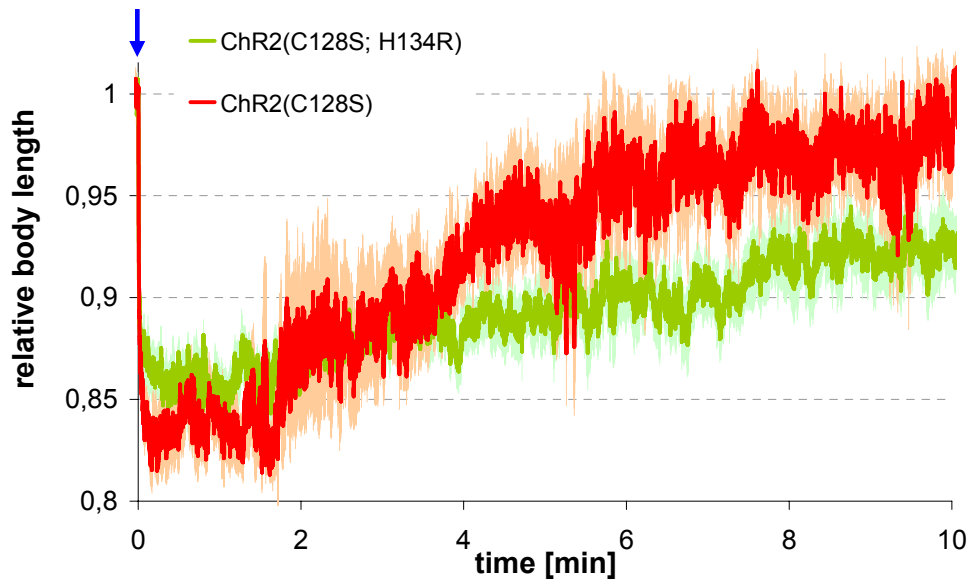
Figure 28: Long-term depolarization of muscle cells
A two second blue light stimulus (0,2 mW/mm²; indicated by the blue arrow) was presented at t=0 to animals expressing either ChR2(C128S) or (C128S; H134R) in BWMs while the relative body length was monitored for 10 minutes; n≥11, given are means ± s.e.m.
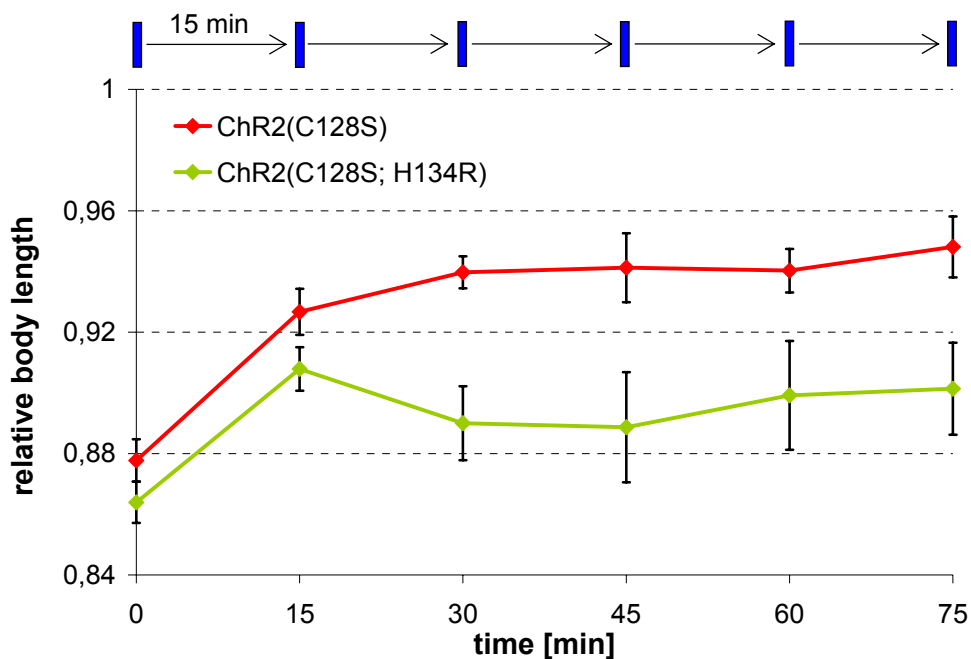
Figure 29: Repeated stimulation of ChR2 variants in muscle cells
Two second blue light stimuli (0,2 mW/mm²; indicated by the blue ticks) were presented every 15 minutes for six times to animals expressing either ChR2(C128S) or (C128S; H134R) in BWMs while the amplitudes of resulting contractions were monitored as changes of the relative body length; n=10, given are means ± s.e.m.

Thus, ChR2(C128S; H134R) combines favorable attributes from both C128S and H134R single mutants, making this variant an even more potent tool for long-term depolarization of excitable cells than ChR2(C128S).

However, while yellow light efficiently closed the channel of ChR2(C128S), inactivation was incomplete for ChR2(C128S; H134R) (**Figure 30**). Possibly, the action spectrum of the double mutant is either broadened or shifted to bathochromic wavelengths so that inactivation by yellow light likewise facilitates the opposite re-activation of ChR2(C128S; H134R). This is supported by contractions that could be evoked by yellow light without preceding photoactivation by blue (**Figure 31**). While this limits temporal control of ChR2(C128S; H134R) mediated depolarizations it also allows the long-term stimulation of neurons with red-shifted wavelength.
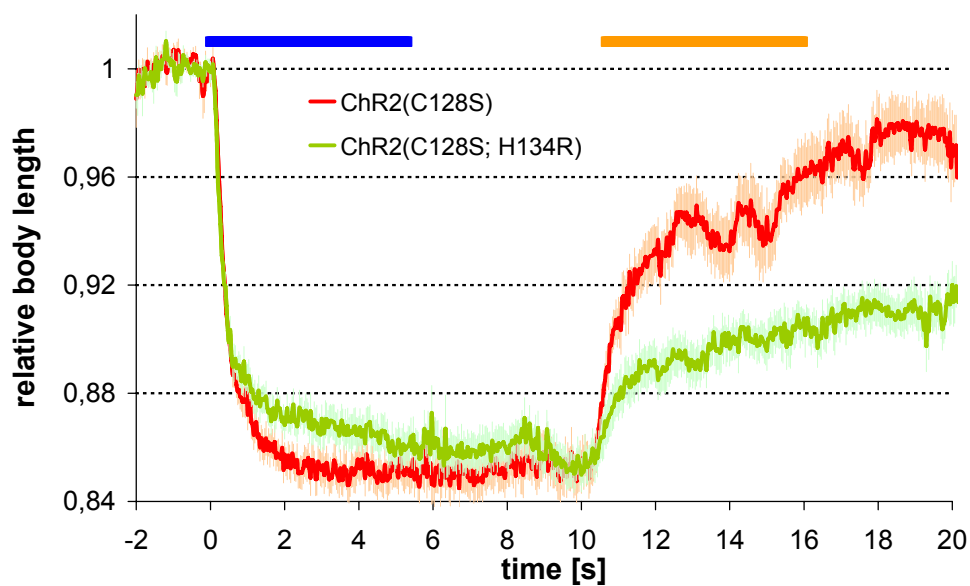
Figure 30: Photoinactivation of ChR2 variants by yellow light
To test photoinactivation by yellow light, ChR2(C128S) or (C128S; H134R) were expressed in BWMs and the relative body length was recorded while a five second blue light stimulus (0,2 mW/mm²) was given at t=0, followed by a five second yellow light stimulus (6,9 mW/mm²) at t=10 as indicated by the bars of the respective color; n≥19, given are means ± s.e.m.
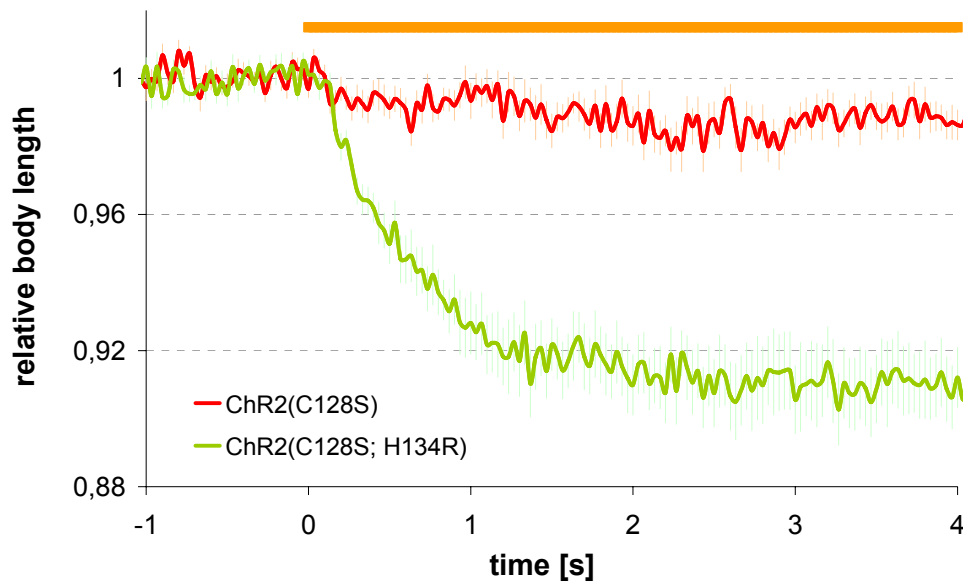
Figure 31: Photoactivation of ChR2 variants by yellow light
Yellow light (6,9 mW/mm²) was presented as indicated by the bar to animals expressing either ChR2(C128S) or (C128S; H134R) in BWMs while the relative body length was recorded; n≥15, given are means ± s.e.m.

The utility of optogenetic tools for the long-term depolarization was demonstrated in this work for the study of synaptic vesicle exocytosis in hyperstimulated motorneurons of *C. elegans* in combination with electron microscopy. Furthermore, prolonged stimulation of either sensory or command interneurons also allowed manipulation of the development or the locomotion of animals in the long-term.

In the future, these optogenetic tools will be useful to study neurobiological processes that either induce or rely on repeated and prolonged excitation of neurons. For instance, sustained stimulation was shown to impact on neuronal functionality, e.g. by affecting synaptic efficacy and organization of synaptic connections to adjacent neurons [65,309,310,341-343]. This neuronal plasticity allows adaptation of the nervous system to environmental stimuli, which is important for processes like learning or memory formation [344,345]. With respect to this, many forms of neuronal plasticity are similarly found in *C. elegans*, though often in a simplified form. For example, the prolonged or repeated experience of chemical or mechanical stimuli can induce adaptation of responses [341,342,346-350], making the nematode a model to study behavioral plasticity [344,351,352].

5.3.1.2. Prospective ChR2 variants for optogenetic applications

In the future, additional optogenetic tools will be introduced that also expand the spectrum for optogenetic manipulation of neuronal activity. For instance, screens in various microbial organisms already identified other rhodopsins that exhibit altered action spectral properties [238,264,266-269,271]. Furthermore, existing proteins can be modified to enhance their utility for optogenetic applications. Here, codon optimization [254,255] and addition of motifs that promote the transport to the plasma membrane [255,256] were applied to improve cell surface expression of ChR2 and NpHR, while molecular engineering yielded various ChR2 mutants with diverse functional properties [219,235,238,257,259,260,269]. With respect to this, a projection map of ChR2 at 6 Å resolution was recently published [353], potentially allowing to assign functional properties to individual amino acids, thus simplifying the mutagenesis for the directed manipulation of functional characteristics in the future. Furthermore, this work also demonstrated that functional properties of distinct ChR2 mutants can potentially be combined in double or triple mutants. With respect to the long-term depolarization, the utility of ChR2(C128S; H134R) could possibly be further improved through introduction of mutants that enhance the surface expression or the channel conductance for specific ions [259,260]. Likewise, another mutant was recently described in which channel closing is decelerated (D156A; [235]). In combination with C128S, the endurance of the open intermediate could be further enhanced in the resulting double mutant. This ChR2 variant was already used to induce prolonged depolarizations in mammalian neurons [269].

5.3.2. Optogenetic tools for the synthesis of second messengers

5.3.2.1. Light-driven synthesis of cAMP using PACα

While neuronal activity is the trigger, intracellular signaling cascades finally implement plastic changes. Here, the $G\alpha_s$ pathway plays a prominent role through synthesis of the second messenger cAMP. Thus it was shown for different organisms that cAMP induces mobilization of synaptic vesicles [156,162], alters expression of numerous proteins [157-160,163,164], and also re-organizes terminal varicosities in dependence of neuronal activity [309,310]. Yet, molecular mechanisms of these

processes are not completely understood. With respect to this, the *photoactivated adenylyl cyclase* (PAC)α from *Euglena gracilis* was established in this work as optogenetic tool for the light-controlled synthesis of cAMP in *C. elegans*. Hence it was also demonstrated, that photo-induced cAMP production in motorneurons of the nematode enhanced synaptic activity and by this also affected locomotory behaviors of the animals. Prospectively, PACα and ChR2 variants for the long-term depolarization of neurons will be useful to study neurobiological processes induced by elevated cAMP levels or prolonged neuronal stimulation in the nervous system of *C. elegans*. With respect to this, methods developed in this work can be applied to enhance cellular specificity for optogenetic intervention and to facilitate the versatile analysis of resulting effects.

5.3.2.2. Prospective optogenetic tools for the light-driven synthesis of second messengers

For the light-driven synthesis of cAMP, additional *photoactivated adenylyl cyclases* were discovered in other organisms. While AlPAC from *A. longa* is not fully characterized yet [275], PAC from *Beggiatoa spec* (bPAC) was probed recently for optogenetic applications [354,355]. In contrast to PACα from *Euglena*, bPAC exhibits reduced dark activity and hence allows a higher dynamic range of cAMP synthesis by light. However, on- and off-kinetics in bPAC are comparably slow, favoring *Euglena* PAC for temporally precise control of cAMP production whereas bPAC is preferred to induce lasting increases of cAMP levels with relative low light intensities. Furthermore, site directed mutagenesis within the active site of bPAC generated a variant (bPGC) with shifted substrate specificity for the synthesis of cGMP [354]. cGMP is an important second messenger, e.g. involved in signal transduction in mammals through cGMP driven ion channels [356] and relaxation of smooth muscle cells [357,358]. In *C. elegans*, several sensory neurons similarly express cGMP-gated ion channels (mostly TAX-2/4; [303,305]) and sensory guanylyl cyclases [359,360] that induce depolarizations in neurons upon sensation of environmental stimuli. Thus, bPGC potentially constitutes a powerful optogenetic tool to study intracellular events induced by cGMP.

Finally, optogenetic tools are not localized to distinct compartments of the cells and thus exert their effects without intracellular specificity. However, the physiological activity of cAMP and cGMP within the cells is spatially regulated by means of local

synthesis and degradation but also by recruitment of proteins like PKA to specific regions [361-363]. Thus, further engineering of optogenetic proteins should aim at their subcellular or intracellular targeting. This might possibly be done by the coupling to endogenous sorting sequences or binding motifs. Thereby, light-induced effects could be limited to distinct and relevant regions of the cell, hence also reducing required expression levels.

Thus, the introduction of new optogenetic tools and the modification of existing ones will help to expand the optogenetic line-up for the manipulation of the membrane potential and second messenger concentrations, adapted to individual purposes. Ideally, these tools combine with conventional techniques for the genetic manipulation of *C. elegans* and sophisticated approaches for the analysis of effects from optogenetic intervention to constitute powerful methods for neurobiological research.

5.4. Future applications of optogenetics

5.4.1. Optogenetic applications in *C. elegans*

The heterologous expression of photoactivated proteins for the manipulation of neuronal processes by light bears great potential for neurobiological research. With respect to this, most light-driven proteins used by optogenetics operate in the millisecond time-range, thus conferring temporally precise control over intervention, while small and transparent organisms like the nematode *C. elegans* ideally also allow the non-invasive application in live and freely moving animals.

To improve applicability of optogenetics in the nematode, several approaches were developed in this work that enhance the cellular specificity of optogenetic intervention and that expand the spectrum of possible applications for the long-term depolarization and the synthesis of the second messenger cAMP. Making use of these improvements, optogenetic techniques could further be combined with other methods like for instance electron microscopy, electrophysiology, and behavioral assays to constitute powerful approaches for the functional characterization of synaptic transmission and the functional dissection of neural networks in *C. elegans*. Furthermore, these techniques ideally also allow the investigation of mechanisms of synaptic plasticity or simple forms of learning and memory formation that are found in the nematode. For the study of these basic neurobiological processes, *C. elegans* is

a favorable model organism as it possesses a rather simple nervous system with a well-characterized morphology. Furthermore, many functions of the nervous systems are conserved from the worm to mammals, allowing in numerous cases the transfer of information to other organisms.

5.4.2. Optogenetic applications in other organisms

Developed for *C. elegans*, it is conceivable that advances made to optogenetic approaches in this work are likely adaptable to other organisms, too. Here, the fruitfly *Drosophila melanogaster* and the zebrafish *Danio rerio* are other common model organisms in neurobiology in which optogenetic techniques were already applied for the investigation of basic neurobiological processes like synaptic transmission [364], ordinary forms of learning and habituation [365-367] and mechanisms for the integration of sensory stimuli [368-370].

Conceivably, ChR2(C128S; H134R) and PACα can also be used in the fruitfly and zebrafish to study effects of prolonged depolarization or enhanced cAMP levels in neurons. Here, this could be useful for the investigation of mechanisms of synaptic plasticity or to study the SV cycle in combination with high-pressure freeze electron microscopy. While PACα was already established as optogenetic tool in *Drosophila* [278,285], ChR2 variants for the long-term depolarization of neurons were not yet implemented in the fruitfly or zebrafish. However, ChR2(C128S; H134R) could improve several aspects of optogenetic stimulation in both organisms. On the one hand, this ChR2 variant allows the optogenetic depolarization of neurons under minimal light-invasive conditions to reduce phototactic responses in *Drosophila* [223] and zebrafish [365,371,372]. Furthermore, compared to other ChR2 variants for the prolonged depolarization, the enhanced off-retinal stability of ChR2(C128S; H134R) is potentially useful for experimental approaches in *Drosophila* which requires the exogenous supplementation of this cofactor [223].

Likewise, optogenetics are nowadays also widely applied in mammals like mouse and rat and even in primates like the macaque [220,221,253,373-375]. With respect to this, sophisticated techniques were established to optimize transfection of these organisms (for review see [376]) and to allow the photoactivation of optogenetic tools in live and freely-moving animals [253,377-381]. Given the high developmental degree of nervous systems in these organisms, optogenetics were applied here to

study complex behaviors like e.g. breathing [382], awakening [383], anxiety [380], or conditioned fear [384,385]. Furthermore, optogenetics were also implicated in various disease models as for example Parkinson's disease, retinal degeneration, cocaine conditioning, and depressions [379,380,386-389].

However, to fully understand these complex functions of nervous systems – and to allow adequate therapeutic treatment in case of defects – likewise requires knowledge of molecular mechanisms of basic neurobiological processes as e.g. synaptic transmission. Here, small model organisms like *C. elegans* are best-suited for the investigation of these conserved processes. Thus, findings from the nematode ideally complement functional relations discovered in mammals. Taken together, optogenetics constitute powerful tools for the functional characterization of diverse neurobiological processes in various organisms. In the future, these techniques will largely contribute to complete the still enigmatic understanding of the functionality of nervous systems.

6. <u>Zusammenfassung</u>

In Nervensystemen werden zahlreiche Informationen wahrgenommen und verarbeitet um ein adäquates Verhalten hervorzurufen. Für die Untersuchung der funktionellen Zusammenhänge hierbei wurden verschiedene Methoden entwickelt, die eine gezielte Manipulation neuronaler Prozesse ermöglichen. Durch Analyse der resultierenden Effekte können dabei synaptische Proteine, einzelne Neuronen oder neuronale Netzwerke funktionell charakterisiert werden. Bisherige Ansätze verfügen jedoch nur über eine geringe zeitliche und räumliche Auflösung oder erlauben lediglich eine eingeschränkte Anwendung im frei beweglichen Tier.

Diese Nachteile können durch die heterologe Expression von lichtgesteuerten, mikrobiellen Rhodopsinen zur gezielten Manipulation des Membranpotentials umgangen werden. So induziert die Photoaktivierung des Kationenkanals Channelrhodopsin-2 (ChR2; [219]) eine Depolarisation, während die Chloridpumpe Halorhodopsin (NpHR; [221]) für die Hyperpolarisation verwendet werden kann. Dabei ermöglichen die schnellen Kinetiken der Rhodopsine eine zeitlich präzise Steuerung des Membranpotentials. Durch Auswahl geeigneter Promotoren ist zudem oftmals eine zell-spezifische Expression möglich. Dieser Ansatz wird daher allgemein als Optogenetik bezeichnet.

In der vorliegenden Arbeit wurden zunächst konventionelle Techniken genutzt, um die Funktion von zwei assoziierten Proteinen eines Acetylcholin-Rezeptors in *C. elegans* zu untersuchen. Des Weiteren wurden verschiedene Methoden für den Fadenwurm entwickelt und angewendet, die die Vorteile optogenetischer Techniken für die funktionelle Charakterisierung synaptischer Proteine und neuronaler Netzwerke nutzbar machen. Hierbei erlaubt die Transparenz von *C. elegans* die optogenetische Stimulation im lebenden Organismus unter nicht-invasiven Bedingungen. Weitere Vorteile von *C. elegans* als neurobiologischem Modellorganismus liegen in seiner einfachen Handhabung [3] und der stereotypen Entwicklung seines Nervensystems mit bekannten anatomischen Ausprägungen [12,13,15]. Durch ihre Häufigkeit und die experimentelle Zugänglichkeit wird hierbei die neuromuskuläre Synapse oftmals zur Erforschung der synaptischen Reizweiterleitung genutzt [48]. Durch pharmakologische [54,55,215,216] und elektrische Stimulation [55] können dabei Defekte der Transmission hervorgehoben

werden, während Verhaltensexperimente oder elektrophysiologische Messungen der post-synaptischen Ströme in Muskelzellen eine quantitative Analyse ermöglichen [55].

Diese Methoden wurden für die funktionelle Charakterisierung von NRA-2 und NRA-4 verwendet, die beide als akzessorische Proteine zusammen mit dem Levamisol-sensitiven Acetylcholin-Rezeptor der Körperwandmuskelzellen aufgereinigt wurden [184]. Dabei konnte gezeigt werden, dass NRA-2 und NRA-4 im Endoplasmatischen Retikulum (ER) der Muskelzellen einen Komplex bilden, der die Sensitivität von beiden nikotinischen Acetylcholin-Rezeptoren gegenüber verschiedenen cholinergen Agonisten verändert. In diesem Zusammenhang wurde auch nachgewiesen, dass die Oberflächenexpression einzelner Untereinheiten der beiden Rezeptoren durch NRA-2/4 beeinflusst wird. Diese Resultate legen die Vermutung nahe, dass beide Proteine die Zusammensetzung der Rezeptoren und somit ihre pharmakologischen Eigenschaften modulieren. Denkbar ist dabei eine regulatorische Funktion bei der Assemblierung verschiedener Untereinheiten zu einem funktionellen Rezeptor oder bei der Kontrolle des ER-Austritts von Rezeptoren mit bestimmter Zusammensetzung. In dieser Hinsicht konnte jedoch keine Interaktion von NRA-2/4 mit der Notch-Signalkaskade nachgewiesen werden, wie sie für die homologen Proteine nicalin und NOMO in Vertebraten gezeigt wurde [280,281].

Für die Untersuchung synaptischer Proteine durch optogenetische Techniken wurde ChR2(H134R) selektiv in cholinergen oder GABAergen Motorneuronen exprimiert, um die akute und lichtgesteuerte Freisetzung des jeweiligen Neurotransmitters zu ermöglichen. Die resultierende Stimulation bzw. Inhibition von Muskelzellen wurde hierbei durch elektrophysiologische Messungen der post-synaptischen Ströme und durch Analyse von Kontraktionen respektive Relaxationen untersucht. Dabei wurde gezeigt, dass Störungen der synaptischen Reizweiterleitung die Ausprägung und Dynamik dieser lichtinduzierten Effekte beeinflussen und dadurch charakterisiert werden können. So zeigten beispielsweise Mutanten von Synaptojanin und Endophilin nachlassende Effekte bei anhaltender oder wiederholter Stimulation, was durch die gestörte Regeneration synaptischer Vesikel erklärt werden kann [130,132,133].

Die hohe Sensitivität dieser Methode wurde im Nachfolgenden dazu verwendet, die Inhibition cholinerger Motorneuronen durch den metabotropen $GABA_B$-Rezeptor zu untersuchen, der in *C. elegans* aus den beiden Untereinheiten GBB-1 und GBB-2

gebildet wird [65,298]. Dabei konnte zunächst gezeigt werden, dass diese heterosynaptische Inhibition verschiedene lokomotorische Verhaltensweisen der Tiere beeinflusst. Für die mechanistische Untersuchung wurden anschließend cholinerge Motorneuronen durch ChR2(H134R) photoaktiviert, während resultierende Kontraktionseffekte in Abhängigkeit von GBB-1/2 analysiert wurden. Um hierbei die Funktion von GBB-1/2 durch erhöhte GABA-Konzentrationen hervorzuheben, wurden zusätzlich GABAerge Motorneuronen optogenetisch stimuliert oder die Wiederaufnahme von GABA aus dem synaptischen Spalt durch Mutation des Membran-ständigen GABA-Transporters blockiert. So konnte gezeigt werden, dass GBB-1/2 eine akute Inhibition der cholinergen Motorneuronen bewirken, was vermutlich für die Regulation von Bewegungsabläufen eine wichtige Rolle spielt. Die geringe Dynamik der GBB-1/2 induzierten Effekte deutet allerdings darauf hin, dass die synaptische Aktivität durch den metabotropen Rezeptor kaum nachhaltig moduliert wird.

In nachfolgenden Versuchen wurde die optogenetische Stimulation von Motorneuronen außerdem mit der elektronenmikroskopischen Analyse der präsynaptischen Feinstruktur kombiniert. Dadurch konnte die Dynamik der Exozytose und Endozytose synaptischer Vesikel (SV) in Abhängigkeit von neuronaler Aktivität untersucht werden. So wurde gezeigt, dass synaptische Vesikel nahe der aktiven Zone während einer 30-sekündigen Hyperstimulation nahezu komplett aufgebraucht waren. Die vollständige Regeneration der SV Pools benötigte anschließend etwa 12 Sekunden und erfolgte zunächst in der Peripherie der aktiven Zone, was auf eine laterale Heranführung der Vesikel schließen lässt. Nach etwa 20 Sekunden erholte sich ebenfalls die Wirksamkeit der Stimulation von Muskelzellen durch die Motorneuronen, was durch elektrophysiologische Messungen der photo-induzierten post-synaptischen Ströme gezeigt wurde. Während der Hyperstimulation bildeten sich außerdem große vesikuläre Strukturen, die sich anschließend nach etwa acht Sekunden wieder aufgelöst hatten. In Analogie zu vergleichbaren Experimenten in anderen Organismen liegt die Vermutung nahe, dass es sich dabei um Zwischenprodukte der so genannten *Bulk Phase* Endozytose handelt, die das Clathrin-abhängige Recycling von synaptischen Vesikeln bei starker neuronaler Aktivität ergänzt [141,318,319]. Bemerkenswerterweise war der Abbau der vesikulären Strukturen in Synaptojanin- und Endophilin-defizienten Tieren stark verzögert. Denkbar ist, dass beide Proteine für die Synthese von synaptischen

Vesikeln aus den vesikulären Zwischenprodukten der *Bulk Phase* Endozytose wichtig sind, analog zur ihrer Funktion bei der Clathrin-abhängigen Endozytose an der Plasmamembran.

Durch die zielgerichtete Manipulation der Zellaktivität ermöglichen optogenetische Techniken außerdem die funktionelle Charakterisierung von Neuronen und neuronalen Netzwerken. Um die zelluläre Spezifität dieses Ansatzes zu erhöhen, wurde ein Tracking-System entwickelt das die Position frei beweglicher Tiere in Echtzeit bestimmt und nachverfolgt. Dadurch konnte die Photoaktivierung optogenetischer Proteine auf definierte Bereiche der Fadenwürmer und somit auf ausgewählte Neuronen innerhalb der Expressionsmuster von verwendeten Promotoren eingeschränkt werden. Des Weiteren ermöglichte hierbei die Auswertung translatorischer Parameter die Analyse verschiedener lokomotorischer Merkmale wie Geschwindigkeit, Bewegungsbahn oder Ausprägung der Körperbiegungen. Dieses System wurde beispielhaft für die konzertierte Photoaktivierung durch ChR2(H134R) bzw. Photoinhibition durch MAC von zwei verschiedenen Gruppen von Neuronen angewendet, um die Integration mechanosensorischer Informationen durch *Command Interneuronen* zu untersuchen. In diesem Zusammenhang wurde zudem eine Rekombinase-basierte Methode für optogenetische Proteine adaptiert, die die Transkription auf die zelluläre Schnittmenge von zwei verschiedenen Promotoren einschränkt und somit die Spezifität der Expression erhöht. Idealerweise kann dieser Ansatz außerdem mit der gezielten Photoaktivierung kombiniert werden, um die zelluläre Selektivität optogenetischer Anwendungen weiter zu verbessern.

Weiterhin ist die Anwendung optogenetischer Techniken bisher durch intrinsische Eigenschaften der verwendeten Rhodopsine auf die relativ kurzzeitige Manipulation des Membranpotentials von Zellen beschränkt. So benötigt ChR2 durch die schnelle Schließung seines offenen Kanals eine kontinuierliche Photoaktivierung, um eine andauernde Depolarisation hervorzurufen. Dies ist jedoch potentiell mit phototoxischen und – besonders bei *C. elegans* – phototaktischen Nebeneffekten verbunden. Deswegen wurden diverse Mutanten von ChR2 mit stark verlangsamter Inaktivierung [261] für ihren Nutzen zur Langzeit-Stimulation von erregbaren Zellen im Nematode getestet. Dabei wurde gezeigt, dass ChR2(C128S) durch einen kurzen Photostimulus mit vergleichsweise niedriger Intensität eine anhaltende Depolarisation über mehrere Minuten auslösen kann. Die wiederholte Stimulation in ASJ Neuronen ermöglichte zudem eine langzeitige Depolarisation über mehrere Tage, wodurch die

genetisch veranlagte Entwicklung von Tieren manipuliert werden konnte. Durch gezielte Punktmutation konnten außerdem relevante Eigenschaften von ChR2(C128S) für die Langzeit-Stimulation weiter verbessert werden.

Als weiteres optogenetisches Werkzeug wurde zudem die *Photoaktivierbare Adenylatzyklase alpha* (PACα) aus *Euglena gracilis* [274,275,278] für die akute und lichtgetriebene Synthese des sekundären Botenstoffs cAMP in *C. elegans* etabliert. Die Photoaktivierung von PACα in cholinergen Motorneuronen verstärkte dabei die Neurotransmitterfreisetzung und induzierte hyperlokomotorische Phänotypen, vergleichbar zu Mutanten mit erhöhten cAMP-Konzentrationen.

Zusammengefasst wurden diverse optogenetische Techniken für *C. elegans* entwickelt und optimiert, die die zellspezifische und nicht-invasive Manipulation des Membranpotentials beziehungsweise die Synthese des sekundären Botenstoffs cAMP durch Licht im frei beweglichen Tier ermöglichen. Diese Methoden können zur gezielten Störung neuronaler Aktivität angewendet werden, um dadurch neurobiologische Fragestellungen im Fadenwurm zu untersuchen. Dies wurde beispielhaft für die Erforschung der synaptischen Reizweiterleitung und die funktionelle Analyse neuronaler Netzwerke demonstriert. Denkbar ist außerdem, diese für *C. elegans* etablierten Methoden vergleichbar in anderen Modellorganismen anzuwenden. So sind die Fruchtfliege ebenso wie der Zebrafisch-Embryo bereits für optogenetische Techniken erprobt [365,367]. Für Säugetiere wie die Maus, die Ratte und den Makaken wurden zudem bereits Ansätze entwickelt, die die gezielte Photostimulation in lebenden und frei beweglichen Tieren ermöglichen [253,269,377,390].

7. Publications arising from the thesis

7.1. Personal contributions to the publications

(*: equal contribution)

7.1.1. Publication I: „An ER-resident membrane protein complex regulates nicotinic acetylcholine receptor subunit composition at the synapse"

EMBO Journal; Volume 28(17); 2009

Ruta B Almedom*, Jana F Liewald*, Guillermina Hernando, Christian Schultheis, Diego Rayes, Jie Pan, Thorsten Schedletzky, Harald Hutter, Cecilia Bouzat, Alexander Gottschalk

In this publication, the proteins NRA-2 and NRA-4 were characterized by pharmacological and electrophysiological techniques with respect to their functional role for AChR maturation in muscle cells. Therefore, mutant alleles of both genes were used for the analysis of related phenotypes. For this, I conducted biochemical experiments to analyze transcription of residual fragments in deletion mutant alleles of nra-4 (hd127 and tm2656).

7.1.2. Publication II: „Optogenetic analysis of synaptic function"

Nature Methods; Volume 5(10); 2008

Jana F Liewald*, Martin Brauner*, Greg J Stephens, Magali Bouhours, Christian Schultheis, Mei Zhen, Alexander Gottschalk

In this paper, the use of optogenetic tools for the characterization of synaptic transmission in C. elegans is described. The method was further expanded for analyses of defects in various mutants affecting synaptic transmission. Therefore, I generated worm strains that conjointly contained ChR2(H134R) expressed in GABAergic motorneurons (transgene zxIs3) and mutant alleles of synaptogyrin (sng-1(ok234)), synaptotagmin (snt-1(md290)), the vesicular GABA transporter (unc-47(e307)), and the ionotropic GABA receptor (unc-49(e407)).

7.1.3. Publication III: „Optogenetic analysis of GABA_B receptor signaling in *Caenorhabditis elegans* motor neurons"

Journal of Neurophysiology; Volume 106(2); 2011

<u>Christian Schultheis</u>*, Martin Brauner*, Jana F Liewald, Alexander Gottschalk

In this publication, the negative feedback on cholinergic motorneurons mediated by the GABA_B receptor GBB-1/2 was investigated by optogenetic stimulation techniques in combination with electrophysiological and behavioral analyses. To this work, I contributed rescue constructs for GBB-2 and created the respective transgenic strains as well as strains with snf-11(ok156) mutant background. Furthermore, I performed behavioral experiments for these worm strains and assays for analysis of body thrashing frequencies, crawling velocity, bending angles, and trajectories. I also wrote the script for Gnu R that was used for computational analysis of trajectories.

7.1.4. Publication IV: „Real-time multimodal optical control of neurons and muscles in freely behaving *Caenorhabditis elegans*"

Nature Methods; Volume 8(2); 2011

Jeffrey N Stirman, Matthew M Crane, Steven J Husson, Sebastian Wabnig, <u>Christian Schultheis</u>, Alexander Gottschalk, Hang Lu

This publication describes an approach for real-time tracking of freely moving C. elegans and simultaneous, targeted multi-color photoactivation of distinct optogenetic tools. Exemplary, this technique was used to demonstrate that command interneurons integrate information from mechanosensory neurons to evoke adequate locomotory behaviors. Here, I provided constructs for the selective optogenetic inhibition of command interneurons by NpHR.

7.1.5. Publication V: „Optogenetic long-term manipulation of behavior and animal development"

PLoS One; Volume 6(4); 2011

Christian Schultheis, Jana F Liewald, Ernst Bamberg, Georg Nagel, Alexander Gottschalk

In this publication Channelrhodopsin-2 variants with altered kinetics were characterized for their utility to evoke prolonged depolarizations in excitable cells of C. elegans. For this, I generated the Channelrhodopsin-2 constructs with mutated Cys128 residue for expression in various cells of the worm, created the respective worm strains, and performed the behavioral experiments.

7.1.6. Publication VI: „PACα – an optogenetic tool for *in-vivo* manipulation of cellular cAMP levels, neurotransmitter release, and behavior in *Caenorhabditis elegans*"

Simone Weissenberger*, Christian Schultheis*, Jana F Liewald*, Karen Erbguth, Georg Nagel, Alexander Gottschalk

This work characterizes effects of light-driven cAMP synthesis in cholinergic motorneurons of C. elegans through photoactivated adenylyl cyclase (PAC)α. For this, I performed behavioral assays, namely analysis of crawling velocity on solid medium (with light intensities of 2 mW/mm²), number of long reversals, average bending angles, relative body length, and head-tail contacts. Furthermore, I designed custom-written scripts for ImageJ and Gnu R that allowed computational analysis of bending angles and the relative body length.

8. References

[1] Altun ZF, Herndon LA, Crocker C, Lints R, Hall DH: "Wormatlas"; *http://www.Wormatlas.org* (2010).

[2] Maupas É: "Modes et formes de reproduction des Nématodes"; *Archives De Zoologie Experimentale Et Generale* (1900), 8:463-624.

[3] Hope IA: *C. elegans: a practical approach*. Oxford: Oxford University Press; 1999.

[4] Byerly L, Cassada RC, Russell RL: "The life cycle of the nematode Caenorhabditis elegans"; *Dev Biol* (1976), 51:23-33.

[5] Cassada RC, Russell RL: "The dauerlarva, a post-embryonic developmental variant of the nematode Caenorhabditis elegans"; *Dev Biol* (1975), 46:326-342.

[6] Golden JW, Riddle DL: "A pheromone influences larval development in the nematode Caenorhabditis elegans"; *Science* (1982), 218:578-580.

[7] N.D.: "The C. elegans lifecycle"; *http://withscienceforlife.wordpress.com/tag/c-elegans/*.

[8] Adams JM: "Ways of dying: multiple pathways to apoptosis"; *Genes Dev* (2003), 17:2481-2495.

[9] Danial NN, Korsmeyer SJ: "Cell death: critical control points"; *Cell* (2004), 116:205-219.

[10] Horvitz HR: "Worms, life, and death (Nobel lecture)"; *Chembiochem* (2003), 4:697-711.

[11] Kimble J, Hirsh D: "The postembryonic cell lineages of the hermaphrodite and male gonads in Caenorhabditis elegans"; *Dev Biol* (1979), 70:396-417.

[12] Sulston JE, Horvitz HR: "Post-embryonic cell lineages of the nematode, Caenorhabditis elegans"; *Dev Biol* (1977), 56:110-156.

[13] White JG, Southgate E, Thomson JN, Brenner S: "The Structure of the Nervous System of the Nematode Caenorhabditis elegans"; *Philos Trans R Soc Lond B Biol Sci* (1986), 314:1-340.

[14] Hall DH, Russell RL: "The posterior nervous system of the nematode Caenorhabditis elegans: serial reconstruction of identified neurons and complete pattern of synaptic interactions"; *J Neurosci* (1991), 11:1-22.

[15] Varshney LR, Chen BL, Paniagua E, Hall DH, Chklovskii DB: "Structural properties of the Caenorhabditis elegans neuronal network"; *PLoS Comput Biol* (2011), 7:e1001066.

[16] Consortium TCeS: "Genome sequence of the nematode C. elegans: a platform for investigating biology"; *Science* (1998), 282:2012-2018.

[17] Nelson GA, Schubert WW, Marshall TM, Benton ER, Benton EV: "Radiation effects in Caenorhabditis elegans, mutagenesis by high and low LET ionizing radiation"; *Mutat Res* (1989), 212:181-192.

[18] De Stasio EA, Dorman S: "Optimization of ENU mutagenesis of Caenorhabditis elegans"; *Mutat Res* (2001), 495:81-88.

[19] Brenner S: "The genetics of Caenorhabditis elegans"; *Genetics* (1974), 77:71-94.

[20] Chalfie M, Sulston J: "Developmental genetics of the mechanosensory neurons of Caenorhabditis elegans"; *Dev Biol* (1981), 82:358-370.

[21] Frokjaer-Jensen C, Davis MW, Hollopeter G, Taylor J, Harris TW, Nix P, Lofgren R, Prestgard-Duke M, Bastiani M, Moerman DG, et al.: "Targeted gene

deletions in C. elegans using transposon excision"; *Nat Methods* (2010), 7:451-453.

[22] Frokjaer-Jensen C, Davis MW, Hopkins CE, Newman BJ, Thummel JM, Olesen SP, Grunnet M, Jorgensen EM: "Single-copy insertion of transgenes in Caenorhabditis elegans"; *Nat Genet* (2008), 40:1375-1383.

[23] Fire A, Xu S, Montgomery MK, Kostas SA, Driver SE, Mello CC: "Potent and specific Interference by double-stranded RNA in Caenorhabditis elegans"; *Nature* (1998), 391:806-810.

[24] Tabara H, Grishok A, Mello CC: "RNAi in C. elegans: soaking in the genome sequence"; *Science* (1998), 282:430-431.

[25] Timmons L, Court DL, Fire A: "Ingestion of bacterially expressed dsRNAs can produce specific and potent genetic interference in Caenorhabditis elegans"; *Gene* (2001), 263:103-112.

[26] Fraser AG, Kamath RS, Zipperlen P, Martinez-Campos M, Sohrmann M, Ahringer J: "Functional genomic analysis of C. elegans chromosome I by systematic RNA interference"; *Nature* (2000), 408:325-330.

[27] Kamath RS, Fraser AG, Dong Y, Poulin G, Durbin R, Gotta M, Kanapin A, Le Bot N, Moreno S, Sohrmann M, et al.: "Systematic functional analysis of the Caenorhabditis elegans genome using RNAi"; *Nature* (2003), 421:231-237.

[28] Mello CC, Kramer JM, Stinchcomb D, Ambros V: "Efficient gene transfer in C.elegans: extrachromosomal maintenance and integration of transforming sequences"; *Embo J* (1991), 10:3959-3970.

[29] Mello C, Fire A: "DNA transformation"; *Methods Cell Biol* (1995), 48:451-482.

[30] Nonet M: "C. elegans"; *http://neuroscience.wustl.edu/nonetlab/*.

[31] Chalfie M, Sulston JE, White JG, Southgate E, Thomson JN, Brenner S: "The neural circuit for touch sensitivity in Caenorhabditis elegans"; *J Neurosci* (1985), 5:956-964.

[32] Bargmann CI: "Chemosensation in C. elegans"; *WormBook* (2006):1-29.

[33] Hilliard MA, Bargmann CI, Bazzicalupo P: "C. elegans responds to chemical repellents by integrating sensory inputs from the head and the tail"; *Curr Biol* (2002), 12:730-734.

[34] Bergamasco C, Bazzicalupo P: "Chemical sensitivity in Caenorhabditis elegans"; *Cell Mol Life Sci* (2006), 63:1510-1522.

[35] Chang AJ, Chronis N, Karow DS, Marletta MA, Bargmann CI: "A distributed chemosensory circuit for oxygen preference in C. elegans"; *PLoS Biol* (2006), 4:e274.

[36] Zimmer M, Gray JM, Pokala N, Chang AJ, Karow DS, Marletta MA, Hudson ML, Morton DB, Chronis N, Bargmann CI: "Neurons detect increases and decreases in oxygen levels using distinct guanylate cyclases"; *Neuron* (2009), 61:865-879.

[37] Hart AC, Kass J, Shapiro JE, Kaplan JM: "Distinct signaling pathways mediate touch and osmosensory responses in a polymodal sensory neuron"; *J Neurosci* (1999), 19:1952-1958.

[38] Bargmann CI, Hartwieg E, Horvitz HR: "Odorant-selective genes and neurons mediate olfaction in C. elegans"; *Cell* (1993), 74:515-527.

[39] Mori I, Ohshima Y: "Neural regulation of thermotaxis in Caenorhabditis elegans"; *Nature* (1995), 376:344-348.

[40] Perkins LA, Hedgecock EM, Thomson JN, Culotti JG: "Mutant sensory cilia in the nematode Caenorhabditis elegans"; *Dev Biol* (1986), 117:456-487.

[41] Ward A, Liu J, Feng Z, Xu XZ: "Light-sensitive neurons and channels mediate phototaxis in C. elegans"; *Nat Neurosci* (2008), 11:916-922.

[42] Liu J, Ward A, Gao J, Dong Y, Nishio N, Inada H, Kang L, Yu Y, Ma D, Xu T, et al.: "C. elegans phototransduction requires a G protein-dependent cGMP pathway and a taste receptor homolog"; *Nat Neurosci* (2010), 13:715-722.

[43] Culotti JG, Russell RL: "Osmotic avoidance defective mutants of the nematode Caenorhabditis elegans"; *Genetics* (1978), 90:243-256.

[44] Herman RK: "Touch sensation in Caenorhabditis elegans"; *Bioessays* (1996), 18:199-206.

[45] Goodman MB: "Eppendorf essay winner. Deconstructing C. elegans sensory mechanotransduction"; *Science* (2004), 306:427-428.

[46] Garcia-Anoveros J, Corey DP: "The molecules of mechanosensation"; *Annu Rev Neurosci* (1997), 20:567-594.

[47] Wicks SR, Rankin CH: "The integration of antagonistic reflexes revealed by laser ablation of identified neurons determines habituation kinetics of the Caenorhabditis elegans tap withdrawal response"; *J Comp Physiol [A]* (1996), 179:675-685.

[48] Von Stetina SE, Treinin M, Miller DM, 3rd: "The motor circuit"; *Int Rev Neurobiol* (2006), 69:125-167.

[49] Francis R, Waterston RH: "Muscle cell attachment in Caenorhabditis elegans"; *J Cell Biol* (1991), 114:465-479.

[50] Liu Q, Chen B, Gaier E, Joshi J, Wang ZW: "Low conductance gap junctions mediate specific electrical coupling in body-wall muscle cells of Caenorhabditis elegans"; *J Biol Chem* (2006), 281:7881-7889.

[51] Liu P, Chen B, Wang ZW: "Gap junctions synchronize action potentials and Ca2+ transients in Caenorhabditis elegans body-wall muscle"; *J Biol Chem* (2011).

[52] Schuske K, Beg AA, Jorgensen EM: "The GABA nervous system in C. elegans"; *Trends Neurosci* (2004), 27:407-414.

[53] McIntire SL, Jorgensen E, Kaplan J, Horvitz HR: "The GABAergic nervous system of Caenorhabditis elegans"; *Nature* (1993), 364:337-341.

[54] McIntire SL, Jorgensen E, Horvitz HR: "Genes required for GABA function in Caenorhabditis elegans"; *Nature* (1993), 364:334-337.

[55] Richmond JE, Jorgensen EM: "One GABA and two acetylcholine receptors function at the C. elegans neuromuscular junction"; *Nat Neurosci* (1999), 2:791-797.

[56] Almedom RB, Liewald JF, Hernando G, Schultheis C, Rayes D, Pan J, Schedletzky T, Hutter H, Bouzat C, Gottschalk A: "An ER-resident membrane protein complex regulates nicotinic acetylcholine receptor subunit composition at the synapse"; *Embo J* (2009), 28:2636-2649.

[57] Touroutine D, Fox RM, Von Stetina SE, Burdina A, Miller DM, 3rd, Richmond JE: "acr-16 encodes an essential subunit of the levamisole-resistant nicotinic receptor at the Caenorhabditis elegans neuromuscular junction"; *J Biol Chem* (2005), 280:27013-27021.

[58] Francis MM, Evans SP, Jensen M, Madsen DM, Mancuso J, Norman KR, Maricq AV: "The Ror receptor tyrosine kinase CAM-1 is required for ACR-16-mediated synaptic transmission at the C. elegans neuromuscular junction"; *Neuron* (2005), 46:581-594.

[59] Lewis JA, Elmer JS, Skimming J, McLafferty S, Fleming J, McGee T: "Cholinergic receptor mutants of the nematode Caenorhabditis elegans"; *J Neurosci* (1987), 7:3059-3071.

[60] Lewis JA, Fleming JT, McLafferty S, Murphy H, Wu C: "The levamisole receptor, a cholinergic receptor of the nematode Caenorhabditis elegans"; *Mol Pharmacol* (1987), 31:185-193.

[61] Fleming JT, Squire MD, Barnes TM, Tornoe C, Matsuda K, Ahnn J, Fire A, Sulston JE, Barnard EA, Sattelle DB, et al.: "Caenorhabditis elegans levamisole resistance genes lev-1, unc-29, and unc-38 encode functional nicotinic acetylcholine receptor subunits"; *J Neurosci* (1997), 17:5843-5857.

[62] Culetto E, Baylis HA, Richmond JE, Jones AK, Fleming JT, Squire MD, Lewis JA, Sattelle DB: "The Caenorhabditis elegans unc-63 gene encodes a levamisole-sensitive nicotinic acetylcholine receptor alpha subunit"; *J Biol Chem* (2004), 279:42476-42483.

[63] Lanzafame AA, Christopoulos A, Mitchelson F: "Cellular signaling mechanisms for muscarinic acetylcholine receptors"; *Receptors Channels* (2003), 9:241-260.

[64] Zhang B, Luo S, Dong XP, Zhang X, Liu C, Luo Z, Xiong WC, Mei L: "Beta-catenin regulates acetylcholine receptor clustering in muscle cells through interaction with rapsyn"; *J Neurosci* (2007), 27:3968-3973.

[65] Dittman JS, Kaplan JM: "Behavioral impact of neurotransmitter-activated G-protein-coupled receptors: muscarinic and GABAB receptors regulate Caenorhabditis elegans locomotion"; *J Neurosci* (2008), 28:7104-7112.

[66] Combes D, Fedon Y, Toutant JP, Arpagaus M: "Acetylcholinesterase genes in the nematode Caenorhabditis elegans"; *Int Rev Cytol* (2001), 209:207-239.

[67] Kolson DL, Russell RL: "New acetylcholinesterase-deficient mutants of the nematode Caenorhabditis elegans"; *J Neurogenet* (1985), 2:69-91.

[68] Kolson DL, Russell RL: "A novel class of acetylcholinesterase, revealed by mutations, in the nematode Caenorhabditis elegans"; *J Neurogenet* (1985), 2:93-110.

[69] Johnson CD, Duckett JG, Culotti JG, Herman RK, Meneely PM, Russell RL: "An acetylcholinesterase-deficient mutant of the nematode Caenorhabditis elegans"; *Genetics* (1981), 97:261-279.

[70] Culotti JG, Von Ehrenstein G, Culotti MR, Russell RL: "A second class of acetylcholinesterase-deficient mutants of the nematode Caenorhabditis elegans"; *Genetics* (1981), 97:281-305.

[71] Okuda T, Okamura M, Kaitsuka C, Haga T, Gurwitz D: "Single nucleotide polymorphism of the human high affinity choline transporter alters transport rate"; *J Biol Chem* (2002), 277:45315-45322.

[72] Matthies DS, Fleming PA, Wilkes DM, Blakely RD: "The Caenorhabditis elegans choline transporter CHO-1 sustains acetylcholine synthesis and motor function in an activity-dependent manner"; *J Neurosci* (2006), 26:6200-6212.

[73] Rand JB: "Acetylcholine"; *WormBook* (2007):1-21.

[74] Mullen GP, Mathews EA, Saxena P, Fields SD, McManus JR, Moulder G, Barstead RJ, Quick MW, Rand JB: "The Caenorhabditis elegans snf-11 gene encodes a sodium-dependent GABA transporter required for clearance of synaptic GABA"; *Mol Biol Cell* (2006), 17:3021-3030.

[75] Jiang G, Zhuang L, Miyauchi S, Miyake K, Fei YJ, Ganapathy V: "A Na+/Cl- -coupled GABA transporter, GAT-1, from Caenorhabditis elegans: structural and functional features, specific expression in GABA-ergic neurons, and involvement in muscle function"; *J Biol Chem* (2005), 280:2065-2077.

[76] Schultheis C, Brauner M, Liewald JF, Gottschalk A: "Optogenetic analysis of GABA(B) receptor signaling in Caenorhabditis elegans motor neurons"; *J Neurophysiol* (2011), 106:817-827.

[77] Bargmann CI: "Neurobiology of the Caenorhabditis elegans genome"; *Science* (1998), 282:2028-2033.

[78] Yu FH, Yarov-Yarovoy V, Gutman GA, Catterall WA: "Overview of molecular relationships in the voltage-gated ion channel superfamily"; *Pharmacol Rev* (2005), 57:387-395.

[79] Raizen DM, Avery L: "Electrical activity and behavior in the pharynx of Caenorhabditis elegans"; *Neuron* (1994), 12:483-495.

[80] Gao S, Zhen M: "Action potentials drive body wall muscle contractions in Caenorhabditis elegans"; *Proc Natl Acad Sci U S A* (2011), 108:2557-2562.

[81] Mellem JE, Brockie PJ, Madsen DM, Maricq AV: "Action potentials contribute to neuronal signaling in C. elegans"; *Nat Neurosci* (2008), 11:865-867.

[82] Lockery SR, Goodman MB: "The quest for action potentials in C. elegans neurons hits a plateau"; *Nat Neurosci* (2009), 12:377-378.

[83] Lockery SR, Goodman MB, Faumont S: "First report of action potentials in a C. elegans neuron is premature"; *Nat Neurosci* (2009), 12:365-366; author reply 366.

[84] Starich T, Sheehan M, Jadrich J, Shaw J: "Innexins in C. elegans"; *Cell Commun Adhes* (2001), 8:311-314.

[85] Rostaing P, Weimer RM, Jorgensen EM, Triller A, Bessereau JL: "Preservation of immunoreactivity and fine structure of adult C. elegans tissues using high-pressure freezing"; *J Histochem Cytochem* (2004), 52:1-12.

[86] Rizzoli SO, Betz WJ: "Synaptic vesicle pools"; *Nat Rev Neurosci* (2005), 6:57-69.

[87] Heuser JE, Reese TS, Dennis MJ, Jan Y, Jan L, Evans L: "Synaptic vesicle exocytosis captured by quick freezing and correlated with quantal transmitter release"; *J Cell Biol* (1979), 81:275-300.

[88] Elmqvist D, Quastel DM: "A quantitative study of end-plate potentials in isolated human muscle"; *J Physiol* (1965), 178:505-529.

[89] Harata N, Pyle JL, Aravanis AM, Mozhayeva M, Kavalali ET, Tsien RW: "Limited numbers of recycling vesicles in small CNS nerve terminals: implications for neural signaling and vesicular cycling"; *Trends Neurosci* (2001), 24:637-643.

[90] Richards DA, Guatimosim C, Rizzoli SO, Betz WJ: "Synaptic vesicle pools at the frog neuromuscular junction"; *Neuron* (2003), 39:529-541.

[91] Rizzoli SO, Betz WJ: "The structural organization of the readily releasable pool of synaptic vesicles"; *Science* (2004), 303:2037-2039.

[92] Kuromi H, Kidokoro Y: "Two distinct pools of synaptic vesicles in single presynaptic boutons in a temperature-sensitive Drosophila mutant, shibire"; *Neuron* (1998), 20:917-925.

[93] Weimer RM, Gracheva EO, Meyrignac O, Miller KG, Richmond JE, Bessereau JL: "UNC-13 and UNC-10/rim localize synaptic vesicles to specific membrane domains"; *J Neurosci* (2006), 26:8040-8047.

[94] Gracheva EO, Burdina AO, Holgado AM, Berthelot-Grosjean M, Ackley BD, Hadwiger G, Nonet ML, Weimer RM, Richmond JE: "Tomosyn inhibits synaptic vesicle priming in Caenorhabditis elegans"; *PLoS Biol* (2006), 4:e261.

[95] Weimer RM, Richmond JE, Davis WS, Hadwiger G, Nonet ML, Jorgensen EM: "Defects in synaptic vesicle docking in unc-18 mutants"; *Nat Neurosci* (2003), 6:1023-1030.

[96] Nonet ML, Staunton JE, Kilgard MP, Fergestad T, Hartwieg E, Horvitz HR, Jorgensen EM, Meyer BJ: "Caenorhabditis elegans rab-3 mutant synapses exhibit impaired function and are partially depleted of vesicles"; *J Neurosci* (1997), 17:8061-8073.

[97] Gracheva EO, Hadwiger G, Nonet ML, Richmond JE: "Direct interactions between C. elegans RAB-3 and Rim provide a mechanism to target vesicles to the presynaptic density"; *Neurosci Lett* (2008), 444:137-142.

[98] Koushika SP, Richmond JE, Hadwiger G, Weimer RM, Jorgensen EM, Nonet ML: "A post-docking role for active zone protein Rim"; *Nat Neurosci* (2001), 4:997-1005.

[99] Garcia-Anoveros J, Ma C, Chalfie M: "Regulation of Caenorhabditis elegans degenerin proteins by a putative extracellular domain"; *Curr Biol* (1995), 5:441-448.

[100] Saifee O, Wei L, Nonet ML: "The Caenorhabditis elegans unc-64 locus encodes a syntaxin that interacts genetically with synaptobrevin"; *Mol Biol Cell* (1998), 9:1235-1252.

[101] Nonet ML, Saifee O, Zhao H, Rand JB, Wei L: "Synaptic transmission deficits in Caenorhabditis elegans synaptobrevin mutants"; *J Neurosci* (1998), 18:70-80.

[102] Richmond JE, Weimer RM, Jorgensen EM: "An open form of syntaxin bypasses the requirement for UNC-13 in vesicle priming"; *Nature* (2001), 412:338-341.

[103] Hammarlund M, Palfreyman MT, Watanabe S, Olsen S, Jorgensen EM: "Open syntaxin docks synaptic vesicles"; *PLoS Biol* (2007), 5:e198.

[104] Maruyama IN, Brenner S: "A phorbol ester/diacylglycerol-binding protein encoded by the unc-13 gene of Caenorhabditis elegans"; *Proc Natl Acad Sci U S A* (1991), 88:5729-5733.

[105] Sassa T, Harada S, Ogawa H, Rand JB, Maruyama IN, Hosono R: "Regulation of the UNC-18-Caenorhabditis elegans syntaxin complex by UNC-13"; *J Neurosci* (1999), 19:4772-4777.

[106] Sudhof TC: "The synaptic vesicle cycle: a cascade of protein-protein interactions"; *Nature* (1995), 375:645-653.

[107] Frokjaer-Jensen C, Kindt KS, Kerr RA, Suzuki H, Melnik-Martinez K, Gerstbreih B, Driscol M, Schafer WR: "Effects of voltage-gated calcium channel subunit genes on calcium influx in cultured C. elegans mechanosensory neurons"; *J Neurobiol* (2006), 66:1125-1139.

[108] Wojcik SM, Brose N: "Regulation of membrane fusion in synaptic excitation-secretion coupling: speed and accuracy matter"; *Neuron* (2007), 55:11-24.

[109] Steger KA, Shtonda BB, Thacker C, Snutch TP, Avery L: "The C. elegans T-type calcium channel CCA-1 boosts neuromuscular transmission"; *J Exp Biol* (2005), 208:2191-2203.

[110] Davis AF, Bai J, Fasshauer D, Wolowick MJ, Lewis JL, Chapman ER: "Kinetics of synaptotagmin responses to Ca2+ and assembly with the core SNARE complex onto membranes"; *Neuron* (1999), 24:363-376.

[111] Jorgensen EM, Hartwieg E, Schuske K, Nonet ML, Jin Y, Horvitz HR: "Defective recycling of synaptic vesicles in synaptotagmin mutants of Caenorhabditis elegans"; *Nature* (1995), 378:196-199.

[112] Richmond J: "Synaptic function"; *WormBook* (2005):1-14.

[113] Nonet ML, Holgado AM, Brewer F, Serpe CJ, Norbeck BA, Holleran J, Wei L, Hartwieg E, Jorgensen EM, Alfonso A: "UNC-11, a Caenorhabditis elegans AP180 homologue, regulates the size and protein composition of synaptic vesicles"; *Mol Biol Cell* (1999), 10:2343-2360.

[114] Ahle S, Ungewickell E: "Purification and properties of a new clathrin assembly protein"; *Embo J* (1986), 5:3143-3149.

[115] Ye W, Lafer EM: "Clathrin binding and assembly activities of expressed domains of the synapse-specific clathrin assembly protein AP-3"; *J Biol Chem* (1995), 270:10933-10939.

[116] Hirst J, Robinson MS: "Clathrin and adaptors"; *Biochim Biophys Acta* (1998), 1404:173-193.

[117] Zhang JZ, Davletov BA, Sudhof TC, Anderson RG: "Synaptotagmin I is a high affinity receptor for clathrin AP-2: implications for membrane recycling"; *Cell* (1994), 78:751-760.

[118] Gu M, Schuske K, Watanabe S, Liu Q, Baum P, Garriga G, Jorgensen EM: "Mu2 adaptin facilitates but is not essential for synaptic vesicle recycling in Caenorhabditis elegans"; *J Cell Biol* (2008), 183:881-892.

[119] Kirchhausen T: "Clathrin"; *Annu Rev Biochem* (2000), 69:699-727.

[120] Arneson LS, Kunz J, Anderson RA, Traub LM: "Coupled inositide phosphorylation and phospholipase D activation initiates clathrin-coat assembly on lysosomes"; *J Biol Chem* (1999), 274:17794-17805.

[121] Grant B, Hirsh D: "Receptor-mediated endocytosis in the Caenorhabditis elegans oocyte"; *Mol Biol Cell* (1999), 10:4311-4326.

[122] Bai J, Hu Z, Dittman JS, Pym EC, Kaplan JM: "Endophilin functions as a membrane-bending molecule and is delivered to endocytic zones by exocytosis"; *Cell* (2010), 143:430-441.

[123] Schmidt A, Wolde M, Thiele C, Fest W, Kratzin H, Podtelejnikov AV, Witke W, Huttner WB, Soling HD: "Endophilin I mediates synaptic vesicle formation by transfer of arachidonate to lysophosphatidic acid"; *Nature* (1999), 401:133-141.

[124] Clark SG, Shurland DL, Meyerowitz EM, Bargmann CI, van der Bliek AM: "A dynamin GTPase mutation causes a rapid and reversible temperature-inducible locomotion defect in C. elegans"; *Proc Natl Acad Sci U S A* (1997), 94:10438-10443.

[125] Sweitzer SM, Hinshaw JE: "Dynamin undergoes a GTP-dependent conformational change causing vesiculation"; *Cell* (1998), 93:1021-1029.

[126] Takei K, McPherson PS, Schmid SL, De Camilli P: "Tubular membrane invaginations coated by dynamin rings are induced by GTP-gamma S in nerve terminals"; *Nature* (1995), 374:186-190.

[127] Faelber K, Posor Y, Gao S, Held M, Roske Y, Schulze D, Haucke V, Noe F, Daumke O: "Crystal structure of nucleotide-free dynamin"; *Nature* (2011), 477:556-560.

[128] Ford MG, Jenni S, Nunnari J: "The crystal structure of dynamin"; *Nature* (2011), 477:561-566.

[129] Chappie JS, Mears JA, Fang S, Leonard M, Schmid SL, Milligan RA, Hinshaw JE, Dyda F: "A pseudoatomic model of the dynamin polymer identifies a hydrolysis-dependent powerstroke"; *Cell* (2011), 147:209-222.

[130] Harris TW, Hartwieg E, Horvitz HR, Jorgensen EM: "Mutations in synaptojanin disrupt synaptic vesicle recycling"; *J Cell Biol* (2000), 150:589-600.

[131] Marie B, Sweeney ST, Poskanzer KE, Roos J, Kelly RB, Davis GW: "Dap160/intersectin scaffolds the periactive zone to achieve high-fidelity endocytosis and normal synaptic growth"; *Neuron* (2004), 43:207-219.

[132] Verstreken P, Koh TW, Schulze KL, Zhai RG, Hiesinger PR, Zhou Y, Mehta SQ, Cao Y, Roos J, Bellen HJ: "Synaptojanin is recruited by endophilin to promote synaptic vesicle uncoating"; *Neuron* (2003), 40:733-748.

[133] Schuske KR, Richmond JE, Matthies DS, Davis WS, Runz S, Rube DA, van der Bliek AM, Jorgensen EM: "Endophilin is required for synaptic vesicle endocytosis by localizing synaptojanin"; *Neuron* (2003), 40:749-762.

[134] Ceccarelli B, Hurlbut WP, Mauro A: "Turnover of transmitter and synaptic vesicles at the frog neuromuscular junction"; *J Cell Biol* (1973), 57:499-524.

[135] Gandhi SP, Stevens CF: "Three modes of synaptic vesicular recycling revealed by single-vesicle imaging"; *Nature* (2003), 423:607-613.

[136] Klyachko VA, Jackson MB: "Capacitance steps and fusion pores of small and large-dense-core vesicles in nerve terminals"; *Nature* (2002), 418:89-92.

[137] Albillos A, Dernick G, Horstmann H, Almers W, Alvarez de Toledo G, Lindau M: "The exocytotic event in chromaffin cells revealed by patch amperometry"; *Nature* (1997), 389:509-512.

[138] He L, Wu XS, Mohan R, Wu LG: "Two modes of fusion pore opening revealed by cell-attached recordings at a synapse"; *Nature* (2006), 444:102-105.

[139] Zenisek D, Steyer JA, Feldman ME, Almers W: "A membrane marker leaves synaptic vesicles in milliseconds after exocytosis in retinal bipolar cells"; *Neuron* (2002), 35:1085-1097.

[140] Ceccarelli B, Hurlbut WP: "Ca2+-dependent recycling of synaptic vesicles at the frog neuromuscular junction"; *J Cell Biol* (1980), 87:297-303.

[141] Miller TM, Heuser JE: "Endocytosis of synaptic vesicle membrane at the frog neuromuscular junction"; *J Cell Biol* (1984), 98:685-698.

[142] Maycox PR, Deckwerth T, Hell JW, Jahn R: "Glutamate uptake by brain synaptic vesicles. Energy dependence of transport and functional reconstitution in proteoliposomes"; *J Biol Chem* (1988), 263:15423-15428.

[143] Arata Y, Nishi T, Kawasaki-Nishi S, Shao E, Wilkens S, Forgac M: "Structure, subunit function and regulation of the coated vesicle and yeast vacuolar (H(+))-ATPases"; *Biochim Biophys Acta* (2002), 1555:71-74.

[144] Fykse EM, Fonnum F: "Amino acid neurotransmission: dynamics of vesicular uptake"; *Neurochem Res* (1996), 21:1053-1060.

[145] Alfonso A, Grundahl K, Duerr JS, Han HP, Rand JB: "The Caenorhabditis elegans unc-17 gene: a putative vesicular acetylcholine transporter"; *Science* (1993), 261:617-619.

[146] McIntire SL, Reimer RJ, Schuske K, Edwards RH, Jorgensen EM: "Identification and characterization of the vesicular GABA transporter"; *Nature* (1997), 389:870-876.

[147] Reynolds NK, Schade MA, Miller KG: "Convergent, RIC-8-dependent Galpha signaling pathways in the Caenorhabditis elegans synaptic signaling network"; *Genetics* (2005), 169:651-670.

[148] Rhee JS, Betz A, Pyott S, Reim K, Varoqueaux F, Augustin I, Hesse D, Sudhof TC, Takahashi M, Rosenmund C, et al.: "Beta phorbol ester- and diacylglycerol-induced augmentation of transmitter release is mediated by Munc13s and not by PKCs"; *Cell* (2002), 108:121-133.

[149] Schade MA, Reynolds NK, Dollins CM, Miller KG: "Mutations that rescue the paralysis of Caenorhabditis elegans ric-8 (synembryn) mutants activate the G alpha(s) pathway and define a third major branch of the synaptic signaling network"; *Genetics* (2005), 169:631-649.

[150] Renden RB, Broadie K: "Mutation and activation of Galpha s similarly alters pre- and postsynaptic mechanisms modulating neurotransmission"; *J Neurophysiol* (2003), 89:2620-2638.

[151] Aravamudan B, Broadie K: "Synaptic Drosophila UNC-13 is regulated by antagonistic G-protein pathways via a proteasome-dependent degradation mechanism"; *J Neurobiol* (2003), 54:417-438.

[152] Miller KG, Emerson MD, Rand JB: "Goalpha and diacylglycerol kinase negatively regulate the Gqalpha pathway in C. elegans"; *Neuron* (1999), 24:323-333.

[153] Ahnert-Hilger G, Wiedenmann B: "Requirements for exocytosis in permeabilized neuroendocrine cells. Possible involvement of heterotrimeric G proteins associated with secretory vesicles"; *Ann N Y Acad Sci* (1994), 733:298-305.

[154] Robatzek M, Niacaris T, Steger K, Avery L, Thomas JH: "eat-11 encodes GPB-2, a Gbeta(5) ortholog that interacts with G(o)alpha and G(q)alpha to regulate C. elegans behavior"; *Curr Biol* (2001), 11:288-293.

[155] Perez-Mansilla B, Nurrish S: "A network of G-protein signaling pathways control neuronal activity in C. elegans"; *Adv Genet* (2009), 65:145-192.

[156] Kuromi H, Kidokoro Y: "Tetanic stimulation recruits vesicles from reserve pool via a cAMP-mediated process in Drosophila synapses"; *Neuron* (2000), 27:133-143.

[157] Langan TA: "Histone phosphorylation: stimulation by adenosine 3',5'-monophosphate"; *Science* (1968), 162:579-580.

[158] Marek KW, Ng N, Fetter R, Smolik S, Goodman CS, Davis GW: "A genetic analysis of synaptic development: pre- and postsynaptic dCBP control transmitter release at the Drosophila NMJ"; *Neuron* (2000), 25:537-547.

[159] Beavo JA, Brunton LL: "Cyclic nucleotide research -- still expanding after half a century"; *Nat Rev Mol Cell Biol* (2002), 3:710-718.

[160] Steward O: "mRNA localization in neurons: a multipurpose mechanism?" *Neuron* (1997), 18:9-12.

[161] Zhong Y, Wu CF: "Altered synaptic plasticity in Drosophila memory mutants with a defective cyclic AMP cascade"; *Science* (1991), 251:198-201.

[162] Charlie NK, Thomure AM, Schade MA, Miller KG: "The Dunce cAMP phosphodiesterase PDE-4 negatively regulates G alpha(s)-dependent and G alpha(s)-independent cAMP pools in the Caenorhabditis elegans synaptic signaling network"; *Genetics* (2006), 173:111-130.

[163] Jeanclos EM, Lin L, Treuil MW, Rao J, DeCoster MA, Anand R: "The chaperone protein 14-3-3eta interacts with the nicotinic acetylcholine receptor alpha 4 subunit. Evidence for a dynamic role in subunit stabilization"; *J Biol Chem* (2001), 276:28281-28290.

[164] Muratake T, Hayashi S, Ichikawa T, Kumanishi T, Ichimura Y, Kuwano R, Isobe T, Wang Y, Minoshima S, Shimizu N, et al.: "Structural organization and chromosomal assignment of the human 14-3-3 eta chain gene (YWHAH)"; *Genomics* (1996), 36:63-69.

[165] Liu Z, Chen CY, Bonham AC: "Metabotropic glutamate receptors depress vagal and aortic baroreceptor signal transmission in the NTS"; *Am J Physiol* (1998), 275:H1682-1694.

[166] Hille B: "G protein-coupled mechanisms and nervous signaling"; *Neuron* (1992), 9:187-195.

[167] Absalom NL, Lewis TM, Schofield PR: "Mechanisms of channel gating of the ligand-gated ion channel superfamily inferred from protein structure"; *Exp Physiol* (2004), 89:145-153.

[168] Colquhoun D, Sivilotti LG: "Function and structure in glycine receptors and some of their relatives"; *Trends Neurosci* (2004), 27:337-344.

[169] Lester HA, Dibas MI, Dahan DS, Leite JF, Dougherty DA: "Cys-loop receptors: new twists and turns"; *Trends Neurosci* (2004), 27:329-336.

[170] Unwin N: "Refined structure of the nicotinic acetylcholine receptor at 4A resolution"; *J Mol Biol* (2005), 346:967-989.

[171] Grenningloh G, Gundelfinger E, Schmitt B, Betz H, Darlison MG, Barnard EA, Schofield PR, Seeburg PH: "Glycine vs GABA receptors"; *Nature* (1987), 330:25-26.

[172] Schofield PR, Darlison MG, Fujita N, Burt DR, Stephenson FA, Rodriguez H, Rhee LM, Ramachandran J, Reale V, Glencorse TA, et al.: "Sequence and functional expression of the GABA A receptor shows a ligand-gated receptor super-family"; *Nature* (1987), 328:221-227.

[173] Betz H: "Ligand-gated ion channels in the brain: the amino acid receptor superfamily"; *Neuron* (1990), 5:383-392.

[174] Green WN, Wanamaker CP: "The role of the cystine loop in acetylcholine receptor assembly"; *J Biol Chem* (1997), 272:20945-20953.

[175] Grutter T, de Carvalho LP, Dufresne V, Taly A, Edelstein SJ, Changeux JP: "Molecular tuning of fast gating in pentameric ligand-gated ion channels"; *Proc Natl Acad Sci U S A* (2005), 102:18207-18212.

[176] Sine SM: "The nicotinic receptor ligand binding domain"; *J Neurobiol* (2002), 53:431-446.

[177] Karlin A: "Emerging structure of the nicotinic acetylcholine receptors"; *Nat Rev Neurosci* (2002), 3:102-114.

[178] Sugiyama N, Boyd AE, Taylor P: "Anionic residue in the alpha-subunit of the nicotinic acetylcholine receptor contributing to subunit assembly and ligand binding"; *J Biol Chem* (1996), 271:26575-26581.

[179] Gelman MS, Chang W, Thomas DY, Bergeron JJ, Prives JM: "Role of the endoplasmic reticulum chaperone calnexin in subunit folding and assembly of nicotinic acetylcholine receptors"; *J Biol Chem* (1995), 270:15085-15092.

[180] Blount P, Merlie JP: "BIP associates with newly synthesized subunits of the mouse muscle nicotinic receptor"; *J Cell Biol* (1991), 113:1125-1132.

[181] Forsayeth JR, Gu Y, Hall ZW: "BiP forms stable complexes with unassembled subunits of the acetylcholine receptor in transfected COS cells and in C2 muscle cells"; *J Cell Biol* (1992), 117:841-847.

[182] Keller SH, Lindstrom J, Taylor P: "Involvement of the chaperone protein calnexin and the acetylcholine receptor beta-subunit in the assembly and cell surface expression of the receptor"; *J Biol Chem* (1996), 271:22871-22877.

[183] Keller SH, Lindstrom J, Taylor P: "Inhibition of glucose trimming with castanospermine reduces calnexin association and promotes proteasome degradation of the alpha-subunit of the nicotinic acetylcholine receptor"; *J Biol Chem* (1998), 273:17064-17072.

[184] Gottschalk A, Almedom RB, Schedletzky T, Anderson SD, Yates JR, Schafer WR: "Identification and characterization of novel nicotinic receptor-associated proteins in Caenorhabditis elegans"; *EMBO J* (2005), 24:2566-2578.

[185] Wanamaker CP, Christianson JC, Green WN: "Regulation of nicotinic acetylcholine receptor assembly"; *Ann N Y Acad Sci* (2003), 998:66-80.

[186] Wang JM, Zhang L, Yao Y, Viroonchatapan N, Rothe E, Wang ZZ: "A transmembrane motif governs the surface trafficking of nicotinic acetylcholine receptors"; *Nat Neurosci* (2002), 5:963-970.

[187] Whiting PJ, Lindstrom JM: "Characterization of bovine and human neuronal nicotinic acetylcholine receptors using monoclonal antibodies"; *J Neurosci* (1988), 8:3395-3404.

[188] Muslin AJ, Tanner JW, Allen PM, Shaw AS: "Interaction of 14-3-3 with signaling proteins is mediated by the recognition of phosphoserine"; *Cell* (1996), 84:889-897.

[189] Halevi S, McKay J, Palfreyman M, Yassin L, Eshel M, Jorgensen E, Treinin M: "The C. elegans ric-3 gene is required for maturation of nicotinic acetylcholine receptors"; *Embo J* (2002), 21:1012-1020.

[190] Eimer S, Gottschalk A, Hengartner M, Horvitz HR, Richmond J, Schafer WR, Bessereau JL: "Regulation of nicotinic receptor trafficking by the transmembrane Golgi protein UNC-50"; *Embo J* (2007), 26:4313-4323.

[191] DeChiara TM, Bowen DC, Valenzuela DM, Simmons MV, Poueymirou WT, Thomas S, Kinetz E, Compton DL, Rojas E, Park JS, et al.: "The receptor tyrosine kinase MuSK is required for neuromuscular junction formation in vivo"; *Cell* (1996), 85:501-512.

[192] Gautam M, Noakes PG, Moscoso L, Rupp F, Scheller RH, Merlie JP, Sanes JR: "Defective neuromuscular synaptogenesis in agrin-deficient mutant mice"; *Cell* (1996), 85:525-535.

[193] Gautam M, Noakes PG, Mudd J, Nichol M, Chu GC, Sanes JR, Merlie JP: "Failure of postsynaptic specialization to develop at neuromuscular junctions of rapsyn-deficient mice"; *Nature* (1995), 377:232-236.

[194] Sanes JR, Lichtman JW: "Induction, assembly, maturation and maintenance of a postsynaptic apparatus"; *Nat Rev Neurosci* (2001), 2:791-805.

[195] Wang ZZ, Mathias A, Gautam M, Hall ZW: "Metabolic stabilization of muscle nicotinic acetylcholine receptor by rapsyn"; *J Neurosci* (1999), 19:1998-2007.

[196] Gally C, Eimer S, Richmond JE, Bessereau JL: "A transmembrane protein required for acetylcholine receptor clustering in Caenorhabditis elegans"; *Nature* (2004), 431:578-582.

[197] Rapti G, Richmond J, Bessereau JL: "A single immunoglobulin-domain protein required for clustering acetylcholine receptors in C. elegans"; *Embo J* (2011), 30:706-718.

[198] Swope SL, Moss SI, Raymond LA, Huganir RL: "Regulation of ligand-gated ion channels by protein phosphorylation"; *Adv Second Messenger Phosphoprotein Res* (1999), 33:49-78.

[199] Khiroug L, Sokolova E, Giniatullin R, Afzalov R, Nistri A: "Recovery from desensitization of neuronal nicotinic acetylcholine receptors of rat chromaffin cells is modulated by intracellular calcium through distinct second messengers"; *J Neurosci* (1998), 18:2458-2466.

[200] Liu Q, Berg DK: "Actin filaments and the opposing actions of CaM kinase II and calcineurin in regulating alpha7-containing nicotinic receptors on chick ciliary ganglion neurons"; *J Neurosci* (1999), 19:10280-10288.

[201] Hedgecock EM, Culotti JG, Hall DH, Stern BD: "Genetics of cell and axon migrations in Caenorhabditis elegans"; *Development* (1987), 100:365-382.

[202] Avery L, Horvitz HR: "Pharyngeal pumping continues after laser killing of the pharyngeal nervous system of C. elegans"; *Neuron* (1989), 3:473-485.

[203] Avery L, Raizen D, Lockery S: "Electrophysiological methods"; *Methods Cell Biol* (1995), 48:251-269.

[204] Lockery SR, Goodman MB: "Tight-seal whole-cell patch clamping of Caenorhabditis elegans neurons"; *Methods Enzymol* (1998), 293:201-217.

[205] Goodman MB, Hall DH, Avery L, Lockery SR: "Active currents regulate sensitivity and dynamic range in C. elegans neurons"; *Neuron* (1998), 20:763-772.

[206] Demaurex N, Frieden M: "Measurements of the free luminal ER Ca(2+) concentration with targeted "cameleon" fluorescent proteins"; *Cell Calcium* (2003), 34:109-119.

[207] Nakai J, Ohkura M, Imoto K: "A high signal-to-noise Ca(2+) probe composed of a single green fluorescent protein"; *Nat Biotechnol* (2001), 19:137-141.

[208] Zhao Y, Araki S, Wu J, Teramoto T, Chang YF, Nakano M, Abdelfattah AS, Fujiwara M, Ishihara T, Nagai T, et al.: "An expanded palette of genetically encoded Ca(2) indicators"; *Science* (2011), 333:1888-1891.

[209] Tian L, Hires SA, Mao T, Huber D, Chiappe ME, Chalasani SH, Petreanu L, Akerboom J, McKinney SA, Schreiter ER, et al.: "Imaging neural activity in worms, flies and mice with improved GCaMP calcium indicators"; *Nat Methods* (2009), 6:875-881.

[210] Piggott BJ, Liu J, Feng Z, Wescott SA, Xu XZS: "The Neural Circuits and Synaptic Mechanisms Underlying Motor Initiation in C. elegans"; *Cell* (2011), 147:922-933.

[211] Kimble J: "Alterations in cell lineage following laser ablation of cells in the somatic gonad of Caenorhabditis elegans"; *Dev Biol* (1981), 87:286-300.

[212] Zheng Y, Brockie PJ, Mellem JE, Madsen DM, Maricq AV: "Neuronal control of locomotion in C. elegans is modified by a dominant mutation in the GLR-1 ionotropic glutamate receptor"; *Neuron* (1999), 24:347-361.

[213] Chelur DS, Chalfie M: "Targeted cell killing by reconstituted caspases"; *Proceedings of the National Academy of Sciences of the United States of America* (2007), 104:2283.

[214] Nhan TQ, Liles WC, Schwartz SM: "Physiological functions of caspases beyond cell death"; *Am J Pathol* (2006), 169:729-737.

[215] Miller KG, Alfonso A, Nguyen M, Crowell JA, Johnson CD, Rand JB: "A genetic selection for Caenorhabditis elegans synaptic transmission mutants"; *Proc Natl Acad Sci U S A* (1996), 93:12593-12598.

[216] Lewis JA, Wu CH, Levine JH, Berg H: "Levamisole-resistant mutants of the nematode Caenorhabditis elegans appear to lack pharmacological acetylcholine receptors"; *Neuroscience* (1980), 5:967-989.

[217] Callaway EM, Katz LC: "Photostimulation using caged glutamate reveals functional circuitry in living brain slices"; *Proc Natl Acad Sci U S A* (1993), 90:7661-7665.

[218] Szobota S, Gorostiza P, Del Bene F, Wyart C, Fortin DL, Kolstad KD, Tulyathan O, Volgraf M, Numano R, Aaron HL, et al.: "Remote control of neuronal activity with a light-gated glutamate receptor"; *Neuron* (2007), 54:535-545.

[219] Nagel G, Brauner M, Liewald JF, Adeishvili N, Bamberg E, Gottschalk A: "Light activation of channelrhodopsin-2 in excitable cells of Caenorhabditis elegans triggers rapid behavioral responses"; *Curr Biol* (2005), 15:2279-2284.

[220] Boyden ES, Zhang F, Bamberg E, Nagel G, Deisseroth K: "Millisecond-timescale, genetically targeted optical control of neural activity"; *Nat Neurosci* (2005), 8:1263-1268.

[221] Zhang F, Wang L, Brauner M, Liewald J, Kay K, Watzke N, Wood P, Bamberg E, Nagel G, Gottschalk A, et al.: "Multimodal fast optical interrogation of neural circuitry." *Nature* (2007), 446:633 - 639.

[222] Deisseroth K, Feng G, Majewska AK, Miesenbock G, Ting A, Schnitzer MJ: "Next-generation optical technologies for illuminating genetically targeted brain circuits"; *J Neurosci* (2006), 26:10380-10386.

[223] Xiang Y, Yuan Q, Vogt N, Looger LL, Jan LY, Jan YN: "Light-avoidance-mediating photoreceptors tile the Drosophila larval body wall"; *Nature* (2010), 468:921-926.

[224] Nagel G, Szellas T, Huhn W, Kateriya S, Adeishvili N, Berthold P, Ollig D, Hegemann P, Bamberg E: "Channelrhodopsin-2, a directly light-gated cation-selective membrane channel"; *Proc Natl Acad Sci U S A* (2003), 100:13940-13945.

[225] Hegemann P, Fuhrmann M, Kateriya S: "Algal sensory photoreceptors"; *Journal of Phycology* (2001), 37:668-676.

[226] Hausser M, Smith SL: "Neuroscience: controlling neural circuits with light"; *Nature* (2007), 446:617-619.

[227] Kateriya S, Nagel G, Bamberg E, Hegemann P: ""Vision" in single-celled algae"; *News Physiol Sci* (2004), 19:133-137.

[228] Bamberg E: "Retinal proteins light-gated ion channels and light-driven ion pumps and their application in neuro and cell biology"; *http://www.biophys.mpg.de/en/bamberg.html*.

[229] Nagel G, Szellas T, Kateriya S, Adeishvili N, Hegemann P, Bamberg E: "Channelrhodopsins: directly light-gated cation channels"; *Biochem Soc Trans* (2005), 33:863-866.

[230] Sineshchekov OA, Jung KH, Spudich JL: "Two rhodopsins mediate phototaxis to low- and high-intensity light in Chlamydomonas reinhardtii"; *Proc Natl Acad Sci U S A* (2002), 99:8689-8694.

[231] Stehfest K, Hegemann P: "Evolution of the channelrhodopsin photocycle model"; *Chemphyschem* (2010), 11:1120-1126.

[232] Radu I, Bamann C, Nack M, Nagel G, Bamberg E, Heberle J: "Conformational changes of channelrhodopsin-2"; *J Am Chem Soc* (2009), 131:7313-7319.

[233] Bamann C, Kirsch T, Nagel G, Bamberg E: "Spectral characteristics of the photocycle of channelrhodopsin-2 and its implication for channel function"; *J Mol Biol* (2008), 375:686-694.

[234] Ritter E, Stehfest K, Berndt A, Hegemann P, Bartl FJ: "Monitoring light-induced structural changes of Channelrhodopsin-2 by UV-visible and Fourier transform infrared spectroscopy"; *J Biol Chem* (2008), 283:35033-35041.

[235] Bamann C, Gueta R, Kleinlogel S, Nagel G, Bamberg E: "Structural guidance of the photocycle of channelrhodopsin-2 by an interhelical hydrogen bond"; *Biochemistry* (2010), 49:267-278.

[236] Feldbauer K, Zimmermann D, Pintschovius V, Spitz J, Bamann C, Bamberg E: "Channelrhodopsin-2 is a leaky proton pump"; *Proc Natl Acad Sci U S A* (2009), 106:12317-12322.

[237] Hegemann P, Ehlenbeck S, Gradmann D: "Multiple photocycles of channelrhodopsin"; *Biophys J* (2005), 89:3911-3918.

[238] Lin JY, Lin MZ, Steinbach P, Tsien RY: "Characterization of engineered channelrhodopsin variants with improved properties and kinetics"; *Biophys J* (2009), 96:1803-1814.

[239] Bruun S, Naumann H, Kuhlmann U, Schulz C, Stehfest K, Hegemann P, Hildebrandt P: "The chromophore structure of the long-lived intermediate of the C128T channelrhodopsin-2 variant"; *FEBS Lett* (2011).

[240] Stehfest K, Ritter E, Berndt A, Bartl F, Hegemann P: "The branched photocycle of the slow-cycling channelrhodopsin-2 mutant C128T"; *J Mol Biol* (2010), 398:690-702.

[241] Schoenenberger P, Gerosa D, Oertner TG: "Temporal control of immediate early gene induction by light"; *PLoS One* (2009), 4:e8185.

[242] Soliman GSH, Truper HG: "Halobacterium pharaonis sp. nov., a new, extremely haloalkaliphilic archaebacterium with low magnesium requirement"; *Zbl Bakt Hyg* (1982):318-329.

[243] Lanyi JK, Duschl A, Hatfield GW, May K, Oesterhelt D: "The primary structure of a halorhodopsin from Natronobacterium pharaonis. Structural, functional and evolutionary implications for bacterial rhodopsins and halorhodopsins"; *J Biol Chem* (1990), 265:1253-1260.

[244] Falb M, Pfeiffer F, Palm P, Rodewald K, Hickmann V, Tittor J, Oesterhelt D: "Living with two extremes: conclusions from the genome sequence of Natronomonas pharaonis"; *Genome Res* (2005), 15:1336-1343.

[245] Stoeckenius W: "The rhodopsin-like pigments of halobacteria: light-energy and signal transducers in an archaebacterium"; *Trends Biochem Sci* (1985), 10:483-486.

[246] Kouyama T, Kanada S, Takeguchi Y, Narusawa A, Murakami M, Ihara K: "Crystal structure of the light-driven chloride pump halorhodopsin from Natronomonas pharaonis"; *J Mol Biol* (2010), 396:564-579.

[247] Pettersen EF, Goddard TD, Huang CC, Couch GS, Greenblatt DM, Meng EC, Ferrin TE: "UCSF Chimera--a visualization system for exploratory research and analysis"; *J Comput Chem* (2004), 25:1605-1612.

[248] Duschl A, Lanyi JK, Zimanyi L: "Properties and photochemistry of a halorhodopsin from the haloalkalophile, Natronobacterium pharaonis"; *J Biol Chem* (1990), 265:1261-1267.

[249] Kulcsar A, Groma GI, Lanyi JK, Varo G: "Characterization of the proton-transporting photocycle of pharaonis halorhodopsin"; *Biophys J* (2000), 79:2705-2713.

[250] Chizhov I, Engelhard M: "Temperature and halide dependence of the photocycle of halorhodopsin from Natronobacterium pharaonis"; *Biophys J* (2001), 81:1600-1612.

[251] Hackmann C, Guijarro J, Chizhov I, Engelhard M, Rodig C, Siebert F: "Static and time-resolved step-scan Fourier transform infrared investigations of the photoreaction of halorhodopsin from Natronobacterium pharaonis: consequences for models of the anion translocation mechanism"; *Biophys J* (2001), 81:394-406.

[252] Shibata M, Saito Y, Demura M, Kandori H: "Deprotonation of Glu234 during the photocycle of Natronomonas pharaonis halorhodopsin"; *Chemical Physics Letters* (2006), 432:545-547.

[253] Han X, Qian X, Bernstein JG, Zhou HH, Franzesi GT, Stern P, Bronson RT, Graybiel AM, Desimone R, Boyden ES: "Millisecond-timescale optical control of neural dynamics in the nonhuman primate brain"; *Neuron* (2009), 62:191-198.

[254] Zhang F, Wang LP, Boyden ES, Deisseroth K: "Channelrhodopsin-2 and optical control of excitable cells"; *Nat Methods* (2006), 3:785-792.

[255] Gradinaru V, Thompson KR, Deisseroth K: "eNpHR: a Natronomonas halorhodopsin enhanced for optogenetic applications"; *Brain Cell Biol* (2008), 36:129-139.

[256] Gradinaru V, Zhang F, Ramakrishnan C, Mattis J, Prakash R, Diester I, Goshen I, Thompson KR, Deisseroth K: "Molecular and cellular approaches for diversifying and extending optogenetics"; *Cell* (2010), 141:154-165.

[257] Gunaydin LA, Yizhar O, Berndt A, Sohal VS, Deisseroth K, Hegemann P: "Ultrafast optogenetic control"; *Nat Neurosci* (2010), 13:387-392.

[258] Freund TF: "Interneuron Diversity series: Rhythm and mood in perisomatic inhibition"; *Trends Neurosci* (2003), 26:489-495.

[259] Berndt A, Schoenenberger P, Mattis J, Tye KM, Deisseroth K, Hegemann P, Oertner TG: "High-efficiency channelrhodopsins for fast neuronal stimulation at low light levels"; *Proc Natl Acad Sci U S A* (2011), 108:7595-7600.

[260] Kleinlogel S, Feldbauer K, Dempski RE, Fotis H, Wood PG, Bamann C, Bamberg E: "Ultra light-sensitive and fast neuronal activation with the Ca(2)+-permeable channelrhodopsin CatCh"; *Nat Neurosci* (2011), 14:513-518.

[261] Berndt A, Yizhar O, Gunaydin LA, Hegemann P, Deisseroth K: "Bi-stable neural state switches"; *Nat Neurosci* (2009), 12:229-234.

[262] Gordeliy VI, Labahn J, Moukhametzianov R, Efremov R, Granzin J, Schlesinger R, Buldt G, Savopol T, Scheidig AJ, Klare JP, et al.: "Molecular basis of transmembrane signalling by sensory rhodopsin II-transducer complex"; *Nature* (2002), 419:484-487.

[263] Waschuk SA, Bezerra AG, Jr., Shi L, Brown LS: "Leptosphaeria rhodopsin: bacteriorhodopsin-like proton pump from a eukaryote"; *Proc Natl Acad Sci U S A* (2005), 102:6879-6883.

[264] Chow BY, Han X, Dobry AS, Qian X, Chuong AS, Li M, Henninger MA, Belfort GM, Lin Y, Monahan PE, et al.: "High-performance genetically targetable optical neural silencing by light-driven proton pumps"; *Nature* (2010), 463:98-102.

[265] Husson SJ, Liewald JF, Stirman JN, Lu H, Gottschalk A: "Microbial light-activatable proton pumps as circuit breakers to functionally dissect neuronal networks in C. elegans"; *submitted* (2011).

[266] Ernst OP, Sanchez Murcia PA, Daldrop P, Tsunoda SP, Kateriya S, Hegemann P: "Photoactivation of channelrhodopsin"; *J Biol Chem* (2008), 283:1637-1643.

[267] Zhang F, Prigge M, Beyriere F, Tsunoda SP, Mattis J, Yizhar O, Hegemann P, Deisseroth K: "Red-shifted optogenetic excitation: a tool for fast neural control derived from Volvox carteri"; *Nat Neurosci* (2008), 11:631-633.

[268] Govorunova EG, Spudich EN, Lane CE, Sineshchekov OA, Spudich JL: "New channelrhodopsin with a red-shifted spectrum and rapid kinetics from Mesostigma viride"; *MBio* (2011), 2:e00115-00111.

[269] Yizhar O, Fenno LE, Prigge M, Schneider F, Davidson TJ, O'Shea DJ, Sohal VS, Goshen I, Finkelstein J, Paz JT, et al.: "Neocortical excitation/inhibition balance in information processing and social dysfunction"; *Nature* (2011), 477:171-178.

[270] Erbguth K, Gottschalk A. Edited by; 2011.

[271] Wen L, Wang H, Tanimoto S, Egawa R, Matsuzaka Y, Mushiake H, Ishizuka T, Yawo H: "Opto-current-clamp actuation of cortical neurons using a strategically designed channelrhodopsin"; *PLoS One* (2010), 5:e12893.

[272] Yaroslavsky AN, Schulze PC, Yaroslavsky IV, Schober R, Ulrich F, Schwarzmaier HJ: "Optical properties of selected native and coagulated human brain tissues in vitro in the visible and near infrared spectral range"; *Phys Med Biol* (2002), 47:2059-2073.

[273] Ghetti F, Colombetti G, Lenci F, Campani E, Polacco E, Quaglia M: "Fluorescence of Euglena gracilis photoreceptor pigment: An in vivo microspectrofluorometric study"; *Photochem Photobiol* (1985), 42:29-33.

[274] Iseki M, Matsunaga S, Murakami A, Ohno K, Shiga K, Yoshida K, Sugai M, Takahashi T, Hori T, Watanabe M: "A blue-light-activated adenylyl cyclase mediates photoavoidance in Euglena gracilis"; *Nature* (2002), 415:1047-1051.

[275] Ntefidou M, Iseki M, Watanabe M, Lebert M, Hader DP: "Photoactivated adenylyl cyclase controls phototaxis in the flagellate Euglena gracilis"; *Plant Physiol* (2003), 133:1517-1521.

[276] Anderson S, Dragnea V, Masuda S, Ybe J, Moffat K, Bauer C: "Structure of a novel photoreceptor, the BLUF domain of AppA from Rhodobacter sphaeroides"; *Biochemistry* (2005), 44:7998-8005.

[277] Gauden M, van Stokkum IH, Key JM, Luhrs D, van Grondelle R, Hegemann P, Kennis JT: "Hydrogen-bond switching through a radical pair mechanism in a flavin-binding photoreceptor"; *Proc Natl Acad Sci U S A* (2006), 103:10895-10900.

[278] Schroder-Lang S, Schwarzel M, Seifert R, Strunker T, Kateriya S, Looser J, Watanabe M, Kaupp UB, Hegemann P, Nagel G: "Fast manipulation of cellular cAMP level by light in vivo"; *Nat Methods* (2007), 4:39-42.

[279] Nagahama T, Suzuki T, Yoshikawa S, Iseki M: "Functional transplant of photoactivated adenylyl cyclase (PAC) into Aplysia sensory neurons"; *Neurosci Res* (2007), 59:81-88.

[280] Haffner C, Frauli M, Topp S, Irmler M, Hofmann K, Regula J, Bally-Cuif L, Haass C: "Nicalin and its binding partner Nomo are novel Nodal signaling antagonists"; *EMBO J* (2004), 23:3041-3050.

[281] Haffner C, Dettmer U, Weiler T, Haass C: "The Nicastrin-like protein Nicalin regulates assembly and stability of the Nicalin-nodal modulator (NOMO) membrane protein complex"; *J Biol Chem* (2007), 282:10632-10638.

[282] Macosko EZ, Pokala N, Feinberg EH, Chalasani SH, Butcher RA, Clardy J, Bargmann CI: "A hub-and-spoke circuit drives pheromone attraction and social behaviour in C. elegans"; *Nature* (2009), 458:1171-1175.

[283] Voutev R, Hubbard EJ: "A "FLP-Out" system for controlled gene expression in Caenorhabditis elegans"; *Genetics* (2008), 180:103-119.

[284] Davis MW, Morton JJ, Carroll D, Jorgensen EM: "Gene activation using FLP recombinase in C. elegans"; *PLoS Genet* (2008), 4:e1000028.

[285] Bucher D, Buchner E: "Stimulating PACalpha increases miniature excitatory junction potential frequency at the Drosophila neuromuscular junction"; *J Neurogenet* (2009), 23:220-224.

[286] Liewald JF, Brauner M, Stephens GJ, Bouhours M, Schultheis C, Zhen M, Gottschalk A: "Optogenetic analysis of synaptic function"; *Nat Methods* (2008), 5:895-902.

[287] Liu Q, Chen B, Yankova M, Morest DK, Maryon E, Hand AR, Nonet ML, Wang ZW: "Presynaptic ryanodine receptors are required for normal quantal size at the Caenorhabditis elegans neuromuscular junction"; *J Neurosci* (2005), 25:6745-6754.

[288] Broadie K, Bellen HJ, DiAntonio A, Littleton JT, Schwarz TL: "Absence of synaptotagmin disrupts excitation-secretion coupling during synaptic transmission"; *Proc Natl Acad Sci U S A* (1994), 91:10727-10731.

[289] Geppert M, Goda Y, Hammer RE, Li C, Rosahl TW, Stevens CF, Sudhof TC: "Synaptotagmin I: a major Ca2+ sensor for transmitter release at a central synapse"; *Cell* (1994), 79:717-727.

[290] Ringstad N, Nemoto Y, De Camilli P: "The SH3p4/Sh3p8/SH3p13 protein family: binding partners for synaptojanin and dynamin via a Grb2-like Src homology 3 domain"; *Proc Natl Acad Sci U S A* (1997), 94:8569-8574.

[291] Haffner C, Takei K, Chen H, Ringstad N, Hudson A, Butler MH, Salcini AE, Di Fiore PP, De Camilli P: "Synaptojanin 1: localization on coated endocytic

intermediates in nerve terminals and interaction of its 170 kDa isoform with Eps15"; *FEBS Lett* (1997), 419:175-180.

[292] Bettler B, Kaupmann K, Mosbacher J, Gassmann M: "Molecular structure and physiological functions of GABA(B) receptors"; *Physiol Rev* (2004), 84:835-867.

[293] Luscher C, Jan LY, Stoffel M, Malenka RC, Nicoll RA: "G protein-coupled inwardly rectifying K+ channels (GIRKs) mediate postsynaptic but not presynaptic transmitter actions in hippocampal neurons"; *Neuron* (1997), 19:687-695.

[294] Schuler V, Luscher C, Blanchet C, Klix N, Sansig G, Klebs K, Schmutz M, Heid J, Gentry C, Urban L, et al.: "Epilepsy, hyperalgesia, impaired memory, and loss of pre- and postsynaptic GABA(B) responses in mice lacking GABA(B(1))"; *Neuron* (2001), 31:47-58.

[295] Simonds WF: "G protein regulation of adenylate cyclase"; *Trends Pharmacol Sci* (1999), 20:66-73.

[296] Calver AR, Davies CH, Pangalos M: "GABA(B) receptors: from monogamy to promiscuity"; *Neurosignals* (2002), 11:299-314.

[297] Sakaba T, Neher E: "Direct modulation of synaptic vesicle priming by GABA(B) receptor activation at a glutamatergic synapse"; *Nature* (2003), 424:775-778.

[298] Vashlishan AB, Madison JM, Dybbs M, Bai J, Sieburth D, Ch'ng Q, Tavazoie M, Kaplan JM: "An RNAi screen identifies genes that regulate GABA synapses"; *Neuron* (2008), 58:346-361.

[299] Abramoff MD, Magelhaes PJ, Ram SJ: "Image Processing with ImageJ"; *Biophotonics International* (2004), 11:36-42.

[300] Team RDC: *R: A Language and Environment for Statistical Computing*; 2008.

[301] Stirman JN, Crane MM, Husson SJ, Wabnig S, Schultheis C, Gottschalk A, Lu H: "Real-time multimodal optical control of neurons and muscles in freely behaving Caenorhabditis elegans"; *Nat Methods* (2011), 8:153-158.

[302] Wicks SR, Rankin CH: "Integration of mechanosensory stimuli in Caenorhabditis elegans"; *J Neurosci* (1995), 15:2434-2444.

[303] Fielenbach N, Antebi A: "C. elegans dauer formation and the molecular basis of plasticity"; *Genes Dev* (2008), 22:2149-2165.

[304] Schackwitz WS, Inoue T, Thomas JH: "Chemosensory neurons function in parallel to mediate a pheromone response in C. elegans"; *Neuron* (1996), 17:719-728.

[305] Birnby DA, Link EM, Vowels JJ, Tian H, Colacurcio PL, Thomas JH: "A Transmembrane Guanylyl Cyclase (DAF-11) and Hsp90 (DAF-21) Regulate a Common Set of Chemosensory Behaviors in Caenorhabditis elegans"; *Genetics* (2000), 155:85-104.

[306] Kim K, Sato K, Shibuya M, Zeiger DM, Butcher RA, Ragains JR, Clardy J, Touhara K, Sengupta P: "Two chemoreceptors mediate developmental effects of dauer pheromone in C. elegans"; *Science* (2009), 326:994-998.

[307] Vowels JJ, Thomas JH: "Multiple chemosensory defects in daf-11 and daf-21 mutants of Caenorhabditis elegans"; *Genetics* (1994), 138:303-316.

[308] Bargmann CI, Horvitz HR: "Control of larval development by chemosensory neurons in Caenorhabditis elegans"; *Science* (1991), 251:1243-1246.

[309] Zhong Y, Budnik V, Wu CF: "Synaptic plasticity in Drosophila memory and hyperexcitable mutants: role of cAMP cascade"; *J Neurosci* (1992), 12:644-651.

[310] Mansuy IM, Mayford M, Jacob B, Kandel ER, Bach ME: "Restricted and regulated overexpression reveals calcineurin as a key component in the transition from short-term to long-term memory"; *Cell* (1998), 92:39-49.

[311] Berger AJ, Hart AC, Kaplan JM: "G alphas-induced neurodegeneration in Caenorhabditis elegans"; *J Neurosci* (1998), 18:2871-2880.

[312] Kaiser M, Varier S: "Evolution and development of Brain Networks: From Caenorhabditis elegans to Homo sapiens"; *Network: Computation in Neural Systems* (2011), 22:143-147.

[313] Sieburth D, Ch'ng Q, Dybbs M, Tavazoie M, Kennedy S, Wang D, Dupuy D, Rual JF, Hill DE, Vidal M, et al.: "Systematic analysis of genes required for synapse structure and function"; *Nature* (2005), 436:510-517.

[314] Crane MM, Chung K, Stirman J, Lu H: "Microfluidics-enabled phenotyping, imaging, and screening of multicellular organisms"; *Lab Chip* (2010), 10:1509-1517.

[315] Stirman JN, Brauner M, Gottschalk A, Lu H: "High-throughput study of synaptic transmission at the neuromuscular junction enabled by optogenetics and microfluidics"; *J Neurosci Methods* (2010), 191:90-93.

[316] Slepnev VI, De Camilli P: "Accessory factors in clathrin-dependent synaptic vesicle endocytosis"; *Nat Rev Neurosci* (2000), 1:161-172.

[317] Dittman J, Ryan TA: "Molecular circuitry of endocytosis at nerve terminals"; *Annu Rev Cell Dev Biol* (2009), 25:133-160.

[318] Heuser JE, Reese TS: "Evidence for recycling of synaptic vesicle membrane during transmitter release at the frog neuromuscular junction"; *J Cell Biol* (1973), 57:315-344.

[319] Richards DA, Guatimosim C, Betz WJ: "Two endocytic recycling routes selectively fill two vesicle pools in frog motor nerve terminals"; *Neuron* (2000), 27:551-559.

[320] Schultheis C: "Modifikation von Channelrhodopsin-2 und Halorhodopsin zur vereinfachten und zellspezifischeren Anwendung in erregbaren Zellen von Caenorhabditis elegans"; Diploma. Frankfurt: Goethe-University: 2007.

[321] Schertler GF, Bartunik HD, Michel H, Oesterhelt D: "Orthorhombic crystal form of bacteriorhodopsin nucleated on benzamidine diffracting to 3.6 A resolution"; *J Mol Biol* (1993), 234:156-164.

[322] Kolbe M, Besir H, Essen LO, Oesterhelt D: "Structure of the light-driven chloride pump halorhodopsin at 1.8 A resolution"; *Science* (2000), 288:1390-1396.

[323] Feinberg EH, Vanhoven MK, Bendesky A, Wang G, Fetter RD, Shen K, Bargmann CI: "GFP Reconstitution Across Synaptic Partners (GRASP) defines cell contacts and synapses in living nervous systems"; *Neuron* (2008), 57:353-363.

[324] Zhang S, Ma C, Chalfie M: "Combinatorial marking of cells and organelles with reconstituted fluorescent proteins"; *Cell* (2004), 119:137-144.

[325] Harbury PB, Kim PS, Alber T: "Crystal structure of an isoleucine-zipper trimer"; *Nature* (1994), 371:80-83.

[326] Ghosh I, Hamilton AD, Regan L: "Antiparallel leucine zipper-directed protein reassembly: application to the green fluorescent protein"; *Journal of the American Chemical Society* (2000), 122:5658-5659.

[327] Jansen G, Thijssen KL, Werner P, van der Horst M, Hazendonk E, Plasterk RH: "The complete family of genes encoding G proteins of Caenorhabditis elegans"; *Nat Genet* (1999), 21:414-419.

[328] Maricq AV, Peckol E, Driscoll M, Bargmann CI: "Mechanosensory signalling in C. elegans mediated by the GLR-1 glutamate receptor"; *Nature* (1995), 378:78-81.

[329] Schwarz V, Pan J, Voltmer-Irsch S, Hutter H: "IgCAMs redundantly control axon navigation in Caenorhabditis elegans"; *Neural Dev* (2009), 4:13.

[330] Kim K, Li C: "Expression and regulation of an FMRFamide-related neuropeptide gene family in Caenorhabditis elegans"; *J Comp Neurol* (2004), 475:540-550.

[331] Rogers C, Reale V, Kim K, Chatwin H, Li C, Evans P, de Bono M: "Inhibition of Caenorhabditis elegans social feeding by FMRFamide-related peptide activation of NPR-1"; *Nat Neurosci* (2003), 6:1178-1185.

[332] Schultheis C, Liewald JF, Bamberg E, Nagel G, Gottschalk A: "Optogenetic long-term manipulation of behavior and animal development"; *PLoS One* (2011), 6:e18766.

[333] O'Hagan R, Chalfie M, Goodman MB: "The MEC-4 DEG/ENaC channel of Caenorhabditis elegans touch receptor neurons transduces mechanical signals"; *Nat Neurosci* (2005), 8:43-50.

[334] Zhao Y, Araki S, Wu J, Teramoto T, Chang YF, Nakano M, Abdelfattah AS, Fujiwara M, Ishihara T, Nagai T, et al.: "An expanded palette of genetically encoded Ca(2+) indicators"; *Science* (2011), 333:1888-1891.

[335] Hilliard MA, Apicella AJ, Kerr R, Suzuki H, Bazzicalupo P, Schafer WR: "In vivo imaging of C. elegans ASH neurons: cellular response and adaptation to chemical repellents"; *Embo J* (2005), 24:63-72.

[336] Ezcurra M, Tanizawa Y, Swoboda P, Schafer WR: "Food sensitizes C. elegans avoidance behaviours through acute dopamine signalling"; *Embo J* (2011), 30:1110-1122.

[337] Chatzigeorgiou M, Schafer WR: "Lateral facilitation between primary mechanosensory neurons controls nose touch perception in C. elegans"; *Neuron* (2011), 70:299-309.

[338] Esposito G, Di Schiavi E, Bergamasco C, Bazzicalupo P: "Efficient and cell specific knock-down of gene function in targeted C. elegans neurons"; *Gene* (2007), 395:170-176.

[339] Stryer L: "Transducin and the cyclic GMP phosphodiesterase: amplifier proteins in vision"; *Cold Spring Harb Symp Quant Biol* (1983), 48 Pt 2:841-852.

[340] Stryer L: "The molecules of visual excitation"; *Sci Am* (1987), 257:42-50.

[341] Colbert HA, Bargmann CI: "Odorant-specific adaptation pathways generate olfactory plasticity in C. elegans"; *Neuron* (1995), 14:803-812.

[342] Saeki S, Yamamoto M, Iino Y: "Plasticity of chemotaxis revealed by paired presentation of a chemoattractant and starvation in the nematode Caenorhabditis elegans"; *J Exp Biol* (2001), 204:1757-1764.

[343] Chao MY, Komatsu H, Fukuto HS, Dionne HM, Hart AC: "Feeding status and serotonin rapidly and reversibly modulate a Caenorhabditis elegans chemosensory circuit"; *Proc Natl Acad Sci U S A* (2004), 101:15512-15517.

[344] Rankin CH, Beck CD, Chiba CM: "Caenorhabditis elegans: a new model system for the study of learning and memory"; *Behav Brain Res* (1990), 37:89-92.

[345] Rose JK, Rankin CH: "Analyses of habituation in Caenorhabditis elegans"; *Learn Mem* (2001), 8:63-69.

[346] Colbert HA, Bargmann CI: "Environmental signals modulate olfactory acuity, discrimination, and memory in Caenorhabditis elegans"; *Learn Mem* (1997), 4:179-191.

[347] Wicks SR, Rankin CH: "Effects of tap withdrawal response habituation on other withdrawal behaviors: the localization of habituation in the nematode Caenorhabditis elegans"; *Behav Neurosci* (1997), 111:342-353.

[348] Cheung BH, Cohen M, Rogers C, Albayram O, de Bono M: "Experience-dependent modulation of C. elegans behavior by ambient oxygen"; *Curr Biol* (2005), 15:905-917.

[349] Sanyal S, Wintle RF, Kindt KS, Nuttley WM, Arvan R, Fitzmaurice P, Bigras E, Merz DC, Hebert TE, van der Kooy D, et al.: "Dopamine modulates the plasticity of mechanosensory responses in Caenorhabditis elegans"; *Embo J* (2004), 23:473-482.

[350] Kindt KS, Quast KB, Giles AC, De S, Hendrey D, Nicastro I, Rankin CH, Schafer WR: "Dopamine mediates context-dependent modulation of sensory plasticity in C. elegans"; *Neuron* (2007), 55:662-676.

[351] Gannon TN, Rankin CH: "Methods of studying behavioral plasticity in Caenorhabditis elegans"; *Methods Cell Biol* (1995), 48:205-223.

[352] Mah KB, Rankin CH: "An analysis of behavioral plasticity in male Caenorhabditis elegans"; *Behav Neural Biol* (1992), 58:211-221.

[353] Muller M, Bamann C, Bamberg E, Kuhlbrandt W: "Projection structure of channelrhodopsin-2 at 6 a resolution by electron crystallography"; *J Mol Biol* (2011), 414:86-95.

[354] Ryu MH, Moskvin OV, Siltberg-Liberles J, Gomelsky M: "Natural and engineered photoactivated nucleotidyl cyclases for optogenetic applications"; *J Biol Chem* (2010), 285:41501-41508.

[355] Stierl M, Stumpf P, Udwari D, Gueta R, Hagedorn R, Losi A, Gartner W, Petereit L, Efetova M, Schwarzel M, et al.: "Light modulation of cellular cAMP by a small bacterial photoactivated adenylyl cyclase, bPAC, of the soil bacterium Beggiatoa"; *J Biol Chem* (2011), 286:1181-1188.

[356] Fesenko EE, Kolesnikov SS, Lyubarsky AL: "Induction by cyclic GMP of cationic conductance in plasma membrane of retinal rod outer segment"; *Nature* (1985), 313:310-313.

[357] Furchgott RF, Zawadzki JV: "The obligatory role of endothelial cells in the relaxation of arterial smooth muscle by acetylcholine"; *Nature* (1980), 288:373-376.

[358] Rapoport RM, Waldman SA, Ginsburg R, Molina CR, Murad F: "Effects of glyceryl trinitrate on endothelium-dependent and -independent relaxation and cyclic GMP levels in rat aorta and human coronary artery"; *J Cardiovasc Pharmacol* (1987), 10:82-89.

[359] Inada H, Ito H, Satterlee J, Sengupta P, Matsumoto K, Mori I: "Identification of guanylyl cyclases that function in thermosensory neurons of Caenorhabditis elegans"; *Genetics* (2006), 172:2239-2252.

[360] Hallem EA, Spencer WC, McWhirter RD, Zeller G, Henz SR, Ratsch G, Miller DM, 3rd, Horvitz HR, Sternberg PW, Ringstad N: "Receptor-type guanylate cyclase is required for carbon dioxide sensation by Caenorhabditis elegans"; *Proc Natl Acad Sci U S A* (2011), 108:254-259.

[361] Michel JJ, Scott JD: "AKAP mediated signal transduction"; *Annu Rev Pharmacol Toxicol* (2002), 42:235-257.

[362] Chen Q, Lin RY, Rubin CS: "Organelle-specific targeting of protein kinase AII (PKAII). Molecular and in situ characterization of murine A kinase anchor proteins that recruit regulatory subunits of PKAII to the cytoplasmic surface of mitochondria"; *J Biol Chem* (1997), 272:15247-15257.

[363] Dodge KL, Khouangsathiene S, Kapiloff MS, Mouton R, Hill EV, Houslay MD, Langeberg LK, Scott JD: "mAKAP assembles a protein kinase A/PDE4 phosphodiesterase cAMP signaling module"; *Embo J* (2001), 20:1921-1930.

[364] Pulver SR, Hornstein NJ, Land BL, Johnson BR: "Optogenetics in the teaching laboratory: using channelrhodopsin-2 to study the neural basis of behavior and synaptic physiology in Drosophila"; *Adv Physiol Educ* (2011), 35:82-91.

[365] Arrenberg AB, Del Bene F, Baier H: "Optical control of zebrafish behavior with halorhodopsin"; *Proc Natl Acad Sci U S A* (2009), 106:17968-17973.

[366] Larkin A, Karak S, Priya R, Das A, Ayyub C, Ito K, Rodrigues V, Ramaswami M: "Central synaptic mechanisms underlie short-term olfactory habituation in Drosophila larvae"; *Learn Mem* (2010), 17:645-653.

[367] Schroll C, Riemensperger T, Bucher D, Ehmer J, Voller T, Erbguth K, Gerber B, Hendel T, Nagel G, Buchner E, et al.: "Light-induced activation of distinct modulatory neurons triggers appetitive or aversive learning in Drosophila larvae"; *Curr Biol* (2006), 16:1741-1747.

[368] Douglass AD, Kraves S, Deisseroth K, Schier AF, Engert F: "Escape behavior elicited by single, channelrhodopsin-2-evoked spikes in zebrafish somatosensory neurons"; *Curr Biol* (2008), 18:1133-1137.

[369] Bellmann D, Richardt A, Freyberger R, Nuwal N, Schwarzel M, Fiala A, Stortkuhl KF: "Optogenetically Induced Olfactory Stimulation in Drosophila Larvae Reveals the Neuronal Basis of Odor-Aversion behavior"; *Front Behav Neurosci* (2010), 4:27.

[370] Stortkuhl KF, Fiala A: "The Smell of Blue Light: A New Approach toward Understanding an Olfactory Neuronal Network"; *Front Neurosci* (2011), 5:72.

[371] Mueller KP, Neuhauss SC: "Behavioral neurobiology: how larval fish orient towards the light"; *Curr Biol* (2010), 20:R159-161.

[372] Mueller KP, Neuhauss SC: "Quantitative measurements of the optokinetic response in adult fish"; *J Neurosci Methods* (2010), 186:29-34.

[373] Wang H, Peca J, Matsuzaki M, Matsuzaki K, Noguchi J, Qiu L, Wang D, Zhang F, Boyden E, Deisseroth K, et al.: "High-speed mapping of synaptic connectivity using photostimulation in Channelrhodopsin-2 transgenic mice"; *Proc Natl Acad Sci U S A* (2007), 104:8143-8148.

[374] Arenkiel BR, Peca J, Davison IG, Feliciano C, Deisseroth K, Augustine GJ, Ehlers MD, Feng G: "In vivo light-induced activation of neural circuitry in transgenic mice expressing channelrhodopsin-2"; *Neuron* (2007), 54:205-218.

[375] Zhao S, Cunha C, Zhang F, Liu Q, Gloss B, Deisseroth K, Augustine GJ, Feng G: "Improved expression of halorhodopsin for light-induced silencing of neuronal activity"; *Brain Cell Biol* (2008), 36:141-154.

[376] Yizhar O, Fenno LE, Davidson TJ, Mogri M, Deisseroth K: "Optogenetics in neural systems"; *Neuron* (2011), 71:9-34.

[377] Wentz CT, Bernstein JG, Monahan P, Guerra A, Rodriguez A, Boyden ES: "A wirelessly powered and controlled device for optical neural control of freely-behaving animals"; *J Neural Eng* (2011), 8:046021.

[378] Aravanis AM, Wang LP, Zhang F, Meltzer LA, Mogri MZ, Schneider MB, Deisseroth K: "An optical neural interface: in vivo control of rodent motor cortex with integrated fiberoptic and optogenetic technology"; *J Neural Eng* (2007), 4:S143-156.

[379] Witten IB, Lin SC, Brodsky M, Prakash R, Diester I, Anikeeva P, Gradinaru V, Ramakrishnan C, Deisseroth K: "Cholinergic interneurons control local circuit activity and cocaine conditioning"; *Science* (2010), 330:1677-1681.

[380] Tye KM, Prakash R, Kim SY, Fenno LE, Grosenick L, Zarabi H, Thompson KR, Gradinaru V, Ramakrishnan C, Deisseroth K: "Amygdala circuitry mediating reversible and bidirectional control of anxiety"; *Nature* (2011), 471:358-362.

[381] Bernstein JG, Han X, Henninger MA, Ko EY, Qian X, Franzesi GT, McConnell JP, Stern P, Desimone R, Boyden ES: "Prosthetic systems for therapeutic optical activation and silencing of genetically-targeted neurons"; *Proc Soc Photo Opt Instrum Eng* (2008), 6854:68540H.

[382] Abbott SB, Stornetta RL, Fortuna MG, Depuy SD, West GH, Harris TE, Guyenet PG: "Photostimulation of retrotrapezoid nucleus phox2b-expressing neurons in vivo produces long-lasting activation of breathing in rats"; *J Neurosci* (2009), 29:5806-5819.

[383] Adamantidis AR, Zhang F, Aravanis AM, Deisseroth K, de Lecea L: "Neural substrates of awakening probed with optogenetic control of hypocretin neurons"; *Nature* (2007), 450:420-424.

[384] Johansen JP, Wolff SB, Luthi A, Ledoux JE: "Controlling the Elements: An Optogenetic Approach to Understanding the Neural Circuits of Fear"; *Biol Psychiatry* (2011).

[385] Haubensak W, Kunwar PS, Cai H, Ciocchi S, Wall NR, Ponnusamy R, Biag J, Dong HW, Deisseroth K, Callaway EM, et al.: "Genetic dissection of an amygdala microcircuit that gates conditioned fear"; *Nature* (2011), 468:270-276.

[386] Gradinaru V, Mogri M, Thompson KR, Henderson JM, Deisseroth K: "Optical deconstruction of parkinsonian neural circuitry"; *Science* (2009), 324:354-359.

[387] Covington HE, 3rd, Lobo MK, Maze I, Vialou V, Hyman JM, Zaman S, LaPlant Q, Mouzon E, Ghose S, Tamminga CA, et al.: "Antidepressant effect of optogenetic stimulation of the medial prefrontal cortex"; *J Neurosci* (2010), 30:16082-16090.

[388] Busskamp V, Duebel J, Balya D, Fradot M, Viney TJ, Siegert S, Groner AC, Cabuy E, Forster V, Seeliger M, et al.: "Genetic reactivation of cone photoreceptors restores visual responses in retinitis pigmentosa"; *Science* (2010), 329:413-417.

[389] Kravitz AV, Freeze BS, Parker PR, Kay K, Thwin MT, Deisseroth K, Kreitzer AC: "Regulation of parkinsonian motor behaviours by optogenetic control of basal ganglia circuitry"; *Nature* (2010), 466:622-626.

[390] Zhang F, Aravanis AM, Adamantidis A, de Lecea L, Deisseroth K: "Circuit-breakers: optical technologies for probing neural signals and systems"; *Nat Rev Neurosci* (2007), 8:577-581.

[391] Brauner M: "Entwicklung optogenetischer Methoden zur Erforschung des Nervensystems des Nematoden Caenorhabditis elegans"; PhD. Frankfurt: Goethe-University Frankfurt: 2010.

[392] Emanuelsson O, Brunak S, von Heijne G, Nielsen H: "Locating proteins in the cell using TargetP, SignalP and related tools"; *Nat Protoc* (2007), 2:953-971.

[393] Thompson JD, Higgins DG, Gibson TJ: "CLUSTAL W: improving the sensitivity of progressive multiple sequence alignment through sequence weighting, position-specific gap penalties and weight matrix choice"; *Nucleic Acids Res* (1994), 22:4673-4680.

[394] Tusnady GE, Simon I: "The HMMTOP transmembrane topology prediction server"; *Bioinformatics* (2001), 17:849-850.

[395] Jones DT: "Improving the accuracy of transmembrane protein topology prediction using evolutionary information"; *Bioinformatics* (2007), 23:538-544.

[396] Notredame C, Higgins DG, Heringa J: "T-Coffee: A novel method for fast and accurate multiple sequence alignment"; *J Mol Biol* (2000), 302:205-217.

[397] Krogh A, Larsson B, von Heijne G, Sonnhammer EL: "Predicting transmembrane protein topology with a hidden Markov model: application to complete genomes"; *J Mol Biol* (2001), 305:567-580.

[398] Hirokawa T, Boon-Chieng S, Mitaku S: "SOSUI: classification and secondary structure prediction system for membrane proteins"; *Bioinformatics* (1998), 14:378-379.

9. <u>Abbreviations</u>

A	Ampère
Å	Ångström
aa	amino acid
ACh	acetylcholine
AChE	acetylcholine esterase
AChR	acetylcholine receptor
AMP	adenosine monophosphate
ATP	adenosine triphosphate
ATR	all-*trans* retinal
AZ	active zone
BLUF	sensor of blue light using FAD
bp	base pair
bPAC	*photoactivated adenylyl cyclase* from *Beggiatoa spec*
bPGC	*photoactivated guanylyl cyclase* from *Beggiatoa spec*
BR	Bacteriorhodopsin
BWM	body wall muscle cell
C. elegans	*Caenorhabditis elegans*
CaMKII	calmodulin-dependent protein kinase II
cAMP	cyclic adenosine monophosphate
CFP	cyan fluorescent protein
CGC	*Caenorhabditis* Genetics Center
cGMP	cyclic guanosine monophosphate
ChR1	Channelrhodopsin-1
ChR2	Channelrhodopsin-2
CNG	cyclic nucleotide gated
Cre	cyclization recombination
CRE	cAMP response element
CREB	cAMP response element binding
DAG	diacylglycerol
DIC	differential interference contrast
DNA	deoxyribonucleic acid
DNC	dorsal nerve cord
DPSS	diode pumped solid state laser
dsRNA	double-stranded RNA
e.g.	exempli gratia/for example
EM	electron microscopy

EMS	ethyl methane sulfonate
ER	endoplasmatic reticulum
ERAD	ER associated degradation
f	femto
FAD	flavin adenine dinucleotide
FMN	flavin mononucleotide
FRT	flippase recognition target
GABA	γ-amino butyric acid
GECI	genetically encoded calcium indicator
GEF	guanine nucleotide exchange factor
GFP	green fluorescent protein
GPCR	G-protein coupled receptor
HPF	high-pressure freeze
Hz	Hertz
IBMX	3-isobutyl-1-methylxanthin
k	kilo
L-AChR	levamisole-sensitive acetylcholine receptor
LGIC	ligand gated ion channel
m	milli/meter
µ	micro
MN	motorneuron
mPSC	miniature post-synaptic current
n	nano
nAChR	nicotinic acetylcholine receptor
N-AChR	nicotine-sensitive acetylcholine receptor
n.d.	not determined
NGM	nematode growth medium
NMJ	neuromuscular junction
NpHR	halorhodopsin from *Natronomonas pharaonis*
p	pico
PA	phosphatidic acid
PAB	autofluorescent paraxonemal body
PAC	*photoactivated adenylyl cyclase*
PCR	polymerase chain reaction
PDE	phosphodiesterase
PIP$_2$	phosphatidylinositol-4,5-bisphosphate
PLCβ	phospholipase Cβ
PKA	(cAMP-dependent) protein kinase A
PTP	post-tetanic potentiation

RGS	regulator of G-protein signaling
RNA	ribonucleic acid
RNAi	RNA-interference
RP	reserve pool
RRP	readily-releasable pool
RT	reverse transcriptase
s	second
S	Siemens
s.e.m.	standard error of the mean
SNAP25	synaptosomal-associated protein 25
SNARE	soluble n-ethyl-maleimide sensitive factor attachment receptor
SV	synaptic vesicle
TMP	trimethylpsoralen
UV	ultraviolet
VNC	ventral nerve cord
W	Watt
YFP	yellow fluorescent protein
ZX	systematic number of a *C. elegans* strain with in the Gottschalk-Lab
zxEx	systematic number of an extrachromosomal transgene
zxIs	systematic number of a genomically integrated transgene

10. Acknowledgements

11. Appendix

11.1. Additional material and methods

This section contains additional information about experiments that are presented in "*Discussion and outlook*" and that are not described in the attached publications.

11.1.1. *C. elegans* culture and transgenic animals

C. elegans were cultivated and prepared for experiments as described in publication V. Standard microinjection techniques were applied for the generation of transgenic animals. Unless stated differently, the following concentrations were used for injection markers: *lin-15$^+$*: 80 ng/µl; *rol-6d*: 80 ng/µl. Optionally, some transgenes were integrated into the genome using UV irradiation. The following strains were used (the concentration of plasmids in the injection mix is given in brackets; unless stated differently, *ChR2* refers to *ChR2(H134R)*):

No ZX-Number: *lin-15(n765ts$^-$); zxEx [pmyo3::ChR2 (Helix 1, Met1-Thr74) (50 ng/µl); pmyo-3::ChR2 (Helices 2-7, Lys76-Thr314) (50 ng/µl); lin-15$^+$]*

No ZX-Number: *lin-15(n765ts$^-$); zxEx [pmyo3::ChR2 (Helices 1-2, Met1-Pro105) (50 ng/µl); pmyo-3::ChR2 (Helices 3-7, Ser106-Thr314) (50 ng/µl); lin-15$^+$]*

No ZX-Number: *lin-15(n765ts$^-$); zxEx [pmyo3::ChR2 (Helices 1-2, Met1-Pro105) (50 ng/µl); pmyo-3::ChR2-SigSeq::ChR2 (Helices 3-7, Ser106-Thr314) (50 ng/µl); lin-15$^+$]*

No ZX-Number: *lin-15(n765ts$^-$); zxEx [pmyo3::ChR2 (Helices 1-5, Met1-Gly199) (50 ng/µl); pmyo3::ChR2 (Helices 6-7, Tyr200-Thr314) (50 ng/µl); lin-15$^+$]*

No ZX-Number: *lin-15(n765ts$^-$); zxEx [pmyo3::NpHR (Hel. 1-2; Met1-Gly88) (50 ng/µl); pmyo3::NpHR (Hel. 3-7; Leu89-Asp291)::eCFP (50 ng/µl); lin-15$^+$]*

No ZX-Number: *lin-15(n765ts$^-$); zxEx [pmyo3::pat-3 SigSeq::spGFP11::(GGGGS)1::NpHR (Hel. 3-7; His100-Asp291) (50 ng/µl); pmyo3::NpHR (Hel. 1-2; Met1-Gly99)::(GGGGS)1::spGFP1-10 (50 ng/µl); lin-15$^+$]*

No ZX-Number: *lin-15(n765ts$^-$); zxEx [pmyo3::pat-3 SigSeq::spGFP11:: (GGGGS)1::NpHR (Hel. 3-7; His100-Asp291) (50 ng/µl); pmyo3::NpHR SigSeq::NpHR (Hel. 1-2; Met1-Gly99)::(GGGGS)1::spGFP1-10 (50 ng/µl); lin-15$^+$]*

No ZX-Number: *lin-15(n765ts⁻); zxEx [pmyo3::pat-3 SigSeq::spGFP11::(GGGGS)2::NpHR (Hel. 3-7; His100-Asp291) (50 ng/µl); pmyo3::NpHR (Hel. 1-2; Met1-Gly99)::(GGGGS)2::spGFP1-10 (50 ng/µl); lin-15⁺]*

No ZX-Number: *lin-15(n765ts⁻); zxEx [pmyo3::pat-3 SigSeq::spGFP11::(GGGGS)2::NpHR (Hel. 3-7; His100-Asp291) (50 ng/µl); pmyo3::NpHR SigSeq::NpHR (Hel. 1-2; Met1-Gly99)::(GGGGS)2::spGFP1-10 (50 ng/µl); lin-15⁺]*

No ZX-Number: *lin-15(n765ts⁻); zxEx [pmyo3::NpHR (Hel. 1-2; Met1-Gly99) (50 ng/µl); pmyo3::NpHR (Hel. 3-7; His100-Asp291)::eCFP (50 ng/µl); lin-15⁺]*

No ZX-Number: *lin-15(n765ts⁻); zxEx [pgpa-14b::FLP recombinase (100 ng/µ); pglr-1::FRT::mCherry::FRT::ChR2(H134R)::YFP (100 ng/µ); lin-15⁺]*

No ZX-Number: *lin-15(n765ts⁻); zxEx [pglr-1::FLP recombinase (100 ng/µ); pgpa-14b::FRT::mCherry::FRT::ChR2(H134R)::YFP (100 ng/µ); lin-15⁺]*

No ZX-Number: *lin-15(n765ts⁻); zxEx [prig-3::FLP recombinase (100 ng/µ); pflp-18::FRT::mCherry::FRT::ChR2(H134R):YFP (100 ng/µ); lin-15⁺]*

No ZX-Number: *lin-15(n765ts⁻); zxEx [pflp-18::FLP recombinase (100 ng/µ); prig-3::FRT::mCherry::FRT::ChR2(H134R)::YFP (100 ng/µ); lin-15⁺]*

ZX460: N2; *zxIs6 [punc-17::ChR2(H134R)::YFP (80 ng/µ); lin-15⁺ (160 ng/µl)]*

ZX477: N2; *zxEx35 [pmyo3::nzYFP::ChR2 (Helices3-7; Ala111-Thr314) (100 ng/µl); pmyo3::ChR2 (Helices1-2; Met1-Leu110)::czCFP (100 ng/µl); rol-6d]*

ZX478: N2; *zxEx36 [pmyo3::ChR2-SigSeq::nzYFP::ChR2 (Helices3-7; Ala111-Thr314) (20 ng/µl); pmyo3::ChR2 (Helices1-2; Met1-Leu110)::czCFP (20 ng/µl); rol-6d]*

ZX480: N2; *zxEx38 [pmyo3::nzYFP::ChR2 (Helices4-7; Asn143-Thr314) (50 ng/µl); pmyo3::ChR2 (Helices1-3; Met1-Ser142)::czCFP (50 ng/µl); rol-6d]*

ZX481: N2; *zxEx39 [pmyo-3::nzYFP::ChR2 (Helices 6-7; Tyr200-Thr314) (50 ng/µl); pmyo3::ChR2 (Helices1-5; Met1-Gly199)::czCFP (50 ng/µl); rol-6d]*

ZX488: N2; *zxEx46 [pmyo3::NpHR (Helices1-3; Met1-Ser144) (100 ng/µl); pmyo-3::NpHR (Helices 4-7; Ser144-Asp291)::eCFP (100 ng/µl); rol-6d]*

ZX489: N2; *zxEx47 [pmyo3::NpHR-SigSeq::NpHR (Helices1-3; Met1-Ser144) (100 ng/µl); pmyo-3::NpHR (Helices 4-7; Ser144-Asp291)::eCFP (100 ng/µl); rol-6d]*

ZX511: *unc-26(s1710); zxIs6 [punc-17::ChR2(H134R)::YFP (80 ng/µ); lin-15⁺ (160 ng/µl)]*

ZX634:   *unc-57(e406); zxIs6 [punc-17::ChR2(H134R)::YFP (80 ng/µ); lin-15*[+] *(160 ng/µl)]*

ZX833:   *lin-15(n765ts*[-]*); lite-1 (ce314); zxEx702 [pgpa-14b::Cre recombinase (80 ng/µ); pglr-1::LoxP*::LacZ::LoxP::ChR2(H134R)::mCherry (80 ng/µ); lin-15*[+]*]*

ZX916:   N2; *zxIs6 [punc-17::ChR2(C128S)::YFP (100 ng/µ); lin-15*[+] *]*

ZX954:   *lin-15(n765ts*[-]*); zxEx468 [pmyo-3::ChR2(C128S; H134R)::YFP (80 ng/µ); lin-15*[+]*]*

Strain **ZX833** was generated by C. Schmitt; strains **ZX460**, **ZX511**, and **ZX634** were generated by M. Brauner [391]; strains **ZX477**, **ZX478**, **ZX480**, **ZX481**, **ZX488**, and **ZX489** were generated in the diploma thesis preceding this work [320].

11.1.2. Molecular biology

The following plasmids were kindly provided:

TU#712 (*nzYFP = YFP(aa1-157)::zipper*) (by M. Chalfie; [324]),

TU#715 (*czCFP = zipper::CFP(aa155-239)*) (by M. Chalfie; [324]),

spGFP1-10 (GFP(aa1-214)) (by C. Bargmann; [323]),

spGFP11 (pat-3-signalpeptide::GFP(aa215-230)) (by C. Bargmann; [323]),

pNM165   (*pglr-1::LoxP*::LacZ::LoxP::ChR2(H134R)::mCherry*) (by C. Bargmann; [282]),

pNP259 (*pgpa-14b::Cre recombinase*) (by C. Bargmann; [282]),

pWD172 (*FLP recombinase*) (by E. Jorgensen; [284]),

pWD178 (*FRT::mCherry::FRT::GFP*) (by E. Jorgensen; [284]),

The first 29 amino acids of the ChR2 primary structure were recognized as eukaryotic signal sequence by computational analysis (SignalP; [392]) and were referred to as ChR2-signal sequence. Similarly, using an alternative upstream start codon within the genome of *Natronomonas pharaonis* for expression of NpHR added additional 19 amino acids to the amino-terminus which were recognized as eukaryotic signal peptide using SignalP [392]. This sequence was termed NpHR-signal sequence.

Sites of fragmentation within ChR2(H134R) and NpHR were selected in loop-regions in order to minimize impact on functionality of the respective rhodopsin. For this, the primary structure of ChR2(H134R) and NpHR were aligned with the highly homologous rhodopsins of known structure – Bacteriorhodopsin [321] and

Halorhodopsin [322] from *Halobacterium salinarium* – using the tools ClustalW [393], HMMTOP [394], MEMSAT3 [395], and T-Coffee [396]. Furthermore, structural information about ChR2(H134R) was contributed by P. Wood and E. Bamberg from the Max-Planck Institute for Biophysics in Frankfurt (MPI-BP) and for NpHR by L. Forrest (MPI-BP). The topology of individual fragments was analyzed using the algorithms of TMHMM [397] and SOSUI [398].

The *glr-1* promoter was taken from **pCS106** (*pglr-1::ChR2(C128S)::YFP*; [332]) and the promoters *pflp-18* (4,15 kbps upstream of the start codon), and *prig-3* (3,1 kbps) were PCR-amplified from genomic *C. elegans* DNA. The plasmids **pAG54** (*pmyo-3::ChR2(H134R)::YFP*; [219]), **pCS10** (*pmyo-3::NpHR-Sigseq::NpHR::eCFP*; [320]), **pCS86** (*pmyo-3::ChR2(C128S)::YFP*; [332]) and plasmids/sequences described above were used to generate the following plasmids employing standard cloning techniques (unless stated differently *ChR2* refers to *ChR2(H134R)*):

pCS1: *pmyo3::nzYFP::ChR2 (Helices3-7; Ala111-Thr314)*

pCS1+: *pmyo3::ChR2-SigSeq::nzYFP::ChR2 (Helices3-7; Ala111-Thr314)*

pCS2: *pmyo3::ChR2 (Helices1-2; Met1-Leu110)::czCFP*

pCS3: *pmyo3::nzYFP::ChR2 (Helices4-7; Asn143-Thr314)*

pCS4: *pmyo3::ChR2 (Helices1-3; Met1-Ser142)::czCFP*

pCS5: *pmyo3::NpHR-SigSeq::NpHR::eCFP*

pCS6: *pmyo3::ChR2 (Helices1-5; Met1-Gly206)::czCFP*

pCS14: *pmyo3::NpHR (Helices1-3; Met1-Ser144)*

pCS14+: *pmyo3::NpHR-SigSeq::NpHR (Helices1-3; Met1-Ser144)*

pCS16: *pmyo-3::NpHR (Helices 4-7; Ser144-Asp291)::eCFP*

pCS20: *pmyo3::ChR2 (Helix 1, Met1-Thr74)*

pCS21: *pmyo3::ChR2 (Helices 1-2, Met1-Pro105)*

pCS22: *pmyo3::ChR2 (Helices 1-5, Met1-Gly199)*

pCS23: *pmyo-3::ChR2 (Helices 2-7, Lys76-Thr314)*

pCS24: *pmyo-3::ChR2 (Helices 3-7, Ser106-Thr314)*

pCS24+: *pmyo-3::ChR2-SigSeq::ChR2 (Helices 3-7, Ser106-Thr314)*

pCS25: *pmyo3::ChR2 (Helices 6-7, Tyr200-Thr314)*

pCS80: *pmyo3::NpHR (Hel. 1-2; Met1-Gly88)*

pCS82: *pmyo3::NpHR (Hel. 3-7; Leu89-Asp291)::eCFP*

pCS89: *pmyo3::pat-3 SigSeq::spGFP11::(GGGGS)$_1$::NpHR (Hel. 3-7; His100-Asp291)*

pCS89+: *pmyo3::pat-3 SigSeq::spGFP11::(GGGGS)$_2$::NpHR (Hel. 3-7; His100-Asp291)*

pCS90: *pmyo3::NpHR (Hel. 1-2; Met1-Gly99)::(GGGGS)$_1$::spGFP1-10*

pCS90+: *pmyo3::NpHR (Hel. 1-2; Met1-Gly99)::(GGGGS)$_2$::spGFP1-10*

pCS91: *pmyo3::NpHR SigSeq::NpHR (Hel. 1-2; Met1-Gly99)::(GGGGS)$_1$::spGFP1-10*

pCS91+: *pmyo3::NpHR SigSeq::NpHR (Hel. 1-2; Met1-Gly99)::(GGGGS)$_2$::spGFP1-10*

pCS92: *pmyo3::NpHR (Hel. 1-2; Met1-Gly99)*

pCS93: *pmyo3::NpHR SigSeq::NpHR (Hel. 1-2; Met1-Gly99)*

pCS94: *pmyo3::NpHR (Hel. 3-7; His100-Asp291)::eCFP*

pCS101: *pflp-18::FLP recombinase*

pCS102: *prig-3::FLP recombinase*

pCS116: *pmyo-3::ChR2(C128S; H134R)::YFP*

pCS131: *pflp-18::FRT::mCherry::FRT::ChR2:YFP*

pCS132: *prig-3::FRT::mCherry::FRT::ChR2:YFP*

pCS133: *pgpa-14b::FLP recombinase*

pCS134: *pglr-1::FLP recombinase*

pCS135: *pgpa-14b::FRT::mCherry::FRT::ChR2:YFP*

pCS136: *pglr-1::FRT::mCherry::FRT::ChR2:YFP*

The plasmids **pCS1**, **pCS1+**, **pCS2**, **pCS3**, **pCS4**, **pCS5**, **pCS6**, **pCS14**, **pCS14+,** and **pCS16** were generated in the diploma thesis preceding this work [320].

11.1.3. Behavioral experiments

Experiments were essentially performed as described in publication V. Light for excitation of rhodopsins was provided by an HB050 or HB0100 mercury bulb with joined band-pass filters (blue: 450-490 nm for excitation of ChR2 and variants; yellow: 565-595 nm for excitation of NpHR and inactivation of ChR2 variants; see [332]). Unless stated differently, intensities of light were adjusted to 2,2 mW/mm² (blue) and 6,9 mW/mm² (yellow), respectively. For optogenetic stimulation, single worms were placed on plain NGM-plates and recorded using a G5 or G9 digital

camera (Canon) coupled either to an Axiovert 40CFL or Axiovert 200 microscope (both Zeiss) with 10x magnification.

For electron-microscopic analyses, *C. elegans* expressing either ChR2(H134R) or ChR2(C128S) in cholinergic neurons were photostimulated for the indicated times using a DPSS Laser (473 nm; 22,6 mW/mm²; Pusch OptoTech) and a computer-controlled shutter (Sutter instruments) (performed by M. Brauner and C. Schultheis). Subsequent high-pressure freezing and electron-microscopic analyses were performed by J. Hegermann and M. Kittelmann as described recently [85]. Electrophysiological recordings from muscle cells were performed by J. Liewald as described in publication II.

For measurement of evoked contractions or relaxations of complementary fragments of ChR2(H134R) and NpHR, blue (1,6 mW/mm²) or yellow light (6,1 mW/mm²) was presented to transgenic animals. After extraction of single frames, the median of worms was analyzed manually for the last frame before and the frame including 566 ms of illumination using ImageJ. The change in body length is given by the ratio of both values. Notably, transgenic lines generated in the diploma thesis preceding this work were also analyzed in the course of the diploma thesis [320].

To determine responsiveness of animals expressing ChR2(H134R) in AVA, blue light was applied for one second to 30 forward moving animals per genotype and the fraction of reversing animals (that is reversals of more than half of the body length) was determined.

For measurement of repetitive excitability of single worms expressing ChR2(C128S) or (C128S; H134R) in muscle cells, animals were illuminated for two seconds every 15 minutes (6 times in total) with 0,2 mW/mm² of blue light. The mean body length for one second intervals directly before and four to five seconds after onset of illumination were measured as described in publication II to calculate the relative change of body length.

11.1.4. Statistics

Unless stated differently data are given as means ± standard error of the mean (s.e.m.).

An ER-resident membrane protein complex regulates nicotinic acetylcholine receptor subunit composition at the synapse

Ruta B Almedom[1,5], Jana F Liewald[1,5], Guillermina Hernando[2], Christian Schultheis[1], Diego Rayes[2], Jie Pan[3], Thorsten Schedletzky[1], Harald Hutter[3], Cecilia Bouzat[2] and Alexander Gottschalk[1,4,*]

[1]Department of Biochemistry, Chemistry and Pharmacy, Johann Wolfgang Goethe-University, Institute of Biochemistry, Frankfurt, Germany, [2]Instituto de Investigaciones Bioquimicas, Universidad Nacional del Sur-CONICET, Bahia Blanca, Argentina, [3]Department of Biological Sciences, Simon Fraser University, University Drive, Burnaby, British Columbia, Canada and [4]Cluster of Excellence Frankfurt—Macromolecular Complexes (CEF-MC), Goethe-University, Frankfurt, Germany

Nicotinic acetylcholine receptors (nAChRs) are homo- or heteropentameric ligand-gated ion channels mediating excitatory neurotransmission and muscle activation. Regulation of nAChR subunit assembly and transfer of correctly assembled pentamers to the cell surface is only partially understood. Here, we characterize an ER transmembrane (TM) protein complex that influences nAChR cell-surface expression and functional properties in *Caenorhabditis elegans* muscle. Loss of either type I TM protein, NRA-2 or NRA-4 (<u>n</u>icotinic <u>r</u>eceptor <u>a</u>ssociated), affects two different types of muscle nAChRs and causes *in vivo* resistance to cholinergic agonists. Sensitivity to subtype-specific agonists of these nAChRs is altered differently, as demonstrated by whole-cell voltage-clamp of dissected adult muscle, when applying exogenous agonists or after photo-evoked, channelrhodopsin-2 (ChR2) mediated acetylcholine (ACh) release, as well as in single-channel recordings in cultured embryonic muscle. These data suggest that nAChRs desensitize faster in *nra-2* mutants. Cell-surface expression of different subunits of the 'levamisole-sensitive' nAChR (L-AChR) is differentially affected in the absence of NRA-2 or NRA-4, suggesting that they control nAChR subunit composition or allow only certain receptor assemblies to leave the ER.

*Corresponding author. Department of Biochemistry, Johann Wolfgang Goethe-University Frankfurt, Cluster of Excellence Frankfurt—Macromolecular Complexes, Max-von-Laue-Str. 9, Frankfurt 60438, Germany. Tel.: +49 69 7982 9261; Fax: +49 69 7982 9495; E-mail: a.gottschalk@em.uni-frankfurt.de
[5]These authors contributed equally to this work

Introduction

Nicotinic acetylcholine receptors (nAChRs) are homo- or heteropentamers composed of α- and non-α-subunits, which mediate fast synaptic transmission in neurons and muscles (Changeux and Edelstein, 2005). The agonist binds at the interface between an α-subunit and either another α- or a non-α-subunit (Chiara and Cohen, 1997). Two or three acetylcholine (ACh) molecules need to bind for maximal activation (Karlin, 2002; Rayes *et al*, 2009); thus, functional properties of nAChRs are affected by the number of α-subunits, and the presence of particular subunits in the pentamer. In vertebrates, α-, β-, δ-, γ- and ε-subunits are found in muscle, and nAChRs are of $\alpha_2\beta\delta\gamma$ or $\alpha_2\beta\delta\epsilon$ composition, depending on the developmental stage (Mishina *et al*, 1986); in neurons, 9 α- and 3 β-subunits form α_5- or $\alpha_2\beta_3$-type receptors. The nAChR subunit repertoire of *Caenorhabditis elegans* is even more complex: its genome encodes 29 confirmed nAChR subunits (Jones *et al*, 2007), of which at least seven are expressed in muscle, based on microarray profiling and biochemical purification (Gottschalk *et al*, 2005; Touroutine *et al*, 2005; Fox *et al*, 2007). However, expression of additional nAChRs in muscle was demonstrated (Treinin *et al*, 1998).

Regulating nAChR subunit composition is an important way to fine-tune cholinergic signalling. Subunit combinations can be predetermined by cell-specific expression, and many potential assembly intermediates may be unstable due to incompatible subunit interfaces. In vertebrate neurons, a vast variety of nAChRs could be generated; however, only few combinations were detected experimentally (Gotti *et al*, 2007). Out of the 208 possible combinations of vertebrate muscle nAChR subunits, only one is found in mature muscle. To some extent, this is explained by sequence-specific interactions within the N-terminal, as well as the first transmembrane (TM) domains, according to different models (Gu *et al*, 1991; Kreienkamp *et al*, 1995; Wang *et al*, 1996; Keller and Taylor, 1999; Wanamaker *et al*, 2003). HSP70 chaperones and the ER quality control assist in nAChR assembly (Blount and Merlie, 1991; Keller *et al*, 1996, 1998; Keller and Taylor, 1999). The ER-resident TM protein RIC-3 and the Golgi-associated protein UNC-50 are also required for efficient nAChR assembly, maturation or trafficking from the ER and beyond (Halevi *et al*, 2002; Eimer *et al*, 2007), and 14-3-3 proteins further assist nAChRs in leaving the ER (Jeanclos *et al*, 2001). Immature assemblies and single subunits are retained in the ER, as they expose retention motifs in the first TM helix, which are masked only on closed pentamer formation (Wang *et al*, 2002). Yet, no factors are known that select particular subunits for incorporation into mature receptors, particularly in cells expressing many different nAChR subunits. It is further unknown whether there is active sorting that allows only particular nAChRs to exit the ER.

The *C. elegans* 'levamisole-sensitive' nAChR (L-AChR) is expressed in muscle cells, but some of its subunits are also found in neurons. Genetic screens based on levamisole-induced paralysis defined three essential subunits: UNC-38, UNC-63 (both α-subunits) and UNC-29 (non-α; Lewis *et al*, 1987; Fleming *et al*, 1997; Culetto *et al*, 2004). Additional L-AChR subunits, LEV-8 (α) and LEV-1 (non-α), are considered non-essential as their loss confers weak levamisole resistance (Lewis *et al*, 1987; Culetto *et al*, 2004; Towers *et al*, 2005). Co-expression of these five subunits in *Xenopus* oocytes, together with essential L-AChR biogenesis factors, RIC-3, UNC-50 and UNC-74, sufficed to constitute levamisole-activated currents (Boulin *et al*, 2008). An electrophysiologically defined 'nicotine-sensitive' N-AChR contributes to ACh currents at neuromuscular junctions (NMJs). This apparently homopentameric receptor consists of ACR-16 subunits (Francis *et al*, 2005; Touroutine *et al*, 2005).

To define proteins contributing to L-AChR function, we previously purified the L-AChR by tandem affinity purification and identified co-purified proteins by mass spectrometry (Gottschalk *et al*, 2005). In addition to the five genetically identified L-AChR subunits, we found two more α-subunits, ACR-8 and ACR-12. Although ACR-12 is expressed in neurons only, ACR-8 is expressed in body wall muscle cells. Thus, seven nAChR subunits are implicated in L-AChR function *in vivo*, suggesting that L-AChRs may represent a mixed population of pentamers with variable subunit composition, and/or that their composition could depend on the particular cell. Non-nAChR proteins that co-purified with the L-AChR were screened for effects on the *in vivo* sensitivity to cholinergic agonists (Gottschalk *et al*, 2005). Among proteins causing reduced agonist sensitivity was the product of gene T05F1.1, subsequently termed *nra-2*.

Here, we show that NRA-2, in complex with a second protein, NRA-4, acts in the ER to affect functional properties and subunit composition of L-AChRs expressed at synapses. Electrophysiological properties of L- and N-AChRs are altered in *nra-2* and *nra-4* mutants, as well as single-channel L-AChR properties in embryonic muscle, consistent with faster desensitization of L-AChRs. Synaptic expression of UNC-29 and, particularly, UNC-38 subunits are characteristically altered in *nra-2* and *nra-4* mutants. Mutations in *acr-8* suppress *nra-2* phenotypes, and synaptic expression of ACR-8 is increased in *nra-2* mutants, uncovering a reciprocal regulation of UNC-38 versus ACR-8 α-subunit incorporation into synaptic nAChRs by NRA-2. Thus, NRA-2 and NRA-4 affect L-AChR properties by altering subunit composition and/or the relative abundance of particular L-AChR subtypes at the synapse.

Results

NRA-2 and NRA-4 are type I TM proteins associated with L-AChRs

NRA-2 is a type I TM protein, consisting of a 518 amino acid (aa) luminal domain and an 18 aa cytosolic tail (Figure 1A and B), and contains a peptidase domain, likely inactive, as certain amino acids are non-conserved (Supplementary Figure 1). NRA-2 resembles vertebrate Nicalin (nicastrin-like protein; Supplementary Figures 2 and 3). Nicastrins are subunits of the integral membrane peptidase γ-secretase (Yu *et al*, 2000). Nicalin, which is not part of γ-secretase, antagonizes TGFβ signalling in an ill-defined manner, acting

in complex with a second type I TM protein, termed NOMO (nodal modulator) in the ER (Haffner *et al*, 2004, 2007). Nicalin and NOMO were shown to stabilize each other in this complex. Interestingly, the *C. elegans* homologue of NOMO (gene C02E11.1; Figure 1A; Supplementary Figures 4 and 5), was among the proteins we co-purified with the L-AChR (Gottschalk *et al*, 2005). We termed this protein NRA-4. NRA-4 has a 1068 aa luminal domain, a 30 aa cytosolic tail and no motifs suggesting a function (Figure 1B). Both *nra-2* and *nra-4* produce only single-splice variants, based on published ESTs (www.wormbase.org) and sequencing of full-length cDNAs obtained from Y Kohara. Deletion alleles of *nra-2* (*tm1453* and *ok1731*) and *nra-4* (*hd127* and *tm2656*) were obtained for further study (Figure 1; Supplementary Figures 2 and 4).

Mutants in *nra-2(ok1731)* were slightly uncoordinated, and *nra-2(ok1731)* and *nra-4(tm2656)* mutants showed reduced brood size (data not shown). The *nra-2* alleles truncate the NRA-2 protein C-terminal, leaving only 294 (*tm1453*) or 212 (*ok1731*) aa of the luminal domain (Supplementary Figure 6). Alleles of *nra-4* delete N- (*hd127*) or C-terminal (*tm2656*) sequences. *hd127* is predicted to remove 183 nt of the promoter and the first 48 aa, including a leader sequence (Figure 1; Supplementary Figure 6). As the second exon, unaffected by *hd127*, begins with an ATG, a protein without leader sequence could be made. RT–PCR analysis confirmed the presence of an *nra-4* transcript lacking exon 1 in *hd127* mutants (data not shown). However, it is unclear whether the truncated promoter expresses in the same tissues as the full-length promoter, or whether any functional protein is made in this mutant. The *nra-4(tm2656)* allele removes aa 816–920 of the luminal domain in-frame, leaving TM domain and cytosolic tail intact (Figure 1; Supplementary Figure 6). As most assays used in this work showed no phenotypes of *nra-4(tm2656)*, we consider it at most a reduction-of-function allele (see Supplementary Figure 7 for a summary of experiments involving *nra-4(tm2656)*).

NRA-2 and NRA-4 affect in vivo sensitivity to cholinergic, but not GABAergic agonists, and act cell autonomously in muscle

We tested the *nra-2* and *nra-4* mutants in paralysis assays for altered *in vivo* sensitivity to cholinergic agonists (nicotine and levamisole), and to aldicarb, an ACh-esterase inhibitor that causes ACh accumulation in the synaptic cleft. Both alleles of *nra-2* as well as *nra-4(hd127)* caused mild resistance to either drug, indicating reduced activity of muscle nAChRs (Figure 1C and D; Supplementary Figure 8). The paralysis phenotypes could be reversed by expression of the *nra-2* cDNA in muscle only (using *pmyo-3*), and *nra-4* under its own promoter, in the respective mutants (Figure 1C and D; Supplementary Figure 9A). Thus, at least NRA-2 acts cell autonomously in muscle. Double mutants of *nra-2* and *nra-4* (and double RNAi; data not shown) showed no exacerbation of the single-mutant effects in paralysis assays, indicating that NRA-2 and NRA-4 act in the same pathway.

To test whether NRA-2 and NRA-4 generally affect ligand-gated ion channels at the NMJ, we assayed function of the inhibitory GABA$_A$ receptor. Swimming behaviour was analysed in the presence of muscimol, a GABA$_A$R agonist that slows down swimming rate. Muscimol sensitivity was unaffected in *nra-2*, *nra-4* or *nra-2; nra-4* double mutants,
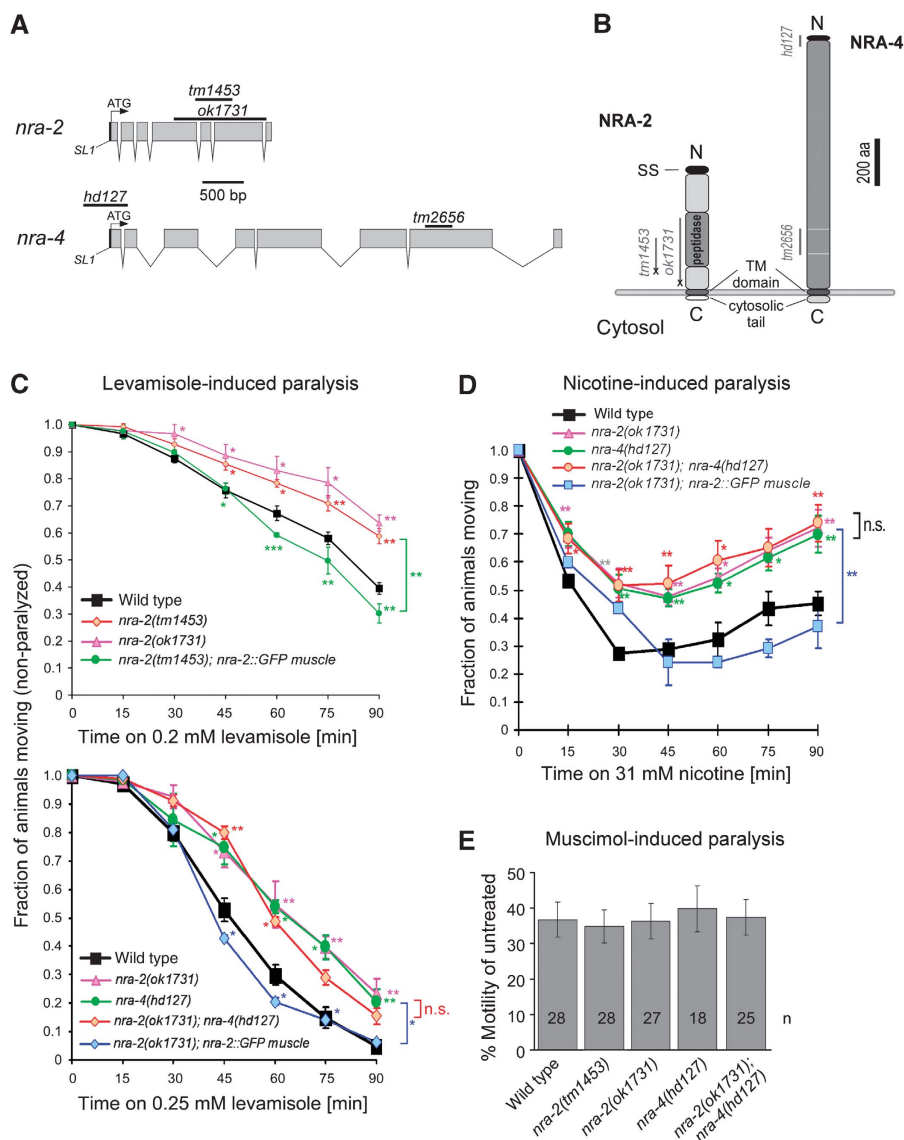
Figure 1 Cholinergic agonist-induced phenotypes are altered in *nra-2* and *nra-4* mutants, and rescued by muscle-specific expression. (**A**) The *nra-2* and *nra-4* genes, as annotated in www.wormbase.org, were confirmed by sequencing cDNAs kindly provided by Y Kohara. Sequences deleted in the alleles used are indicated by bars. (**B**) The *nra-2* and *nra-4* genes encode predicted type I TM proteins with signal sequences (SS), thus they are expected to be synthesized into the ER lumen, exposing a short C-terminal cytosolic tail. Deletion/insertion alleles *tm1453* and *ok1731* truncate NRA-2, bringing stop codons (X) in frame. *nra-4(hd127)* removes part of the promoter and exon I including SS and start codon and *tm2656* is a predicted in-frame deletion. (C, D) Paralysis time-course of wild-type and mutant animals exposed to 0.2 or 0.25 mM levamisole (**C**) or 31 mM nicotine (**D**). The fraction of non-paralyzed animals was counted every 15 min. Experiments were repeated 3–7 times (30 animals tested each time), data represent mean ± s.e.m., statistically significant differences to wild type are indicated (*$P < 0.05$; **$P < 0.01$; ***$P < 0.001$). Brackets indicate overall significant differences between genotypes, if they were different for at least three time points. (**E**) Swimming cycles of animals immersed for 1 h in M9 buffer with 8 mM muscimol, a GABA$_A$R agonist, were normalized to swimming cycles of untreated control animals.

indicating that *nra-2* and *nra-4* do not act on GABA$_A$Rs (Figure 1E).

Human Nicalin partially functions in C. elegans, likely independent of TGFβ signalling

The Nicalin/NOMO ER protein complex was shown to act in signalling through the *nodal* TGFβ pathway, but a potential function in vertebrate nAChR biology was not investigated (Haffner *et al*, 2004). We thus asked whether human Nicalin could rescue *nra-2* cholinergic phenotypes. Human Nicalin cDNA, fused to GFP, was expressed in muscle cells of *nra-2(ok1731)* mutants, which caused partial rescue of

levamisole and nicotine resistance phenotypes (Supplementary Figure 9B), indicating potential conservation of an nAChR-associated function of Nicalin. However, transgenic animals were small, slightly uncoordinated, and Nicalin::GFP partially aggregated (Supplementary Figure 9C), possibly preventing full rescue.

As *nra-2* and *nra-4* mutants may affect cholinergic signalling indirectly through TGFβ pathways, we tested mutants in these pathways for cholinergic phenotypes. *C. elegans* has five TGFβ ligands (Savage-Dunn, 2005): two are of unknown function, DAF-7 controls the dauer larval state (Ren *et al*, 1996), whereas DBL-1 affects body size (Suzuki *et al*, 1999)

and GABA signalling at the NMJ (Vashlishan *et al*, 2008), neither of which is altered in *nra-2* or *nra-4* mutants. UNC-129 affects dorsoventral axon guidance of some motor neurons, and could thus affect the NMJ (Colavita *et al*, 1998). We analysed levamisole and nicotine paralysis in the mutants *unc-129(ev554)*, *dbl-1(wk70)*, *daf-7(e1372)* and in TGFβ receptor mutants *daf-1(m402)* and *sma-6(wk7)* (Supplementary Figure 10A and B). *dbl-1(wk70)* and *sma-6(wk7)* animals were hypersensitive to nicotine and levamisole. For *dbl-1*, this was previously shown to be caused by a GABA signalling defect (Vashlishan *et al*, 2008). *sma-6(wk7)* mutants were sick and paralyzed immediately, likely indicating a cuticle defect. The other mutants had normal sensitivity to cholinergic agonists. Effects of *nra-2* and *nra-4* alleles on TGFβ signalling are most likely not causing the observed cholinergic defects, though we cannot completely rule out that the two TGFβ ligands of unknown function may affect NMJs.

NRA-2 and NRA-4 form a protein complex in the ER and co-localize with the L-AChR

NRA-2 and NRA-4 may affect nAChR biogenesis and/or function either in the ER, in which the vertebrate homologues form a complex, in the Golgi, the secretory pathway or at synapses. To determine the site of action of these proteins, we analysed their subcellular localization using fluorescent proteins as tags. NRA-2::GFP, NRA-2::mCherry and NRA-4::GFP showed a reticular pattern reminiscent of the ER in muscles (for NRA-2 and NRA-4; Figures 2 and 3) and other cells (for
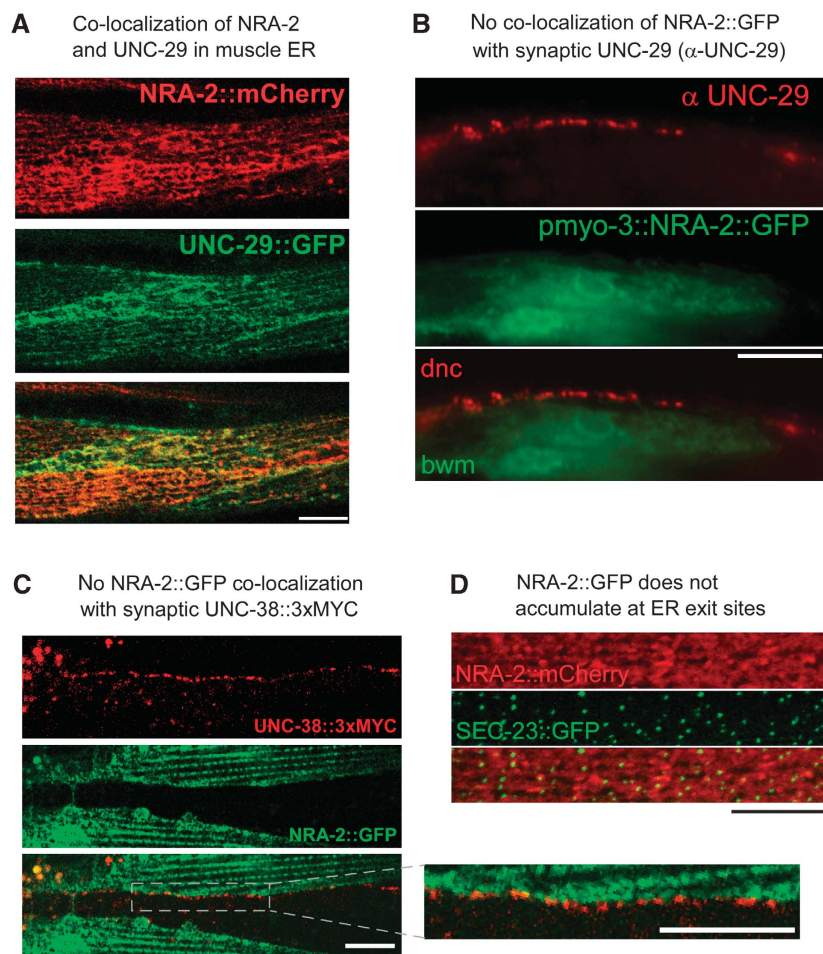
NRA-4::GFP only; Figure 2B; *pnra-4* and *pnra-2* are active in muscles, neurons and other tissues; Supplementary Figure 11). NRA-2::GFP also co-localized with an ER marker in HeLa cells (data not shown). To study whether NRA-2 and NRA-4 physically interact *in vivo*, we used bimolecular fluorescence complementation (BiFC; Chen *et al*, 2007; Shyu *et al*, 2008). Indeed, NRA-2 and NRA-4 interact within the ER membrane (Figure 2C), whereas NRA-4 and an unrelated control membrane protein, the stomatin UNC-1, do not (Figure 2D). Thus, NRA-2 and NRA-4 form a membrane protein complex in the ER of muscle cells, in which they may interact with nAChRs during biogenesis and assembly.

Consistent with this idea, NRA-2::mCherry and the L-AChR subunit UNC-29::GFP largely co-localized in ER membranes (Figure 3A). Although L-AChR subunits are visible in the ER only when over-expressed (endogenous L-AChRs are only detectable at synapses; Figure 3B; Gally *et al*, 2004), a diffuse localization of nascent nAChRs in the ER is not unexpected. Several additional observations argue against direct interactions of NRA-2/NRA-4 with L-AChRs at synapses: (1) NRA-2::GFP and NRA-4::GFP did not accumulate at the plasma membrane or the tips of muscle arms, in which NMJ postsynaptic elements are found (Gottschalk *et al*, 2005; Gottschalk and Schafer, 2006; Eimer *et al*, 2007). (2) The endogenous L-AChR subunit UNC-29 does not co-localize with NRA-2::GFP (Figure 3B). (3) NRA-2::GFP does not co-localize with the synaptic UNC-38::3xMYC L-AChR subunit (Figure 3C; the latter one immuno-labelled at the cell surface, using fluorescent antibodies
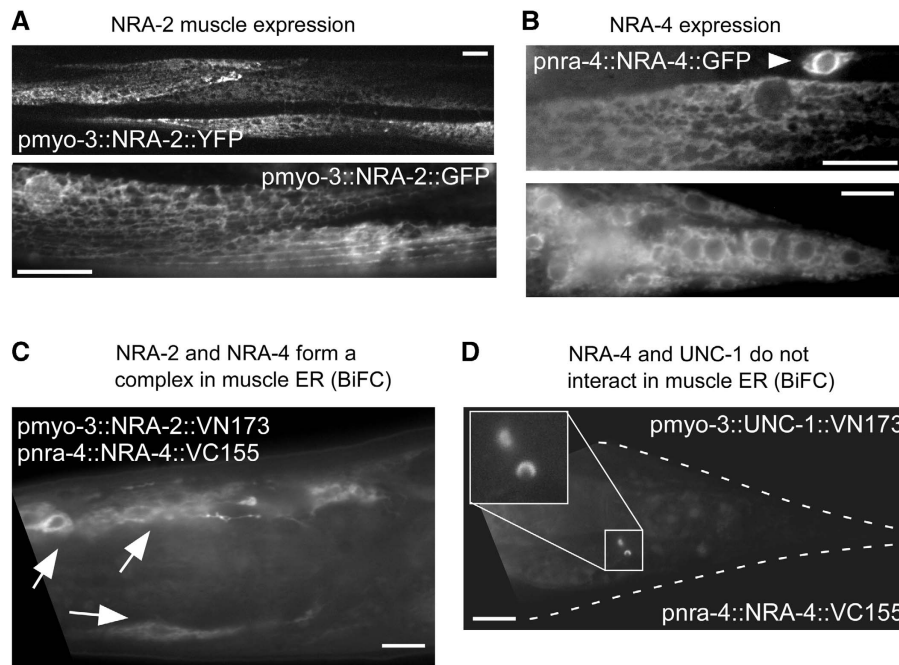
Figure 2 NRA-2 and NRA-4 are expressed in the ER and interact in a complex. (**A**) NRA-2::YFP (upper panel, single confocal plane) or NRA-2::GFP (lower panel, epifluorescence) were expressed from the muscle-specific *pmyo-3* promoter. Reticular expression, reminiscent of the ER was found. (**B**) NRA-4::GFP was expressed from the endogenous *pnra-4* promoter. Intracellular, reticular expression was observed in muscle cells (upper panel) and neurons (arrowhead), and in other tissues (lower panel: muscles, neurons and hypodermal cells in the tail). (**C**) NRA-2 and NRA-4 form a complex, as shown by bimolecular fluorescence complementation (BiFC). NRA-2 was fused to the VN173 fragment of Venus, and NRA-4 to the VC155 fragment. Fluorescence was restored in muscle ER (arrows point to muscle cell nuclei surrounded by ER), in which the two proteins were co-expressed. (**D**) NRA-4::VC155 does not interact in the ER with the stomatin UNC-1::VN173, expressed in muscle (a gift by ZW Wang). Occasionally, vesicular fluorescent structures were observed, possibly representing lysosomes in which the fusion proteins are degraded and in whose membranes their cytosolic tails (and Venus fragments) accumulate. Size bars are 10 μm.

A   Co-localization of NRA-2
       and UNC-29 in muscle ER

B   No co-localization of NRA-2::GFP
       with synaptic UNC-29 (α-UNC-29)

C   No NRA-2::GFP co-localization
       with synaptic UNC-38::3xMYC

D   NRA-2::GFP does not
       accumulate at ER exit sites

Figure 3 NRA-2 co-localizes with L-AChR subunits in the ER, but not at synapses. (**A**) NRA-2::mCherry (expressed from the *pmyo-3* promoter) was co-expressed with the L-AChR subunit UNC-29::GFP (expressed from *punc-29*) and co-localization was observed by confocal microscopy (single confocal plane of midbody muscle cells). (**B**) Endogenous UNC-29 protein was immunolabelled with specific antibodies in animals expressing NRA-2::GFP in muscles (GFP fluorescence was preserved during fixation). Dorsal nerve cord (dnc) and adjacent muscle cells (bwm) are shown near the pharyngeal terminal bulb. No co-localization of NRA-2::GFP and UNC-29 was apparent. (**C**) NRA-2::GFP was co-expressed in muscle with epitope-tagged UNC-38::3xMYC (expressed from *punc-38*). UNC-38, exposing the MYC tag on the cell surface, was labelled with Cy3-conjugated anti-MYC antibodies injected into the body cavity. The ventral nerve cord was imaged by confocal microscopy (single focal plane), showing punctate cell-surface L-AChR clusters that contain UNC-38. NRA-2::GFP is adjacent to L-AChR clusters, but not co-localizing with them (inset: enlarged region). (**D**) SEC-23::GFP, a COPII coat component that labels ER exit sites, and NRA-2::mCherry were co-expressed in muscle and imaged by confocal microscopy. Puncta of SEC-23 accumulation contained also NRA-2; however, NRA-2 did not accumulate at these sites. Z-stack of confocal sections. Size bars are 10 μm.

injected into the body cavity; Gottschalk *et al*, 2005; Gottschalk and Schafer, 2006; Eimer *et al*, 2007). (4) Minor amounts of cell-surface NRA-2 were detected with extracellular anti-HA antibody in animals expressing 3xHA::NRA-2::GFP, in clusters along muscle cell boundaries (Supplementary Figure 12), but this did not accumulate at nerve cords, in which synaptic L-AChRs are found. Cell-surface expression of 3xHA::NRA-2::GFP may be due to overexpression (its binding partner NRA-4 was not overexpressed). In sum, our observations do not support an interaction of NRA-2 with L-AChRs at synapses.

NRA-2 may interact with L-AChRs during assembly, or when they are sorted for ER exit. However, NRA-2::mCherry and SEC-23::GFP, a COPII coat component localizing to ER exit sites and secretory vesicles (Roberts *et al*, 2003) showed different localization patterns: SEC-23::GFP was found in punctate intracellular clusters, whereas NRA-2::mCherry was not enriched at these sites (Figure 3D). Thus, NRA-2 is likely not part of the ER exit machinery.

Cholinergic inward currents in muscle cells are reduced in *nra-2* and *nra-4* mutants

To directly measure nAChR and GABA$_A$R function in muscle, we recorded postsynaptic currents (PSCs) evoked by pressure-applied ACh, levamisole, nicotine and GABA under whole-cell voltage-clamp (Supplementary Table 1; Richmond and Jorgensen, 1999; Francis *et al*, 2003; Richmond, 2006; Liewald *et al*, 2008). Levamisole- and nicotine-evoked PSCs were significantly reduced in both *nra-2* mutants (*ok1731*: levamisole: $62 \pm 6\%$, normalized to wild type, $P < 0.01$, *t*-test; nicotine: $57 \pm 5\%$, $P < 0.001$; *tm1453*: levamisole: $74 \pm 9\%$, $P < 0.05$; nicotine: $72 \pm 8\%$, $P < 0.05$), as well as in *nra-4(hd127)* mutants (levamisole: $61 \pm 5\%$, $P < 0.05$; nicotine: $76 \pm 6\%$, $P < 0.05$), indicating that both L-AChRs and N-AChRs, were functionally compromised in these animals (Figure 4A and B). GABA-evoked PSCs were not affected (*nra-2(tm1453)*: $103 \pm 17\%$; Figure 4C). Levamisole-induced PSCs in *nra-2(ok1731)*; *nra-4(hd127)* double mutants were not further reduced than in single
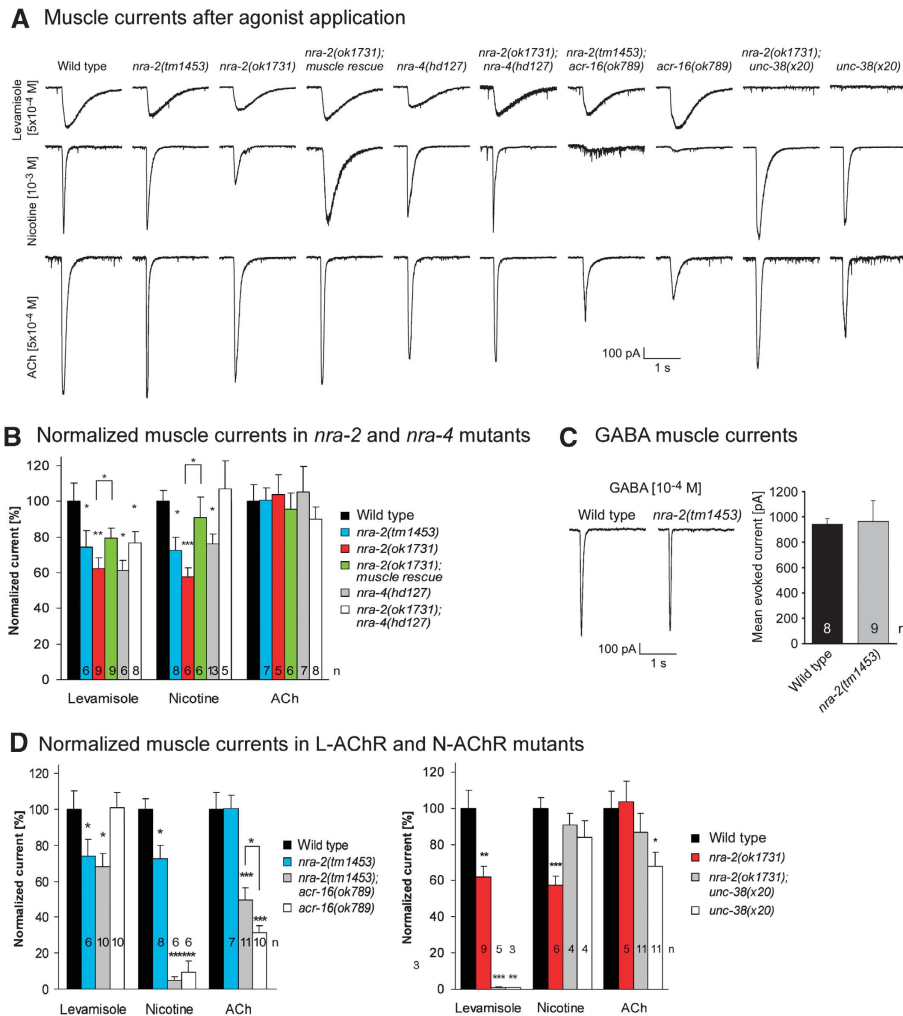
Figure 4 Whole-cell voltage-clamp analysis of muscle cells reveals altered nAChR function in *nra-2* and *nra-4* mutants. (**A**) Representative traces for levamisole- (top), nicotine- (middle) and ACh-evoked (bottom) muscle currents in wild-type animals and various mutants of *nra-2*, *nra-4*, L- and N-AChR subunits. (**B**) Normalized mean peak values of levamisole-, nicotine- and ACh-mediated muscle currents in wild-type animals and various *nra-2* and *nra-4* mutants, and *nra-2(ok1731)* animals rescued in muscle by NRA-2::GFP expression. Only GFP-positive cells were patched. (**C**) Representative traces (left) and mean peak values (right) of GABA-mediated muscle currents were not altered in *nra-2(tm1453)* mutants, compared with wild type. (**D**) Normalized mean peak values of levamisole-, nicotine- and ACh-mediated muscle currents in wild-type animals, *nra-2(tm1453* or *ok1731)* mutants as well as in mutants lacking the N-AChR (*acr-16(ok789)*; left) or L-AChR (*unc-38(x20)*; right), and respective double mutants. Displayed are means ± s.e.m., statistically significant differences to the wild type are indicated (*$P<0.05$; **$P<0.01$; ***$P<0.001$), as well as the number of animals.

mutants, again indicating a function of NRA-2 and NRA-4 in the same pathway. Yet, nicotine-evoked PSCs were normal in these double mutants. Possibly, some *nra-2* and *nra-4* effects on L- and N-AChRs are allele specific, and such effects may be partly compensated in double mutants, for example, due to direct physical interactions of NRA-2 and NRA-4. Levamisole- and nicotine-induced PSCs in *nra-2(ok1731)* mutants were rescued by muscle-specific expression of NRA-2::GFP (Figure 4A and B), confirming the cell-autonomous function of NRA-2.

Short-term ACh sensitivity of L- and possibly N-AChRs is increased in *nra-2* mutants

On the basis of agonist-evoked PSCs, both L- and N-AChRs are affected in *nra-2* and *nra-4* mutants. This is not seen in paralysis assays, as *acr-16* mutants are not resistant to either agonist, in contrast to L-AChR mutants (Supplementary

Figure 13), stressing differences between behavioural and electrophysiological phenotypes of L- versus N-AChR mutations. These could depend on the duration of agonist exposure, as L-AChRs desensitize much more slowly than N-AChRs. Surprisingly, PSCs in response to short-term ACh application in both *nra-2* alleles, in *nra-4(hd127)* mutants and in several double-mutant combinations, were indistinguishable from the wild type (Figure 4A and B; Supplementary Figure 14). This was unexpected, as L- and N-AChRs are the only nAChRs contributing to cholinergic signalling at the NMJ (Richmond and Jorgensen, 1999; Francis *et al*, 2005; Touroutine *et al*, 2005).

Our findings indicated that sensitivity of the two nAChRs was altered in an agonist-specific manner, that is, reduced for levamisole and nicotine, but largely unaltered for ACh. As both nAChRs contribute to ACh PSCs, they could be differently affected for ACh sensitivity. To examine this, we assayed

properties of each AChR individually, in *acr-16(ok789)* or *unc-38(x20)* mutants, in *nra-2* or *nra-4* backgrounds (Figure 4A and D; Supplementary Figure 14).

In *acr-16(ok789); nra-2(tm1453)* mutants, in which only the L-AChR contributes to PSCs, levamisole sensitivity was reduced as in *nra-2(tm1453)* mutants ($68 \pm 7\%$, $P < 0.05$), whereas nicotine sensitivity was abolished ($5 \pm 2\%$, $P < 0.001$), as in *acr-16(ok789)* single mutants ($6 \pm 1\%$, $P < 0.001$). However, ACh sensitivity in the *acr-16*; *nra-2(tm1453)* double mutants ($50 \pm 7\%$, $P < 0.001$, versus wild type) was significantly increased when compared with the *acr-16* single mutant ($32 \pm 5\%$, $P < 0.001$, versus wild type; $P < 0.05$, versus *acr-16* mutant). This indicates that ACh sensitivity of the L-AChR was increased by *nra-2(tm1453)*, even though sensitivity to the L-AChR-specific agonist levamisole was decreased. Thus, functional properties of the L-AChR may be altered in *nra-2(tm1453)* animals. In *acr-16(ok789)*; *nra-4(hd127)* double mutants, ACh PSCs were not increased. These animals also had normal levamisole responses, but reduced nicotine responses (Supplementary Figure 14). This discrepancy to *nra-2* mutant phenotypes may be due to allele-specific effects, or could point to different functions of the two proteins in the heteromeric complex.

Mean ACh sensitivity of the N-AChR was affected similarly when *unc-38(x20)* single mutants and *nra-2(ok1731)*; *unc-38(x20)* double mutants were compared. Although ACh PSCs were significantly reduced in *unc-38* mutants ($68 \pm 8\%$, $P < 0.05$), they were not significantly different from wild type ($87 \pm 10\%$) in the *nra-2*; *unc-38* double mutant, possibly suggesting that ACh sensitivity of also the N-AChR is increased by *nra-2(ok1731)*. Interestingly, nicotine sensitivity of the N-AChR, which was significantly reduced in *nra-2(ok1731)* single mutants ($57 \pm 5\%$ of wild type, $P < 0.001$), was not altered in *nra-2(ok1731)*; *unc-38(x20)* double or *unc-38(x20)* single mutants ($91 \pm 6\%$ and $84 \pm 9\%$ of wild type, respectively), possibly due to compensatory changes induced by lack of the L-AChR (Figure 4A and D). Although *nra-2* effects were not as clear as for the L-AChR, our findings indicate that also N-AChR functional properties are altered in *nra-2* mutants in an agonist-specific manner.

PSCs after prolonged optogenetic ACh release reveal altered nAChR desensitization in nra-2 mutants

Somewhat contrasting our electrophysiological results, in which no reduction of acute ACh responses was seen in *nra-2* mutants, these animals showed a slight resistance in aldicarb assays, in which endogenous ACh accumulates in the synaptic cleft (Supplementary Figure 8). This could indicate reduced postsynaptic AChR sensitivity, or reduced presynaptic ACh release. Aldicarb assays take 1–2 h, whereas the 'puff' application of ACh in electrophysiological assays lasts only 70 ms, using non-physiological amounts of ACh, broadly sprayed over the muscle cell. Thus, long-term effects such as altered desensitization may cause different results in both types of experiments. To examine this, we used the light-gated cation channel channelrhodopsin-2 (ChR2) to stimulate ACh release at the NMJ, at endogenous levels, only at synapses, and for short or long durations (Liewald *et al*, 2008).

We photo-stimulated sustained release of ACh (1000 ms), which evokes large peak currents, followed by small steady-state currents that occur after nAChR desensitization. In *acr-16*
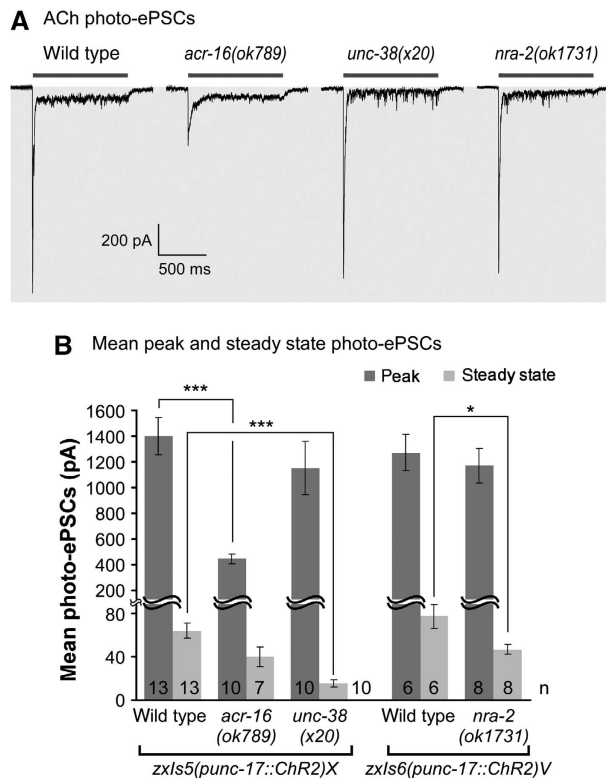

Figure 5 Optogenetic analysis of ACh transmission in cholinergic and *nra-2* mutants using channelrhodopsin-2 (ChR2). (**A**) Whole-cell voltage-clamp was used to record photo-ePSCs in animals expressing ChR2 in cholinergic motor neurons (*punc-17* promoter), in response to a 1000 ms photo-stimulus, as described earlier (Liewald *et al*, 2008). Representative peak and steady-state currents were compared in wild type, *acr-16(ok789)*, *unc-38(x20)* and *nra-2(ok1731)* mutants. Duration of light stimulus is indicated by a bar. (**B**) Mean peak and steady-state photo-ePSCs, obtained using two different integrated transgenes, as indicated. Displayed are mean currents ± s.e.m., statistically significant differences to the wild type are indicated (*t*-test; *$P < 0.05$; ***$P < 0.001$), as is the number of animals used.

mutants (i.e. when only the L-AChR is present), we observed largely reduced peak, but unaltered steady-state currents. In *unc-38(x20)* mutants (N-AChR only), we observed reduced steady-state currents, and no major effects on peak currents (Figure 5). The differences in steady-state currents are likely explained by different rates of desensitization of the two nAChRs, and can thus help distinguishing which of the two nAChRs is affected. In *nra-2(ok1731)* mutants, we observed no significant differences in the peak photo-ePSCs (Figure 5), whereas steady-state currents were significantly smaller than in wild type. Our results rule out presynaptic defects, and indicate that alterations in the desensitization rate of L-AChRs may cause the slight aldicarb resistance of *nra-2* mutants.

Single-channel L-AChR properties are altered in nra-2 mutant embryonic muscle

To assay L-AChR properties in more detail, we recorded single-channel currents from cell-attached patches of cultured embryonic muscle cells, which show activity of L- but not of N-AChRs (Rayes *et al*, 2007). We compared channels from wild type and *nra-2(ok1731)* mutants in the presence of different concentrations of ACh or levamisole.
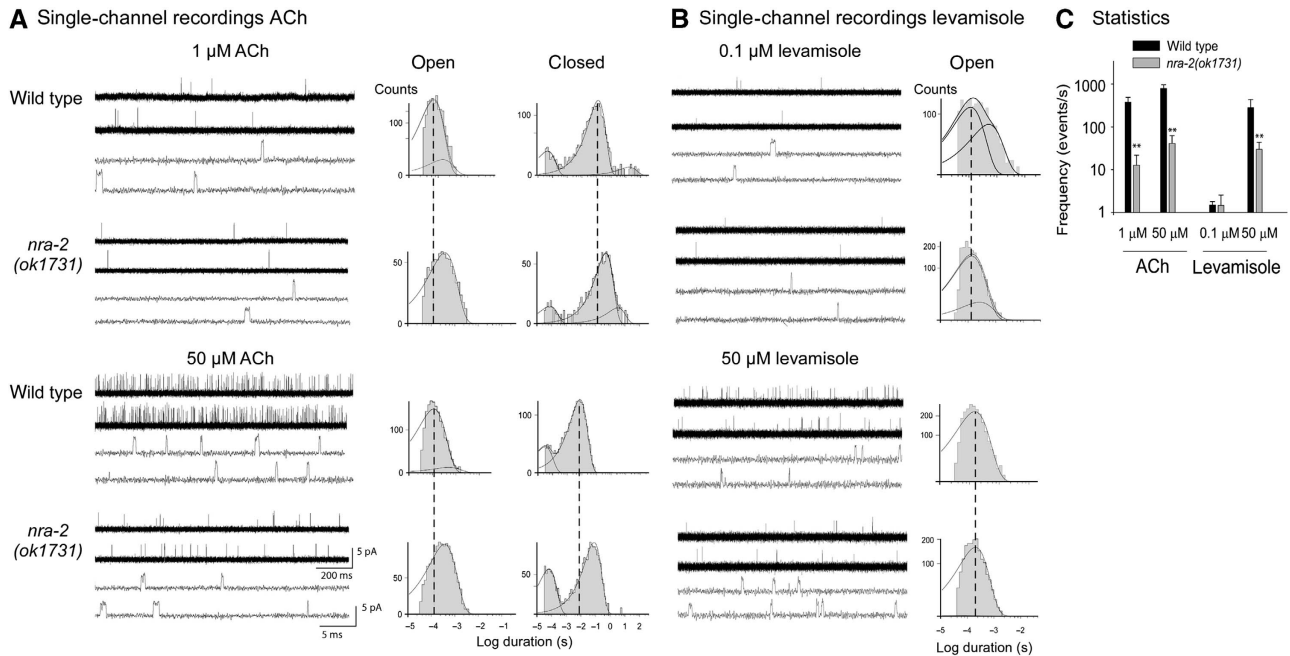
Figure 6 Single-channel properties of the L-AChR in cell-attached patches of cultured embryonic muscle cells are altered in *nra-2(ok1731)* mutants. (**A**) Single-channel currents recorded from wild type and *nra-2(ok1731)* muscle cells in the presence of 1 μM (upper panel) and 50 μM (lower panel) ACh. Shown are representative traces (left) and open and closed time histograms (right). (**B**) Single-channel currents activated by 0.1 μM (upper panel) and 50 μM (lower panel) levamisole; representative traces (left) and open time histograms (right). (**C**) Frequency of channel openings in mutant and wild-type animals. Channel events were counted within the first minute of recording and plotted as events/s. Holding potential in all recordings was −100 mV. Displayed are means ± s.d.

Single-channel openings of about 3.5 pA activated by ACh or levamisole were detected in *nra-2(ok1731)* mutant muscle cells at −100 mV (Figure 6A and B). For both agonists, opening frequency increased with agonist concentration but was strongly reduced in *nra-2(ok1731)* mutants (Figure 6C), as observed in the closed time histogram by displacement of the main component to longer durations. This could reflect lower cell-surface density and/or altered open probability and/or increased desensitization of L-AChRs in the patch. Open time distributions of L-AChRs activated by 1 μM ACh in wild type cells are fitted by two exponential components (Rayes *et al*, 2007); duration of the main component (relative area <0.85) is 100 ± 20 μs (Figure 6A). Significant changes in the open time distributions were observed in *nra-2* mutants. For ACh, the mean open duration was three-fold longer than that of wild type L-AChRs; open time histograms showed a single component of 350 ± 50 μs (Figure 6A). For channels activated by 0.1 μM levamisole, open time histograms are fitted by two components in wild type and *nra-2* mutants. Yet, the mean open time of the slowest component was significantly briefer in levamisole-activated channels recorded from *nra-2* mutant cells (τ_{on} = 310 ± 50 μs, relative area 0.1 ± 0.08) with respect to wild type (τ_{on} = 600 ± 70 μs, relative area 0.35; Figure 6B). Higher levamisole concentrations produce open-channel block, which is observed as a reduction in the mean open time. The decreased frequency of opening events, increased closed times and decreased open durations of levamisole-activated L-AChRs from *nra-2* mutants are in line with the reduced levamisole-induced PSCs in adult *nra-2* mutants (Figure 4A and B). The comparison is not straight-forward for ACh responses, as the increase in open duration but not the reduction in opening frequency supports increased ACh sensitivity. Yet, the reduced frequency may be explained by an increase in desensitization, consistent with the results from the optogenetic ACh release experiments. In sum, our single-channel recordings confirm that L-AChR functional properties differ significantly in *nra-2* mutants, indicating agonist-specific kinetic changes of L-AChRs.

Contribution of ACR-8 and LEV-8 to L-AChR function in nra-2 and nra-4 mutants

How do *nra-2* and *nra-4* mutations affect L-AChR properties? Receptor properties could be determined by posttranslational modifications, or by subunit composition of the pentamer. In purified L-AChRs, we identified seven subunits, more than the five present in any individual channel: ACR-8, ACR-12, UNC-63, UNC-38, UNC-29, LEV-8 and LEV-1 (Gottschalk *et al*, 2005). Co-expression of the latter five subunits reconstitutes levamisole-specific currents in *Xenopus* oocytes (Boulin *et al*, 2008). ACR-12 is expressed only in motor neurons, but a potential contribution of ACR-8, also expressed in muscle (Gottschalk *et al*, 2005), was not tested in oocytes. Different L-AChR populations with variable subunit content could exist, and the relative contribution of individual subunits to L-AChRs could be controlled by NRA-2/NRA-4. As essential subunits, UNC-38, UNC-63 and UNC-29 should be present in every L-AChR pentamer. Yet, receptors containing more than one of the essential subunits, for example, two copies of UNC-38, may exist, and one of them may be replaced with a non-essential α-subunit, LEV-8 and ACR-8, preserving function, but possibly altering functional properties. Thus, we investigated the contribution of ACR-8 and LEV-8 to NMJ function, in *nra-2*, *lev-8* or *acr-8* single mutants, or in combination.
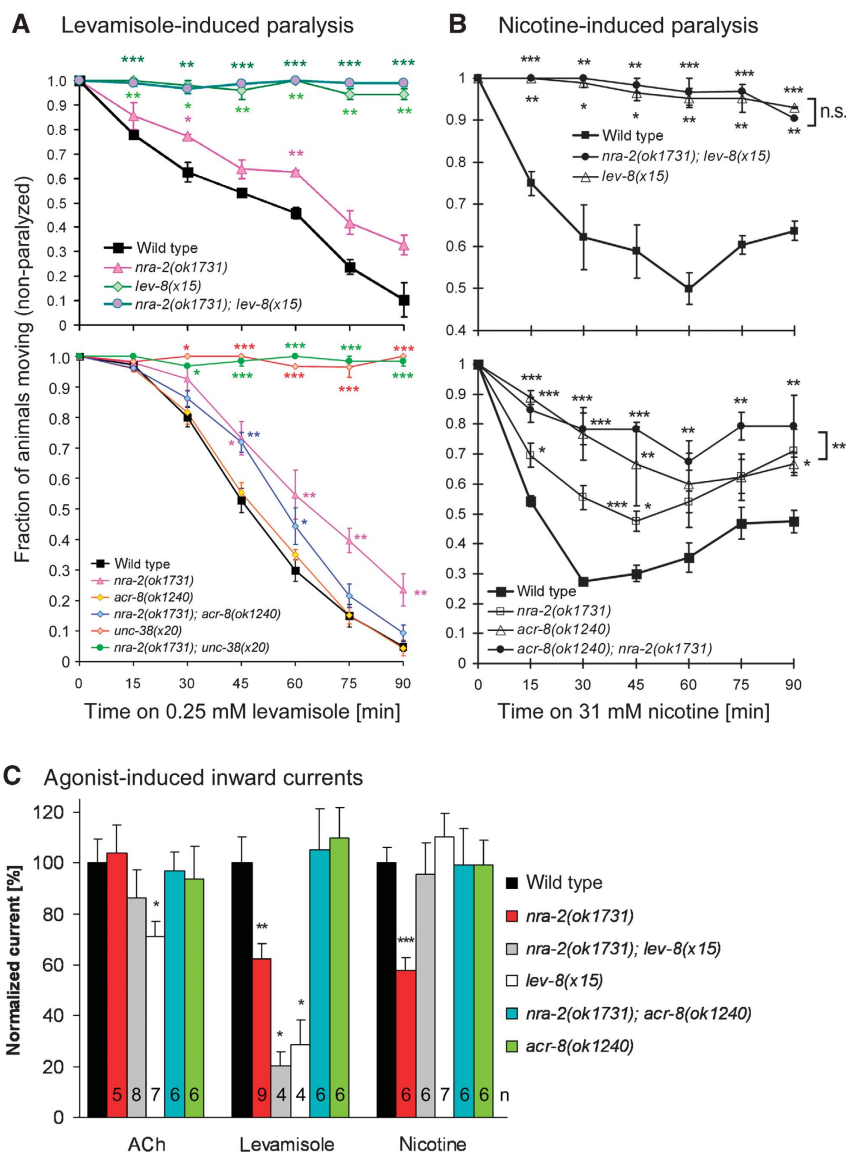
Figure 7 Contribution of essential and non-essential L-AChR subunits to cholinergic agonist sensitivity in *nra-2(ok1731)* mutants. (**A, B**) Paralysis assays (*n* = 2–7; 30 animals each) in response to levamisole (A) and nicotine (B) of mutants in *nra-2(ok1731)*, *lev-8(x15)*, *acr-8(ok1240)* and *unc-38(x20)*, and in double-mutant combinations as indicated. (**C**) Normalized mean peak values of ACh-, levamisole- and nicotine-induced muscle PSCs in wild-type animals, *nra-2(ok1731)* mutants, and mutants of the non-essential L-AChR α-subunits *lev-8(x15)* and *acr-8(ok1240)* as well as respective double mutants. Displayed are means ± s.e.m., number of animals and significant differences to wild type (*t*-test; *$P < 0.05$; **$P < 0.01$; ***$P < 0.001$) are indicated.

Mutants lacking LEV-8 showed strong levamisole- and nicotine-resistance in paralysis assays, just like mutants in the essential subunit UNC-38 (Figure 7A and B); however, *lev-8(x15)* mutants were special in that only head and neck region of the animals were resistant. Consistent with our behavioural assays and a previous report (Towers *et al*, 2005), *lev-8(x15)* mutants showed largely reduced levamisole-induced PSCs (28 ± 10%, $P < 0.05$; Figure 7C), whereas nicotine PSCs were normal. Surprisingly, this was also the case in *lev-8; nra-2* double mutants, even though *nra-2(ok1731)* mutants have reduced nicotine PSCs. Either, in the absence of NRA-2, LEV-8 assembles with ACR-16, thus explaining altered nicotine PSCs, or, as in *unc-38(x20)* mutants, N-AChRs undergo compensatory changes in *lev-8* mutants.

Mutants of *acr-8(ok1240)* showed no levamisole resistance, but a significant resistance to nicotine in paralysis assays, which was slightly elevated in the *acr-8(ok1240); nra-2(ok1731)* double mutants (Figure 7A and B). To our surprise, PSCs for ACh, levamisole, or nicotine did not differ between wild type, *acr-8(ok1240)* and *acr-8(ok1240); nra-2(ok1731)* double mutants, even though *nra-2(ok1731)* alone significantly reduces levamisole and nicotine PSCs (Figure 7C). Thus, the *acr-8* mutation suppresses *nra-2(ok1731)* effects on L- and N-AChRs. This could be explained if NRA-2 prevents ACR-8 subunits from assembling with other subunits. In *nra-2* mutants, ACR-8 could be integrated in L- and N-AChRs, thus altering their physiological properties, which cannot occur in *acr-8* mutants.

Relative expression of individual L-AChR subunits is altered in nra-2 and nra-4 mutants

Our findings suggested that NRA-2/NRA-4 could affect nAChR properties by influencing the representation of particular subunits in the mature receptors. We thus probed synaptic expression of LEV-1 (4xHA tagged), UNC-38 (3xMYC tagged), LEV-8 (3xHA) and ACR-8 (6xHA) by antibody injection, and of UNC-29 by immunostaining relative to the presynaptic UNC-17 vesicular ACh transporter, in wild type, nra-2 and nra-4 mutants (Figure 8).

For UNC-38 (essential α-subunit), synaptic expression was significantly reduced in nra-2(tm1453 and ok1731), and in nra-4(hd127) animals. UNC-29 (essential non-α) was reduced in nra-2(ok1731) animals, and, intriguingly, significantly increased in nra-4(hd127) animals. LEV-1 cell-surface expression levels were not affected in either mutant (Figure 8A and C). Effects of NRA-2 on LEV-8 and ACR-8 synaptic expression were assayed relative to UNC-38. The synaptic expression pattern of LEV-8 was peculiar, and could explain our observations in paralysis assays (resistance in head and neck):
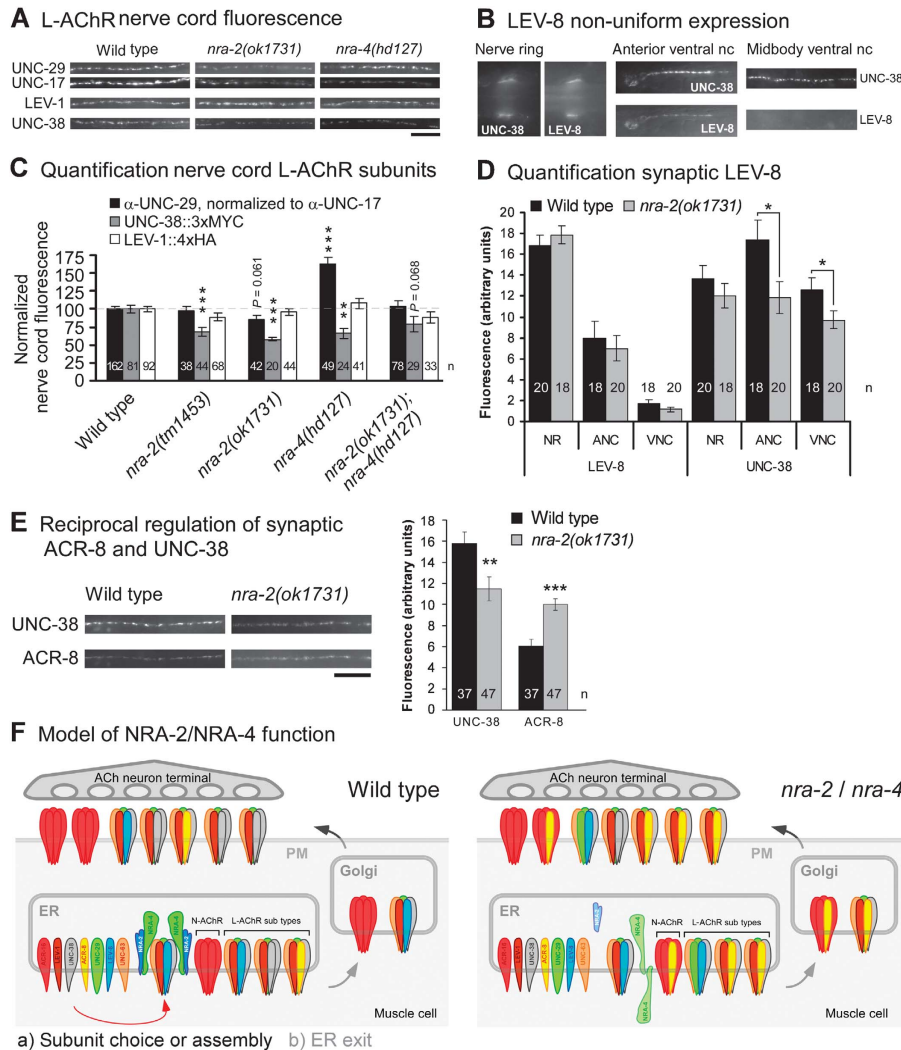
Figure 8 Individual L-AChR subunit levels at postsynaptic elements vary in nra-2 and nra-4 mutants reciprocally. (**A**, **B**, **E**) Synaptic expression of different L-AChR subunits was analysed by quantitative fluorescence microscopy. Endogenous, postsynaptic UNC-29, as well as the presynaptic UNC-17 (vAChT), were immunolabelled with specific 1° and different fluorescent 2° antibodies, then UNC-29 fluorescence was normalized to UNC-17 and compared in the indicated mutants. Also, transgenic animals expressing epitope-tagged LEV-1 (4 HA tags), UNC-38 (3 MYC tags), LEV-8 (3 HA tags) or ACR-8 (6 HA tags) were injected into the body cavity with fluorescent tag-specific antibodies. Size bar: 10 μm. (B) LEV-8 is non-uniformly expressed in the nervous system, as compared with UNC-38. Shown is expression of both subunits in the nerve ring, and the anterior and midbody ventral nerve cords (nc). (**C**, **D**, E) Fluorescence in the ventral cord was quantified (as linescans, followed by background correction) either in fixed animals (UNC-29, UNC-17), or in live animals after a recovery period of >6 h (during which excess antibody is cleared from the extracellular fluid by scavenger cells). Shown is mean fluorescence ± s.e.m. (normalized to wild type in C, arbitrary units in D and E), number of animals and significant differences to wild type are indicated (t-test; *P<0.05; **P<0.01; ***P<0.001). (**F**) Model of NRA-2/NRA-4 function. Left, NRA-2/NRA-4 either influence the choice of particular subunits (indicated by different colours) to be assembled into pentameric nAChRs, or they determine to which extent pentamers of particular subunit composition are allowed to leave the ER (less favoured, as no obvious accumulation of NRA-2 was seen at ER exit sites). ACR-16 N-AChRs and L-AChRs, rarely incorporating ACR-8 subunits (yellow) are preferably formed. Right, In the nra-2 or nra-4 mutants, nAChRs of other composition are found, for example, containing ACR-8 or UNC-29 subunits more often. Depending on the allele, NRA-2 and NRA-4 proteins could either be completely absent, not bound to ER membranes and secreted, or of inverted topology.

we found the protein in L-AChR clusters in the nerve ring and the anterior ends of ventral and dorsal nerve cords, together with UNC-38 (largely co-expressed in the same synaptic clusters; Supplementary Figure 15). Interestingly, LEV-8 was almost not detectable in the rest of the body (Figure 8B); synaptic LEV-8 expression was not affected in the *nra-2(ok1731)* mutant (Figure 8D).

ACR-8 and UNC-38 expression was found in all regions of the nerve cords (Figure 8E); however, as we observed earlier, ACR-8 was present in many clusters that did not contain UNC-38, in addition to clusters in which both proteins were co-expressed (Supplementary Figure 15; Gottschalk *et al*, 2005). This indicates that ACR-8 is either found in (unknown) receptors that are different from the L-AChR, or that there are L-AChRs in which ACR-8 replaced UNC-38. In *nra-2(ok1731)* mutants, while synaptic UNC-38 levels were reduced, expression of ACR-8 was significantly increased (Figure 8E). Thus, NRA-2 function affects synaptic expression of UNC-38 and ACR-8 α-subunits reciprocally. In sum, NRA-2 and NRA-4 affect the relative composition of the synaptic L-AChR in a (subunit) gene-, and (*nra-2/nra-4*) allele-specific manner.

Discussion

In this work, we showed that NRA-2 and NRA-4, evolutionarily conserved type I TM proteins forming a protein complex in the ER, affect synaptic nAChR subunit composition in *C. elegans*. Mutants lacking these proteins exhibited moderate resistance to cholinergic but not GABAergic agonists, verifying that in muscle they affect nAChRs, and not GABA$_A$Rs. The cholinergic deficits were accompanied by defects in agonist sensitivity in whole-cell voltage-clamp analyses: sensitivities of the L-AChR and the N-AChR to their 'specific' agonists, levamisole and nicotine, were reduced, whereas sensitivity for short-term applied ACh was either unaffected (N-AChR) or increased (L-AChR). These effects may sum up such that overall ACh PSC are unaffected in *nra-2* mutants; however, compensatory changes when both L- and N-AChRs are present in *nra-2* mutants cannot be ruled out. Yet, optogenetic, prolonged application of ACh demonstrated increased desensitization of L-AChRs, even though N-AChRs were present. We further showed that in the absence of NRA-2 or NRA-4, the NMJ contained L-AChRs of different subunit composition, or altered relative amounts of different L-AChRs with specific subunit compositions, particularly UNC-38 and ACR-8. Thus, NRA-2 and NRA-4 either influence choice of subunits for assembly in the ER, or the extent to which particular pentamers are allowed to leave the ER and reach the NMJ (see model in Figure 8F).

Altered L-AChR single-channel properties in nra-2 mutants
Our conclusions are supported by analyses of single-channel properties of embryonic L-AChRs, which indicated changes in the functional properties of receptors in *nra-2* mutants versus wild type, and which appeared to originate from changes in L-AChR subunit composition. The main kinetic change was an increase in the open duration of channels activated by ACh, and a decrease when levamisole was the agonist. These agonist-specific changes parallel the sensitivity changes observed in whole-cell experiments of adult muscle. However,

correlating results from single-channel experiments with whole-cell currents is not trivial. For levamisole, both single channel and macroscopic currents showed decreased responses. Single-channel recordings of L-AChRs activated by ACh showed reduced frequency in the *nra-2* mutant, whereas macroscopic currents were unaltered. One explanation is that desensitization is affected in the *nra-2* mutant L-AChR. Single-channel recordings occur in the continuous presence of agonist, thus enhanced desensitization to ACh will appear as a decrease in single-channel opening frequency, as we observed, and in agreement with our results obtained after long-term photo-evoked ACh release, which uncovered increased desensitization of the L-AChR in *nra-2* mutants. Another explanation for these differences is that embryonic, extrasynaptic L-AChRs are compared with synaptic adult L-AChRs, in which subunit composition may change during development, and interaction with additional proteins could occur, for example, LEV-10 (Gally *et al*, 2004). Also, more than one type of L-AChR may be present in adult muscle cells, though we only detect a single main functional population in embryonic cells. This L-AChR population is kinetically different in *nra-2* mutants, likely due to altered subunit composition.

NRA-2 and NRA-4 affect subunit composition of synaptic nAChRs
The effects of *nra-2* and *nra-4* mutants on synaptic L-AChR subunit representation were subunit dependent. In particular, the α-subunit UNC-38 was reduced in these mutants, whereas the non-α-subunit UNC-29 was increased in *nra-4(hd127)* animals. The non-α-subunit LEV-1 was unaltered, as was the α-subunit LEV-8. In contrast, the α-subunit ACR-8 was increased in *nra-2* mutants, and thus may compensate for the reduction in UNC-38 levels. This could explain the observed increase in short-term applied ACh sensitivity of L-AChRs, and the increased desensitization in long-term ACh application (either optically, or in response to aldicarb). In *nra-4* mutants, in which UNC-38 is reduced and UNC-29 increased, fewer α-subunits, and thus fewer ACh-binding sites should be present in synaptic L-AChRs. This may explain why in *nra-4; acr-16* double mutants compared with *acr-16* single mutants ACh sensitivity of the L-AChR was not increased (Supplementary Figure 14). In this regard, we recently showed that channel activation rate and agonist sensitivity increase with the number of functional binding sites in homomeric Cys-loop receptors (Rayes *et al*, 2009). Yet, as we do not know the number of ACh-binding sites in the L-AChR or the number of bound agonist molecules required for maximal activation, ACh sensitivity in *nra-2* or *nra-4* mutants may mainly be affected by altering ACh-dependent desensitization rather than ACh binding, as suggested by optogenetic experiments and single-channel recordings.

Mode of action of NRA-2 and NRA-4 in L-AChR assembly
Our findings suggest that NRA-2/NRA-4 interact with L-AChRs in the ER. How do NRA-2 and NRA-4 influence L-AChR subunit composition? They may interact with RIC-3, an ER protein that affects biogenesis and/or trafficking of several types of nAChRs (Halevi *et al*, 2002; Gottschalk *et al*, 2005; Gottschalk and Schafer, 2006; Biala *et al*, 2009). We tested for possible genetic interactions between *ric-3* and *nra-2* by analysing swimming behaviour as an indirect

measure for NMJ function. *ric-3* mutants showed significantly less swimming cycles, which were further reduced in the *ric-3; nra-2* double mutants (data not shown). Thus, RIC-3 and NRA-2 likely act in separate pathways.

An intriguing alternative is indicated by findings made for the NRA-2/Nicalin homologue Nicastrin: this γ-secretase component was implicated as 'gate-keeper' of the intramembrane peptidase and regulates substrate access by binding their N-termini (Shah *et al*, 2005). NRA-2/NRA-4 could act as a 'nucleation centre' for nAChR assembly and regulate inclusion of particular subunits during pentamer assembly. L-AChRs require essential subunits UNC-29, UNC-38 and UNC-63; remaining positions are occupied by non-essential subunits. NRA-2/NRA-4 could sort certain subunits into the pentamer, while excluding others, for example, ACR-8. Also N-AChR properties were altered in *nra-2* and *nra-4* mutants, which could be explained by NRA-2/NRA-4 ensuring that only ACR-16 is assembled. As *nra-2* effects on N-AChRs were reversed by *lev-8* and *acr-8* mutations, these subunits may assemble with ACR-16 in the absence of NRA-2/NRA-4. Alternatively, NRA-2/NRA-4 could control which nAChR pentamer of particular composition is allowed to leave the ER. However, our observation that NRA-2/NRA-4 is not enriched at ER exit sites argues against this idea.

Evolutionary conservation and additional functions of NRA-2 and NRA-4

The *nra-4* expression pattern was broad, extending beyond the neuromuscular system, and also the *nra-2* promoter was active in tissues in addition to muscles and neurons. *nra-2* and *nra-4* mutants had reduced broodsize, indicating additional functions. Furthermore, these genes are conserved across all phyla, that is, also in species that do not express nAChRs (Supplementary Figures 2–5). Vertebrate homologues of NRA-2/NRA-4 (NOMO/Nicalin) antagonistically influence cell-surface signalling events through the *nodal* type of TGFβ ligands (Haffner *et al*, 2004, 2007), but how these signalling pathways are influenced by the ER proteins NOMO/Nicalin was not further investigated. Possibly, they may affect receptors for TGFβ-like ligands, that is, heterodimeric activin receptors. TGFβ receptors are antagonized by other membrane-associated co-receptors or inhibitors that bind to the complex (e.g. 'Cripto'; Gray *et al*, 2003), and secretion or cell-surface expression of such antagonists could be influenced by ER-resident proteins. A role for TGFβ in *Drosophila* NMJ formation was shown (Rawson *et al*, 2003), thus we cannot rule out the possibility that NRA-2 and NRA-4 affect nAChRs indirectly through TGFβ pathways. Yet, though some mutants in TGFβ pathways we tested showed increased levamisole or nicotine sensitivity, the effects are likely indirect (e.g. through GABA signalling for *dbl-1*; Vashlishan *et al*, 2008). Furthermore, our co-purification of NRA-2/NRA-4 with L-AChRs argues for direct interactions (Gottschalk *et al*, 2005).

Are Nicalin and NOMO involved in nAChR assembly in vertebrates? This is not unlikely, given the conservation of the proteins, and the fact that human Nicalin, expressed in *C. elegans* muscle, partially rescued *nra-2* phenotypes. However, as vertebrate muscle does not express such a large set of nAChR subunits as *C. elegans* muscle, it may be worthwhile to study the function of Nicalin/NOMO in nAChR subunit choice or assembly in neurons.

Materials and methods

C. elegans strains

Nematodes were grown under standard conditions (Brenner, 1974). Mutant strains were backcrossed four to six times. Transgenic strains were generated following standard procedures (Fire, 1986). *nra-4(hd127)* was isolated from an EMS mutagenized library by a poison primer approach (Edgley *et al*, 2002), using primers 5′-GATTACGGTTCCCGGTCTTAAC-3′, 5′-CATCAACAAATGGATTCATGCT-3′ and 5′-TCGACTATTCCCAGTTGAAGGT-3′.

Strains used or generated: N2 (wild type), *lin-15(n765ts)*, **ZZ37:** *unc-63(x37)*, **ZZ20:** *unc-38(x20)*, **RB1195:** *acr-8(ok1240)*, **ZZ15:** *lev-8(x15)*, **RB918:** *acr-16(ok789)*, **RM509:** *ric-3(md1181)*, **NW987:** *unc-129(ev554)*, **ZX383:** *nra-2(tm1453)*, **RB1480:** *nra-2(ok1731)*, **ZX441:** *nra-4(hd127)*, **ZX544:** *nra-4(tm2656)*, **ZX453:** *nra-2(ok1731); nra-4(hd127)*, **ZX455:** *nra-2(tm1453); nra-4(hd127)*, **ZX543:** *nra-2(ok1731); nra-4(tm2656)*, **ZX395:** *nra-2(tm1453); unc-38(x20)*, **ZX502:** *nra-2(ok1731); unc-38(x20)*, **ZX500:** *nra-2(ok1731); acr-8(ok1240)*, **ZX621:** *nra-2(ok1731); lev-8(x15)*, **ZX445:** *nra-2(tm1453); acr-16(ok789)*, **ZX575:** *nra-4(hd127); acr-16(ok789)*, **ZX501:** *nra-2(tm1453); ric-3(md1181)*, **LT186:** *sma-6(wk7)*, **DR960:** *daf-1(m402)*, **LT121:** *dbl-1(wk70)*, **CB1372:** *daf-7(e1372)*.

Transgenic strains: **ZX15:** *ljEx42[punc-38::unc-38::MYC::6xHIS::2xMYC; rol-6d]*, **ZX56:** *zxEx51[punc-38::unc-38::MYC::6xHIS-2xMYC; podr-2::odr-2::HA; rol-6d]*, **ZX275:** *zxIs1[plev-1::lev-1::HA-6xHIS-3xHA; rol-6]* (ZX15, 56, 275 were as described; (Gottschalk and Schafer, 2006), **ZX387:** *nra-2(tm1453); zxIs1*, **ZX386:** *nra-2(ok1731); zxIs1*, **ZX568:** *nra-4(hd127); zxIs1*, **ZX569:** *nra-2(ok1731); nra-4(hd127); zxIs1*, **ZX525:** *nra-2(tm1453); ljEx42*, **ZX524:** *nra-2(ok1731); ljEx42*, **ZX523:** *nra-4(hd127); ljEx42*, **ZX522:** *nra-2(ok1731); nra-4(hd127); ljEx42*, **ZX574:** *zxEx52[pnra-4::GFP; rol-6d]*, **ZX556:** *nra-2(tm1453); zxEx53[pmyo3::nra-2(cDNA)::GFP; rol-6d]*, **ZX578:** *nra-2(ok1731); ljEx42; zxEx54[pmyo-3::nra-2(cDNA)::GFP; lin15+]*, **ZX640:** *nra-2(ok1731); lin-15(n765ts); zxEx54*, **ZX579:** *zxEx55[pmyo-3::nra-2(cDNA)::YFP; rol-6d]*, **ZX576:** *zxEx56[pmyo-3::nra-2(cDNA)::mCherry; punc-29::unc-29::GFP; rol-6d]*, **ZX577:** *zxEx57[pmyo-3::nra-2(cDNA)::mCherry; psec23::sec23::GFP; rol-6d]*, **ZX628:** *nra-2(ok1731); zxEx58[pmyo-3::Nicalin(human cDNA)::GFP; rol-6d]*, **ZX629:** *nra-4(hd127); zxEx59[pnra-4::nra-4(cDNA)::GFP; rol-6d]*, **ZX636:** *lin-15(n765ts); zxEx60[pnra-4::nra-4(cDNA)::VC155; lin-15+]; zxEx61[pmyo-3::nra-2(cDNA)::VN173; rol-6d]*, **ZX639:** *lin-15(n765ts); zxEx60; zxEx62[pmyo-3::unc-1::VN173; rol-6d]*, **ZX627:** *nra-2(ok1731); zxEx63[pmyo-3::3xHA::nra-2(cDNA)::GFP; rol-6d]*, **ZX699:** *N2; zxEx64[plev-8::lev-8::3xHA; punc-38::unc-38-MYC::6xHIS-2xMYC; rol-6d]*, **ZX700:** *nra-2(ok1731); zxEx64*, **ZX701:** *N2; zxEx65[pacr-8::acr-8::6xHIS-3xHA::6xHIS-3xHA; punc-38::unc-38-MYC::6xHIS-2xMYC; rol-6d]*, **ZX702:** *nra-2(ok1731); zxEx65*, **ZX703:** *N2; zxEx66[pnra-2::GFP; rol-6d]*, **ZX460:** *N2; zxIs6[punc-17::ChR2(H134R)::YFP; lin-15+]IV* ((Liewald *et al*, 2008)), **ZX499:** *N2; zxIs5[punc-17::ChR2(H134R)::YFP; lin-15+]X*, **ZX704:** *nra-2(ok1731); zxIs6*, **ZX705:** *acr-16(ok789); zxIs5*, **ZX706:** *unc-38(x20); zxIs5*.

Bimolecular fluorescence complementation

BiFC experiments were essentially as described (Chen *et al*, 2007; Shyu *et al*, 2008). pnra-4::nra-4(cDNA)::VC155 was first injected (10 ng/μl) into *lin-15(n765ts)* animals. Stable lines were obtained, and into one of those, either pmyo-3::nra-2(cDNA)::VN173 (7 ng/μl), or, as a negative control, pmyo-3::UNC-1::VN173 (wp646; 15 ng/μl) were injected with *rol-6d*(pRF4) as a marker. Stable lines were analysed for reconstituted Venus fluorescence.

Behavioural assays

Paralysis assays, as well as swimming assays, were as described (Gottschalk *et al*, 2005).

Electrophysiology

Recordings of agonist- or photo-induced PSCs from dissected *C. elegans* body muscle cells were as described (Liewald *et al*, 2008; Biala *et al*, 2009). Single-channel recordings from embryonic muscle cells were as described earlier (Christensen *et al*, 2002; Rayes *et al*, 2007).

More detailed and additional Materials and methods are presented in Supplementary data.

References

Biala Y, Liewald JF, Cohen Ben-Ami H, Gottschalk A, Treinin M (2009) The conserved RIC-3 coiled-coil domain mediates receptor-specific interactions with nicotinic acetylcholine receptors. *Mol Biol Cell* **20:** 1419–1427

Blount P, Merlie JP (1991) BIP associates with newly synthesized subunits of the mouse muscle nicotinic receptor. *J Cell Biol* **113:** 1125–1132

Boulin T, Gielen M, Richmond JE, Williams DC, Paoletti P, Bessereau JL (2008) Eight genes are required for functional reconstitution of the Caenorhabditis elegans levamisole-sensitive acetylcholine receptor. *Proc Natl Acad Sci USA* **105:** 18590–18595

Brenner S (1974) The genetics of Caenorhabditis elegans. *Genetics* **77:** 71–94

Changeux J, Edelstein S (2005) *Nicotinic Acetylcholine Receptors*. New York: Odile Jacob Publishing Corporation

Chen B, Liu Q, Ge Q, Xie J, Wang ZW (2007) UNC-1 regulates gap junctions important to locomotion in C. elegans. *Curr Biol* **17:** 1334–1339

Chiara DC, Cohen JB (1997) Identification of amino acids contributing to high and low affinity d-tubocurarine sites in the Torpedo nicotinic acetylcholine receptor. *J Biol Chem* **272:** 32940–32950

Christensen M, Estevez A, Yin X, Fox R, Morrison R, McDonnell M, Gleason C, Miller III DM, Strange K (2002) A primary culture system for functional analysis of C. elegans neurons and muscle cells. *Neuron* **33:** 503–514

Colavita A, Krishna S, Zheng H, Padgett RW, Culotti JG (1998) Pioneer axon guidance by UNC-129, a C. elegans TGF-beta. *Science* **281:** 706–709

Culetto E, Baylis HA, Richmond JE, Jones AK, Fleming JT, Squire MD, Lewis JA, Sattelle DB (2004) The Caenorhabditis elegans unc-63 gene encodes a levamisole-sensitive nicotinic acetylcholine receptor alpha subunit. *J Biol Chem* **279:** 42476–42483

Edgley M, D'Souza A, Moulder G, McKay S, Shen B, Gilchrist E, Moerman D, Barstead R (2002) Improved detection of small deletions in complex pools of DNA. *Nucleic Acids Res* **30:** e52

Eimer S, Gottschalk A, Hengartner M, Horvitz HR, Richmond J, Schafer WR, Bessereau JL (2007) Regulation of nicotinic receptor trafficking by the transmembrane Golgi protein UNC-50. *EMBO J* **26:** 4313–4323

Fire A (1986) Integrative transformation of Caenorhabditis elegans. *EMBO J* **5:** 2673–2680

Fleming JT, Squire MD, Barnes TM, Tornoe C, Matsuda K, Ahnn J, Fire A, Sulston JE, Barnard EA, Sattelle DB, Lewis JA (1997) Caenorhabditis elegans levamisole resistance genes lev-1, unc-29, and unc-38 encode functional nicotinic acetylcholine receptor subunits. *J Neurosci* **17:** 5843–5857

Fox RM, Watson JD, Von Stetina SE, McDermott J, Brodigan TM, Fukushige T, Krause M, Miller III DM (2007) The embryonic muscle transcriptome of Caenorhabditis elegans. *Genome Biol* **8:** R188

Francis MM, Evans SP, Jensen M, Madsen DM, Mancuso J, Norman KR, Maricq AV (2005) The Ror receptor tyrosine kinase CAM-1 is required for ACR-16-mediated synaptic transmission at the C. elegans neuromuscular junction. *Neuron* **46:** 581–594

Francis MM, Mellem JE, Maricq AV (2003) Bridging the gap between genes and behavior: recent advances in the electrophysiological analysis of neural function in Caenorhabditis elegans. *Trends Neurosci* **26:** 90–99

Gally C, Eimer S, Richmond JE, Bessereau JL (2004) A transmembrane protein required for acetylcholine receptor clustering in Caenorhabditis elegans. *Nature* **431:** 578–582

Gotti C, Moretti M, Gaimarri A, Zanardi A, Clementi F, Zoli M (2007) Heterogeneity and complexity of native brain nicotinic receptors. *Biochem Pharmacol* **74:** 1102–1111

Gottschalk A, Almedom RB, Schedletzky T, Anderson SD, Yates JR, Schafer WR (2005) Identification and characterization of novel nicotinic receptor-associated proteins in Caenorhabditis elegans. *EMBO J* **24:** 2566–2578

Gottschalk A, Schafer WR (2006) Visualization of integral and peripheral cell surface proteins in live Caenorhabditis elegans. *J Neurosci Methods* **154:** 68–79

Gray PC, Harrison CA, Vale W (2003) Cripto forms a complex with activin and type II activin receptors and can block activin signaling. *Proc Natl Acad Sci USA* **100:** 5193–5198

Gu Y, Camacho P, Gardner P, Hall ZW (1991) Identification of two amino acid residues in the epsilon subunit that promote mammalian muscle acetylcholine receptor assembly in COS cells. *Neuron* **6:** 879–887

Haffner C, Dettmer U, Weiler T, Haass C (2007) The Nicastrin-like protein Nicalin regulates assembly and stability of the Nicalin-nodal modulator (NOMO) membrane protein complex. *J Biol Chem* **282:** 10632–10638

Haffner C, Frauli M, Topp S, Irmler M, Hofmann K, Regula J, Bally-Cuif L, Haass C (2004) Nicalin and its binding partner Nomo are novel Nodal signaling antagonists. *EMBO J* **23:** 3041–3050

Halevi S, McKay J, Palfreyman M, Yassin L, Eshel M, Jorgensen E, Treinin M (2002) The C. elegans ric-3 gene is required for maturation of nicotinic acetylcholine receptors. *EMBO J* **21:** 1012–1020

Jeanclos EM, Lin L, Treuil MW, Rao J, DeCoster MA, Anand R (2001) The chaperone protein 14-3-3eta interacts with the nicotinic acetylcholine receptor alpha 4 subunit. Evidence for a dynamic role in subunit stabilization. *J Biol Chem* **276:** 28281–28290

Jones AK, Davis P, Hodgkin J, Sattelle DB (2007) The nicotinic acetylcholine receptor gene family of the nematode Caenorhabditis elegans: an update on nomenclature. *Invert Neurosci* **7:** 129–131

Karlin A (2002) Emerging structure of the nicotinic acetylcholine receptors. *Nat Rev Neurosci* **3:** 102–114

Keller SH, Lindstrom J, Taylor P (1996) Involvement of the chaperone protein calnexin and the acetylcholine receptor beta-subunit in the assembly and cell surface expression of the receptor. *J Biol Chem* **271:** 22871–22877

Keller SH, Lindstrom J, Taylor P (1998) Inhibition of glucose trimming with castanospermine reduces calnexin association and promotes proteasome degradation of the alpha-subunit of the nicotinic acetylcholine receptor. *J Biol Chem* **273:** 17064–17072

Keller SH, Taylor P (1999) Determinants responsible for assembly of the nicotinic acetylcholine receptor. *J Gen Physiol* **113:** 171–176

Kreienkamp HJ, Maeda RK, Sine SM, Taylor P (1995) Intersubunit contacts governing assembly of the mammalian nicotinic acetylcholine receptor. *Neuron* **14:** 635–644

Lewis JA, Fleming JT, McLafferty S, Murphy H, Wu C (1987) The levamisole receptor, a cholinergic receptor of the nematode Caenorhabditis elegans. *Mol Pharmacol* **31:** 185–193

Liewald JF, Brauner M, Stephens GJ, Bouhours M, Schultheis C, Zhen M, Gottschalk A (2008) Optogenetic analysis of synaptic function. *Nat Methods* **5:** 895–902

Mishina M, Takai T, Imoto K, Noda M, Takahashi T, Numa S, Methfessel C, Sakmann B (1986) Molecular distinction between fetal and adult forms of muscle acetylcholine receptor. *Nature* **321:** 406–411

Rawson JM, Lee M, Kennedy EL, Selleck SB (2003) Drosophila neuromuscular synapse assembly and function require the TGF-beta type I receptor saxophone and the transcription factor Mad. *J Neurobiol* **55:** 134–150

Rayes D, De Rosa MJ, Sine SM, Bouzat C (2009) Number and locations of agonist binding sites required to activate homomeric Cys-loop receptors. *J Neurosci* **29:** 6022–6032

Rayes D, Flamini M, Hernando G, Bouzat C (2007) Activation of single nicotinic receptor channels from Caenorhabditis elegans muscle. *Mol Pharmacol* **71:** 1407–1415

Ren P, Lim CS, Johnsen R, Albert PS, Pilgrim D, Riddle DL (1996) Control of C. elegans larval development by neuronal expression of a TGF-beta homolog. *Science* **274:** 1389–1391

Richmond JE (2006) Electrophysiological recordings from the neuromuscular junction of *C. elegans*. In *The C. elegans Research Community*, WormBook (ed). doi:10.1895/wormbook.1.112.1, http://www.wormbook.org

Richmond JE, Jorgensen EM (1999) One GABA and two acetylcholine receptors function at the C. elegans neuromuscular junction. *Nat Neurosci* **2:** 791–797

Roberts B, Clucas C, Johnstone IL (2003) Loss of SEC-23 in Caenorhabditis elegans causes defects in oogenesis, morphogenesis, and extracellular matrix secretion. *Mol Biol Cell* **14:** 4414–4426

Savage-Dunn C (2005) TGF-β signaling. In *The C. elegans Research Community*, WormBook (ed). doi:10.1895/wormbook.1.22.1, http://www.wormbook.org

Shah S, Lee SF, Tabuchi K, Hao YH, Yu C, LaPlant Q, Ball H, Dann III CE, Sudhof T, Yu G (2005) Nicastrin functions as a gamma-secretase-substrate receptor. *Cell* **122:** 435–447

Shyu YJ, Hiatt SM, Duren HM, Ellis RE, Kerppola TK, Hu CD (2008) Visualization of protein interactions in living Caenorhabditis elegans using bimolecular fluorescence complementation analysis. *Nat Protoc* **3:** 588–596

Suzuki Y, Yandell MD, Roy PJ, Krishna S, Savage-Dunn C, Ross RM, Padgett RW, Wood WB (1999) A BMP homolog acts as a dose-dependent regulator of body size and male tail patterning in Caenorhabditis elegans. *Development* **126:** 241–250

Touroutine D, Fox RM, Von Stetina SE, Burdina A, Miller III DM, Richmond JE (2005) acr-16 encodes an essential subunit of the levamisole-resistant nicotinic receptor at the Caenorhabditis elegans neuromuscular junction. *J Biol Chem* **280:** 27013–27021

Towers PR, Edwards B, Richmond JE, Sattelle DB (2005) The Caenorhabditis elegans lev-8 gene encodes a novel type of nicotinic acetylcholine receptor alpha subunit. *J Neurochem* **93:** 1–9

Treinin M, Gillo B, Liebman L, Chalfie M (1998) Two functionally dependent acetylcholine subunits are encoded in a single Caenorhabditis elegans operon. *Proc Natl Acad Sci USA* **95:** 15492–15495

Vashlishan AB, Madison JM, Dybbs M, Bai J, Sieburth D, Ch'ng Q, Tavazoie M, Kaplan JM (2008) An RNAi screen identifies genes that regulate GABA synapses. *Neuron* **58:** 346–361

Wanamaker CP, Christianson JC, Green WN (2003) Regulation of nicotinic acetylcholine receptor assembly. *Ann N Y Acad Sci* **998:** 66–80

Wang JM, Zhang L, Yao Y, Viroonchatapan N, Rothe E, Wang ZZ (2002) A transmembrane motif governs the surface trafficking of nicotinic acetylcholine receptors. *Nat Neurosci* **5:** 963–970

Wang ZZ, Hardy SF, Hall ZW (1996) Assembly of the nicotinic acetylcholine receptor. The first transmembrane domains of truncated alpha and delta subunits are required for heterodimer formation *in vivo*. *J Biol Chem* **271:** 27575–27584

Yu G, Nishimura M, Arawaka S, Levitan D, Zhang L, Tandon A, Song YQ, Rogaeva E, Chen F, Kawarai T, Supala A, Levesque L, Yu H, Yang DS, Holmes E, Milman P, Liang Y, Zhang DM, Xu DH, Sato C *et al* (2000) Nicastrin modulates presenilin-mediated notch/glp-1 signal transduction and betaAPP processing. *Nature* **407:** 48–54

Optogenetic analysis of synaptic function

Jana F Liewald[1,5], Martin Brauner[1,5], Greg J Stephens[2], Magali Bouhours[3], Christian Schultheis[1], Mei Zhen[3] & Alexander Gottschalk[1,4]

We introduce optogenetic investigation of neurotransmission (OptIoN) for time-resolved and quantitative assessment of synaptic function via behavioral and electrophysiological analyses. We photo-triggered release of acetylcholine or γ-aminobutyric acid at *Caenorhabditis elegans* neuromuscular junctions using targeted expression of *Chlamydomonas reinhardtii* Channelrhodopsin-2. In intact Channelrhodopsin-2 transgenic worms, photostimulation instantly induced body elongation (for γ-aminobutyric acid) or contraction (for acetylcholine), which we analyzed acutely, or during sustained activation with automated image analysis, to assess synaptic efficacy. In dissected worms, photostimulation evoked neurotransmitter-specific postsynaptic currents that could be triggered repeatedly and at various frequencies. Light-evoked behaviors and postsynaptic currents were significantly ($P \leq 0.05$) altered in mutants with pre- or postsynaptic defects, although the behavioral phenotypes did not unambiguously report on synaptic function in all cases tested. OptIoN facilitates the analysis of neurotransmission with high temporal precision, in a neurotransmitter-selective manner, possibly allowing future investigation of synaptic plasticity in *C. elegans*.

Much of our understanding of the mechanisms of chemical synaptic transmission comes from the analysis of mutants that are compromised in pre- or postsynaptic functions. Such mutants could be affected in synaptic-vesicle biogenesis, neurotransmitter loading, active zone translocation, vesicle priming, fusion and recycling[1,2] or biogenesis, surface expression and function of neurotransmitter receptors[3]. Lesions in synaptic transmission are analyzed at the single-synapse level by electrophysiology or imaging[4] and at the behavioral level using pharmacological synaptic perturbation[5].

The neuromuscular junction of the nematode *C. elegans* is a key genetic model for examining molecular mechanisms of neurotransmission[6,7]. The basic protein machineries involved in mammalian neurotransmission are conserved in *C. elegans*[1,2,5,8]. Most *C. elegans* mutants with severe neurotransmission defects are viable, and adult worms can thus be analyzed. However, many state-of-the-art physiological tools are technically challenging to implement in the worm. For electrophysiological analysis at neuromuscular junctions, worms must be dissected to access the muscle cells for patch-clamp analysis, and motoneurons are stimulated by electric or osmotic shock, which activates the readily releasable pool of synaptic vesicles[6,7]. This is challenging because of the small size of the preparation. Also, the current protocol is limited in its utility. First, the approach cannot be used to distinguish between cholinergic and γ-aminobutyric acid (GABA)-ergic inputs. Second, electric shocks are variable and cause tissue damage, thus only low-frequency electrical stimulation has been reported[9]. Furthermore, methods allowing physiological *in vivo* synaptic stimulation, which could facilitate analysis of synaptic efficacy and plasticity in intact worms, are not established. To this end, we previously developed optogenetic methods, using the light-gated cation channel Channelrhodopsin-2 (ChR2), for precise photoinduced depolarization of muscle cells or neurons in live and dissected transgenic *C. elegans*[10–12]. Similar approaches have been reported for vertebrate systems[13–15].
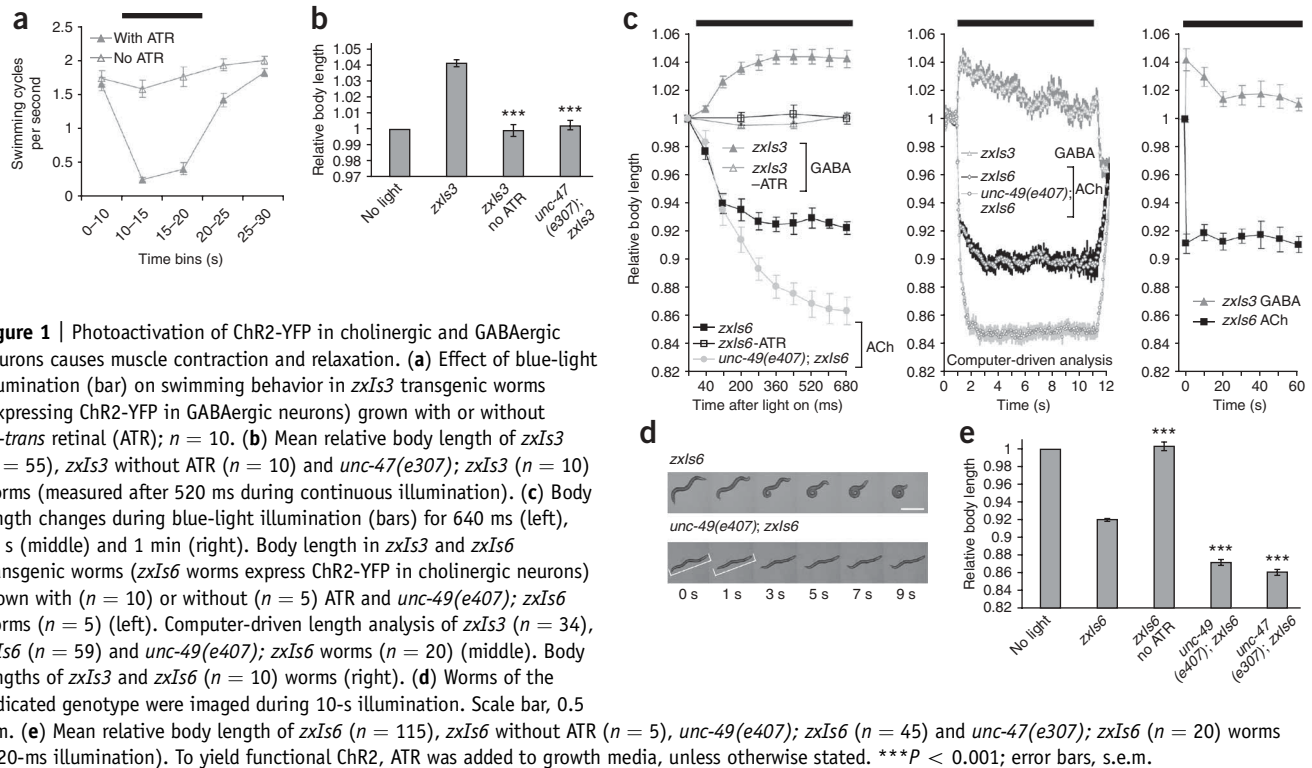
Here we introduce optogenetic investigation of neurotransmission (OptIoN), which allows selective, reproducible and repetitive high-frequency photostimulation of cholinergic or GABAergic neurons. By analyzing in a quantitative and time-resolved manner the photoinduced electrical activity in dissected neuromuscular junctions as well as photo-evoked behavioral changes in the intact worm, we can examine *C. elegans* mutants for defects in various aspects of synaptic function.

RESULTS

Sensitizing cholinergic and GABAergic motoneurons to light

At the *C. elegans* neuromuscular junction, body-wall muscle cells are innervated by both cholinergic (excitatory) and GABAergic (inhibitory) motoneurons[16] (**Supplementary Fig. 1a** online). To selectively sensitize these neurons to light-induced depolarization, we created artificial transgenes to selectively express ChR2 (amino acids 1–315) fused to YFP (GenBank accession AF461397; we also introduced the H134R mutation, as previously described[11]) in these cells, using two cell type–specific promoters: (i) we used P*unc-47*, which normally drives expression of the vesicular GABA transporter vGAT[17], to express ChR2-YFP in GABAergic neurons (from the

Figure 1 | Photoactivation of ChR2-YFP in cholinergic and GABAergic neurons causes muscle contraction and relaxation. (**a**) Effect of blue-light illumination (bar) on swimming behavior in *zxIs3* transgenic worms (expressing ChR2-YFP in GABAergic neurons) grown with or without all-*trans* retinal (ATR); *n* = 10. (**b**) Mean relative body length of *zxIs3* (*n* = 55), *zxIs3* without ATR (*n* = 10) and *unc-47(e307); zxIs3* (*n* = 10) worms (measured after 520 ms during continuous illumination). (**c**) Body length changes during blue-light illumination (bars) for 640 ms (left), 10 s (middle) and 1 min (right). Body length in *zxIs3* and *zxIs6* transgenic worms (*zxIs6* worms express ChR2-YFP in cholinergic neurons) grown with (*n* = 10) or without (*n* = 5) ATR and *unc-49(e407); zxIs6* worms (*n* = 5) (left). Computer-driven length analysis of *zxIs3* (*n* = 34), *zxIs6* (*n* = 59) and *unc-49(e407); zxIs6* worms (*n* = 20) (middle). Body lengths of *zxIs3* and *zxIs6* (*n* = 10) worms (right). (**d**) Worms of the indicated genotype were imaged during 10-s illumination. Scale bar, 0.5 mm. (**e**) Mean relative body length of *zxIs6* (*n* = 115), *zxIs6* without ATR (*n* = 5), *unc-49(e407); zxIs6* (*n* = 45) and *unc-47(e307); zxIs6* (*n* = 20) worms (520-ms illumination). To yield functional ChR2, ATR was added to growth media, unless otherwise stated. ***P < 0.001; error bars, s.e.m.

integrated transgene *zxIs3*); and (ii) we used P*unc-17*, which normally drives expression of the vesicular acetylcholine (ACh) transporter vAChT[18], to express ChR2-YFP in cholinergic neurons (from the integrated transgene *zxIs6*). YFP fluorescence was evident at the plasma membrane of neuronal somata, and along dorsal and ventral nerve cord processes; we verified normal structure of the nervous system in the strains used (**Supplementary Fig. 2** online). To provide the chromophore, essential for ChR2 function, we grew transgenic worms on medium containing all-*trans* retinal.

Light-induced GABA or ACh release alters body length

When we activated ChR2-YFP in *zxIs3* (GABA) worms swimming in liquid by applying 450–490 nm light, normal swimming behavior became almost completely blocked (**Fig. 1a** and **Supplementary Video 1** online). On a solid substrate, illuminated *zxIs3* worms exhibited almost complete paralysis, presumably because of simultaneous relaxation of all body-wall muscle cells (**Supplementary Video 2** online). The body also elongated up to 104.1 ± 0.2% of the initial length, within ∼350 ms (**Fig. 1b,c**; values were measured after 520 ms using graphics software). We could trigger this behavior repeatedly, and it fully reversed in the dark (**Fig. 1c** and data not shown). During 10 s of illumination, worms partially recovered from paralysis after ∼3 s, that is, elongation slowly decreased (**Fig. 1c**), and they resumed moving, though in an uncoordinated fashion and with reduced speed (**Supplementary Video 2** and data not shown). However, worms remained partially elongated even after 60 s, suggesting sustained GABA release (**Fig. 1c**; 101.1 ± 0.4%). Elongation was abolished in *unc-47(e307)* mutants that lacked the vGAT (**Fig. 1b** and **Supplementary Video 3** online), indicating that elongation depended on GABA-filled synaptic vesicles. Neither transgenic worms grown

without all-*trans* retinal (**Fig. 1a–c**), nor wild-type worms grown with or without all-*trans* retinal showed any of these effects when illuminated[11,12].

When we photostimulated cholinergic neurons in worms expressing the transgene *zxIs6*, either for 10 s or 60 s (**Fig. 1c,d**) or 10 ms (**Supplementary Fig. 1b**), worms showed rapid body contraction to 92.0 ± 0.2% of the initial body length (**Fig. 1c,e** and **Supplementary Videos 4** and **5** online). Contractions reached a maximal level after 200–300 ms; however, unless we reported time courses, the reported values were obtained after 520 ms of illumination (**Supplementary Table 1** online). Contractions were sustained during 60 s of illumination (**Fig. 1c**). Additionally, within ∼10 s of illumination, dorsal coiling of the worms was triggered (*n* = 20; **Fig. 1d** and **Supplementary Video 4**). Concomitant GABA release, indirectly triggered by photoactivation of cholinergic neurons innervating GABAergic neurons[16,19] (**Supplementary Fig. 1a**), may cause the coiling and reduce the extent of evoked contractions. Indeed, *unc-49(e407)* worms[20], lacking the ionotropic GABA$_A$ receptor (GABA$_A$R) in muscle, and *unc-47(e307)* vGAT mutants showed no coiling (**Supplementary Video 6** online) and stronger shortening (to 86–87% of the initial length; **Fig. 1c–e**).

As the promoter P*unc-17* is known to be active in a few interneurons as well as in the cholinergic motoneurons, we examined transgenic worms expressing ChR2-YFP from another cholinergic, motoneuron-specific but weaker promoter, P*unc-4*. Again we observed contraction and coiling upon illumination but to a milder degree. Thus, shrinking and coiling appear to be due to ChR2 activity in cholinergic motoneurons, and the extent of the effect depends on the amount of ChR2-YFP expressed (**Supplementary Fig. 1c**). Transgenic *zxIs6* worms grown without all-*trans* retinal neither contracted (**Fig. 1c,e**) nor coiled during illumination.
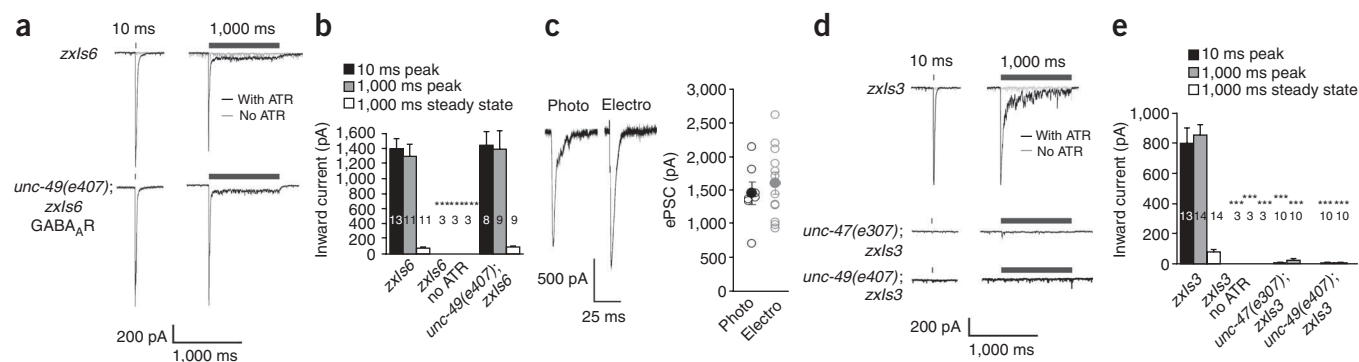
Figure 2 | Light-induced ACh or GABA release evokes postsynaptic currents at the neuromuscular junction. (**a**–**e**) Representative traces for ACh-mediated (**a**) and GABA-mediated (**d**) inward currents evoked by photostimuli (bars) of 10 or 1,000 ms in the presence and absence of all-*trans* retinal (ATR). Mean peak values of currents evoked in the presence of ATR by 10-ms and 1,000-ms illumination (ACh (**b**) and GABA (**e**); *n* values indicated in the bars). GABA photo-ePSCs are outward because of the high Cl⁻ concentration in the patch pipette. Representative traces of PSCs (**c**) evoked by a 10-ms photostimulus or electrostimulus. Mean values of ePSCs did not differ for photo- (*n* = 7) and electrical ePSCs (*n* = 12). ATR was added to growth media, unless otherwise stated.

Quantitative analysis of prolonged light-evoked behaviors

Analyzing the time course of both acute and long-lasting light-evoked behaviors at high temporal resolution could provide information about synaptic performance. Using software we had developed[21], we collected automated measurements of worm body length in individual movie frames before, during and after illumination. As we observed by manual quantification, *zxIs6* worms contracted to about 90% of the original length and remained contracted during the 10-s stimulus, whereas *unc-49(e407);zxIs6* mutants sustained contractions to ~85% (**Fig. 1c** and **Supplementary Fig. 3** online). In *zxIs3* worms, photostimulation triggered elongation within ~500 ms, which lasted for the entire 10 s of illumination, though the length slowly decreased from an initial 104.5% to ~102% (**Fig. 1c**).

Light-induced ACh or GABA release evokes photo-ePSCs

To measure photo-evoked transmitter release at the cellular level, we performed whole-cell voltage-clamp recordings from body-wall muscle cells. The frequency and amplitude of endogenous miniature postsynaptic currents of ChR2-YFP-expressing worms were comparable to those in the wild type (**Supplementary Fig. 4a** online). Postsynaptic physiology was normal in worms expressing ChR2-YFP (**Supplementary Fig. 4b**).

In *zxIs6* and *zxIs3* transgenic worms grown without all-*trans* retinal, photostimulation evoked no postsynaptic currents. However, in *zxIs6* (ACh) worms raised with all-*trans* retinal, 10-ms blue light pulses induced evoked postsynaptic currents (ePSCs) of 1,401 ± 126 pA, which were neurotransmitter-specific, fast and peaked after ~5 ms (**Fig. 2a,b**). These light-induced ePSCs (from now on termed photo-ePSCs) were mediated by ACh only, with no contribution from ACh-induced GABA release, as we observed equivalent photo-ePSCs in *unc-49(e407)* GABA_AR mutants (**Fig. 2a,b**) and the evoked currents could be blocked by tubocurare (**Supplementary Fig. 4c**). Photo-evoked ACh ePSCs generally compared well to electrically evoked ePSCs, displaying similar kinetics, and could be manipulated to comparable amplitudes by modulating the intensity of the stimuli (**Fig. 2c**).

Electric stimulation does not generate GABA ePSCs, for unknown reasons[22]. Notably, using OptIoN, we recorded GABA ePSCs after GABA motoneuron–specific photoactivation: 10-ms

photostimuli on *zxIs3* worms induced photo-ePSCs of 803 ± 102 pA (**Fig. 2d,e**). These photo-ePSCs were GABA-evoked because they were abolished in *unc-47(e307)* vGAT mutants and in *unc-49(e407)* GABA_AR mutants (**Fig. 2d,e**). In addition, they were not affected by the presence of tubocurare (**Supplementary Fig. 4c**).
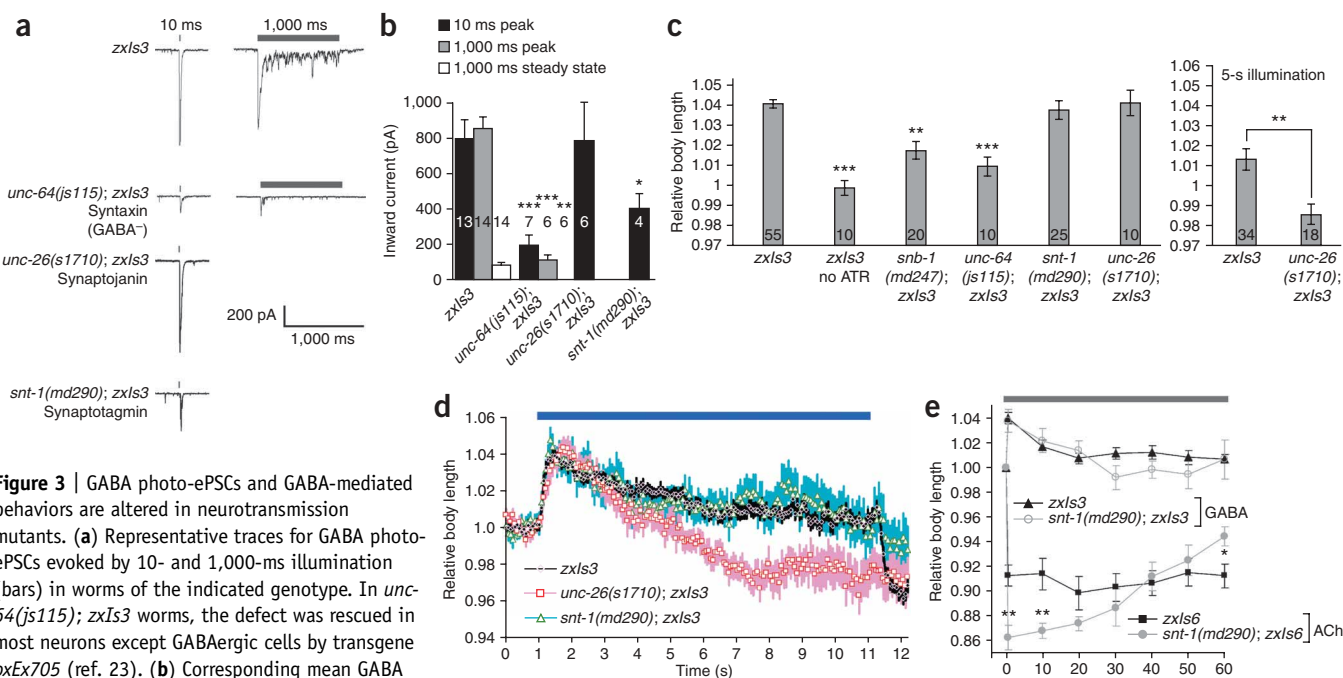
Finally, in contrast to electric stimulation, OptIoN allows prolonged, continuous stimulation. In both *zxIs6* and *zxIs3* strains, 1-s photostimulation induced peak ePSCs (ACh, 1,299 ± 157 pA; GABA, 855 ± 65 pA; **Fig. 2a,b,d,e**). Currents decreased to small steady-state levels persisting as long as the illumination (ACh, 79 ± 8 pA (6% of peak); GABA, 80 ± 17 pA (9% of peak)). How these ePSCs correlate with the activity of motoneurons in intact worms during prolonged illumination and, notably, during normal physiological neurotransmission in the worm, is unknown.

Analyzing defective GABA neurotransmission by OptIoN

Using photo-induced GABA release, we investigated whether GABAergic synaptic defects in various mutants correlated at the behavioral and cellular levels. In *unc-47(e307)* vGAT mutants, which did not show GABA photo-ePSCs (**Fig. 2d,e**), we also could not photo-evoke relaxation (**Fig. 1b**, **Supplementary Video 3** and **Supplementary Table 1**). We made analogous observations in *unc-64(js115)* mutants, which lack the t-SNARE syntaxin specifically in GABAergic neurons[23]. Consistent with syntaxin's role in synaptic-vesicle exocytosis[24], GABA photo-ePSCs were drastically reduced (**Fig. 3a,b**), and photo-evoked relaxation was severely impaired (**Fig. 3c** and **Supplementary Table 2** online).

Our assay appears to be also sufficiently sensitive to reveal defects in weak neurotransmission mutants. *snb-1(md247)* mutants, which harbor a mild reduction-of-function mutation in the v-SNARE synaptobrevin[25], showed reduced body elongation immediately after photostimulation (**Fig. 3c**); however, they displayed a wild-type phenotype after ~1 s of photostimulation (**Supplementary Fig. 3b**). One interpretation of this result is that GABA release in *snb-1(md247)* mutants is initially insufficient to evoke a response, but that sufficient GABA may accumulate at the synaptic cleft during sustained stimulation.

We also analyzed mutants in synaptotagmin, the Ca²⁺ sensor for fast synchronous release of primed synaptic vesicles, which additionally acts in synaptic-vesicle endocytosis[26,27]. *snt-1(md290)*

Figure 3 | GABA photo-ePSCs and GABA-mediated behaviors are altered in neurotransmission mutants. (**a**) Representative traces for GABA photo-ePSCs evoked by 10- and 1,000-ms illumination (bars) in worms of the indicated genotype. In *unc-64(js115)*; *zxIs3* worms, the defect was rescued in most neurons except GABAergic cells by transgene *oxEx705* (ref. 23). (**b**) Corresponding mean GABA photo-ePSCs after 10-ms light pulses as well as peak and steady-state currents after 1,000-ms light pulses. (**c**) Mean relative body length after 520 ms (left) or 5 s (right) of light-induced GABA release in worms of indicated genotypes in the presence of all-*trans* retinal (ATR). *zxIs3* worms grown without ATR were analyzed as a control. (**d**) Relative body length after long-term photostimulation (bar) assayed by computer-driven analysis of worm shape. *zxIs3* (*n* = 39) and mutants with impaired neurotransmission, *snt-1(md290)*; *zxIs3* (*n* = 13) and *unc-26(s1710)*; *zxIs3* (*n* = 18), were compared during light-induced GABA release. (**e**) Long-term photostimulation of transgenic worms of the indicated genotype for 60 s (*n* ≥ 10 for all genotypes). Statistically significant differences in all graphs refer to transgene-only values. ATR was added to growth media, unless otherwise stated. *P < 0.05, **P < 0.01 and ***P < 0.001; error bars, s.e.m. Numbers in **b** and **c** are *n* values for each experiment.

null mutants are severely uncoordinated, and GABA-ePSCs were largely reduced in these worms (**Fig. 3a,b** and **Supplementary Table 2**). Notably, GABA-mediated body elongation did not differ from the wild type, either after short or long-term photostimulation (**Fig. 3c–e**). The reason for this discrepancy between photo-evoked behavior and ePSCs is currently unclear; possibly asynchronous GABA release masked defects during prolonged stimulation.

Analyzing defective ACh neurotransmission by OptIoN
Using photoinduced ACh release, we investigated whether cholinergic synaptic defects in various mutants correlated at the behavioral and cellular levels. In worms with mutations in synaptotagmin, *snt-1(md290)*, the synaptic vesicle priming factor *unc-13*(*n2813* and *e1091*) (ref. 28, partial and strong loss-of-function alleles, respectively), and the phospholipid phosphatase synaptojanin, *unc-26(s1710)* (ref. 29), which is Tgene, required for endocytic recycling of synaptic vesicles, we found drastically reduced ACh photo-ePSCs (**Fig. 4a,b** and **Supplementary Table 2**), consistent with previously reported electrically evoked PSCs in some of these mutants[9,28].

Unexpectedly, the behavioral responses of these mutants did not follow the anticipated pattern. Although OptIoN reported altered behavior for presynaptic mutants upon photo-induced ACh release, the photo-evoked contractions were significantly stronger (*P* ≤ 0.05; **Supplementary Table 1**) when compared to those in wild-type worms, thus contradictory to the decreased ACh photo-ePSCs observed. For instance, light-evoked contractions in *snt-1(md290)* mutants (**Figs. 3e** and **4c,d** and **Supplementary**

Table 1) resulted in relative body lengths of 87.5 ± 1.3% (*n* = 10); compared to 92.0 ± 0.2% for wild type (*P* = 0.0018). We observed increased contractions in all presynaptic mutants tested (**Fig. 4c**), including *snb-1(md247)*, *unc-13(n2813)*, *unc-13(e1091)*, *unc-26(s1710)* (ref. 29) and in a mutant in an AP180 clathrin adaptor homolog involved in endocytosis, *unc-11(e47)* (ref. 30). These paradoxical results are at least partially due to compensatory mechanisms in muscle (**Supplementary Fig. 5** and **Supplementary Results** online). These results emphasize that to characterize a particular synaptic mutation, behavioral assays must be complemented with additional experiments.

Repeated photostimulation at various frequencies
We next tested whether ChR2-YFP could enable repeated, possibly even high-frequency stimulation, which is critical for studying defects in synaptic-vesicle recycling and synaptic plasticity. Repetitive, 10-ms light pulses at frequencies between 0.5 and 50 Hz evoked robust and reliable ACh and GABA photo-ePSCs (**Fig. 5a,b** and **Supplementary Fig. 6** online). The amplitude of subsequent currents decreased to 70–85% of that evoked by the initial stimulus for both ACh and GABA neurons at 0.5 Hz or to 52–57% (GABA) and 48–47% (ACh) at 2 Hz. At 35 Hz, some of the later stimuli did not evoke currents. Photo-ePSCs in response to 50-Hz stimuli resembled permanently illuminated samples, that is, exhibiting 'steady-state' currents (data not shown).

The reduction in the magnitude of consecutive ePSCs could represent presynaptic depression or rundown, or desensitization of postsynaptic receptors. To investigate whether ChR2 desensitization also contributes to the rundown, we applied either single
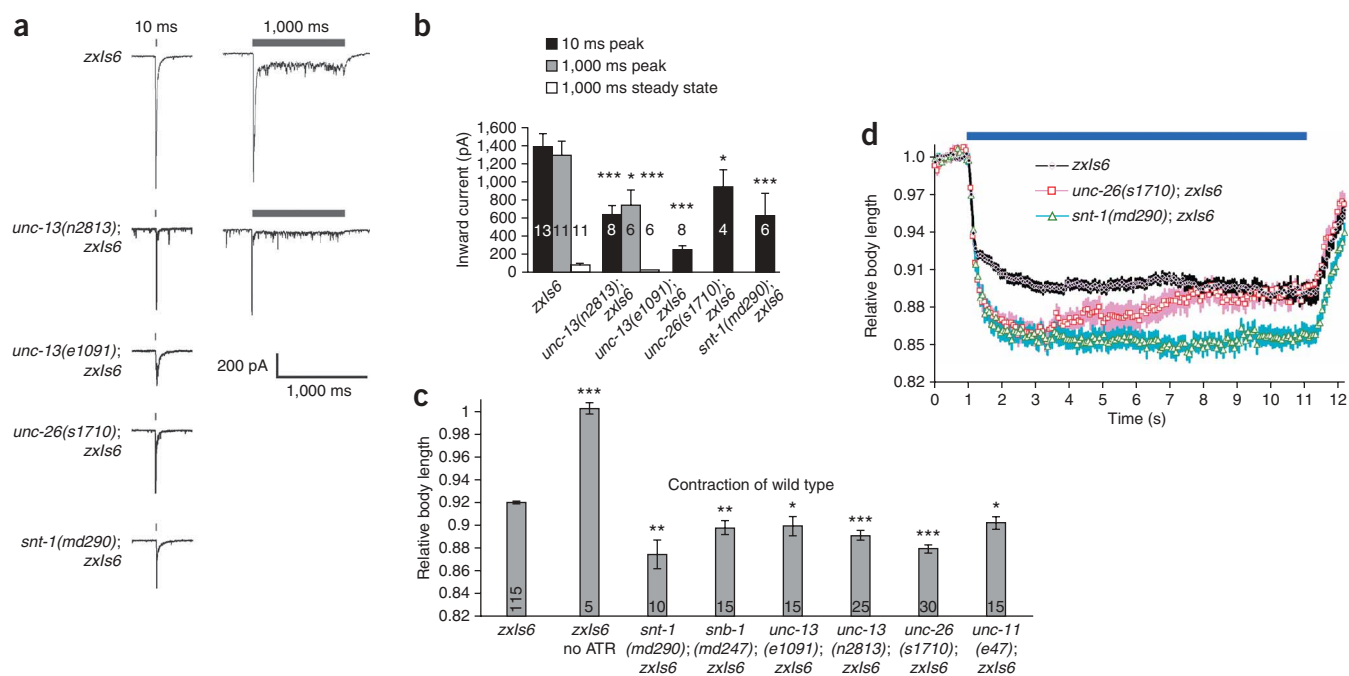
Figure 4 | ACh photo-ePSCs and ACh-mediated behaviors are altered in neurotransmission mutants. (**a**) Representative traces for ACh photo-ePSCs evoked by 10- and 1,000-ms illumination (bars) in worms of the indicated genotype. (**b**) Corresponding mean ACh photo-ePSCs. (**c**) Mean relative body length after 520 ms of light-induced ACh release in worms of the indicated genotypes in the presence of all-*trans* retinal (ATR). As a control, wild-type worms grown in the absence of ATR were also analyzed. Numbers in **b** and **c** are n values for each experiment. (**d**) Relative body length after long-term photostimulation (bar) assayed by computer-driven analysis of worm shape. Wild type ($n = 59$) and mutants with impaired neurotransmission, *snt-1(md290)*; *zxIs6* ($n = 27$) and *unc-26(s1710)*; *zxIs6* ($n = 16$) were compared during light-induced ACh release. ATR was added to growth media, unless otherwise stated. *$P < 0.05$, **$P < 0.01$ and ***$P < 0.001$; error bars, s.e.m.

stimuli or 2-Hz stimulus trains including 20-s or 60-s dark periods (interstimulus or intertrain intervals). We observed that ePSCs after 20-s interstimulus intervals or the first ePSCs in trains with 20-s intertrain intervals recovered to initial values (**Supplementary Figs. 7** and **8** online); thus ChR2 requires 10–20 s for full recovery, as reported in other systems[10,11,13]. Hence, although ChR2 desensitization may contribute to the steep drop from first to second ePSC at higher frequencies, it should not affect rundown in consecutive ePSCs at lower frequencies (0.5 Hz; **Fig. 5a,b** and **Supplementary Fig. 6**).

At intermediate frequencies, photostimulation evoked trains of ePSCs decayed with

similar kinetics as those evoked by electrical stimulation but with higher reproducibility (2 Hz, **Fig. 5c,d**; 0.5 Hz, **Supplementary Fig. 6e,f**; compare also to published results[9]). Electrical stimulation
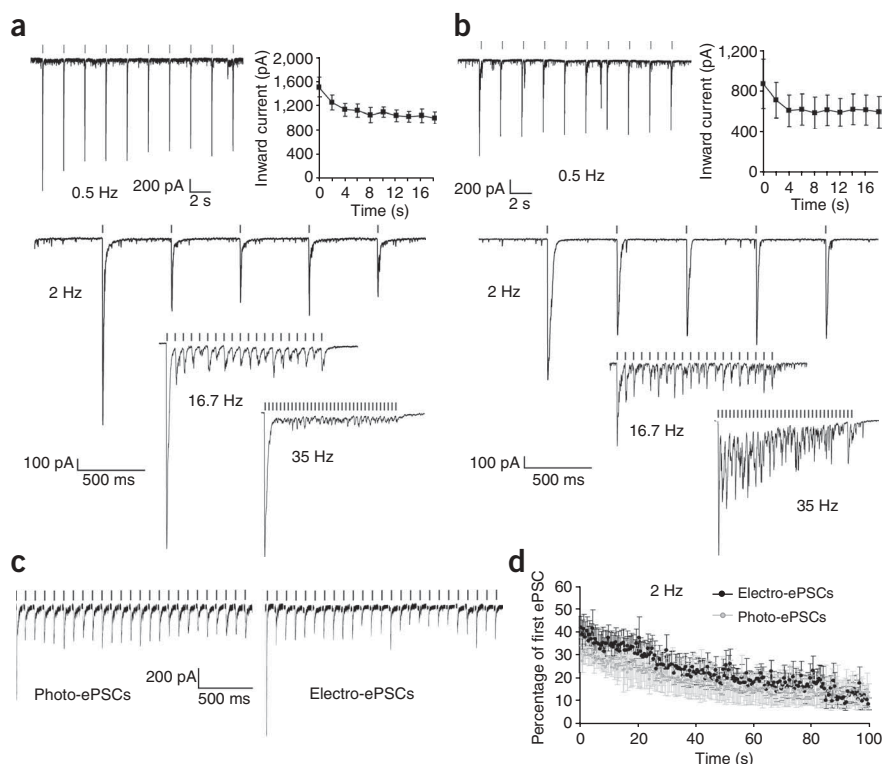
Figure 5 | ACh and GABA photo-ePSCs and ACh-electro-ePSCs during repeated stimulation. (**a,b**) Currents evoked by repeated photostimulation (10-ms pulses) at various frequencies (0.5, 2, 16.7 and 35 Hz) and representative traces for ACh (**a**) and GABA (**b**) photo-ePSCs. Mean inward currents at 0.5 Hz ($n = 5$ each) (top right). Worms were wild type, apart from *zxIs6* (ACh) or *zxIs3* (GABA) transgene. (**c**) Representative traces of ePSCs evoked by repeated stimulation at 2 Hz. (**d**) Mean values of currents normalized relative to the first ePSC were not different for photo-evoked ($n = 6$) and electro-evoked ($n = 11$) ePSCs. ATR was added to growth media, unless otherwise stated. Error bars, s.e.m.

did not evoke more than a handful of ePSCs at 20 Hz (data not shown). Thus, photostimulation is a technically far less demanding, more versatile and more reproducible way to trigger ePSCs at both low and high frequencies in a neurotransmitter-specific fashion.

Analyzing defects in synaptic-vesicle priming and recycling

The frequency-dependent rundown of consecutive ePSCs, which we observed under conditions that challenge the synapse (that is, with repeated photostimulation), is likely to reflect at least to some extent a depletion of the readily releasable pool of synaptic vesicles (**Fig. 5** and **Supplementary Fig. 6**). We reasoned that alterations in the synaptic-vesicle cycle could be reflected in a change in the rate of rundown and could therefore be studied using long-term photostimulation. To investigate whether OptIoN is useful

for electrophysiological analysis of defective synaptic-vesicle priming and recycling, we analyzed mutants with known defects in these processes.

In the absence of UNC-13 function, which primes synaptic vesicles for fusion, the size of the readily releasable pool of synaptic vesicles is reduced, even though the number of docked vesicles is increased[1,24,28]. Photo-ePSCs at 2 Hz in *unc-13(n2813)* and *unc-13 (e1091)* were significantly reduced compared to those in wild-type worms, for all successive stimuli ($P < 0.001$; **Fig. 6a,b**). Normalized ePSCs were also significantly smaller ($P < 0.05$) in *unc-13* mutants for ~20 stimuli (**Fig. 6c** and **Supplementary Fig. 6e**). These results indicate that *unc-13* mutants have decreased synaptic-vesicle fusion, which may be due to impairment in synaptic-vesicle priming for sustained release, but definitively establishing the defective step in the cycle would require further studies. Also, although the wild type
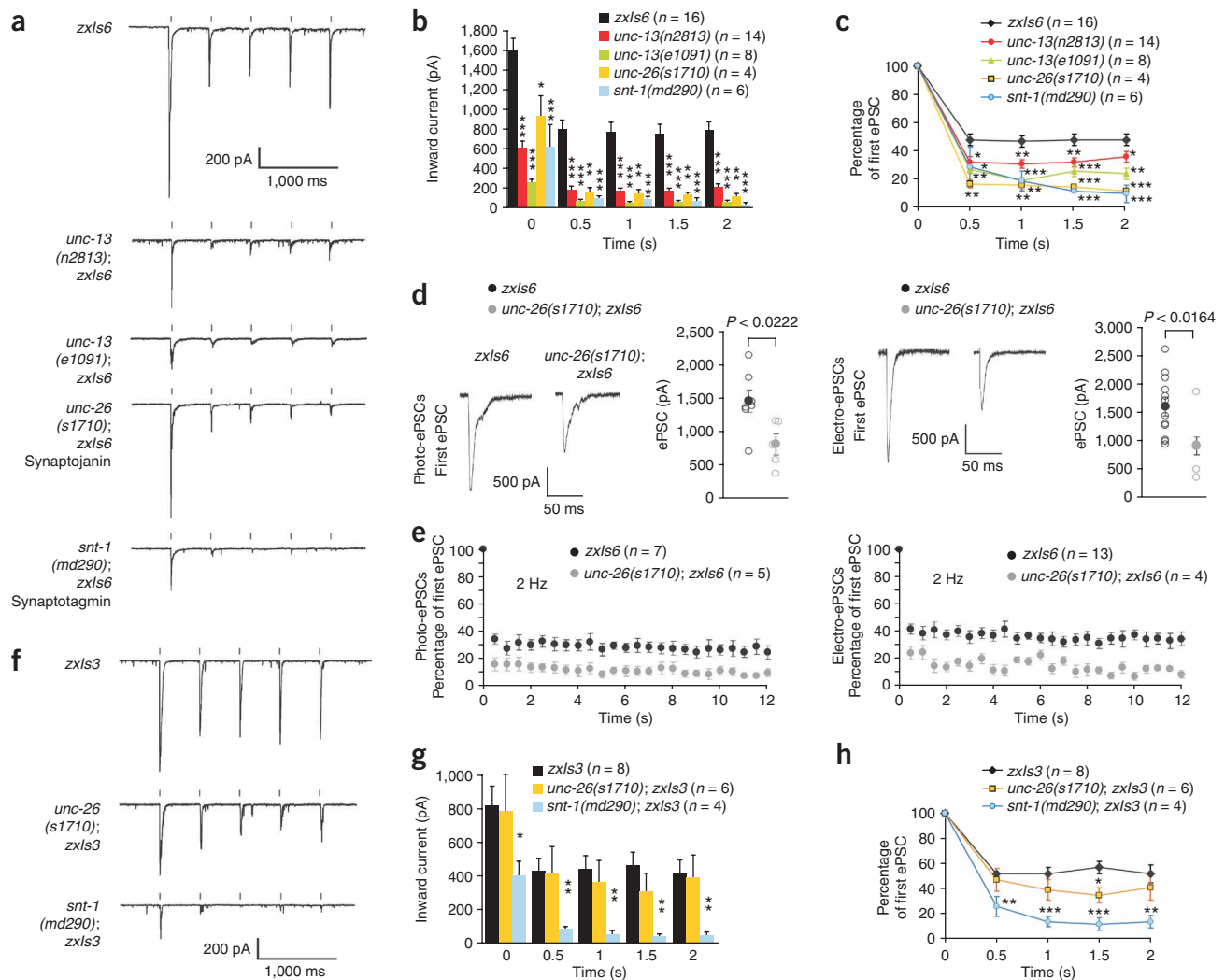
Figure 6 | ACh and GABA photo-ePSCs during repeated photostimulation are altered in neurotransmission mutants implicated in synaptic-vesicle priming and recycling. (**a**) Representative traces for ACh photo-ePSCs evoked by five consecutive 10-ms light pulses at 2 Hz, measured in worms of the indicated genotypes. (**b,c**) Mean ACh photo-ePSCs (**b**) and ACh photo-ePSCs normalized relative to the first evoked current (**c**) in the same worms. All worms carry the *zxIs6* transgene. (**d,e**) Photo- and electro-evoked ACh PSCs compared in *zxIs6* and *unc-26(s1710)*; *zxIs6* worms. (**d**) Representative traces of PSCs evoked by single 10-ms stimuli (left) and mean values of currents evoked by single 10-ms stimuli (right). (**e**) ACh photo- and electro-evoked ePSCs triggered by 2-Hz stimulus trains. (**f**) Representative traces for GABA photo-ePSCs evoked by five consecutive 10-ms light pulses at 2 Hz, measured in worms of the indicated genotypes. All worms carry the transgene *zxIs3*. (**g,h**) Mean GABA photo-ePSCs (**g**) and GABA photo-ePSCs normalized relative to the first evoked current (**h**) in the same worms. ATR was added to growth media. Statistically significant differences in all graphs refer to transgene-only values. *$P < 0.05$, **$P < 0.01$ and ***$P < 0.001$; error bars, s.e.m.

showed less depression in synaptic transmission early during the photostimulus train, after ∼40 photostimuli, normalized photo-ePSCs in the wild type decreased below those in *unc-13(n2813)* (**Supplementary Fig. 6e**). It is possible that the reserve pool of synaptic vesicles in wild type depletes faster than in the *unc-13* mutant because of more efficient priming in the wild type.

Synaptojanin *unc-26(s1710)* mutants are defective in synaptic-vesicle budding and uncoating during clathrin-mediated endocytosis[9,29]. Consistent with previous studies[9,29], the first ACh photo-ePSC was reduced, and consecutive ePSCs (5 stimuli, 2 Hz) were significantly reduced as compared to wild type ($P < 0.01$; **Fig. 6a–c**). Direct comparison of electro- and photostimulus trains (2 Hz; **Fig. 6d,e**; 0.5 Hz, data not shown) in *unc-26(s1710)* mutants confirmed these findings, further proving the power of the photo-stimulation system as an accurate but much easier way of assaying synaptic function.

The recycling defect was also reflected in long-term behavioral analysis: When we photostimulated ACh release for 10 s, wild-type worms sustained constant contraction throughout the illumination, while the initially exaggerated body contraction of *unc-26(s1710)* worms returned to wild-type level after 2–3 s (**Fig. 4d**). We observed similar results during prolonged GABA release: initially normal elongation of *unc-26(s1710)* worms dropped below wild-type level within 4 s (**Fig. 3c,d**). Normalized GABA photo-ePSCs in *unc-26* mutants were significantly different to those in wild type only for the fourth stimulus during a 2-Hz, 5-stimulus train ($P < 0.05$; **Fig. 6f–h**). This was possibly due to the brevity of the experiment; behavioral experiments that showed clear differences lasted longer and involved constant stimulation (10 s; **Fig. 3d**).

Lastly, for synaptotagmin, OptIoN revealed effects consistent with its mediation of fast synchronous synaptic-vesicle release, but also its proposed role in synaptic-vesicle recycling[26]. During 2-Hz stimulus trains, *snt-1(md290)* mutants showed severe decay in consecutive normalized photo-ePSCs in response to stimulation of both cholinergic and GABAergic neurons (**Fig. 6a–c,f–h**). The effect on behavior was also consistent with a defect in synaptic-vesicle recycling in cholinergic neurons, as evoked contractions in response to ACh, though initially stronger in *snt-1(md290)* than in wild-type worms, continuously decreased during a 1-min stimulus until they became weaker than those in the wild type after ∼40 s (**Fig. 3e**).

DISCUSSION

OptIoN greatly simplifies current electrophysiological protocols by obviating the requirement for damaging electrical stimulation[6,7]. Further, photostimulation is technically far more versatile than electrical stimulation: photo-ePSCs can be induced at high frequency and under sustained stimulation. Our method thus opens up the *C. elegans* system to studies of synaptic plasticity. OptIoN also allows, to our knowledge for the first time, to trigger GABA release at the neuromuscular junctions. Therefore it will provide insight into genes that regulate the synaptic function of GABAergic neurons.

OptIoN complements presently available methods for behavioral analysis of neurotransmission in *C. elegans*. Currently postsynaptic defects are most commonly characterized at the behavioral level by measuring the resistance of worms to nicotinic acetylcholine receptor (nAChR) or GABA$_A$R agonists. Presynaptic impairment is typically analyzed by the resistance to the ACh-esterase inhibitor aldicarb; this readout is indirectly also sensitive to defective GABA

transmission. Yet these methods lack the temporal precision of OptIoN: pharmacologically induced paralysis is typically quantified after minutes to hours, whereas light-induced effects occur instantly. Moreover, the light stimulus can be turned off immediately, whereas agonists can not be removed on a reasonable time scale, which impedes repeated stimulation.

Although behavioral analyses by OptIoN can report on the existence of synaptic abnormalities, the physiological nature of synaptic defects cannot be determined solely based on behavioral assays. Presynaptic mutations that reduce ACh release caused increased light-evoked contractions, just as enhanced ACh release in the presence of phorbol esters did (**Supplementary Fig. 5**). Although this is likely due to a compensatory increase in muscle excitability in mutants with reduced ACh release, we cannot exclude other reasons (see **Supplementary Results**). In general, therefore, additional analyses of mutants that show behavioral changes are required. Furthermore, continuous photostimulation caused sustained behavioral changes, whereas steady-state photo-ePSCs were small compared to the initial peak currents. It is thus not clear how sustained behavior and ePSCs (the latter measured in dissected worms) correspond to each other; this may cause discrepancies in results obtained by the two approaches.

Another concern with the behavioral analyses might be that the effects may be sensitive to body size; this is relevant because many presynaptic mutants are smaller than wild-type worms. We compared adult and larval stage four (L4) worms, which are about half the size of adults (**Supplementary Fig. 1d,e**). Normalized GABA-evoked elongations did not differ, and there was a weak positive correlation between body size and extent of ACh-mediated contractions. Thus, if at all, defects in small mutants would only be underestimated.

Postsynaptic mutations can also be analyzed by OptIoN, as exemplified by our analysis of *unc-49* GABA$_A$R mutants. Photo-stimulating endogenous transmitter release has advantages over exogenous agonist application: LED illumination provides sub-millisecond accuracy, and transmitter release is independent of application pipettes, is likely to occur at physiological concentrations and is restricted to synaptic contacts. Thus OptIoN may allow behavioral and physiological analysis also of mutants with dispersed postsynaptic receptors.

Although this study is focused on *C. elegans* neuromuscular junctions, the same principle may be applicable to other model systems such as *Drosophila melanogaster*. Central and peripheral synapses in rodent models may be similarly accessible to optoge-netics-assisted analyses of synaptic function, not only with electro-physiological approaches but possibly also by choosing quantifiable evoked behaviors.

METHODS

Behavioral experiments. Transgenic worms were cultivated in the dark at 20 °C on nematode growth medium (NGM)[8] plates with OP50 bacteria without or with all-*trans* retinal. Plates containing all-*trans* retinal were prepared by spreading 300 μl of OP50 culture mixed with 0.25 μl of 100 mM all-*trans* retinal stock (dissolved in ethanol) onto 5.5-cm plates containing 10 ml of NGM. About 18 h before experiments, L4 larvae, grown on all-*trans* retinal plates, were placed on fresh all-*trans* retinal plates (containing 2 μg/ml phorbol-12-myristate-13-acetate (Sigma), in the case of phorbol ester experiments). Worms were illuminated

with blue light (1.6 mW/mm^2) from a 50-W mercury lamp, filtered through a GFP excitation filter (450–490 nm), on 3.5-cm diameter plates containing 750 µl of NGM, under a 10× objective in a Zeiss Axiovert40 microscope. Duration of illumination was defined by a computer-controlled shutter (Sutter Instruments). Worms were filmed with a Powershot G5 digital camera (Canon) at 320 × 240 resolution, with 4× optical zoom, and body length was determined as previously described[11]. One pixel corresponds to ∼3 µm, and for an adult worm (∼1 mm, or about 300 pixels), the experimental error is ∼0.3% of the body length. For analyzing swimming behavior, worms were washed with M9 buffer and placed into 96-well plates containing 80 µl NGM and 80 µl of M9 buffer per well. Worms were filmed during illumination, and swimming cycles (the worm's body bends twice per cycle), full and half, were counted.

Quantitative behavioral analysis. Individual images, extracted as consecutive frames from video microscopy of behaving worms, were processed using Matlab (Mathworks) to extract the worm's body from background[21]. Cases of self-intersection were excluded from processing. Images of worms were skeletonized to a single-pixel-thick backbone and the body length recorded as the backbone length. Worm lengths were normalized by the mean length (averaged over 15 frames) before the photostimulation and followed over hundreds of consecutive movie frames (at 15 Hz). Length chronograms of multiple worms were then averaged and the profiles compared between wild type and mutants. For all analyses, significance compared to wild type after two-tailed Student's t-test is given as P-values.

Additional methods. Descriptions of plasmid construction, generation of transgenic and mutant worms, electrophysiological recordings and fluorescence microscopy are available in **Supplementary Methods** online.

Note: Supplementary information is available on the Nature Methods website.

AUTHOR CONTRIBUTIONS
J.F.L., Mar.B., Mag.B. and A.G. designed the experiments; J.F.L., Mar.B., Mag.B. and C.S. performed the experiments; G.J.S. wrote software and performed automated analysis of worm shape; J.F.L., Mar.B., M.Z., Mag.B. and A.G. performed all other data analysis; and Mar.B., J.F.L., M.Z., Mag.B. and A.G. wrote the manuscript.

Published online at http://www.nature.com/naturemethods/
Reprints and permissions information is available online at
http://npg.nature.com/reprintsandpermissions/

1. Wojcik, S.M. & Brose, N. Regulation of membrane fusion in synaptic excitation-secretion coupling: speed and accuracy matter. *Neuron* **55**, 11–24 (2007).
2. Richmond, J.E. Synaptic function. In *WormBook* (ed., The *C. elegans* Research Community) (doi/10.1895/wormbook.1.69.1; 2005).
3. Richmond, J.E. & Jorgensen, E.M. One GABA and two acetylcholine receptors function at the *C. elegans* neuromuscular junction. *Nat. Neurosci.* **2**, 791–797 (1999).
4. Guerrero, G. *et al.* Heterogeneity in synaptic transmission along a *Drosophila* larval motor axon. *Nat. Neurosci.* **8**, 1188–1196 (2005).
5. Miller, K.G. *et al.* A genetic selection for *Caenorhabditis elegans* synaptic transmission mutants. *Proc. Natl. Acad. Sci. USA* **93**, 12593–12598 (1996).
6. Richmond, J.E. Electrophysiological recordings from the neuromuscular junction of *C. elegans*. In *WormBook* (ed., The *C. elegans* Research Community) (doi/10.1895/wormbook.1.112.1; 2006).
7. Francis, M.M., Mellem, J.E. & Maricq, A.V. Bridging the gap between genes and behavior: recent advances in the electrophysiological analysis of neural function in *Caenorhabditis elegans*. *Trends Neurosci.* **26**, 90–99 (2003).
8. Brenner, S. The genetics of *Caenorhabditis elegans*. *Genetics* **77**, 71–94 (1974).
9. Schuske, K.R. *et al.* Endophilin is required for synaptic vesicle endocytosis by localizing synaptojanin. *Neuron* **40**, 749–762 (2003).
10. Nagel, G. *et al.* Channelrhodopsin-2, a directly light-gated cation-selective membrane channel. *Proc. Natl. Acad. Sci. USA* **100**, 13940–13945 (2003).
11. Nagel, G. *et al.* Light activation of channelrhodopsin-2 in excitable cells of *Caenorhabditis elegans* triggers rapid behavioral responses. *Curr. Biol.* **15**, 2279–2284 (2005).
12. Zhang, F. *et al.* Multimodal fast optical interrogation of neural circuitry. *Nature* **446**, 633–639 (2007).
13. Boyden, E.S., Zhang, F., Bamberg, E., Nagel, G. & Deisseroth, K. Millisecond-timescale, genetically targeted optical control of neural activity. *Nat. Neurosci.* **8**, 1263–1268 (2005).
14. Li, X. *et al.* Fast noninvasive activation and inhibition of neural and network activity by vertebrate rhodopsin and green algae channelrhodopsin. *Proc. Natl. Acad. Sci. USA* **102**, 17816–17821 (2005).
15. Zhang, Y.P. & Oertner, T.G. Optical induction of synaptic plasticity using a light-sensitive channel. *Nat. Methods* **4**, 139–141 (2007).
16. White, J.G., Southgate, E., Thomson, J.N. & Brenner, S. The structure of the nervous system of the nematode *Caenorhabditis elegans*. *Phil. Trans. R. Soc. Lond. B* **314**, 1–340 (1986).
17. McIntire, S.L., Reimer, R.J., Schuske, K., Edwards, R.H. & Jorgensen, E.M. Identification and characterization of the vesicular GABA transporter. *Nature* **389**, 870–876 (1997).
18. Alfonso, A., Grundahl, K., Duerr, J.S., Han, H.P. & Rand, J.B. The *Caenorhabditis elegans* unc-17 gene: a putative vesicular acetylcholine transporter. *Science* **261**, 617–619 (1993).
19. McIntire, S.L., Jorgensen, E., Kaplan, J. & Horvitz, H.R. The GABAergic nervous system of *Caenorhabditis elegans*. *Nature* **364**, 337–341 (1993).
20. Bamber, B.A., Beg, A.A., Twyman, R.E. & Jorgensen, E.M. The *Caenorhabditis elegans* unc-49 locus encodes multiple subunits of a heteromultimeric GABA receptor. *J. Neurosci.* **19**, 5348–5359 (1999).
21. Stephens, G.J., Johnson-Kerner, B., Bialek, W. & Ryu, W.S. Dimensionality and dynamics in the behavior of *C. elegans*. *PLoS Comput. Biol.* **4**, e1000028 (2008).
22. Liu, Q. *et al.* Presynaptic ryanodine receptors are required for normal quantal size at the *Caenorhabditis elegans* neuromuscular junction. *J. Neurosci.* **25**, 6745–6754 (2005).
23. Hammarlund, M., Palfreyman, M.T., Watanabe, S., Olsen, S. & Jorgensen, E.M. Open syntaxin docks synaptic vesicles. *PLoS Biol.* **5**, e198 (2007).
24. Richmond, J.E., Weimer, R.M. & Jorgensen, E.M. An open form of syntaxin bypasses the requirement for UNC-13 in vesicle priming. *Nature* **412**, 338–341 (2001).
25. Nonet, M.L., Saifee, O., Zhao, H., Rand, J.B. & Wei, L. Synaptic transmission deficits in *Caenorhabditis elegans* synaptobrevin mutants. *J. Neurosci.* **18**, 70–80 (1998).
26. Jorgensen, E.M. *et al.* Defective recycling of synaptic vesicles in synaptotagmin mutants of *Caenorhabditis elegans*. *Nature* **378**, 196–199 (1995).
27. Zhang, J.Z., Davletov, B.A., Sudhof, T.C. & Anderson, R.G. Synaptotagmin I is a high affinity receptor for clathrin AP-2: implications for membrane recycling. *Cell* **78**, 751–760 (1994).
28. Richmond, J.E., Davis, W.S. & Jorgensen, E.M. UNC-13 is required for synaptic vesicle fusion in *C. elegans*. *Nat. Neurosci.* **2**, 959–964 (1999).
29. Harris, T.W., Hartwieg, E., Horvitz, H.R. & Jorgensen, E.M. Mutations in synaptojanin disrupt synaptic vesicle recycling. *J. Cell Biol.* **150**, 589–600 (2000).
30. Nonet, M.L. *et al.* UNC-11, a *Caenorhabditis elegans* AP180 homologue, regulates the size and protein composition of synaptic vesicles. *Mol. Biol. Cell* **10**, 2343–2360 (1999).

Optogenetic analysis of GABA$_B$ receptor signaling in *Caenorhabditis elegans* motor neurons

Christian Schultheis,[1]* **Martin Brauner,**[1]* **Jana F. Liewald,**[1,2] **and Alexander Gottschalk**[1,2]

[1]*Institute of Biochemistry, Department of Biochemistry, Chemistry and Pharmacy and* [2]*Frankfurt Molecular Life Sciences Institute, Goethe-University, Frankfurt, Germany*

Schultheis C, Brauner M, Liewald JF, Gottschalk A. Optogenetic analysis of GABA$_B$ receptor signaling in *Caenorhabditis elegans* motor neurons. *J Neurophysiol* 106: 817–827, 2011. First published May 25, 2011; doi:10.1152/jn.00578.2010.—In the nervous system, a perfect balance of excitation and inhibition is required, for example, to enable coordinated locomotion. In *Caenorhabditis elegans*, cholinergic and GABAergic motor neurons (MNs) effect waves of contralateral muscle contraction and relaxation. Cholinergic MNs innervate muscle as well as GABAergic MNs, projecting to the opposite side of the body, at dyadic synapses. Only a few connections exist from GABAergic to cholinergic MNs, emphasizing that GABA signaling is mainly directed toward muscle. Yet, a GABA$_B$ receptor comprising GBB-1 and GBB-2 subunits, expressed in cholinergic MNs, was shown to affect locomotion, likely by feedback inhibition of cholinergic MNs in response to spillover GABA. In the present study, we examined whether the GBB-1/2 receptor could also affect short-term plasticity in cholinergic MNs with the use of channelrhodopsin-2-mediated photostimulation of GABAergic and cholinergic neurons. The GBB-1/2 receptor contributes to acute body relaxation, evoked by photoactivation of GABAergic MNs, and to effects of GABA on locomotion behavior. Loss of the plasma membrane GABA transporter SNF-11, as well as acute photoevoked GABA release, affected cholinergic MN function in opposite directions. Prolonged stimulation of GABA MNs had subtle effects on cholinergic MNs, depending on stimulus duration and *gbb-2*. Thus GBB-1/2 receptors serve mainly for linear feedback inhibition of cholinergic MNs but also evoke minor plastic changes.

locomotion; metabotropic GABA receptor; plasticity; channelrhodopsin-2; excitatory-inhibitory balance

IN MAMMALS, GABA$_B$ receptors are extrasynaptic, high-affinity G protein-coupled receptors (GPCRs) that either act as presynaptic autoreceptors on GABAergic neurons or detect spillover GABA, released at nearby synapses (Bettler et al. 2004). GABA$_B$ receptors are obligate heterodimers of B1 and B2 subunits (Jones et al. 1998; White et al. 1998) that together with auxiliary subunits (KCTD proteins) appear to form tetramers or even higher order oligomers (Schwenk et al. 2010). GABA$_B$ receptors can modulate the function of excitatory neurons by heterosynaptic inhibition, via signaling through heterotrimeric G proteins (through "released" G$\beta\gamma$ subunits), to inhibit presynaptic voltage-gated Ca^{2+}-channels (Herlitze et al. 1996; Ikeda 1996). Alternatively, they can trigger postsynaptic G protein-activated inward-rectifying potassium (GIRK) channels, again via G$\beta\gamma$ subunits, to induce a slow inhibitory current (Luscher et al. 1997; Schwenk et al. 2010). Furthermore, via Gα_o/Gα_i pathways, mammalian GABA$_B$ receptors can activate or inhibit adenylyl cyclase. At glutamatergic synapses, GABA$_B$ receptors were implicated in synaptic plasticity (Davies et al. 1991; Mott and Lewis 1991), lowering cAMP levels and thus blocking stimulatory effects of increased Ca^{2+} on synaptic vesicle recruitment from the reserve pool (Sakaba and Neher 2003).

Cholinergic motor neurons (MNs) in the *Caenorhabditis elegans* ventral nerve cord activate muscles and GABAergic neurons at dyadic synapses/neuromuscular junctions (NMJs) to coevoke a contralateral inhibition of muscles, thus allowing a bend of the body to occur (Schuske et al. 2004; White et al. 1986). Very few "reverse" connections have been found from GABAergic to cholinergic MNs (White et al. 1986), making it unlikely that these connections contribute much to the excitatory-inhibitory balance. However, a heterodimeric GABA$_B$ receptor, comprising GBB-1 and GBB-2 subunits, was reported to be widely expressed in the nervous system; yet, among MNs, it was exclusively found in cholinergic cells (Dittman and Kaplan 2008). The *gbb-1* or *gbb-2* deletion mutants exhibit alterations in locomotion as well as increased paralysis induced by aldicarb, an inhibitor of acetylcholine (ACh) esterase. Since these effects are not exacerbated in *gbb-1*; *gbb-2* double mutants, it is very likely that these receptors also form hetero(di)mers in *C. elegans*. Because of the aldicarb hypersensitivity of *gbb-1* or *gbb-2* mutants, it is thought that spillover GABA, sensed by the GBB-1/2 receptor, may cause heterosynaptic inhibition of cholinergic MNs. The identity of the G protein that the GBB-1/2 receptor couples to is unknown, although it has been suggested that GBB-1/2 receptors signal through the Gα_o pathway, which inhibits cholinergic transmission by negatively regulating phospholipase C (Lackner et al. 1999). The GBB-1/2 receptor may directly influence cholinergic transmission, i.e., under "steady-state" conditions of GABA transmission, as triggered by ACh release stimulating GABA MNs. In this case, the amount of ACh transmission should linearly feed back on the activity of the cholinergic MNs, since more ACh release would also evoke more GABA release. Alternatively, spillover GABA could induce short-term synaptic plasticity in cholinergic synapses, causing nonlinear feedback regulation of ACh release.

To distinguish between these possibilities, one would ideally measure postsynaptic currents in muscle in response to constant or repeated stimulation of cholinergic MNs. However, the preparation of the *C. elegans* NMJ does not permit such experiments to be performed in a meaningful way (Richmond and Jorgensen 1999), because *1*) commissural connections between cholinergic and GABAergic MNs are cut; *2*) basal

* C. Schultheis and M. Brauner contributed equally to this work.
Address for reprint requests and other correspondence: A. Gottschalk, Institute of Biochemistry, Dept. of Biochemistry, Chemistry and Pharmacy, Goethe-Univ., Max-von-Laue-Strasse 9, D-60438 Frankfurt, Germany (e-mail: a.gottschalk@em.uni-frankfurt.de).

membranes surrounding the NMJs, which would certainly affect the diffusion of spillover GABA, are digested by collagenase treatment; and *3*) the recording is done under buffer flow, which strongly dilutes any spillover transmitter. However, prolonged activation of *C. elegans* neurons in live animals and an indirect analysis of synaptic transmission can be achieved noninvasively by using optogenetic techniques (Nagel et al. 2005; Zhang et al. 2007). Channelrhodopsin-2 (ChR2), expressed and photoactivated in cholinergic cells, causes a simultaneous contraction of all body wall muscles, which depends on the efficacy of synaptic transmission and can easily be measured by automated video analysis (Liewald et al. 2008). Likewise, GABAergic neurons (expressing ChR2) also can be triggered by photostimulation, evoking body relaxation due to simultaneous inhibition of all body wall muscles, an effect that can be macroscopically measured to deduce defects or alterations in GABAergic signaling.

We were able to show that GBB-1/2 receptors contribute to the behavioral effects of photoinduced GABA release. The relaxation effects were completely abolished only if GBB subunits as well as the ionotropic GABA$_A$ receptor UNC-49 were eliminated. Deletion of *gbb-2* had effects on locomotion that could be rescued or even overcompensated by expressing GBB-2(A484V; V572A) specifically in cholinergic MNs, indicating that these cells are the focus of GBB-2 activity. Furthermore, depending on photostimulus strength, duration, and frequency, we observed subtle influences of *gbb-2* deletion on the effects of photoinduced ACh release. Thus GABA$_B$ receptor signaling in *C. elegans* mainly serves as a feedback control mechanism for cholinergic transmission, yet it also effects subtle plastic alterations in cholinergic MN function.

MATERIALS AND METHODS

Genetics. C. elegans strains were cultivated using standard methods on nematode growth medium (NGM) and fed *Escherichia coli* strain OP50-1 (Brenner 1974). For optogenetic experiments, all-*trans* retinal (0.25 μl of a 100 mM stock in ethanol; Sigma) was added to 300 μl of OP50 culture and spread onto 5.5-cm culture dishes containing 10 ml of NGM. About 18 h before experiments, L4 larvae, grown on all-*trans* retinal plates, were placed on fresh all-*trans* retinal plates. Strains used (outcrossed 4–7 times, where appropriate) were as

follows: N2: wild type (Bristol isolate), RM2710: *snf-11(ok156)*, ZX426: N2; *zxIs3[punc-47::ChR2(H134R)::YFP; lin-15$^+$]I*, ZX460: N2; *zxIs6[punc-17::ChR2(H134R)::YFP; lin-15$^+$]V*, ZX464: *unc-49(e407); zxIs3*, ZX551: *gbb-2(tm1165)*, ZX558: *gbb-1(tm1406)*, ZX572: *gbb-2(tm1165); zxIs3*, ZX585: *gbb-1(tm1406); zxIs3*, ZX586: *gbb-1(tm1406); unc-49(e407); zxIs3*, ZX587: *gbb-2(tm1165); unc-49(e407); zxIs3*, ZX635: *gbb-2(tm1165); zxIs6*, ZX675: N2; *zxIs3; zxIs6*, ZX808: *gbb-2(tm1165); zxIs3; zxIs6*, ZX973: *gbb-2(tm1165); snf-11(ok156); zxIs6*, ZX974: *snf-11(ok156); zxIs6*, ZX1052: *gbb-2(tm1165); zxEx455[punc-47::GBB-2(A484V; V572A); pmyo-2::mCherry]*, ZX1053: *gbb-2(tm1165); zxEx456[punc-17::GBB-2(A484V; V572A); pmyo-2::mCherry]*, ZX1054: *gbb-2(tm1165); unc-49(e407); zxIs3; zxEx457[punc-47::GBB-2(A484V; V572A); pmyo-2::mCherry]*, ZX1055: *gbb-2(tm1165); unc-49(e407); zxIs3; zxEx458[punc-17::GBB-2(A484V; V572A); pmyo-2::mCherry]*, ZX1103: N2; *zxEx465[punc-47::GBB-2(A484V; V572A); pmyo-2::mCherry]*, and ZX1104: N2; *zxEx466[punc-17::GBB-2(A484V; V572A); pmyo-2::mCherry]*.

Molecular biology. The plasmid encoding *pmyo-2::mCherry* (pCFJ90) was a kind gift of E. Jorgensen. Construction of plasmids used to generate *zxIs3* and *zxIs6* integrated transgenes was described previously (Liewald et al. 2008). The GBB-2(A484V; V572A) construct was generated as follows. The full-length GBB-2 cDNA with additional restriction sites at both ends was commercially synthesized (Eurofins MWG Operon) and subcloned into the *punc-47::ChR2(H134R)::YFP* plasmid (Liewald et al. 2008) using *Tth*111I and *Eco*RI. Toxicity of this sequence in various plasmid backbones and *E. coli* strains promoted random mutations in the GBB-2 sequence, which after transformation could be reduced by introducing an artificial intron near the 5′-end of the cDNA. However, the most promising clone of GBB-2 still contained two missense mutations resulting in A484V and V572A changes of the GBB-2 amino acid sequence [pCS150NT: *punc-47::GBB-2(A484V; V572A)*]. With the use of *Nhe*I and *Pvu*I, the GBB-2 fragment was then subcloned into *punc-17::ChR2(H134R)::YFP* (Liewald et al. 2008) to generate pCS152NT [*punc-47::GBB-2(A484V; V572A)*].

Behavioral assays and data analysis. Optogenetic/behavioral assays and automated video analysis for the extraction of worm body length were described previously (Liewald et al. 2008; Schultheis et al. 2011; Stirman et al. 2011; Weissenberger et al. 2011). In brief, for body length measurements, animals were transferred onto plain NGM plates and recorded with a PowerShot G5 or G9 digital camera (Canon) while blue light from a 50-W HBO lamp [450- to 490-nm green fluorescent protein excitation filter; intensity adjusted using neutral density filters (AHF Analysetechnik)] was applied. Light intensities were measured in the focal plane using a light power meter (Thorlabs). Light application was
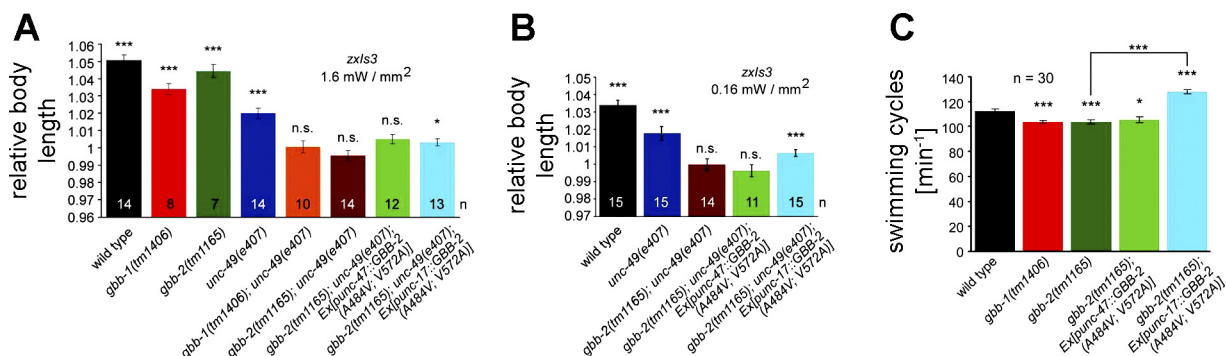

Fig. 1. GABA$_B$ receptors contribute to GABA photoevoked body elongation and affect swimming cycles in cholinergic motor neurons. *A* and *B*: channelrhodopsin-2 (ChR2), expressed in GABAergic motor neurons (MNs) (transgene *zxIs3*; Liewald et al. 2008), was photostimulated to evoke body elongation. Animals of the indicated genotypes were filmed, and the body length during 2 s before and from 0.5 to 2 s during the photostimulation was measured, normalized, and averaged. For an alternative method of analysis, see Fig. 2. Blue light intensities of 1.6 (*A*) and 0.16 mW/mm^2 (*B*) were used. See text for list of strains used. *C*: swimming cycles in M9 buffer were compared in wild-type and *gbb-2(tm1165)* mutant animals in thrashing assays and could be rescued by expression of GBB-2(A484V; V572A) selectively in cholinergic MNs. Values are means ± SE; *n* = no. of animals assayed. Statistically significant differences (*$P < 0.05$; **$P < 0.01$; ***$P < 0.001$; 1-way ANOVA) were assessed with respect to body length before blue light stimulation (*A* and *B*) or to the wild-type level (*C*).

controlled using a computer-controlled shutter (Sutter Instruments). Velocity, bending angles, and trajectories were recorded using tracking software (Stirman et al. 2011) that controls an *x,y*-translational stage and allows photoactivation of ChR2 via a LCD projector (450–490 nm; ~4 mW/mm^2). Ten minutes before the start of these assays, animals were transferred to plain NGM plates. Swimming assays were performed in 96-well plates containing 80 μl of NGM and 80 μl of M9 saline per well. Animals were recorded under ×25 magnification with a PowerShot G9 digital camera (Canon) for 1 min, and swimming cycles were counted.

Electrophysiology. Recordings from dissected *C. elegans* body muscle were performed as described previously (Nagel et al. 2005). After dissection, cells were treated for 8 s with 0.5 mg/ml collagenase (Sigma) in modified Ascaris Ringer's (AR; 150 mM NaCl, 5 mM KCl, 5 mM CaCl$_2$, 1 mM MgCl$_2$, 10 mM glucose, and 15 mM HEPES, pH 7.35, 340 mosM) and washed with AR. Cells were clamped to −60 mV using an EPC10 amplifier with head stage and Pulse software (HEKA). The bath solution was AR; the pipette solution was 120 mM KCl, 20 mM KOH, 4 mM MgCl$_2$, 5 mM Tris·HCl, pH 7.2, 0.25 mM CaCl$_2$, 4 mM ATP, 36 mM sucrose, and 5 mM EGTA (315 mosM). Light activation was performed using an LED lamp (KSL-70; Rapp OptoElectronic, Hamburg, Germany) at a wavelength of 470 nm (maximum: 8 mW/mm^2) and controlled by the HEKA software. Where appropriate, the light intensity of the LED lamp was reduced using the control unit.

RESULTS

GBB-1/2 receptors contribute to GABA effects at the NMJ. We previously analyzed the effects of photoevoked GABA release in animals expressing ChR2 in GABAergic neurons, i.e., containing transgene *zxIs3[punc-47::ChR2(H134R)::YFP; lin-15$^+$]* (Liewald et al. 2008). Animals in which GABA MNs were photostimulated showed a body elongation of up to 5%, depending on photostimulus strength (1.6 vs. 0.16 mW/mm^2), due to simultaneous, flaccid paralysis of all muscles (Fig. 1, *A* and *B*; Supplementary Video 1). (Supplemental material for this article is available online at the *Journal of Neurophysiology* website.) Body length measurements, obtained either by averaging body length over several video frames before and during photostimulation or, when higher numbers of animals were analyzed, in single frames, showed distinguishing significant differences when both absolute and normalized length were compared (Fig. 2, *A–C*). Interestingly, when this was repeated in mutants lacking the sole postsynaptic ionotropic GABA_A receptor UNC-49 (Bamber et al. 1999), the elongation effects were not completely abolished but worms still elongated by up to 2% (Figs. 1, *A* and *B*, and 2, *A–C*; Supplemen-
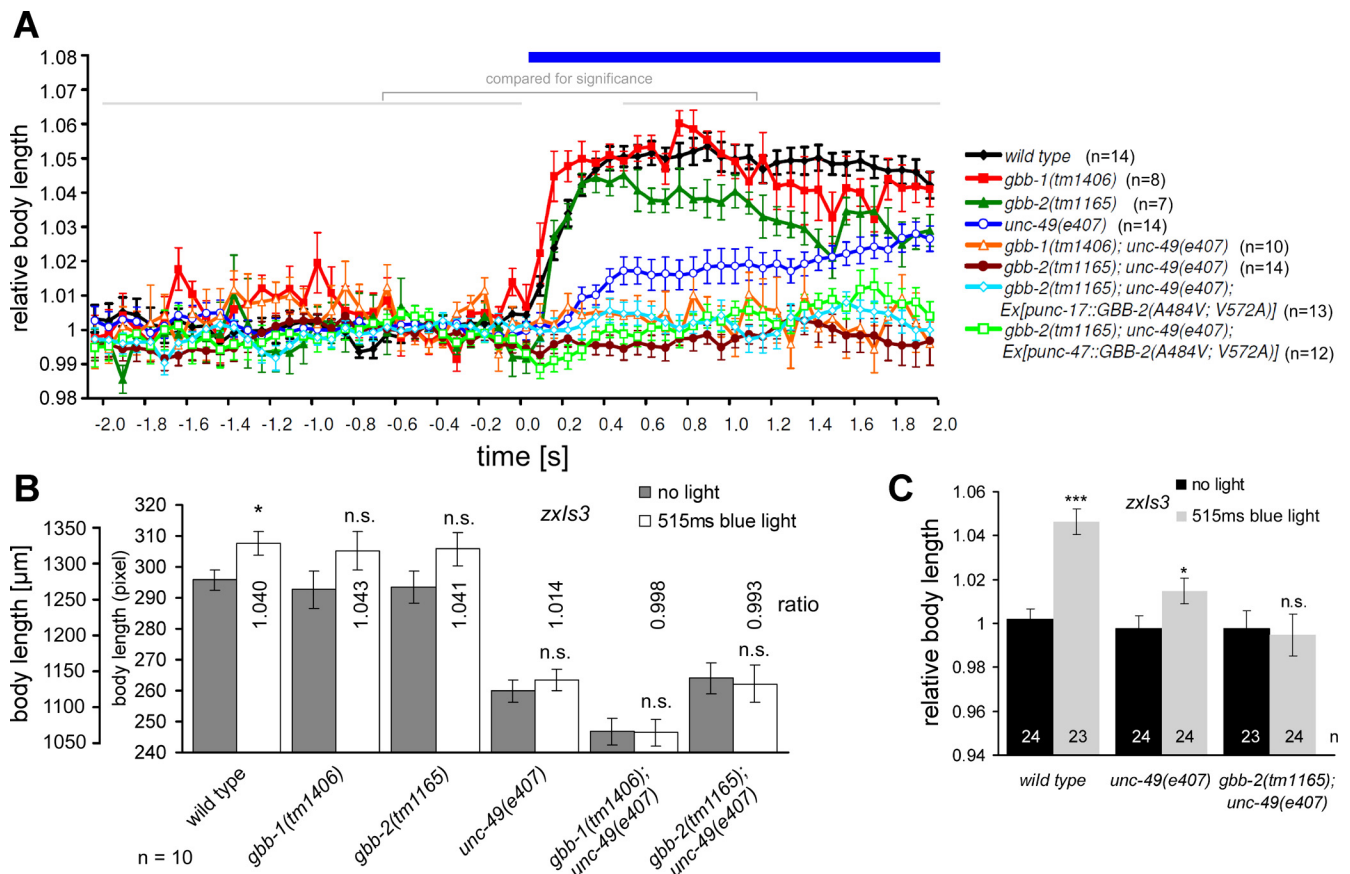

Fig. 2. Analysis of light-evoked elongation in animals expressing ChR2 (transgene *zxIs3*) in GABAergic MNs by averaging over time periods or by comparing single time points and absolute lengths. *A*: animals of the indicated genotypes were filmed before and during a continuous light stimulus (15 frames/s), and body length was deduced from single video frames. The mean length of each animal during the first 30 frames (−2–0 s) was averaged and used to normalize the elongation during the light stimulus. The mean body length before (−2–0 s) and during the stimulus, after full elongation was reached (0.5–2 s), was then averaged for all animals of a genotype and compared, to analyze statistically significant differences (as indicated in Fig. 1*A*). *B*: data for animals from an experiment similar to that in *A* are shown in absolute values (pixels) as obtained from single movie frames (at 515 ms into the continuous stimulus) and compared with the mean length of the 15 frames before illumination onset. The ratio obtained corresponds to the type of data shown in Fig. 1*A*. For *n* = 10 animals each, statistical significance is obtained only for larger size differences. *C*: when larger numbers of animals are analyzed, normalized data for single time points (i.e., not averaged over time periods) allows statistically significant data to be obtained, despite small absolute changes (maximally 4–5% of the initial body length). Values are means ± SE; *n* = no. of animals assayed. *$P < 0.05$; **$P < 0.01$; ***$P < 0.001$; 1-way ANOVA.

tary Video 2). This indicated that an additional GABA receptor may affect this behavioral response, and we wondered whether this could be the GBB-1/2 receptor (Dittman and Kaplan 2008). Genomic deletion of the GBB-1/2 GABA_B receptor on its own did not have any effects on the photoevoked elongation of *zxIs3* animals, indicating that release of GABA was not affected by the *gbb-1/2* mutations (Figs. 1, *A* and *B*, and 2, *A–C*). However, when we analyzed photoevoked GABA-mediated elongation in *gbb-1(tm1406); unc-49(e407)* or *gbb-2(tm1165); unc-49(e407)* double mutants, no effect whatsoever could be detected (Figs. 1, *A* and *B*, and 2, *A–C*). This demonstrated that the slight elongation effects remaining in *unc-49* single mutants were mediated by the GBB-1/2 receptor.

Since the focus of expression in the motor neuron system is cholinergic neurons (Dittman and Kaplan 2008), is it likely that the GBB-1/2 receptor acts by heterosynaptic feedback inhibition of cholinergic neurons. To test this more directly, we turned to cell-specific rescue experiments. The *gbb-2* cDNA was chemically synthesized, verified by sequencing, and then cloned into different promoterless vectors. However, handling any of the constructs containing this cDNA in various *E. coli* strains was problematic, because the sequence was apparently toxic in bacteria. Thus only clones with sequence errors were obtained. To reduce potential toxicity in *E. coli*, we introduced a *C. elegans* intron in the 5′ region. However, even then, the best clone we obtained contained two point mutations, intro-

ducing two amino acid changes: A484V, at the beginning of transmembrane helix 2 (TM2), and V572A, at the end of TM4 (Fig. 3). Since these amino acids likely are embedded in the membrane, and the changes are conservative, we do not expect major effects on the protein. This clone was then introduced into *C. elegans* expression vectors containing promoters for GABAergic (*punc-47*) or cholinergic neurons (*punc-17*) and injected into *gbb-2(tm1165)* and *gbb-2(tm1165); unc-49(e407)* animals containing the *zxIs3* transgene. We obtained several transgenic lines in *gbb-2* single-mutant background. However, despite injecting >100 animals and obtaining several hundred transgenic F1 progeny, we could not obtain any transgenic line in the *gbb-2(tm1165); unc-49(e407)* background. We thus could only test F1 progeny in this genetic background.

Expression of GBB-2(A484V; V572A) in cholinergic neurons slightly, but in a statistically significant manner, restored the *zxIs3*-dependent photoevoked body relaxation in *gbb-2(tm1165); unc-49(e407)* animals, particularly at low photostimulus intensity, whereas expression in GABAergic neurons did not show any statistically significant rescue (Fig. 1, *A* and *B*). Furthermore, we analyzed locomotion of strains lacking *gbb-1* or *gbb-2*, without or with expression of GBB-2(A484V; V572A) in cholinergic or GABAergic neurons, by counting swimming cycles of the animals in M9 buffer (Fig. 1*C*). Whereas *gbb-1* and *gbb-2* mutants exhibited significantly fewer swimming cycles, GBB-2(A484V; V572A) expressed in
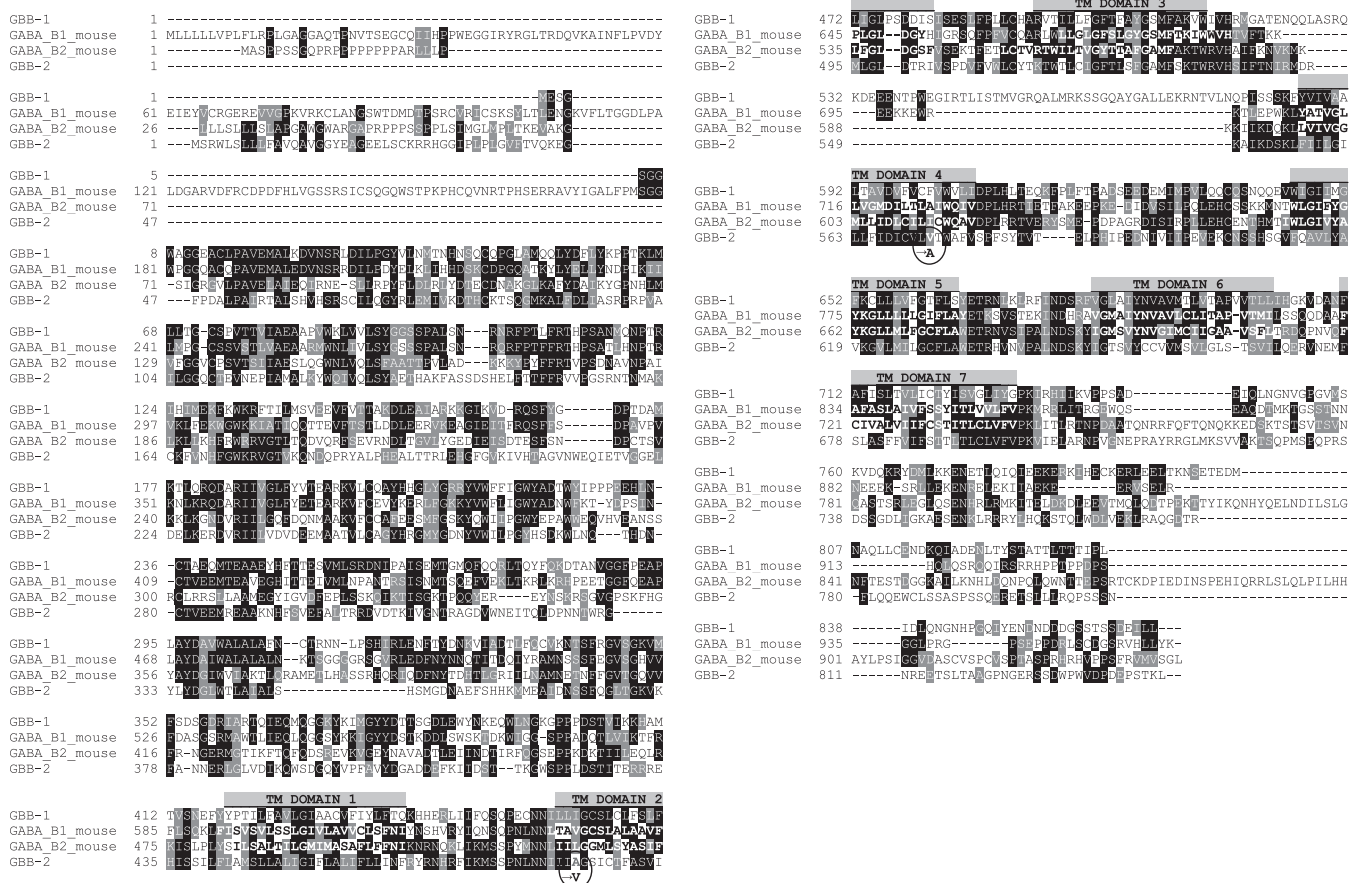
Fig. 3. Amino acid alignment of GBB-1 and GBB-2 subunits with mouse GABA_B1 and GABA_B2 subunits. Transmembrane domains are indicated by shaded bars above the sequence, as well as the point mutations obtained in the cDNA clone of GBB-2 (circled, with mutated residue indicated below the sequence). *gbb-1* is gene Y41G9A.4b, *gbb-2* is gene ZK180.1, and mouse GABA_B1 and GABA_B2 subunits have accession numbers NM_019439.3 and NM_001081141.1, respectively. Alignment was done with ClustalX.

cholinergic but not in GABAergic neurons rescued or even overcompensated the locomotion deficits of *gbb-2(tm1165)* mutants. Although we are cautious in overinterpreting our results due to the mutations in GBB-2 and the analysis of F1 rescue animals in *gbb-2; unc-49* background, the data suggest that the focus of GBB-2 function in locomotion and NMJ function is in cholinergic MNs.

GBB-1/2 receptors affect locomotion in response to light-evoked GABA transmission. Dittman and Kaplan (2008) showed that the GBB-1/2 receptor has an influence on locomotion behavior (e.g., mean speed, directional turns, and area explored per unit time). Confirming these findings, we also observed that *gbb-1* and *gbb-2* mutants performed fewer directional turns per unit time compared with wild type (data not shown). We were interested in analyzing locomotion while GABA transmission was photostimulated, because this might further emphasize effects of the GBB-1/2 receptor. As we previously showed, prolonged photostimulation of GABA neurons via the *zxIs3* transgene causes 4–5% body elongation that declines to 1–2% within 10–20 s, likely due to desensitization of the UNC-49 GABA$_A$ receptor (Liewald et al. 2008), but then, however, GABA effects sustain for several minutes (Schultheis et al. 2011). We thus used a recently developed tracking system, capable of selective photostimulation of freely behaving animals (Stirman et al. 2011), to track locomotion trajectories, speed, and mean bending angles of wild-type and *gbb-2(tm1165)* animals, both containing *zxIs3*. When analyzing animal trajectories, we observed that *gbb-2; zxIs3* animals, while being photostimulated, reached larger maximal distances from the starting point ["R$_{max}$" as defined by Dittman and

Kaplan (2008); note that this is not the absolute distance traveled] during a 120-s period compared with wild type (Fig. 4, *A–C*). When we analyzed the mean bending angles (i.e., the deviation from 180°, averaged over 11 evenly distributed points along the "spine" of the animal), *gbb-2* mutants exhibited much deeper bending angles (~27 vs. ~21° for the wild type) and *gbb-2* animals moved generally faster than wild type (Fig. 4, *D* and *E*). This indicates that the function of the GBB-1/2 receptor may contribute to shaping the body curvature during sinusoidal locomotion, i.e., "smoothening" it. The lack of the receptor, which causes "loopier" locomotion, may thus directly contribute to the overall locomotion speed and, as a consequence of apparently less curved trajectories, to longer R$_{max}$ distances traveled.

Continuous or pulsed photoactivation of cholinergic MNs at different stimulus strength. Because of the innervation pattern in the *C. elegans* nerve cord, cholinergic neurons stimulate GABAergic neurons (White et al. 1986) and apparently detect spillover GABA through the GBB-1/2 receptor as a feedback mechanism. Thus far we have optically manipulated GABA MNs to support this hypothesis. We next asked whether the GBB-1/2 receptor could further act to achieve plastic alterations in cholinergic MNs, e.g., when spillover GABA builds up in the nerve cords for prolonged periods of time. To this end, we used photoactivation of cholinergic neurons via transgene *zxIs6[punc-17::ChR2(H134R)::YFP; lin-15$^+$]*, which we have previously established and extensively characterized (Almedom et al. 2009; Liewald et al. 2008). Prolonged photoevoked ACh transmission, causing concomitant GABA transmission, could for example cause a progressive reduction of further
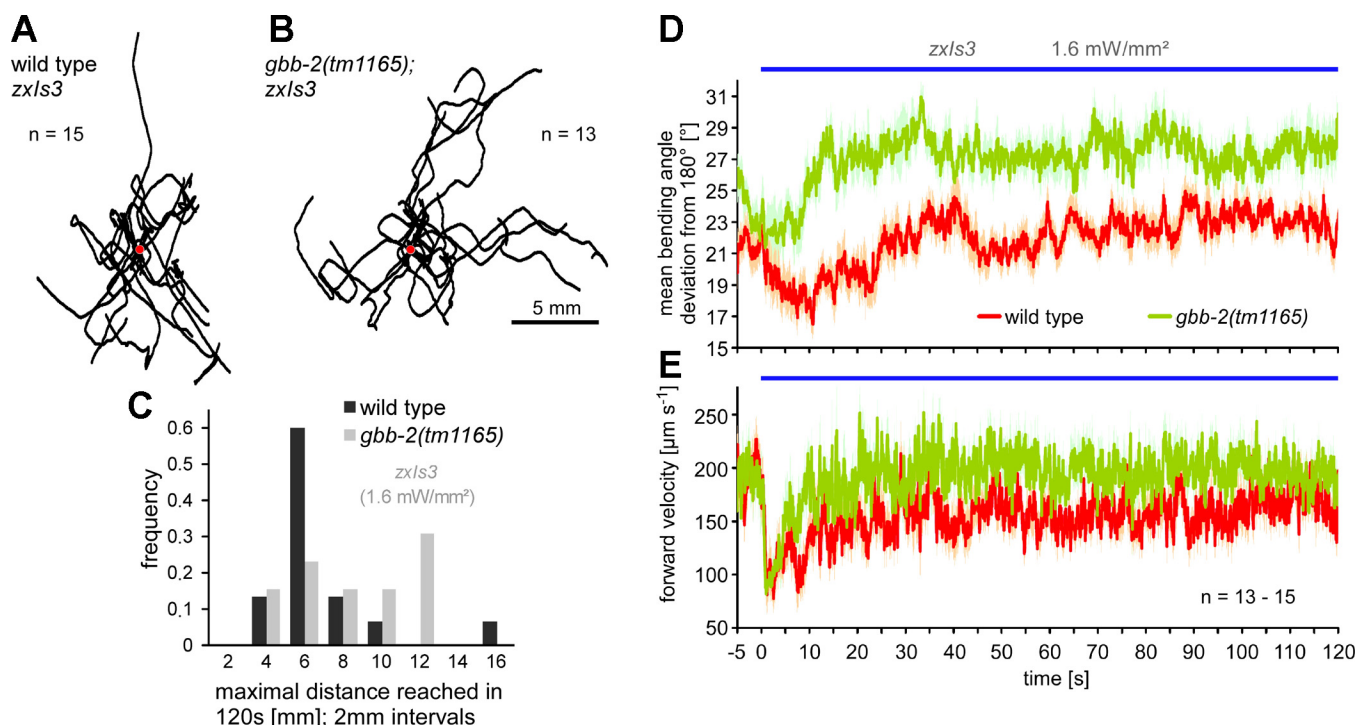

Fig. 4. Locomotion behavior is altered by GBB-2 function when GABA transmission is photostimulated. *A* and *B*: locomotion trajectories of wild-type (*A*) and *gbb-2* mutant animals (*B*) expressing ChR2 in GABAergic MNs were tracked for 120 s under blue light exposure, and the data are superimposed at the origin (red circle). *C*: the maximal distance reached within 120 s [R$_{max}$ as defined by Dittman and Kaplan (2008), i.e., before the animal again moves closer toward the origin] is plotted in a histogram. *D*: mean bending angles were measured between 13 equidistant points along the animals' "backbones" (i.e., 11 angles) at 25 Hz and are expressed as deviation from 180°. *E*: forward velocities of the animals' centroids were measured at 25 Hz and averaged for each genotype. Values are means ± SE, *n* = no. of animals analyzed. Periods of ChR2 photostimulation are indicated by blue bars.

ACh release in response to temporally intensifying GBB-1/2 receptor signaling. We thus measured body contraction in response to continuous, photoevoked ACh transmission in *zxIs6* animals, both in the wild type and in *gbb-2(tm1165)* backgrounds. Contractions in the wild type remained essentially unaltered at ~88% of the initial body length during a 30-s stimulus of 1.6 mW/mm^2 (Fig. 5*A*), and basically identical contractions were observed in *gbb-2(tm1165)* mutants.

Constant photostimulation of cholinergic MNs did not induce a time-dependent alteration of body contractions. Thus no plastic changes were apparent, and ACh transmission remained sufficiently high to cause sustained full body contraction. As we and others previously showed, constant photostimulation of cholinergic MNs causes an initially large postsynaptic inward current (~1,200 pA) that quickly declines to a steady-state current of roughly 80 pA (Almedom et al. 2009; Liewald et al. 2008; Liu et al. 2009). This is in large part due to desensitization of postsynaptic nicotinic ACh receptors and somewhat to depression of cholinergic MNs and partial inactivation of ChR2. Although currents in intact animals may differ, the small, light-induced steady-state currents may suffice to evoke prolonged and sustained muscle contractions, even if much less ACh than initially is released, e.g., by temporal summation. Thus a plastic alteration of cholinergic transmission based on GABA_B receptor signaling may be masked at the behavioral level. We thus asked whether pulsed release of ACh could show time-dependent effects of GABAergic feedback on cholinergic MNs more pronouncedly, because temporal summation would be much less efficient. We presented 10-ms pulses
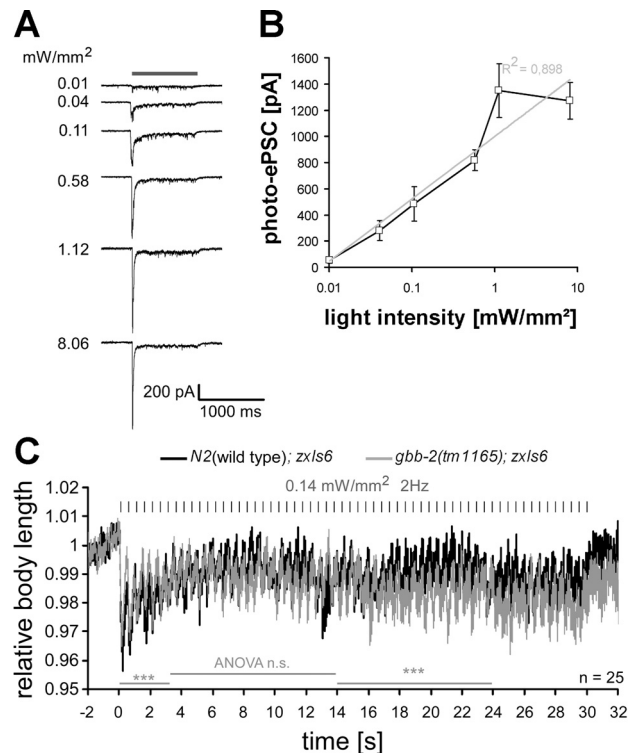
A

B

C

Fig. 6. Graded responses of cholinergic MNs to increasing stimulus strength and different effects of low-intensity stimulus trains on ACh-evoked contractions in wild-type vs. *gbb-2* mutant animals. *A*: photoevoked postsynaptic currents (photo-ePSCs) were measured in wild-type animals expressing ChR2 in cholinergic neurons (transgene *zxIs6*). Currents were recorded from voltage-clamped muscle cells (shown are representative single experiments) in response to a 1-s light pulse (470 nm, indicated by shaded bar) of the indicated light intensity. Peak inward currents were followed by a steady-state current that returned to baseline after the end of the stimulus. *B*: the peak currents were averaged ($n = 6–7$) and fitted with a single exponent. Values are means ± SE. *C*: wild-type or *gbb-2(tm1165)* animals with transgene *zxIs6* were assayed as in Fig. 5*B*, with a light intensity of only 0.14 mW/mm^2, and body contractions were quantified. Values are means ± SE; $n =$ no. of animals analyzed. Two-factorial ANOVAs were used to analyze statistically significant differences (***$P < 0.001$) for time periods indicated by shaded bars.

A

B

Fig. 5. Photostimulated ACh release triggers body contractions that are slightly affected in *gbb-2(tm1165)* mutants and demonstrate synaptic rundown. *A*: ChR2, expressed in cholinergic MNs (transgene *zxIs6*; Liewald et al. 2008), was photostimulated for 30 s to evoke sustained ACh release and, consequently, body contractions (calculated from video frames, obtained at 15 frames/s, before, during, and after illumination with 1.6 mW/mm^2 blue light). Contractions remained essentially constant throughout the illumination period (shaded bar) for wild-type and *gbb-2(tm1165)* mutant animals. *B*: to exaggerate potential plastic alterations in ACh MNs, we used a pulsed illumination protocol (10-ms stimuli, 2 Hz, shaded tick marks). Body contractions declined over the first 5 s of the stimulus train, indicating synaptic rundown. Contractions between 3 and 14 s into the stimulus train differed between wild-type and *gbb-2* mutant animals. Values are means ± SE; $n =$ no. of animals analyzed. Two-factorial ANOVAs were used to analyze statistically significant differences (***$P < 0.001$) for time periods indicated by shaded bars.

of blue light over a period of 30 s, at 2 Hz, to *zxIs6* wild type or *gbb-2(tm1165)* mutant animals. If GBB-1/2 receptors mediate plastic changes over time, contractions might show a depression in the wild type, and this depression should be abolished in the *gbb-2* mutant. In the wild type, the contractions were reduced from ~7% to ~4% over the first 5 s of the stimulus train (93 vs. 96% body length; Fig. 5*B*), which could indeed reflect short-term synaptic depression under these stimulation conditions. Contractions in *gbb-2(tm1165)* mutants essentially showed the same decline over time, although as shown by analysis of variance (ANOVA), body length traces significantly differed 3–14 s into the stimulus train, with *gbb-2* mutants contracting slightly more. Thus a strong stimulus train may possibly evoke some GBB-1/2-mediated plasticity.

Thus far, we "hyper"-stimulated the cholinergic MNs (stimulus intensity 1.6 mW/mm^2), and it appeared possible that the photoactivation was too strong and thus overrode any plastic changes. Because no voltage-gated sodium channels are found in *C. elegans*, cholinergic MNs likely fire no action potentials, and the amount of ACh released depends on membrane depolarization in a graded fashion (Bargmann 1998). As reported previously (Liu et al. 2009), we found that the size of photoevoked postsynaptic currents (photo-ePSCs) in muscle corre-

lated with increasing light intensities and could be fitted with a single exponent (Fig. 6, *A* and *B*), and no all-or-none responses could be observed. To investigate potential plastic effects depending on GBB-1/2 function at low stimulus strength, we lowered the light intensity to approximately one-tenth strength. Photo-ePSCs using 0.11 mW/mm^2 were reduced to ~40% of the maximal photo-ePSCs, which could be reached at 1.12 mW/mm^2 (Fig. 6, *A* and *B*). In behavioral assays, using 0.14 mW/mm^2 caused contractions of the animals to only 96% (Fig. 6*C*; compared with 93% for 1.6 mW/mm^2; Fig. 5*B*). Stimulus trains (2 Hz, 10 ms) at 0.14 mW/mm^2 in wild-type and *gbb-2(tm1165)* mutant animals showed no major differences between genotypes, and although wild-type animals had sig-

nificantly stronger contractions during the first 3 s of the train, a general reduction of the contractions (to 98%) was observed over the first 4–5 s in both genotypes, and significantly less pronounced contractions of the wild type were apparent during the second half of the train.

Altered GABA levels in snf-11 GABA (reuptake) transporter mutants and concomitant photostimulation of GABA/ACh MNs unravels GBB-1/2 effects. We observed slight effects of GABA, released in response to photoevoked ACh transmission and detected by GBB-1/2 receptors, inducing some possibly plastic changes in ACh neurons. However, these effects were subtle, perhaps because the amount of GABA released could have been too small. Thus we wanted to test whether increased
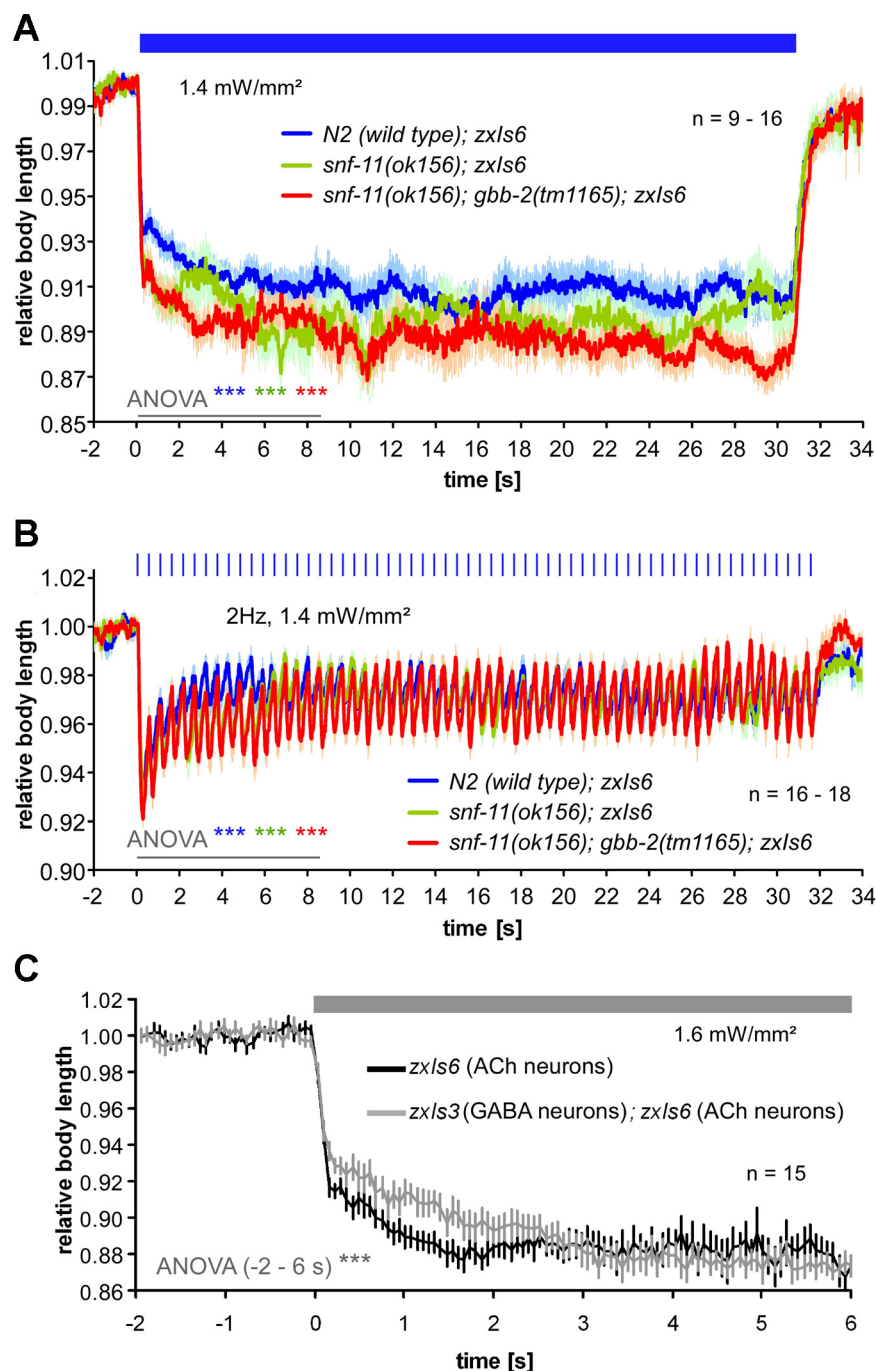
Fig. 7. Increased synaptic GABA by elimination of the GABA (reuptake) transporter SNF-11 or by concomitantly photoevoked GABA release alters ACh-evoked body contractions. Body contractions (means ± SE) were evoked by 30-s continuous (indicated by blue bar in *A*) or by 2-Hz, 10-ms pulsed 1.4 mW/mm^2 photostimulation (indicated by blue tick marks in *B*) of wild-type, *snf-11(ok156)*, and *snf-11(ok156); gbb-2(tm1165)* animals carrying transgene *zxIs6* (ACh). ANOVA for the first 8.5 s of the light stimulus showed significant differences between the wild type and the 2 mutant strains, as well as between mutants. *C*: wild-type animals expressing ChR2 in cholinergic neurons only (*zxIs6*) or in both cholinergic and GABAergic neurons (*zxIs3; zxIs6*) were exposed to a constant light stimulus (indicated by shaded bar), and body contractions were quantified. Values are means ± SE; *n* = no. of animals tested. ANOVA was performed from −2 to 6 s relative to the light stimulus. ***$P < 0.001$.

levels of GABA in the synaptic cleft or increased acute release of GABA could enhance these minor effects.

First, we tried to achieve higher GABA levels in the synaptic cleft at steady state. A high-affinity GABA transporter, SNF-11, has been described, which according to one study is expressed in muscles, as well as some neurons, excluding most of the inhibitory, GABAergic MNs (Mullen et al. 2006). This receptor is likely to act as a reuptake transporter, and not a transporter required in GABAergic MNs to provide GABA for release. Consequently, *snf-11* mutants were shown to be resistant to aldicarb, since higher steady-state inhibition may be

expected due to increased basal levels of GABA in the cleft, and this may even act through the GBB-1/2 receptor. However, in another study, SNF-11 expression was reported for the GABAergic MNs, and when the SNF-11 protein was knocked down by RNA interference, aldicarb hypersensitivity resulted, indicating reduced inhibition (Jiang et al. 2005). The findings of this report thus rather indicate that SNF-11 may be required for recycling of GABA in GABAergic neurons, which also express the GABA biosynthetic enzyme UNC-25 (glutamic acid decarboxlyase). To further investigate the two possibilities suggested by the two studies (Jiang et al. 2005; Mullen et al.
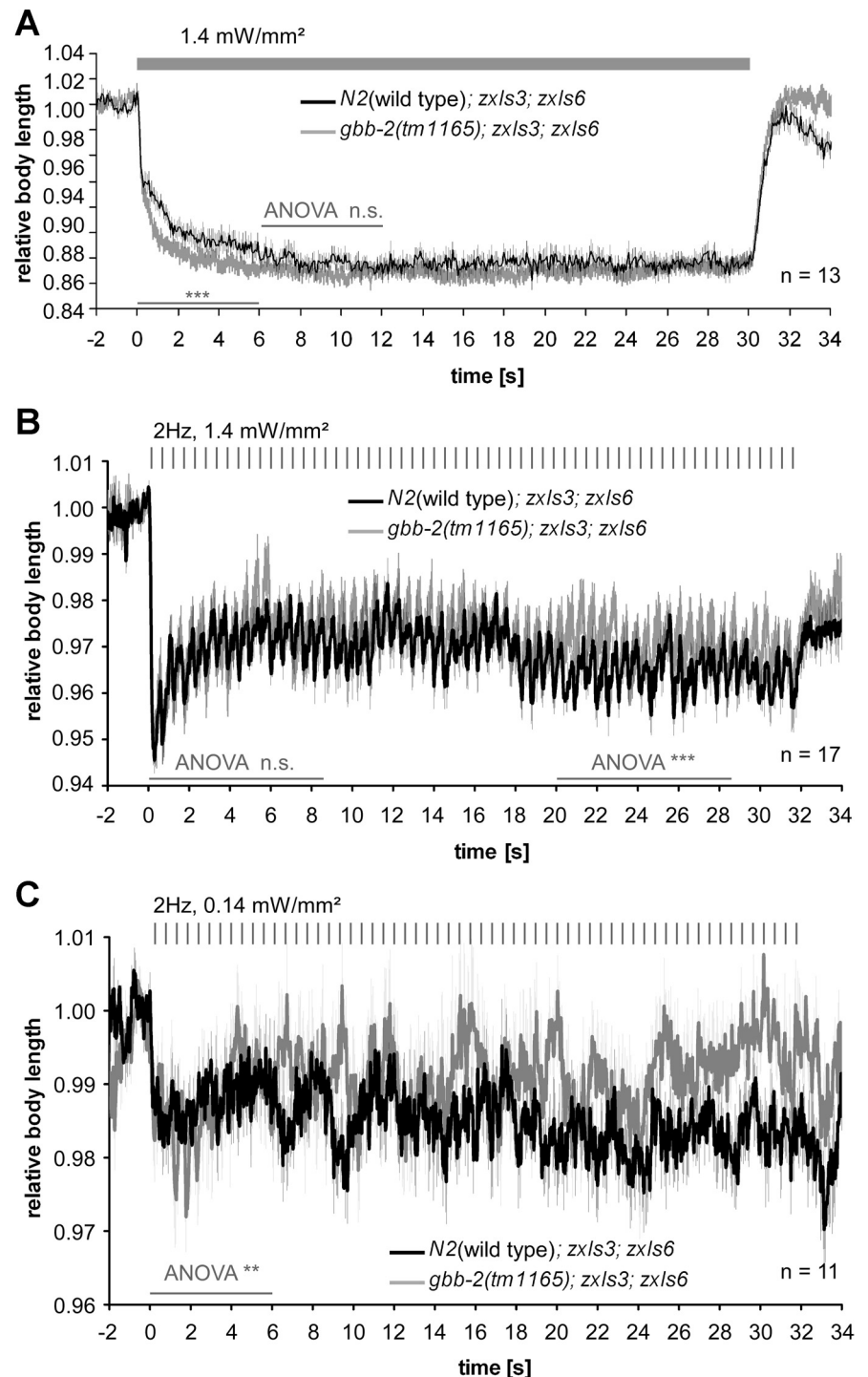
Fig. 8. Concomitant GABA and ACh MN photostimulation shows initial inhibitory effect of GBB-1/2 GABA_B receptors on ACh MNs and small but variable long-term effects. *A*: experiments were as described in Fig. 7*C*, and the genotypes used are indicated. ANOVA was performed for the indicated time periods (thin shaded bars); thick shaded bar indicates illumination period. *B* and *C*: animals of the same genotypes as in *A* were tested with 2-Hz, 10-ms photostimulus trains (tick marks) at 2 different stimulus intensities, 1.4 (*B*) and 0.14 mW/mm² (*C*). Values are means ± SE; *n* = no. of animals tested. ANOVA was performed as indicated by thin shaded bars.

2006), we crossed the *zxIs6* transgene into the *snf-11(ok156)* mutant background. We found that loss of SNF-11 caused significantly increased contractions in response to both continuous and pulsed photostimulation of cholinergic neurons (Fig. 7, *A* and *B*). This could indicate that steady-state levels of GABA in the synaptic cleft are not increased in *snf-11* mutants but that SNF-11 rather functions to provide normal GABA levels in GABAergic MNs. Alternatively, if steady-state GABA levels were increased in *snf-11* mutants, this may have long-term desensitized GABA_A receptors, causing enhanced effects of photoevoked ACh release. ACh effects in *snf-11(ok156)* animals were further increased by additional deletion of *gbb-2* (Fig. 7, *A* and *B*), in line with the hypothesis that GBB-1/2 receptors act in feedback inhibition of cholinergic MNs. The pulsed stimulation of cholinergic neurons in *snf-11* or *snf-11; gbb-2* mutants did not reveal any obviously abolished or enhanced plastic alterations in the contractions, although the differences to wild type were less pronounced toward the end of the 30-s stimulus train for both genotypes.

Because of the likely constantly elevated levels of GABA in the synaptic cleft of *snf-11* mutants, compensatory mechanisms may have occurred, e.g., desensitization of GABA_A (or GABA_B) receptors. To acutely maximize synaptic GABA levels, concomitant with ACh release, we generated a strain expressing ChR2 in both cholinergic and GABAergic neurons (*zxIs3; zxIs6* double transgenic animals). As expected, contractions evoked in these animals were significantly reduced compared with those in the *zxIs6* animals, at least during the first 2.5 s of the stimulation (Fig. 7*C*). Since the initially strong GABA effects diminish over time (Fig. 4, *D* and *E*) (Liewald et al. 2008; Schultheis et al. 2011), this may explain that at later times both strains show similar contractions.

We next compared wild type with *gbb-2(tm1165)* mutant animals, both containing *zxIs3* and *zxIs6* transgenes. On continuous stimulation (Fig. 8*A*), *gbb-2(tm1165)* mutants contracted more strongly than the wild type for the initial 6 s of the stimulus, indicating that under conditions of enhanced GABA release, heterosynaptic inhibition via the GBB-1/2 receptor indeed has a modulating, time-dependent effect on ACh MNs. We also performed similar experiments with 2-Hz pulsed photostimulation, at both high (1.4 mW/mm^2; Fig. 8*B*) and low stimulus intensity (0.14 mW/mm^2; Fig. 8*C*). Whereas at the low stimulus intensity, *gbb-2; zxIs3; zxIs6* animals showed significantly stronger contractions than wild-type *zxIs3; zxIs6* animals during the first 6 s of the stimulus train, the effect was opposite for the remaining train. For the high stimulus intensity, differences were only observed late in the stimulus train, i.e., after 20 s, and wild-type animals contracted more strongly. In essence, there mainly appear to be acute modulating effects of heterosynaptic inhibition of ACh neurons via GBB-1/2 GABA_B receptors, and if at all, only minor long-term plastic effects of GBB-1/2 in ACh MNs.

DISCUSSION

GABA_B receptors, expressed by cholinergic MNs in *C. elegans*, mediate feedback inhibition via spillover GABA, released by GABAergic MNs that are stimulated by the cholinergic MNs. We asked whether this feedback might induce plastic changes at the cholinergic synapse, e.g., a progressive depression upon sustained activity. To investigate this, we used optogenetic methods, i.e., photostimulation of cholinergic neurons, to evoke behavioral changes (contractions) in vivo and analyzed whether these contractions dynamically changed during prolonged activity, dependent on GBB-1/2 receptors. Although we indeed found significant differences in the extent of the light-evoked, ACh-dependent contractions between *gbb-2(tm1165)* mutants and wild-type animals, these alterations were rather small, and their temporal occurrence was not consistent under different experimental conditions (e.g., strong vs. weak, continuous vs. pulsed stimuli). In one case, changing the stimulus protocol even reversed the effects from enhancing cholinergic function to reducing it. Although there may be complex interactions in the motor nervous system that could explain the variability of the observed effects, we cannot explain them satisfyingly and thus suggest that GBB-1/2 receptors mainly serve to provide a negative feedback to cholinergic MNs (model, Fig. 9) that has no major dynamic component. In agreement with this model, locomotion behavior during photostimulation of GABAergic neurons was more exaggerated (deeper body bends, increased speed) in *gbb-2* animals, in line with a partial loss of inhibition, but these differences were roughly constant during the 120-s stimulus period. Our method is able to measure synaptic plasticity at the behavioral level, as we could previously show for mutants affecting synaptic vesicle recycling, e.g., the phospholipid phosphatase synaptojanin UNC-26: these animals showed a progressive reduction of the contractions over time (Liewald et al. 2008). Our method allows to quantitatively address the action of spillover transmitter in intact animals, rather than by electrophysiology in dissected preparations, where such transmitter effects would be abolished by dilution due to bath
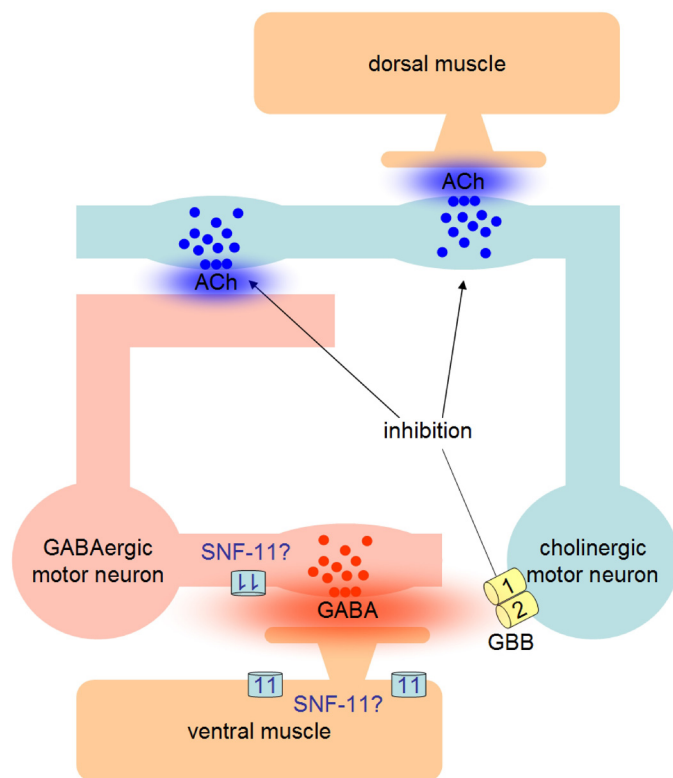

Fig. 9. Model of GBB-1/2 GABA_B receptor function in feedback inhibition of cholinergic MNs at the *Caenorhabditis elegans* neuromuscular junction and putative site of action of the SNF-11 high-affinity GABA transporter.

perfusion. We acknowledge, however, that photostimulation of motor neurons may evoke the co-release of transmitters other than GABA or ACh, since these cells also are likely to contain neuropeptides, whose (modulatory) action could contribute to some of the effects we observed.

GBB-1/2 receptors are responsible for some part of the GABA effects on body relaxation in optogenetic experiments, i.e., upon acute GABA release. We did not find any influence of the GBB-1/2 receptor on the effects of acutely photoevoked ACh release unless we photoevoked GABA release in addition to ACh release. These effects were somewhat dynamic and time dependent, because they were seen only during the initial 2.5-s of a constant stimulation of the two MN classes in *gbb-2 (tm1165)* mutants. Pulsed photostimulation of GABAergic and cholinergic neurons, however, initially showed more pronounced contractions of *gbb-2* animals, whereas later during the stimulus train wild-type animals showed stronger contractions, and this depended on stimulus intensity. It is possible that even lower stimulus intensities may be required to uncover subtle plastic changes better; yet, given the minor extent of the behavioral effects we observed at the lower stimulus intensity we used, we were not confident that they could be accurately measured at even lower stimulus intensities. Instead, we explored whether continuously elevating GABA levels in the synaptic cleft could have effects similar to acute GABA signaling. When the SNF-11 high-affinity GABA transporter was absent, ACh-evoked contractions were stronger, and they were even further enhanced when the GBB-1/2 receptor was missing. This could be in line with a function of SNF-11 as a reuptake transporter or with a possible function of SNF-11 in GABAergic neurons, providing/recycling some of the GABA produced and released by these cells, as suggested by two conflicting previous reports (Jiang et al. 2005; Mullen et al. 2006). However, both continuously elevated and reduced levels of GABA in the cleft may affect compensatory mechanisms in GABA receptors, making it difficult to interpret our findings conclusively.

Although GBB-1/2 receptors are widely expressed in the nervous system (Dittman and Kaplan 2008), their influence on locomotion appears to be exerted in cholinergic MNs. Cell type-specific expression of a mutated version of the GBB-2 subunit (A484V; V572A) in cholinergic MNs at least partially rescued the *gbb-2(tm1165)* phenotypes. Although other GABA receptors are encoded in *C. elegans* [Ringstad et al. (2009) reported GABA-evoked currents when expressing LGC-35 and LGC-38 in *Xenopus* oocytes], no evidence of inhibition in the motor system could be detected in double mutants lacking both the ionotropic GABA_A receptor UNC-49 and the GBB-1/2 receptor.

Using a fast optogenetic approach in vivo, we were able to show that inhibitory signaling via GBB-1/2 receptors likely occurs immediately, since it becomes apparent right upon stimulus onset, when *gbb-2* mutants are compared with wild-type. This indicates that GABA_B receptor signaling acts locally, e.g., to shape *C. elegans* locomotion, possibly to "smoothen" abrupt bending evoked by cholinergic transmission, and our locomotion analyses under GABA neuron photostimulation support this hypothesis. Because of its high affinity, the GBB-1/2 receptor can detect small amounts of free, spillover GABA, and no additional physical connections between GABAergic and cholinergic MNs are required for this

function. The minor dynamic or plastic effects of GABA_B receptor signaling on cholinergic neurons occur more slowly, after a few hundred milliseconds (up to seconds) on the level of our optogenetic behavioral analyses, and do not require extensive stimulus protocols over extended periods, as for example in the induction of long-term synaptic plasticity. These changes, however, may be of minor importance or will require more elaborate experimental approaches to be fully understood.

REFERENCES

Almedom RB, Liewald JF, Hernando G, Schultheis C, Rayes D, Pan J, Schedletzky T, Hutter H, Bouzat C, Gottschalk A. An ER-resident membrane protein complex regulates nicotinic acetylcholine receptor subunit composition at the synapse. *EMBO J* 28: 2636–2649, 2009.

Bamber BA, Beg AA, Twyman RE, Jorgensen EM. The Caenorhabditis elegans unc-49 locus encodes multiple subunits of a heteromultimeric GABA receptor. *J Neurosci* 19: 5348–5359, 1999.

Bargmann CI. Neurobiology of the *Caenorhabditis elegans* genome. *Science* 282: 2028–2033, 1998.

Bettler B, Kaupmann K, Mosbacher J, Gassmann M. Molecular structure and physiological functions of GABA_B receptors. *Physiol Rev* 84: 835–867, 2004.

Brenner S. The genetics of *Caenorhabditis elegans*. *Genetics* 77: 71–94, 1974.

Davies CH, Starkey SJ, Pozza MF, Collingridge GL. GABA autoreceptors regulate the induction of LTP. *Nature* 349: 609–611, 1991.

Dittman JS, Kaplan JM. Behavioral impact of neurotransmitter-activated G-protein-coupled receptors: muscarinic and GABA_B receptors regulate *Caenorhabditis elegans* locomotion. *J Neurosci* 28: 7104–7112, 2008.

Herlitze S, Garcia DE, Mackie K, Hille B, Scheuer T, Catterall WA. Modulation of Ca^{2+} channels by G-protein beta gamma subunits. *Nature* 380: 258–262, 1996.

Ikeda SR. Voltage-dependent modulation of N-type calcium channels by G-protein beta gamma subunits. *Nature* 380: 255–258, 1996.

Jiang G, Zhuang L, Miyauchi S, Miyake K, Fei YJ, Ganapathy V. A Na$^+$/Cl$^-$-coupled GABA transporter, GAT-1, from *Caenorhabditis elegans*: structural and functional features, specific expression in GABA-ergic neurons, and involvement in muscle function. *J Biol Chem* 280: 2065–2077, 2005.

Jones KA, Borowsky B, Tamm JA, Craig DA, Durkin MM, Dai M, Yao WJ, Johnson M, Gunwaldsen C, Huang LY, Tang C, Shen Q, Salon JA, Morse K, Laz T, Smith KE, Nagarathnam D, Noble SA, Branchek TA, Gerald C. GABA_B receptors function as a heteromeric assembly of the subunits GABA_BR1 and GABA_BR2. *Nature* 396: 674–679, 1998.

Lackner MR, Nurrish SJ, Kaplan JM. Facilitation of synaptic transmission by EGL-30 Gqalpha and EGL-8 PLCbeta: DAG binding to UNC-13 is required to stimulate acetylcholine release. *Neuron* 24: 335–346, 1999.

Liewald JF, Brauner M, Stephens GJ, Bouhours M, Schultheis C, Zhen M, Gottschalk A. Optogenetic analysis of synaptic function. *Nat Methods* 5: 895–902, 2008.

Liu Q, Hollopeter G, Jorgensen EM. Graded synaptic transmission at the *Caenorhabditis elegans* neuromuscular junction. *Proc Natl Acad Sci USA* 106: 10823–10828, 2009.

Luscher C, Jan LY, Stoffel M, Malenka RC, Nicoll RA. G protein-coupled inwardly rectifying K$^+$ channels (GIRKs) mediate postsynaptic but not presynaptic transmitter actions in hippocampal neurons. *Neuron* 19: 687–695, 1997.

Mott DD, Lewis DV. Facilitation of the induction of long-term potentiation by GABA$_B$ receptors. *Science* 252: 1718–1720, 1991.

Mullen GP, Mathews EA, Saxena P, Fields SD, McManus JR, Moulder G, Barstead RJ, Quick MW, Rand JB. The *Caenorhabditis elegans* snf-11 gene encodes a sodium-dependent GABA transporter required for clearance of synaptic GABA. *Mol Biol Cell* 17: 3021–3030, 2006.

Nagel G, Brauner M, Liewald JF, Adeishvili N, Bamberg E, Gottschalk A. Light activation of channelrhodopsin-2 in excitable cells of *Caenorhabditis elegans* triggers rapid behavioral responses. *Curr Biol* 15: 2279–2284, 2005.

Richmond JE, Jorgensen EM. One GABA and two acetylcholine receptors function at the C. *elegans* neuromuscular junction. *Nat Neurosci* 2: 791–797, 1999.

Ringstad N, Abe N, Horvitz HR. Ligand-gated chloride channels are receptors for biogenic amines in C. *elegans*. *Science* 325: 96–100, 2009.

Sakaba T, Neher E. Direct modulation of synaptic vesicle priming by GABA$_B$ receptor activation at a glutamatergic synapse. *Nature* 424: 775–778, 2003.

Schultheis C, Liewald JF, Bamberg E, Nagel G, Gottschalk A. Optogenetic long-term manipulation of behavior and animal development. *PLoS ONE* 6: e18766, 2011.

Schuske K, Beg AA, Jorgensen EM. The GABA nervous system in C. *elegans*. *Trends Neurosci* 27: 407–414, 2004.

Schwenk J, Metz M, Zolles G, Turecek R, Fritzius T, Bildl W, Tarusawa E, Kulik A, Unger A, Ivankova K, Seddik R, Tiao JY, Rajalu M, Trojanova J, Rohde V, Gassmann M, Schulte U, Fakler B, Bettler B. Native GABA$_B$ receptors are heteromultimers with a family of auxiliary subunits. *Nature* 465: 231–236, 2010.

Stirman JN, Crane MM, Husson SH, Wabnig S, Schultheis C, Gottschalk A, Lu H. Real-time multimodal optical control of neurons and muscles in freely behaving *Caenorhabditis elegans*. *Nat Methods* 8: 153–158, 2011.

Weissenberger S, Schultheis C, Liewald JF, Erbguth K, Nagel G, Gottschalk A. PACalpha—an optogenetic tool for in vivo manipulation of cellular cAMP levels, neurotransmitter release, and behavior in *Caenorhabditis elegans*. *J Neurochem* 116: 616–625, 2011.

White JG, Southgate E, Thomson JN, Brenner S. The structure of the nervous system of the nematode *Caenorhabditis elegans*. *Philos Trans R Soc Lond B Biol Sci* 314: 1–340, 1986.

White JH, Wise A, Main MJ, Green A, Fraser NJ, Disney GH, Barnes AA, Emson P, Foord SM, Marshall FH. Heterodimerization is required for the formation of a functional GABA$_B$ receptor. *Nature* 396: 679–682, 1998.

Zhang F, Wang L, Brauner M, Liewald J, Kay K, Watzke N, Wood P, Bamberg E, Nagel G, Gottschalk A, Deisseroth K. Multimodal fast optical interrogation of neural circuitry. *Nature* 446: 633–639, 2007.
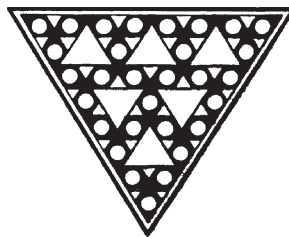
Real-time multimodal optical control of neurons and muscles in freely behaving *Caenorhabditis elegans*

Jeffrey N Stirman[1,2], Matthew M Crane[2], Steven J Husson[3,4], Sebastian Wabnig[3,4], Christian Schultheis[3,4], Alexander Gottschalk[3,4] & Hang Lu[1,2]

The ability to optically excite or silence specific cells using optogenetics has become a powerful tool to interrogate the nervous system. Optogenetic experiments in small organisms have mostly been performed using whole-field illumination and genetic targeting, but these strategies do not always provide adequate cellular specificity. Targeted illumination can be a valuable alternative but it has only been shown in motionless animals without the ability to observe behavior output. We present a real-time, multimodal illumination technology that allows both tracking and recording the behavior of freely moving *C. elegans* while stimulating specific cells that express channelrhodopsin-2 or MAC. We used this system to optically manipulate nodes in the *C. elegans* touch circuit and study the roles of sensory and command neurons and the ultimate behavioral output. This technology enhances our ability to control, alter, observe and investigate how neurons, muscles and circuits ultimately produce behavior in animals using optogenetics.

Understanding the cellular and genetic basis of neural function and behavior of an organism is a central problem in neuroscience. Recently developed optogenetic methods have contributed substantially to our experimental toolbox[1–8]. Using these tools, neurons and muscles can be optically excited or inhibited with millisecond precision in cultured cells as well as in intact animals[4–7,9–12]. The nematode *C. elegans* is an ideal organism for optogenetic studies because it is transparent, has a well characterized nervous system composed of 302 neurons with well known wiring connections, and has a battery of genetic tools available that facilitate its study[13,14]. Probing the neural circuit of *C. elegans* can be performed by ablation experiments or by genetically manipulating neurotransmitters, but these methods have limitations such as their low temporal control and the risk of circuit compensation during development. Optogenetics overcomes many of these drawbacks and has already been successfully applied to investigate neural circuits, synaptic transmission and the cellular basis of behavior in *C. elegans*[5,15–17].

Most optogenetic experiments are done using either whole-field illumination[5], by positioning an optical fiber directly in the

vicinity of the neurons[18,19] or by focusing light onto specific neurons in immobilized animals[20]. Thus, the illumination is either spatially nonspecific or it can only be applied to larger or motionless animals. The expression of transgenes in a subpopulation of cells is routine in *C. elegans*, but precise single-cell expression is often difficult; therefore, whole-body illumination generally does not permit the cell specificity required to interrogate circuits at the single-neuron level. To truly understand a specific circuit, one would ideally probe multiple distinct nodes (cells) with temporally separate signals. It has been shown that in constrained worms, channelrhodopsin-2 (ChR2), a blue light–activated cation channel that can depolarize excitable cells[2,4,5], can be used to stimulate specific spatially separate neurons while Ca^{2+} transients are recorded from neurons connected to them using a commercial digital micromirror device (DMD)[20]. This technique allows the interrogation of neural circuits in a cell-specific manner. However, many behavioral neuroscience problems would further benefit from the ability to control and monitor a particular behavior in a freely moving animal. Furthermore, assembled commercial systems are often prohibitively expensive, and custom-modified DMDs require considerable expertise, making their wide translation to biology laboratories difficult.

Here we demonstrate a method to optogenetically stimulate and silence specific neurons in freely behaving *C. elegans* with spatial, temporal and chromatic precision. Our illumination system allows us to project an illumination pattern onto an animal and maintain the illumination in the intended anatomical position while the animal is moving. We perform simultaneous multicolor illumination, which allows us to activate some cells while silencing others. Furthermore, it allows for high-resolution spatiotemporal and light-intensity control, with changes to stimulation location, intensity and color updated in <40 ms. Finally, because the central component of the illumination system is a modified off-the-shelf liquid crystal display (LCD) projector, the cost and complexity of the system are much lower than those of commercially available illumination systems, while maintaining high performance. To demonstrate the capabilities of this new multimodal illumination

[1]School of Chemical & Biomolecular Engineering, Georgia Institute of Technology, Atlanta, Georgia, USA. [2]Interdisciplinary Program in Bioengineering, Institute of Biosciences and Bioengineering, Georgia Institute of Technology, Atlanta, Georgia, USA. [3]Johann Wolfgang Goethe University, Institute of Biochemistry, Biocenter N220, Frankfurt, Germany. [4]Frankfurt Institute for Molecular Life Sciences, Johann Wolfgang Goethe University, Frankfurt, Germany. Correspondence should be addressed to A.G. (a.gottschalk@em.uni-frankfurt.de) or H.L. (hang@gatech.edu).

technology, we optically manipulated nodes within the *C. elegans* touch circuit to study the roles of sensory and command neurons and the ultimate behavioral output.

RESULTS

Experimental setup

To set up a structured illumination system for exciting and/or silencing optically activatable cells in a moving animal, we used an off-the-shelf, three-color LCD projector integrated with an inverted epifluorescence microscope. Simple modifications were made to both the projector and the microscope (**Fig. 1a,b** and **Supplementary Note 1**). The projector was placed at the epifluorescence illumination port, and the primary image of the projector was demagnified and translated to the specimen plane by a relay lens (**Supplementary Fig. 1**). A three-color LCD was selected because it contains three (red-green-blue, or RGB) distinct light paths, each processed using individual LCDs, thus ensuring simultaneous multicolor illumination. We further filtered each color within the projector to limit the large spectral spread and overlap of the native RGB colors (**Supplementary Fig. 2a**). The intensity of each color is determined by an 8-bit (0–255) value. We calibrated the intensity (with filters inserted) versus pixel value (**Supplementary Fig. 2b**) and found the maximal intensities across the field (**Supplementary Fig. 3**) to be sufficient for most optogenetic experiments[5,7,17].

To track a freely moving animal while stimulating specific neurons, we chose a relatively low-magnification objective (×4). This provided sufficient spatial resolution (14 μm) (**Supplementary Fig. 4**) for stimulation of groups of cells and sufficient field dimensions for whole-animal tracking. Using this system, multicolor optogenetic stimulation and inhibition can be performed with high spatiotemporal resolution while monitoring subsequent behavioral outputs in real time at 25 Hz (**Supplementary Note 2**). Ultimately the accuracy in illumination depends on the speed of the animal and the update rate of the system. In our experiments, the worms' forward velocity was about 250 μm s^{-1}, allowing an accuracy of 10 μm when operating at 25 Hz (**Supplementary Note 2**). To track and illuminate the animals, we created three independent software modules in LabView (2009 with Vision) (**Supplementary Software**).

Qualitative behavior elicited by structured illumination

We performed two simple experiments to show spatiotemporal control over gross *C. elegans* behaviors using structured illumination and ChR2-expression. First, we tracked worms expressing ChR2 in the cholinergic motor neurons (strain ZX460). While the worm was moving forward, we illuminated the head with blue light (430–475 nm) at regular intervals. This produced a dorsal coiling effect[15] when the head was illuminated and resulted in the worm moving in a triangle (**Fig. 1c** and **Supplementary Video 1**).

Figure 1 | Illumination system for live animal tracking and optogenetic stimulation and quantification of behavior elicited by targeted illumination. (**a**) Optical configuration for using a projector for illumination. The normal epifluorescence optical train is replaced by a projector and a relay lens. Projector image planes are indicated, and a motorized *x-y* translational stage is used to track animals. (**b**) Modification of the three-color LCD projector to further narrow the spectrum is accomplished by the addition of filters into the individual RGB light paths. (**c**) Sequential frames from **Supplementary Videos 1** and **2** showing qualitative behavioral responses. Top, use of the dorsal coiling effect to cause a worm to crawl in a triangle; bottom, direct muscular control of a paralyzed worm. Images are false-colored to show illumination pattern. (**d**) Illustration of the positions of the six sensory neurons, and a frame from **Supplementary Video 3** showing the 20-μm bar of blue light, perpendicular to the worm's longitudinal axis, which was scanned at a rate of 12.5% body length per second (~100 μm s^{-1}). (**e**) Two scanning schemes along the A-P axis: head to tail and tail to head. (**f**) Histograms showing the distributions of positions along the A-P axis where the blue light elicited a reversal response. Shown are the distribution of positions where accelerations elicited by the tail-to-head scan were observed (28 out of 52 worms showed an increase in speed 2 s.d. greater than the average speed before illumination) and the distributions of the anatomical positions of the touch neurons in *pmec-4::GFP* worms. Scale bars, 100 μm.
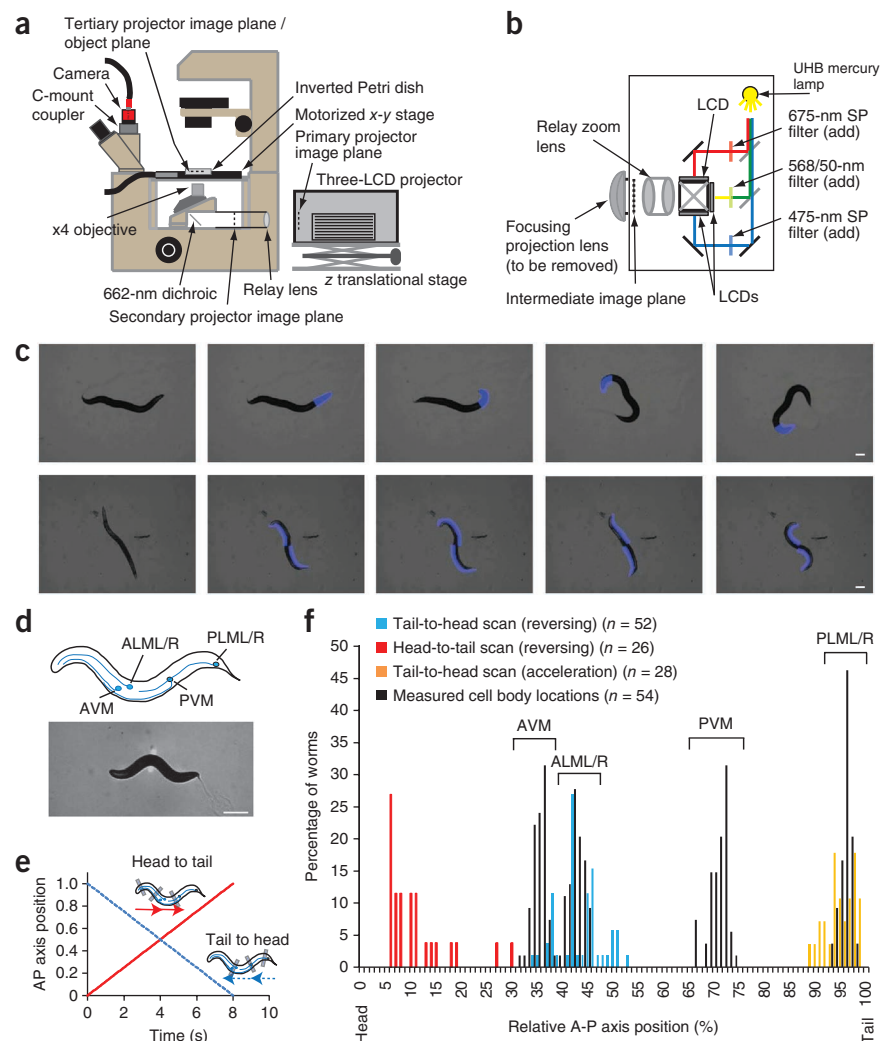
In the second experiment, we controlled the muscles of neuronally paralyzed worms that express ChR2 (strain ZX299)[7] using structured illumination. Ivermectin (0.01 mg ml^{-1} solution), a nematocidal agonist of glutamate-gated Cl$^-$ channels that causes neuronal hyperpolarization, was delivered to the worms; this eliminates the activities of motor neurons—which are known to express ivermectin-sensitive channels—while muscles, which remain excitable[21], were controlled with the light pulses. Partitioning the paralyzed worm into four quadrants (dorsal-anterior, dorsal-posterior, ventral-anterior and ventral-posterior) and exciting the muscles in alternating patterns, we were able to produce S-shaped body postures suggestive of locomotion patterns during crawling (**Fig. 1c** and **Supplementary Video 2**). Although qualitative, these experiments together demonstrate that illumination of optically controllable cells can be well defined, easily controlled and dynamically altered using the projector system.

Spatial activation of sensory and command neurons

To determine the spatial resolution of our system, we performed experiments analyzing the mechanosensory behavior of *C. elegans*. There are six main mechanosensory neurons in *C. elegans*: AVM, ALML and ALMR (anterior), and PVM, PLML and PLMR (posterior)[22,23]. Worms carrying *pmec-4::ChR2* (strain AQ2334) express ChR2 in these six touch neurons (**Fig. 1d**). By traditional touch assays and laser ablation, it has been established that stimulating the anterior neurons causes the worm to move backwards, whereas stimulating the posterior neurons causes forward movement or acceleration[22]. In our experiment, we used a 20-μm-wide bar of blue light and scanned it along a *pmec-4::ChR2* worm's anterior-posterior (A-P) axis at a relative velocity of 12.5% of body length per second (~100 μm s^{-1}) while monitoring the locomotor behavior of the worm (**Fig. 1d**). The line was scanned in both the head-to-tail and tail-to-head directions (**Fig. 1e** and **Supplementary Video 3**). As expected, while illuminating from tail to head, as long as the illumination was in the posterior half of the worm, no reversals were elicited, and as soon as the bar reached the anterior half, worms reversed (**Supplementary Video 3**). It was also evident that illuminations in the posterior initiated acceleration. We quantified the exact body position at which these behaviors

were initiated, as well as the anatomical positions of the touch neurons (**Fig. 1f**). Reversals were initiated most often within the range 40%–48% of the way along the A-P axis in tail-to-head scans, consistent with anatomical data (the positions of the ALM and AVM cell bodies[14]) and with our measurement of neural cell body locations (**Fig. 1f** and **Supplementary Fig. 5**). In the head-to-tail scans, worms showed a high probability of reversal well before the light reached the AVM or ALM cell bodies (**Fig. 1f**), indicating that activation of the ChR2 in the processes is sufficient to elicit a response. This is likely because enough ChR2 is present in neuronal processes to allow sufficient photo-depolarization of the cell (**Supplementary Note 2**). This experiment suggests that the spatial resolution of the system can be used for precise interrogation of the neuronal network at the single-cell level, provided that the cells expressing ChR2 have cell bodies or processes farther apart than the spatial resolution of the system.

In the *C. elegans* touch circuit, command interneurons integrate signals from sensory neurons and ultimately produce locomotor behaviors[22–25] (**Fig. 2a,b**). To quantify these behaviors, we excited the head- or tail-touch neurons and the head or tail interneurons (**Fig. 2b**) using ChR2 and measured the worms' velocity. First, *pmec-4::ChR2* worms were stimulated either in the second 25% or the last 25% of the body. We illuminated a quarter of the body length because this resolution is sufficient to distinguish the anterior and the posterior sensors, and it ensures illumination of the relevant cell bodies in all worms (**Supplementary Note 2** and **Supplementary Video 4**). When the last quarter was illuminated with blue light, thus exciting PLML and PLMR neurons, we observed the expected velocity increase (**Fig. 2c**). Conversely, when the second quarter of the body was illuminated, exciting AVM, ALML and ALMR neurons, we observed a large velocity decrease followed by a reversal (**Fig. 2c**).
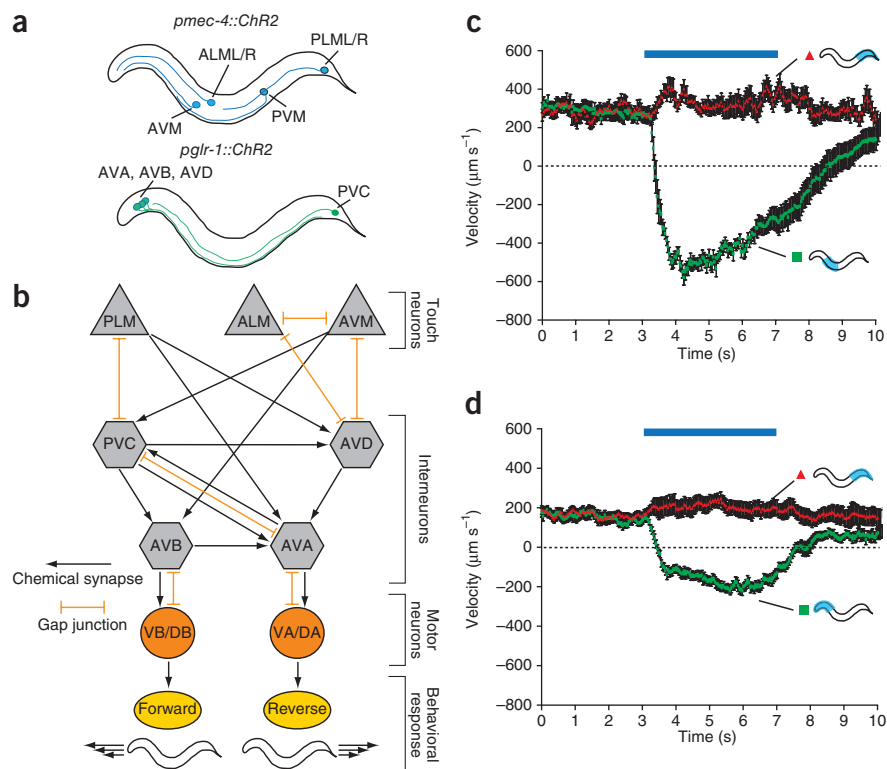
Figure 2 | Optical stimulation of anterior/posterior mechanosensory neurons or forward/backward command interneurons. (**a**) Illustration of the positions of neurons expressing ChR2 in *pmec-4::ChR2* and *pglr-1::ChR2* transgenic worms. (**b**) The touch circuit, showing receptors, command neurons and the resulting behaviors. (**c**) Average velocity plots of *pmec-4::ChR2* worms under illumination conditions (shown as a blue bar above). *n* = 13 (posterior illumination); *n* = 15 (anterior illumination). Error bars, s.e.m. (**d**) Average velocity plots of *pglr-1::ChR2* worms under illumination conditions (shown as a blue bar above). *n* = 24 (posterior illumination); *n* = 12 (anterior illumination). Error bars. s.e.m.

We performed similar experiments on *pglr-1∷ChR2* worms, which express ChR2 in the command interneurons as well as in other neurons[26]. Illuminating the first quarter of the body with blue light excites the interneurons in the head, including AVA, AVD and AVB (**Supplementary Video 4**). Although this stimulation included interneurons for both backward and forward movements, the predominant effect was the backward command. The velocity profile (**Fig. 2d**) showed a robust reversal upon stimulation using this light pattern. Similarly, when the last quarter of the *pglr-1∷ChR2* worms was illuminated and the neuron PVC excited, there was a small but appreciable acceleration. Although we cannot exclude the effects of photostimulation of the other *glr-1*-expressing cells, the experiment shows specific illumination in freely moving animals in ways that are not possible to perform with previous methods. The behavior ares consistent with the known roles of the locomotive interneurons, and the illumination scheme and measured behaviors are reproducible (**Fig. 2c,d** and **Supplementary Fig. 6**).

Spatiotemporal control of the illumination intensity

Traditionally, the study of the *C. elegans* touch circuit has been largely performed using a manual assay that consists of either touching the head or tail of a freely moving worm with an eyelash or tapping on the agar plate that contains the worms[22,25]. One difficulty associated with this assay is controlling and standardizing the force with which animals are stimulated. Microtransducers have been fabricated to allow control of forces[27]. Although precise, these systems are technically demanding, particularly when used on behaving animals and when applied in different positions simultaneously. Using light to drive ChR2, the stimulus intensity (which translates into signal strength in neurons[17,28]) can be easily controlled over a wide range with spatial specificity and in a variety of illumination and intensity profiles. Changing the light intensity in optogenetic experiments normally requires changing the lamp voltage or introducing neutral density filters, which change the light intensity over the entire field of view. With the illumination method described here, one can easily control the local intensity by varying the pixel values.

First we showed that illumination using graded intensities elicited differential behaviors when stimulating the second anterior quarter of *pmec-4∷ChR2* worms with blue light. We recorded the worms' responses to 0.29, 1.17 and 4.67 mW mm^{-2} illumination intensities and recorded whether different stimulation strengths produce reversals with different probabilities (**Fig. 3a**). We grouped the behavior of all the worms analyzed into four categories: a robust, large reversal (defined as a reversal with three or more headswings[29]), a small reversal (defined as a reversal with less than three headswings[29]), a slowing or pausing response but no reversals, and no measurable responses (**Supplementary Video 5**). Regardless of the illumination intensities, we observed that these four categories always existed and were distinguishable (**Fig. 3b**). Grouping the behavioral responses by the illumination intensities, we found that the low-intensity stimulation produced a higher
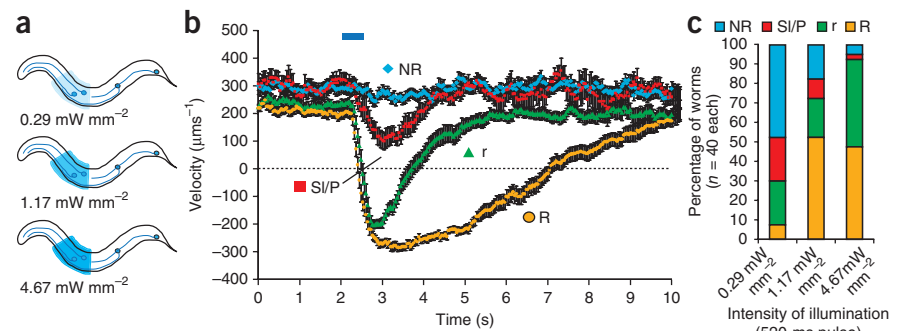
Figure 3 | Quantification of behavioral responses elicited by different anterior illumination intensities. (**a**) Patterns used for illumination location and their intensity. (**b**) Velocity plots from pooled data from worms receiving different illumination intensities (also see **Supplementary Video 5**). NR, no response; Sl/P, a slowing or pausing of the worm with no negative velocity; r, a small reversal; R, a large reversal. n = 40 for each of the three illumination levels. The number of worms showing NR, Sl/P, r and R behaviors were 28, 14, 35 and 43 respectively. Error bars, s.e.m. (**c**) Distribution of the four responses observed at the three intensity levels.

probability of no response and slowing response in the worms, whereas the worms were much more likely to reverse upon stimulation at higher intensities (**Fig. 3c**). This suggests that the illumination intensities affect the sensory neuron responses and ultimately modulate the distribution of the behavioral responses.

Next we asked whether it is possible to simultaneously stimulate neurons in spatially distinct locations and with sophisticated light-intensity patterns. We were interested in the worms' responses to simultaneous stimuli in anterior and posterior regions—that is, the intensity threshold past which a reversal is produced, and how this changes when a competing signal is present—something that would have been impossible using the traditional manual approach. We compared *pmec-4∷ChR2* worms that were stimulated only in the head in an increasing step function, to a maximal intensity of 1.17 mW mm^{-2} (scheme 1; **Fig. 4a**), to worms stimulated with an identical pattern in the head but that also were being stimulated in the tail at a constant intensity of 1.17 mW mm^{-2} (scheme 2; **Fig. 4a** and **Supplementary Video 6**). When the thresholds for a population of worms were compiled, we observed that holding constant tail illumination intensity increased the average head intensity at which worms responded (**Fig. 4b**). To further investigate the integration of competing signals, we stimulated one set of worms with a single light pulse in the anterior and another set with anterior and posterior pulses of the same intensity. There was a decrease in the combined probability of reversals and an increase in the probability of no response when the posterior sensory neurons PLML and PLMR were also excited (**Fig. 4c**). This suggests that the signals from the anterior and posterior sensors are integrated at all times to produce the proper behavior. Additionally, certain combinations of anterior and posterior illumination intensities seemed to constitute conflicting sensory signals and resulted in conflicting commands, as the worms quickly alternated between forward and reverse locomotion (**Supplementary Video 7**).

Simultaneous multicolor illumination

Because many of the available light-sensitive proteins used in optogenetics[2,7,8] are spectrally distinct, an illumination system that can be used to illuminate at different wavelengths would be valuable. For instance, ChR2 is activated in the blue region,

**Figure 4** | Illumination patterns used to explore the integration of anterior and posterior signals and behavior generated from the stimulation. (**a**) Illumination locations and plot of the temporal variation of the intensity for the two patterns tested. Normalized intensity of 1 corresponds to blue light of intensity 1.17 mW mm^{-2}. (**b**) Histogram distributions of intensity at which worms initiated a reversal under two illumination patterns: anterior alone, and anterior and posterior simultaneously ($n = 40$ for each illumination scheme). (**c**) Distributions among the four response states for anterior illumination alone or simultaneous anterior and posterior illumination at the same intensity (1.17mW mm^{-2}) ($n = 40$ for each).
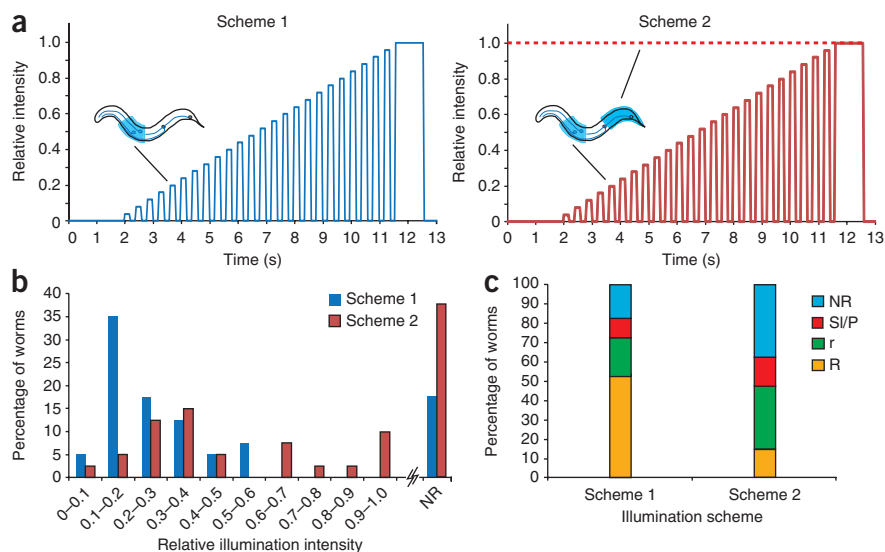
whereas NpHR[7] and MAC[8], both of which can be used to hyperpolarize and thus silence cells, are activated in the green-yellow region. Simultaneously exciting and inhibiting different cells in a circuit, particularly in behaving animals, can greatly enhance our ability to understand circuits and their functions.

Using an LCD projector, we have three independently controllable LCD panels that can be used for three independent illuminations. We used two of these channels to interrogate the mechanosensory circuit using *pmec-4∷ChR2; pglr-1∷MAC* worms. In these worms, MAC inactivates the *glr-1*-expressing interneurons when illuminated by green light (550 nm). Because MAC can also be activated (although less efficiently) by blue light[8], we illuminated the second quarter of the body along the A-P axis (that is, avoiding illumination of *glr-1*-expressing neuron cell bodies) using blue light and the first quarter of the body using green light. This allowed excitation of the ALM and AVM sensory neurons while inhibiting the *glr-1*-expressing neurons only in the anterior part of the worms, thus inhibiting all backward command neurons but only one of two pairs of forward command neurons (**Supplementary Video 8**). Because processes of the *glr-1∷MAC*-expressing cells pass the region of *mec-4∷ChR2* expressing neurons, behaviors evoked in *mec-4* neurons may be

slightly dampened (**Supplementary Note 2**). The behavior of the worms was tracked over time while they were manipulated following two photostimulation schemes (**Fig. 5a**). Velocity averages from multiple worms are shown in **Figure 5b**. When the anterior sensory neurons (ALM and AVM) were stimulated by blue light for 4 s at 1.17 mW mm^{-2} intensity (scheme 1; **Fig. 5a–c**), the worms produced a robust reversal behavior. When ALM and AVM neurons were illuminated the same way while the head interneurons were inhibited by green light 2 s after the blue light came on (scheme 2; **Fig. 5a–c**), the worms first produced the expected reversals, but upon silencing of the interneurons, the reversals were inhibited, and the velocity became positive (**Fig. 5b**). Spontaneous reversals likewise could be inhibited by green illumination (**Supplementary Video 8**), suggesting that this is not an artifact of the optogenetic stimulation but a direct interference with the neuronal circuit. This experiment illustrates our ability to illuminate a behaving animal with spatial, temporal, spectral and intensity control. The method yields quantitative behavior data that cannot be obtained by manual touch assays, laser cell ablation or genetic manipulation of neurotransmitters.
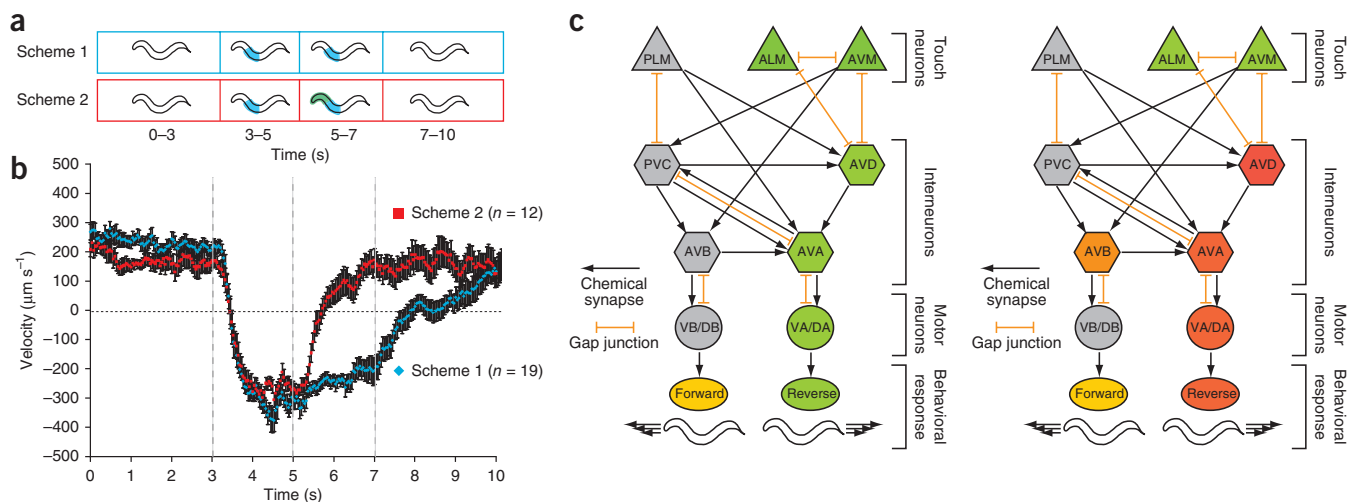
Figure 5 | Simultaneous two-color illumination. (**a**) Illustrations of the two illumination schemes. (**b**) Velocity plots of *pmec-4∷ChR2* and *pglr-1∷MAC∷mCherry* worms subjected to the illumination schemes in **a**. Error bars, s.e.m.; $n = 19$ for scheme 1, $n = 12$ for scheme 2. (**c**) The neural gentle touch circuit showing the neurons that are either stimulated or silenced and the resulting behaviors at different points in the two sets of experiments.

DISCUSSION

Optogenetics has received significant attention owing to the potential for fast, repeatable stimulation of genetically defined neurons. We have shown here, to our knowledge for the first time, that it is possible to track a freely moving *C. elegans* and spatiotemporally excite and/or inhibit specific nodes of neural networks. This illumination system is capable of delivering light stimuli to genetically modified, optically excitable cells with high repeatability and light intensity control. It also enables the use of combinations of optogenetic tools with non-overlapping activation spectra. By using a three-color LCD, we were able to achieve simultaneous multicolor illumination, allowing the spatial and spectral separation to probe neuronal networks more precisely.

Our system uses a modified off-the-shelf projector coupled with a standard microscopy setup, facilitating its adoption by other labs. Single DMD or LCD systems can be similarly applied for single-color illumination. The structured illumination system combined with video tracking could be used to study a variety of biological questions related to the behavior and neuronal function of *C. elegans*, as well as other transparent animals—for example, *Danio rerio* or *Drosophila* larvae. The ultimate resolution of the system depends on the behavior tracking requirements (for example, speed of the animal) and hardware, and one would also have to consider where the light-sensitive proteins are expressed (**Supplementary Note 2**).

In addition to the experiments shown here, multimodal real-time optogenetic control will allow further studies of other sensory circuits. Furthermore, studies related to the integration of different sensory modalities and behaviors will be considerably advanced by the ability to track and stimulate freely moving animals. Real-time illumination and behavior tracking as presented here can also be combined with calcium imaging or with other methods capable of perturbing the circuit, such as using microfluidic devices to deliver well defined sensory stimuli, analyzing animals mutant for particular neurotransmitters or performing laser ablation of cells, axons or synapses to remove single nodes or connections within the circuit. Lastly, one could imagine using the illumination system with other photostimulation methods such as uncaging of small molecules.

METHODS

Methods and any associated references are available in the online version of the paper at http://www.nature.com/naturemethods/.

Note: Supplementary information is available on the Nature Methods website.

AUTHOR CONTRIBUTIONS
J.N.S., M.M.C., A.G. and H.L. designed the experiments. J.N.S. and M.M.C. wrote the software. J.N.S. constructed the illumination system, performed experiments and analyzed the data. S.J.H., S.W. and C.S. contributed to reagents and provided valuable discussions. J.N.S., M.M.C., S.J.H., A.G. and H.L. prepared the manuscript.

1. Zemelman, B., Nesnas, N., Lee, G. & Miesenbock, G. Photochemical gating of heterologous ion channels: Remote control over genetically designated populations of neurons. *Proc. Natl. Acad. Sci. USA* **100**, 1352–1357 (2003).
2. Nagel, G. *et al.* Channelrhodopsin-2, a directly light-gated cation-selective membrane channel. *Proc. Natl. Acad. Sci. USA* **100**, 13940–13945 (2003).
3. Banghart, M., Borges, K., Isacoff, E., Trauner, D. & Kramer, R. Light-activated ion channels for remote control of neuronal firing. *Nat. Neurosci.* **7**, 1381–1386 (2004).
4. Boyden, E., Zhang, F., Bamberg, E., Nagel, G. & Deisseroth, K. Millisecond-timescale, genetically targeted optical control of neural activity. *Nat. Neurosci.* **8**, 1263–1268 (2005).
5. Nagel, G. *et al.* Light activation of channelrhodopsin-2 in excitable cells of *Caenorhabditis elegans* triggers rapid behavioral responses. *Curr. Biol.* **15**, 2279–2284 (2005).
6. Szobota, S. *et al.* Remote control of neuronal activity with a light-gated glutamate receptor. *Neuron* **54**, 535–545 (2007).
7. Zhang, F. *et al.* Multimodal fast optical interrogation of neural circuitry. *Nature* **446**, 633–634 (2007).
8. Chow, B.Y. *et al.* High-performance genetically targetable optical neural silencing by light-driven proton pumps. *Nature* **463**, 98–102 (2010).
9. Schroll, C. *et al.* Light-induced activation of distinct modulatory neurons triggers appetitive or aversive learning in *Drosophila* larvae. *Curr. Biol.* **16**, 1741–1747 (2006).
10. Arenkiel, B. *et al.* In vivo light-induced activation of neural circuitry in transgenic mice expressing channelrhodopsin-2. *Neuron* **54**, 205–218 (2007).
11. Huber, D. *et al.* Sparse optical microstimulation in barrel cortex drives learned behaviour in freely moving mice. *Nature* **451**, 61–67 (2008).
12. Wyart, C. *et al.* Optogenetic dissection of a behavioural module in the vertebrate spinal cord. *Nature* **461**, 407–410 (2009).
13. Brenner, S. Genetics of *Caenorhabditis elegans*. *Genetics* **77**, 71–94 (1974).
14. White, J., Southgate, E., Thomson, J. & Brenner, S. The structure of the nervous-system of the nematode *Caenorhabditis elegans*. *Phil. Trans. R. Soc. Lond. B* **314**, 1–340 (1986).
15. Liewald, J.F. *et al.* Optogenetic analysis of synaptic function. *Nat. Methods* **5**, 895–902 (2008).
16. Mahoney, T. *et al.* Intestinal signaling to GABAergic neurons regulates a rhythmic behavior in *Caenorhabditis elegans*. *Proc. Natl. Acad. Sci. USA* **105**, 16350–16355 (2008).
17. Liu, Q., Hollopeter, G. & Jorgensen, E. Graded synaptic transmission at the *Caenorhabditis elegans* neuromuscular junction. *Proc. Natl. Acad. Sci. USA* **106**, 10823–10828 (2009).
18. Aravanis, A. *et al.* An optical neural interface: in vivo control of rodent motor cortex with integrated fiberoptic and optogenetic technology. *J. Neural Eng.* **4**, S143–S156 (2007).
19. Gradinaru, V. *et al.* Targeting and readout strategies for fast optical neural control in vitro and in vivo. *J. Neurosci.* **27**, 14231–14238 (2007).
20. Guo, Z.V., Hart, A.C. & Ramanathan, S. Optical interrogation of neural circuits in *Caenorhabditis elegans*. *Nat. Methods* **6**, 891–847 (2009).
21. Holden-Dye, L. & Walker, R.J. Anthelmintic drugs. in *WormBook* (ed. The *C. elegans* Research Community) (02 November 2007).
22. Chalfie, M. *et al.* The neural circuit for touch sensitivity in *Caenorhabditis elegans*. *J. Neurosci.* **5**, 956–964 (1985).
23. Goodman, M.B. Mechanosensation. in *WormBook* (ed. The *C. elegans* Research Community) (6 January 2006).
24. Kaplan, J. & Horvitz, H. A dual mechanosensory and chemosensory neuron in *Caenorhabditis elegans*. *Proc. Natl. Acad. Sci. USA* **90**, 2227–2231 (1993).
25. Wicks, S.R. & Rankin, C.H. Integration of mechanosensory stimuli in *Caenorhabditis elegans*. *J. Neurosci.* **15**, 2434–2444 (1995).
26. Brockie, P.J. & Maricq, A.V. Ionotropic glutamate receptors: genetics, behavior and electrophysiology. in *WormBook* (ed. The *C. elegans* Research Community) (19 January 2006).
27. Park, S.J., Goodman, M.B. & Pruitt, B.L. Analysis of nematode mechanics by piezoresistive displacement clamp. *Proc. Natl. Acad. Sci. USA* **104**, 17376–17381 (2007).
28. Mellem, J.E., Brockie, P.J., Madsen, D.M. & Maricq, A.V. Action potentials contribute to neuronal signaling in *C. elegans*. *Nat. Neurosci.* **11**, 865–867 (2008).
29. Gray, J.M., Hill, J.J. & Bargmann, C.I. A circuit for navigation in *Caenorhabditis elegans*. *Proc. Natl. Acad. Sci. USA* **102**, 3184–3191 (2005).

Optogenetic Long-Term Manipulation of Behavior and Animal Development

Christian Schultheis[1,2], Jana Fiona Liewald[1,2], Ernst Bamberg[3], Georg Nagel[4], Alexander Gottschalk[1,2]*

1 Institute of Biochemistry, Goethe-University, Frankfurt, Germany, 2 Frankfurt Institute for Molecular Life Sciences (FMLS), Goethe-University Frankfurt, Frankfurt, Germany, 3 Department of Biophysical Chemistry, Max-Planck-Institute of Biophysics, Frankfurt, Germany, 4 Botanik I, University of Würzburg, Würzburg, Germany

Abstract

Channelrhodopsin-2 (ChR2) is widely used for rapid photodepolarization of neurons, yet, as it requires high-intensity blue light for activation, it is not suited for long-term *in vivo* applications, e.g. for manipulations of behavior, or photoactivation of neurons during development. We used "slow" ChR2 variants with mutations in the C128 residue, that exhibit delayed off-kinetics and increased light sensitivity in *Caenorhabditis elegans*. Following a 1 s light pulse, we could photodepolarize neurons and muscles for minutes (and with repeated brief stimulation, up to days) with low-intensity light. Photoactivation of ChR2(C128S) in command interneurons elicited long-lasting alterations in locomotion. Finally, we could optically induce profound changes in animal development: Long-term photoactivation of ASJ neurons, which regulate larval growth, bypassed the constitutive entry into the "dauer" larval state in *daf-11* mutants. These lack a guanylyl cyclase, which possibly renders ASJ neurons hyperpolarized. Furthermore, photostimulated ASJ neurons could acutely trigger dauer-exit. Thus, slow ChR2s can be employed to long-term photoactivate behavior and to trigger alternative animal development.

Introduction

ChR2 is a light-driven cation channel that enables fast photodepolarization of excitable cells in culture and in live animals ranging from *Caenorhabditis elegans* to primates [1–6]. However, for long-term photodepolarization, e.g. to influence learning or neuron-controlled alternative developmental pathways, ChR2 is not suited: As it requires continuous illumination with blue light of high intensity (≥ 1 mW/mm^2) to keep the channel open a) phototoxicity may arise and b) intrinsic phototactic reactions of animals can occur that interfere with the studied behavior. These limitations may be overcome by the recently described ChR2(C128X) mutants [7–9]. Compared to wild type ChR2 ($\tau_{off} = 11.9$ ms), mutations of C128 to T, A, or S significantly delay the closing of the channel in the dark ($\tau_{off} = 2$ s, 56 s, and 106 s, respectively; [7]). As the open photointermediate P520 accumulates, light of reduced intensity suffices for efficient channel-opening. Once in the open state, C128X mutants can be photoinactivated using green-yellow light, thus they are also termed "step function opsins".

C. elegans is a genetic model for studies of neurobiology and development, among other areas of biology. Its nervous system is mapped down to the individual synapse [10], and its neurons form simple functional units, similar to elementary network units found in higher animals [11]. *C. elegans* exhibits stereotypic behaviors, e.g. escape reflexes in response to particular sensory inputs, and, depending on external conditions, alternative developmental pathways. In a favorable environment, the nematode develops through four larval stages into adult animals [12], while under

harsh conditions, reproductive development is bypassed and animals enter a long-lived "dauer"-state after larval stage L2 [13–15]. Dauer larvae exhibit specialized morphology and metabolism, allowing them to survive harsh conditions for several months [13,16–18]. Importantly, harsh or beneficial conditions are detected by sensory neurons that prevent or instruct entry into, or exit from, the dauer-state [19,20].

We characterized slow ChR2 variants for prolonged photoactivation of excitable cells in *C. elegans*. ChR2(C128X) could photodepolarize body wall muscle (BWM) cells, cholinergic and GABAergic motorneurons for several minutes following a 1 s light pulse. As in other systems, the open state could be terminated by yellow light. Continuous activation of the locomotion command interneurons evoked long-lasting behavioral alterations. Lastly, we could alter the genetically predisposed development of *C. elegans* by long-term photodepolarization of ASJ sensory neurons, to either prevent the constitutive dauer-entry in *daf-11* mutant animals, or to achieve an exit from the dauer-state.

Results

Slow ChR2 mutants enable long-term activation of muscles with low light intensity

First, we expressed three slow ChR2 variants (C128T, A, and S), in BWMs (**Fig. S1a**), as well as ChR2(H134R), which has slightly delayed kinetics and thus larger steady-state conductance than wild type ChR2 [4]. Concomitant depolarization of all BWMs induces a uniform contraction, causing a decrease in body length; thus, body length is a measure for extent and persistence of

BWM depolarization [4]. The proteins localized mostly to the plasma membrane, with variable amounts of intracellular, sometimes aggregated protein. We analyzed expression levels based on fluorescence in individual muscle cells, which showed strong differences: ChR2(C128T and S) both expressed better than ChR2(H134R), while ChR2(C128A) expression was low, showing mosaicisms (data not shown). However, as the proteins aggregated to a variable extent and we could not specifically determine cell surface expression levels, these findings did not allow us to predict which protein may be best suited for long-term applications in *C. elegans*. Thus, to assess this based on function, we monitored the capability of the ChR2 variants to depolarize BWMs. Animals (grown in presence of all-*trans* retinal - ATR) were illuminated for 1 s with blue light (450–490 nm; 0.69 mW/mm^2), and the body length was deduced from videos [5] (**Fig. 1a, b, and Video S1**). ChR2(H134R) induced a ~12% contraction, and animals returned to initial length ~1 s after light-off. ChR2(C128T, A, and S) induced comparable contraction amplitudes, however, relaxation of the body wall was largely delayed, occurring after 5 s, 3 min, and >5 min, for ChR2 C128T, C128A, and C128S, respectively. Measuring ChR2(C128S)-mediated inward photocurrents confirmed the largely delayed channel-closing (**Fig. 1c**, and see below).

We determined the lowest light intensity (0.001–2.2 mW/mm^2) sufficient to achieve saturating ChR2-dependent effects. Contractions >8% were evoked by ChR2(H134R) in BWMs when at least 0.08 mW/mm^2 light were applied. In contrast, photoactivation of ChR2(C128S) with as low as 0.01 mW/mm^2 still evoked full contractions (**Fig. 1d**), that were also prolonged for several minutes (**Fig. S1b, c**), thus establishing ChR2(C128S) as a powerful tool for prolonged depolarization of excitable cells under minimal light-invasive conditions. As daylight already caused marked contraction and uncoordinated locomotion, ChR2(C128S) animals should be kept in the dark and handled under low intensity red light to prevent unwanted photoactivation.

ChR2(C128S) can be repeatedly "switched" on and off with blue an yellow light

As in other systems, we could photo-switch slow ChR2 variants from the open state to the closed dark-state, by using yellow light [7]. We applied alternating blue (450–490 nm; 1 s; 0.01 mW/mm^2) and yellow (565–595 nm; 1 s; 4.4 or 2.5 mW/mm^2) pulses, each followed by an 8 s dark period, and monitored the body length of animals expressing either ChR2(H134R) or ChR2(C128S) in BWMs (**Fig. 1e and Video S1**). In H134R animals, low intensity blue light induced ~2% contraction during illumination, while yellow light had no effect. In contrast, in C128S animals, blue light induced a continuous contraction of ~10% that was completely abolished by the yellow light pulse (**Fig. 1e**), thus allowing full temporal control over ChR2(C128S) induced depolarization.

Long-term stimulation of ChR2(C128S) leads to a partial reduction of function

Potential applications of ChR2(C128S) could be to keep neurons depolarized for hours to days to affect processes like learning or even developmental pathways. However, Schoenenberger et al. (2009) found a progressive inactivation of ChR2(C128A), when in the open state, and in response to repeated stimuli. A fraction of molecules appeared to transition into an ill-defined, non-activatable "lost state", from which they recovered very slowly. We thus assayed for how long ChR2(C128S) may be continuously activated. ChR2(C128S) in

muscles was photoactivated for up to 1 day using two different protocols: a) 1 s blue light every 2 min; or b) 1 s blue, 5 s dark, then 2 s yellow, etc., the latter one to actively prevent loss of ChR2 to inactive states. At 0, 30, 120, 360 minutes and 1 day, animals were given a blue test pulse for full activation, followed by a yellow pulse for inactivation, and the relaxation was measured (**Fig. 1f**). After 30 min, effects were reduced from initially 7.6±1.4% to 4.5±1.0%, after 120 min, and still after 1 day, they were down to 1.4±0.6%. Thus, long-term depolarization via ChR2(C128S) may cause only ~18% of maximal effects and should be considered when using ChR2(C128S) in the range of several hours or days. Nevertheless, depending on the cell type, this remaining functionality for even 24 h may be sufficient for long-term activation of the particular cell and its potential downstream targets.

Slow ChR2 mutants allow activating motorneurons in *C. elegans*

We next tested the applicability of slow ChR2 mutants in neurons. We expressed ChR2(C128S) in cholinergic motorneurons, that cause muscle contraction when photostimulated [5]. As photostimulation of cholinergic neurons causes a coiling phenotype, due to concomitant GABA signaling, we analyzed the effects of ChR2 activation in *unc-49(e407)* mutants that lack the muscular GABA$_A$R. A 1 s, low-intensity (0.01 mW/mm^2) light pulse caused prolonged contractions of ~10%, which were long-lasting (several minutes; **Fig. 2a, d, and Video S2**), and could not be achieved using ChR2(H134R). Also for cholinergic neurons, we could photo-switch ChR2(C128S) from the open state to the closed dark-state, using yellow light, and this could be repeated up to 10 times, with no obvious loss of activity (**Figs. 2b and S2**). As for muscles, the lowest light intensity sufficient to achieve saturating ChR2-dependent effects in cholinergic neurons was 0.01 mW/mm^2 (**Fig. 2c**). At this light intensity, ChR2(H134R) appeared to evoke contractions more efficiently in cholinergic neurons than in BWMs (compare **Figs. 1d and 2c**). This may be due to cell-type specific differences in the environment of the channel, affecting its properties, or because contractions evoked by ChR2 in cholinergic motorneurons are effected by ACh release and postsynaptic nAChRs, which may be more efficient, than directly by photocurrents within BWMs. Similar experiments with ChR2(C128S) and ChR2(H134R) in GABAergic motorneurons (evoking body relaxation; [5]) showed qualitatively comparable results (**Fig. S3**), emphasizing the utility of ChR2(C128S) in several neuron types. Thus, ChR2(C128S) can be used to mimic prolonged synaptic transmission at the neuromuscular junction.

## Long-term alteration of behavior in locomotion command interneurons

We next analyzed whether behavior can be altered in the long-term by depolarizing command interneurons, which regulate certain aspects of locomotion (**Fig. 3a**), particularly the direction and likely also the speed of movement: AVB and PVC neurons trigger forward, whereas AVA and AVD mediate backward locomotion. Each cell type mutually inhibits the opposite type, thus they form a bi-stable switch that fluctuates between backward and forward states. Sensory neuron input alters this balance by depolarizing one command neuron type; in undisturbed animals, forward command neurons dominate, and worms crawl mostly forward, interrupted by brief backward episodes (~2–4 times min^{-1}; [21]). Concomitant activation of all command neurons thus perturbs normal activity and affects locomotion.
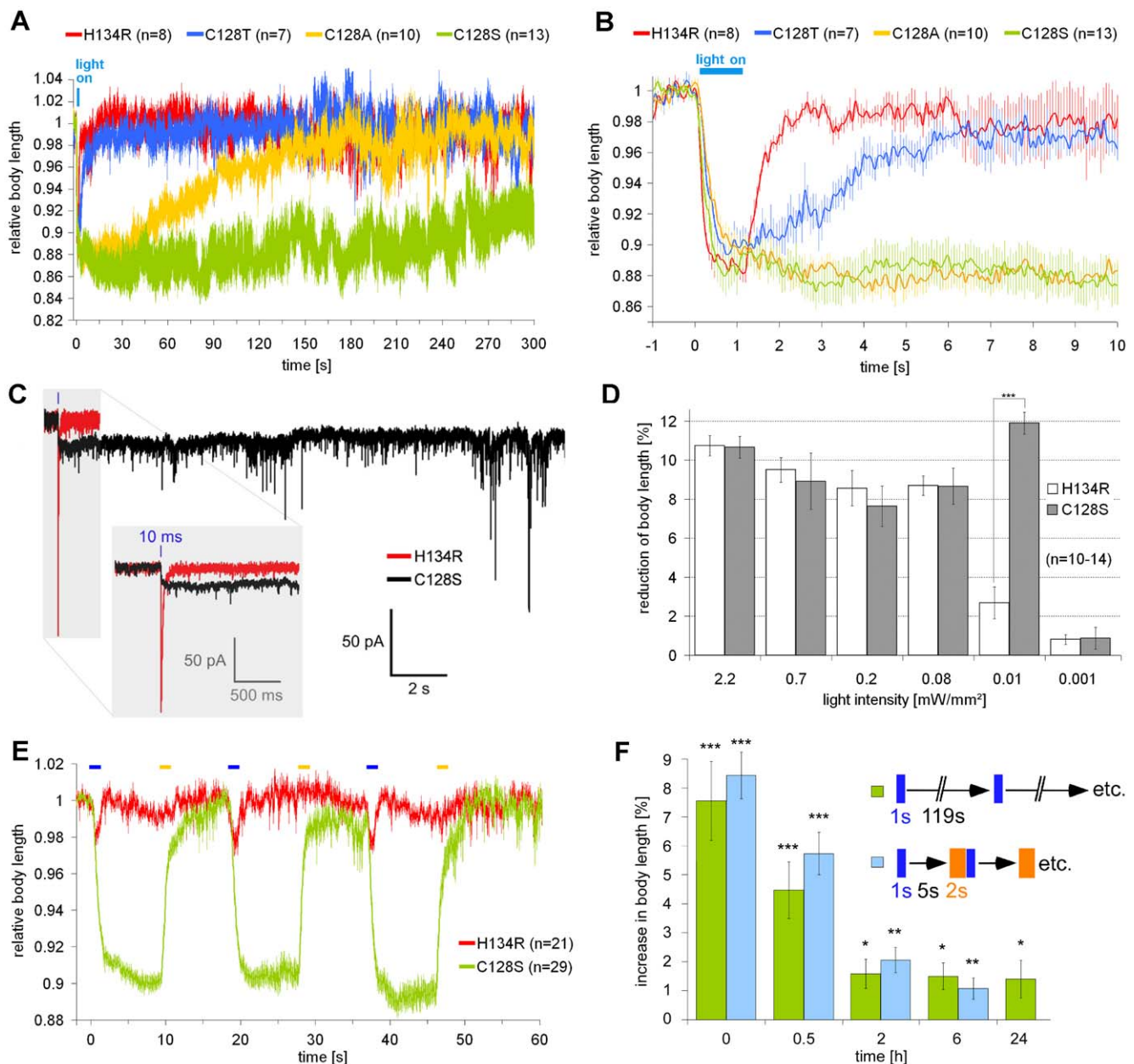
Figure 1. ChR2(C128X) variants induce prolonged depolarization in muscles at reduced light intensities. (**a**) ChR2(H134R), ChR2(C128A, T and S) were expressed in BWMs. Body length of animals during and after a 1 s blue light stimulus (0.69 mW/mm²; 450–490 nm; given at t = 0 s) was calculated relative to the initial length. (**b**) Enlarged (seconds -1 to 10) from (a). (**c**) Representative traces of photocurrents measured in whole-cell voltage clamp of BWMs expressing ChR2(C128S) or ChR2(H134R), evoked by a 10 ms photostimulus (470 nm; 8 mW/mm²); inset shows close-up. (**d**) Comparison of the light-dependence of ChR2(H134R) and ChR2(C128T) in BWMs. Reduction of body length of worms in response to 1 s blue light stimuli (450–490 nm) of various light intensities in the range of 0.001–2.2 mW/mm², presented at t = 0 s; reduction of body length was measured for ChR2(H134R) directly after light off (t = 1 s), for ChR2(C128S), due to the slower onset, 2 s after light off (t = 3 s). (**e**) Relative body length of worms while alternating 1 s blue (0.01 mW/mm²; 450–490 nm) or 1 s yellow (4.4 mW/mm²; 565–595 nm) light pulses were presented, indicated by blue and yellow bars. (**f**) Long-term activity of ChR2(C128S). 1 s blue light pulses (0.05 mW/mm²; 470 nm) were presented either every 120 s or every 8 s (in the latter case, followed by a 5 s dark period and a 2 s yellow light pulse (0.04 mW/mm²; 590 nm)). At the indicated times, animals (n = 9–15) were presented a blue test pulse (2.1 mW/mm²; 450–490 nm), followed by a yellow pulse (6.1 mW/mm²; 565–595 nm) for inactivation and the resulting relaxation was measured. n = number of animals; error bars are s.e.m.; ***: p<0.001, **: p<0.005, *: p<0.01.
doi:10.1371/journal.pone.0018766.g001

We used the *glr-1* promoter to express ChR2(C128S) and ChR2(H134R) in all command neurons and some additional neurons [22] (**Fig. S4**). The ratio of backward movement was assayed for three consecutive 1 min periods, and calculated for the whole period. A 1 s blue light pulse (2.1 mW/mm²) was applied

after the first minute to activate ChR2 variants. After the second minute, yellow light (1 s; 6.1 mW/mm²) was presented for inactivation. Non-transgenic animals (wild type) did not exhibit any significant change in the proportion of backward movement (**Fig. 3b**). For ~40% of ChR2(H134R) expressing animals, a
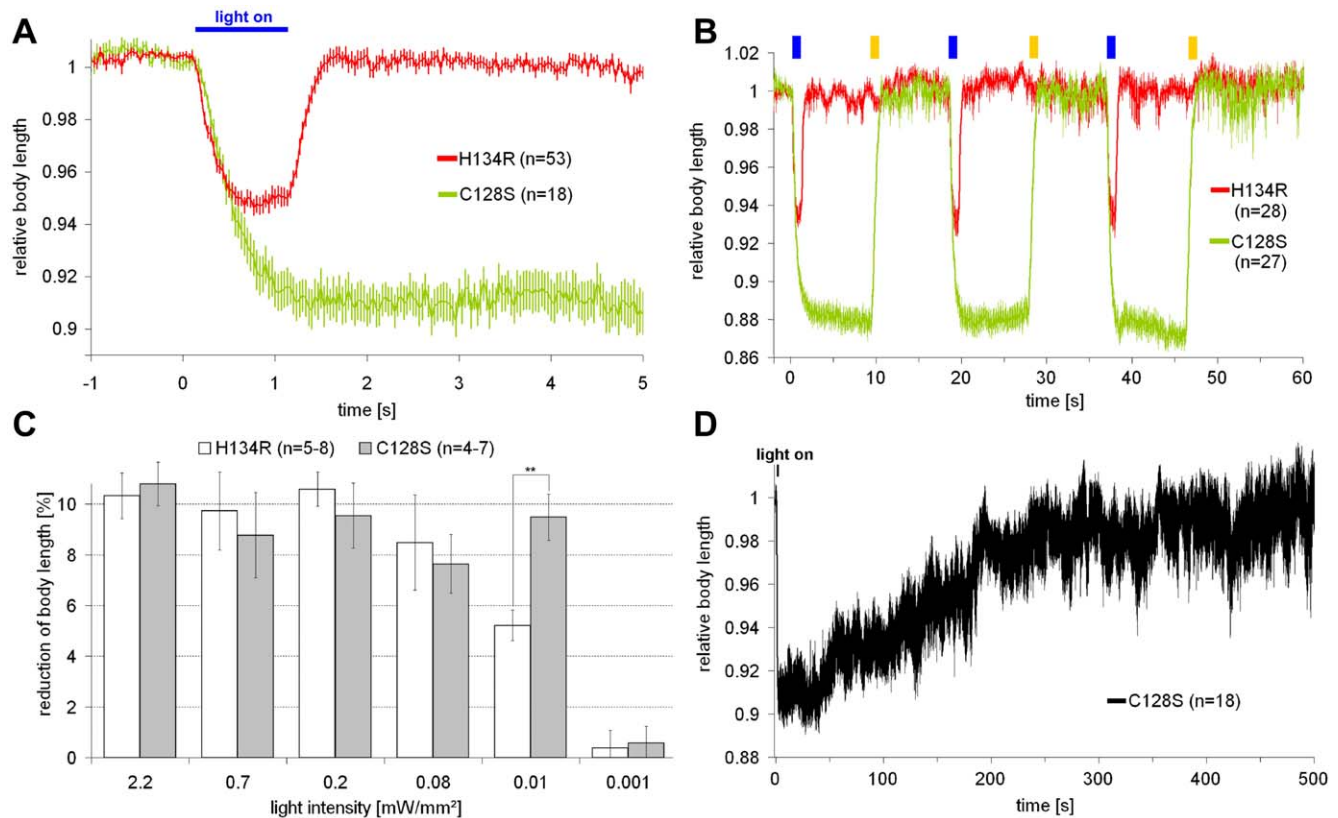
Figure 2. ChR2(C128S) induces prolonged depolarization in cholinergic motorneurons at reduced light intensities. ChR2(H134R) and ChR2(C128S) were expressed in cholinergic motorneurons. To avoid coiling induced by prolonged depolarization of cholinergic neurons [5], we analyzed effects of ChR2 activation in *unc-49(e407)* mutants, lacking GABA$_A$Rs. (**a**) Relative body length of worms while a 1 s blue light stimulus (0.01 mW/mm^2; 450–490 nm) was given at t = 0 s. (**b**) Relative body length of worms while alternating 1 s blue (0.01 mW/mm^2; 450–490 nm) or 1 s yellow (2.5 mW/mm^2; 565–595 nm) light pulses were presented, as indicated. (**c**) Comparison of the light-dependence of ChR2(H134R) and ChR2(C128S). Reduction of body length of worms while a 1 s blue light stimulus (450–490 nm) of various light intensities in the range of 0.001–2.2 mW/mm^2 was given at t = 0; reduction of body length was measured for ChR2(H134R) directly after light off (t = 1 s), and for ChR2(C128S) when full amplitudes were reached, 2 s after light off (t = 3 s). (**d**) Relative body length of worms expressing ChR2(C128S) while a low-intensity 1 s blue light stimulus (0.01 mW/mm^2; 450–490 nm) was given at t = 0 s. n = number of animals; error bars are s.e.m.; **: p<0.005.
doi:10.1371/journal.pone.0018766.g002

reversal was observed right after the blue light photoactivation. However, as these effects were very brief, i.e. restricted to the time of illumination, they did not become evident in the analyzed one-minute proportion of backward locomotion. In contrast, ~71% of ChR2(C128S) animals reversed upon photoactivation and thereafter crawled backwards for extended periods, often even until the inactivating yellow pulse. The proportion of backward movement increased from 19.4±4.2% to 76.8±4.4% during the second minute, which was completely reversed after the inactivating yellow pulse (26.3±5.3%; **Fig. 3b and Video S3**). Thus, command neurons can be optically manipulated in the long-term, to evoke downstream effects across several synapses, emphasizing the utility of ChR2(C128S) in prolonged manipulation of neuronal networks and, as a result, behavior.

Long-term photo-activation of ASJ neurons during animal development

Lastly, we asked whether ChR2(C128S) could sufficiently activate neurons at a timescale of hours to days, e.g. cells relevant for animal development, under low light conditions, to prevent phototoxic effects. We thus turned to neurons that affect larval development. Depending on external signals, *C. elegans* larvae either develop to adulthood, or enter the dauer-state (**Fig. 4a**). In

a simplistic view, but based on results from several studies, favorable external signals are sensed by ADF, ASG, and ASI neurons to prevent dauer-entry and to commit the worm to reproductive development [19,23]. Contrary, ASJ neurons, which can release insulin and possibly other signals to prevent dauer-entry, may rather sense unfavorable cues like pheromones, and thus likely become inhibited [20]. Additionally, ASJ may be involved in dauer-exit, i.e. when conditions become favorable again, by releasing molecules that promote dauer-exit [19]. Unfavorable environmental signals appear to inhibit the guanylyl cyclase DAF-11 (which generates cGMP to activate the cGMP-gated cation-channel TAX-2,-4), thus likely keeping ASJ in a resting or even hyperpolarized state and initiating dauer-arrest [20,24–26] (**Fig. 4a**). *daf-11(m84)* mutants display a constitutive dauer-phenotype (*daf-c*): most larvae become dauers even under favorable conditions [24]. While additional mechanisms affecting dauer larval development need to be considered, (photo-)depolarization of ASJ neurons, at the right time during development, may nonetheless provide a means to prevent dauer-entry and to promote dauer-exit, particularly in *daf-11(m84)* mutants.

To allow cell-specific expression of ChR2(C128S) in ASJ neurons, we used the *trx-1b* promoter, which, however, expresses in ASJ cells only in the context of the genomic locus including the
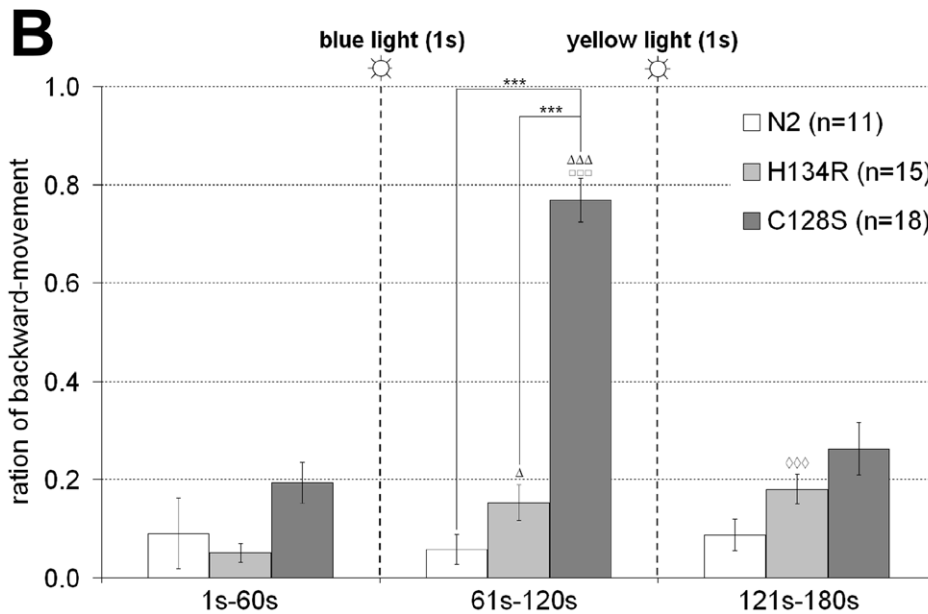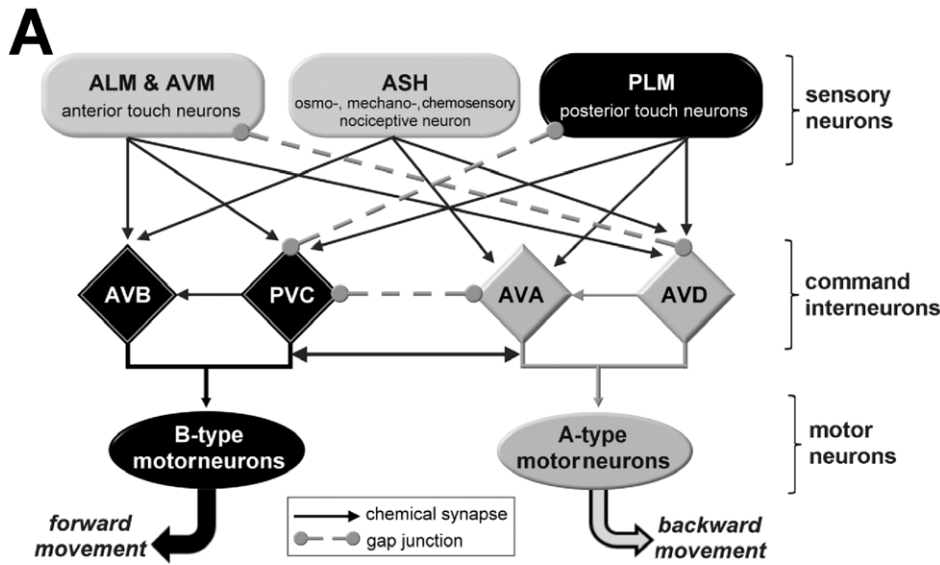
Figure 3. Photoactivated ChR2(C128S) induces long-term behavioral effects in command interneurons. (**a**) Schematic of the neuronal wiring diagram connecting selected sensory neurons, command interneurons and motorneurons that evoke, mediate or are required for forward (indicated in black) or backward locomotion (indicated in grey), respectively. Synaptic strength is omitted, for clarity. (**b**) ChR2(H134R) and ChR2(C128S) were expressed in command interneurons. Animals were placed on NGM plates without food. The ratio of backward locomotion was measured for 3 minutes (binned in 1 min intervals) and compared to wild type animals (N2). After 60 s, a 1 s blue light stimulus (2.1 mW/mm^2; 450–490 nm) and after 120 s, a 1 s yellow light stimulus (6.1 mW/mm^2; 565–595 nm) were given. n = number of animals; error bars are s.e.m.; *: significance between different strains; other symbols: significance within a strain between minute 1 and 2 (Δ), minute 2 and 3 ($\square$), or minute 1 and 3 ($\Diamond$); ***/$\Delta\Delta\Delta$/$\square\square\square$/$\Diamond\Diamond\Diamond$: p<0.001, Δ: p<0.01.
doi:10.1371/journal.pone.0018766.g003

trx-1b coding sequences and introns [27]. We thus needed to fuse ChR2(C128S) to the C-terminus of TRX-1B. Expression of TRX-1B::ChR2(C128S) in ASJ was observed after hatching and through all developmental stages, including the dauer stage (**Fig. S5**). To verify that the ChR2 portion of the TRX-1B::ChR2(C128S) fusion protein is functional, we expressed it also in body wall muscle cells, where it could photo-evoke muscle contractions, albeit to a lesser extent than ChR2(C128S) alone (**Fig. S1a, d**). We also (over)expressed only TRX-1B in ASJ cells, to exclude light-independent effects of TRX-1B on dauer-entry or -exit.

Next, we analyzed whether photoactivation of TRX-1B::ChR2(C128S) in ASJ was able to prevent dauer-entry of *daf-11(m84)* mutant animals. To this end, eggs (from mothers that were kept in the dark at all times) were incubated in the presence of bacterial food, optionally supplemented with ATR, under constant low illumination (~0.12 µW/mm^2 blue light). After 3 days, we scored the fraction of worms in dauer and adult states. Of the *daf-11(m84)* mutant animals, only 16.5±0.9% or 14.9±1.0% (in the absence or presence of ATR, respectively) developed to adulthood (**Fig. 4b**). However, when TRX-1B::ChR2(C128S)::YFP was
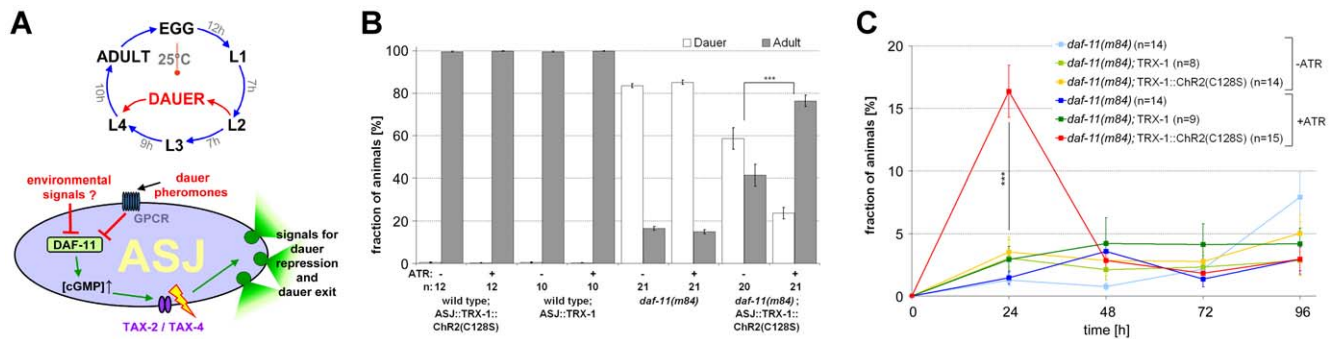
Figure 4. Altering animal development by long-term photostimulation of ASJ neurons. (a) Larval development of *C. elegans*, including the alternative dauer-state (upper panel, simplified; [15,19,20,24–26,33]). Sensory neurons, like ASJ, mediate entry into, exit from, or repression of the dauer-state, in response to environmental signals. The molecular mechanisms in ASJ (lower panel, modified; [26]) are depicted. When depolarized, ASJ releases signals causing dauer-repression and dauer-exit. ASJ is depolarized via cGMP-gated TAX-2/-4 channels. Dauer-pheromones and possibly environmental signals (i.e. absence of food, high temperature) inhibit the guanylyl cyclase DAF-11, thus causing dauer-entry by blocking release of ASJ signals. (b) ChR2(C128S) was expressed in ASJ sensory neurons using the *trx-1* promoter. *daf-11(m84)*, *daf-11(m84);zxIs19[ptrx-1::TRX-1B::ChR2(C128S)::YFP;lin-15+]*, N2;;*zxIs19[ptrx-1::TRX-1B::ChR2(C128S)::YFP;lin-15+]*, and N2; *zxEx450[ptrx-1::TRX-1B;pCFJ90]* adults were allowed to lay eggs in the dark for 10–12 hours on plates with bacterial food, supplemented with or without ATR. Plates were then scored for adult and dauer-animals; n = 10–21 experiments, 30–130 animals each. (c) *daf-11(m84)*, *daf-11(m84); zxIs19[ptrx-1::TRX-1B::ChR2(C128S)::YFP;lin-15+]*, and *daf-11 (m84); zxEx450[ptrx-1::TRX-1B;pmyo-2::mCherry]* animals were allowed to develop into dauers in the dark on plates optionally supplemented with ATR, and then illuminated beginning at t = 0 h. The fraction of animals escaping dauer-arrest was scored at the indicated times post illumination onset. n = 8–15 experiments, 30–60 animals each. Error bars are s.e.m., ***: p<0.001.
doi:10.1371/journal.pone.0018766.g004

expressed in *daf-11(m84)* mutants, photoactivation prevented dauer-formation in 76.4±2.7% of *daf-11(m84)* animals, when ATR was present; a slight positive effect of this transgene was also observed in the absence of ATR (41.4±5.1% adult animals), possibly due to carry-over of some ATR from parental animals. Wild type animals expressing either TRX-1B::ChR2(C128S) or TRX-1B alone yielded close to 100% adult animals, regardless of ATR treatment, and TRX-1B expression in *daf-11(m84)* mutants had no rescuing effect on the dauer-state either (see below, dauer-exit experiment; **Fig. 4c**).

Finally, we investigated whether photoactivation of ASJ could also promote dauer-exit. *daf-11* mutants, optionally expressing TRX-1B::ChR2(C128S) or TRX-1B alone in ASJ, were grown in the dark, in the presence or absence of ATR. Without light-stimulation, animals became dauers, and were only then placed into light, to potentially evoke acute dauer rescue. The fraction of animals developing to adults was scored over 4 days: 2–4% of *daf-11(m84)* dauers and *daf-11(m84)* dauers expressing TRX-1B recovered every 24 h, independent of ATR and light (**Fig. 4c**); yet, within the first 24 h of illumination, 16.4±2.1% of *m84* dauers expressing TRX-1B::ChR2(C128S) in ASJ recovered if ATR was added prior to dauer-entry. At later times, the fraction of adults increased as slowly as for non-transgenic *daf-11(m84)* mutants. Thus, depolarizing ASJ indeed partially induces dauer-exit. However, as this was rather inefficient, additional cells may be required to trigger dauer-exit effectively. Alternatively, as dauers do not feed, ATR may have decayed after the time of dauer entry. We thus analyzed at distinct times after removal from ATR, to what extent ChR2(H134R) and ChR2(C128S) remained functional in muscle cells, by analyzing photo-evoked contractions (**Fig. S6**). While ChR2(H134R) remained fully functional for 24 h, and showed half maximal activity even after 72 h, ChR2(C128S) was surprisingly susceptible to ATR-deprivation: Already after 4 h, functionality was reduced by ~46%, and essentially non-detectable after 48 h (0.5±0.3% contraction; **Fig. S6**). Importantly, ChR2(C128S) remained fully functional in the presence of ATR even after 72 h (8.7±0.6% contraction; **Fig. S6**). In sum, ChR2(C128S) can be used to alter animal

development when expressed in neurons that make developmental decisions, as these can be long-term depolarized using low light intensity.

Discussion

Using *C. elegans*, we showed that: 1) photoactivation of slow ChR2 variants induces prolonged depolarization in BWMs, cholinergic and GABAergic neurons; 2) ChR2(C128S)-mediated depolarization induced by 1 s light lasts several minutes and requires about one order of magnitude less light than ChR2(H134R); 3) blue-light activated ChR2(C128S) can be inactivated by yellow light, enabling full temporal control, thus neurons can be switched "on" and "off"; 4) photoactivation of ChR2(C128S) in command interneurons evokes long-term behavioral effects; and 5) using ChR2(C128S) even animal development can be altered.

Photoactivating command interneurons evoked long-term behavioral changes. Zheng et al. (1999) reported a largely increased frequency of ~40 reversals min^{-1} (the "lurcher" phenotype) after expressing constitutively active GLR-1(A687T) AMPARs in command neurons using the same *glr-1* promoter fragment that we used. Thus, upon permanent strong depolarization, neither forward nor backward command neurons gain dominance, in line with mutual inhibition between the two neuron types. However, we observed a reversal right after photoactivation, often persisting for the whole minute, until yellow light closed ChR2(C128S). Regardless of photoactivation, animals exhibited ~3–4 reversals per minute. How may these opposing results be explained? Unlike ChR2(C128S), GLR-1(A687T) is expressed in its "native environment" (however, in the same cells as ChR2(C128S), as the same promoter was used in both studies), with a likely single-channel conductance in the low pS range, i.e. significantly higher than ChR2 (~40fS; [28]). Thus, stronger depolarization caused by GLR-1(A/T) might account for different behaviors seen in both experiments. Alternatively, GLR-1(A/T) causes depolarization of command neurons from its earliest expression, thus adaptation may occur, evoking different behaviors, while ChR2(C128S) is acutely induced by light during the

experiment. To test this possibility, we photoactivated ChR2(C128S) in command neurons during development and until adulthood, but we found no emerging lurcher phenotype (data not shown). However, as ChR2(C128S) activity dropped to ~18% during long-term experiments (**Fig. 1f**), we may not achieve a long-lasting depolarization to the same extent as the GLR-1(A/T) channel did [21].

Photoactivation of TRX-1B::ChR2(C128S)::YFP in ASJ sufficed to depolarize these neurons for hours, allowing effective dauer-rescue of *daf-11(m84)* mutants. We verified that these effects are specific for the ChR2(C128S) portion of the fusion protein, and that TRX-1B alone had no effects; furthermore, as reported previously, mutation of *trx-1* caused neither *daf-c* nor *daf-d* phenotypes [27]. The photo-evoked dauer rescue was 76.4±2.7%, however, it was not 100%: This may indicate that ChR2(C128S)-induced depolarization was insufficient in some animals, or that additional cellular mechanisms affect dauer-entry in *daf-11* mutants, which could not be overcome by ASJ photodepolarization; clearly the dauer developmental pathway involves many more cells expressing DAF-11 (e.g. ASI, ASK, AWB, and AWC) than just ASJ, and complex signaling pathways that may only inefficiently be triggered via simple depolarization of ASJ neurons. ASJ also promoted dauer-exit in a small, but significant fraction of animals during a 24 h photoactivation period (16.4±2.1%). Possibly, additional neurons, not photoactivated, need to cooperate with ASJ to promote dauer-exit more effectively; yet, more likely, ASJ was insufficiently depolarized due to progressive ChR2(C128S) inactivation, and due to the observed susceptibility of ChR2(C128S) to ATR-deprivation. Nevertheless, to prevent dauer-entry, ASJ is highly efficient on its own.

ChR2(C128S) has some critical properties that should be considered when designing experiments. One is the dependence on the continuous presence of ATR, the other is the partial inactivation by repeated or premature activation. For example, this makes ChR2(C128S) ill-suited for electrophysiological measurements in *C. elegans*, which require dissection of the animals under intense white light, which appears to render a majority of ChR2(C128S) to decay to "lost" states (hence the small photocurrents measured in **Fig. 1c**).

Nonetheless, ChR2(C128S) complements present optogenetic tools and expands their field of application, conceivably also in other animal models. Additional developmental pathways may now be probed, e.g. the likely activity-dependent polarity changes of *C. elegans* DD motorneurons during development [29]. Also adaptation or even associative learning within sensory circuits, which involves long-term neuronal activation [30], may be subjected to optogenetic manipulation using ChR2(C128S).

Materials and Methods

C. elegans culture and transgenic animals

Wild-type and mutant strains used originate from the Bristol strain N2 [31]. Strains were cultivated, optionally in the presence of all-*trans* retinal (Sigma-Aldrich), as described previously [5]. Microinjection of DNA was performed according to standard protocols using 80–100 ng/μl (for constructs with *Pmyo-3* and *Punc-17*), or 200 ng/μl (*Pglr-1* and *Ptrx-1*), and 80 ng/μl for the marker lin-15+ or 2.5 ng/μl for the marker pCFJ90 (*pmyo-2::mCherry*), respectively. The *zxEx434[ptrx-1::TRX-1B::ChR2(C128S)::YFP;lin-15+]* transgene was genomically integrated via UV-irradiation.

Strains used were: **ZX299:** *lin-15(n765ts⁻);zxEx22[pmyo-3::ChR2(H134R)::YFP;lin-15+]* [4], **ZX426:** *N2;zxIs3[punc-47::Ch*

R2(H134R)::YFP;lin-15+] [5], **ZX460:** N2;*zxIs6[punc-17::ChR2(H134R)::YFP;lin-15+]* [5], **ZX497:** *unc-47(e407);zxIs6[punc-17::ChR2(H134R)::YFP;lin-15+]* [5], **ZX836:** *lin-15(n765ts⁻);zxEx421[pmyo-3::ChR2(C128A)::YFP;lin-15+]*, **ZX837:** *lin-15(n765ts⁻);zxEx422[pmyo-3::ChR2(C128T)::YFP;lin-15+]*, **ZX838:** *lin-15(n765ts⁻);zxEx423[pmyo-3::ChR2(C128S)::YFP;lin-15+]*, **ZX839:** *lin-15(n765ts⁻);zxEx424[punc-17::ChR2(C128A)::YFP;lin-15+]*, **ZX840:** *lin-15(n765ts⁻);zxEx425[punc-17::ChR2(C128T)::YFP;lin-15+]*, **ZX841:** *lin-15(n765ts⁻);zxEx426[punc-17::ChR2(C128S)::YFP;lin-15+]*, **ZX842:** *unc-49(e407);lin-15(n765ts⁻);zxEx424[punc-17::ChR2(C128A)::YFP;lin-15+]*, **ZX843:** *unc-49(e407);lin-15(n765ts⁻);zxEx425[punc-17::ChR2(C128T)::YFP;lin-15+]*, **ZX844:** *unc-49(e407);lin-15(n765ts⁻);zxEx426[punc-17::ChR2(C128S)::YFP;lin-15+]*, **ZX845:** *lin-15(n765ts⁻);zxEx428[punc-47::ChR2(C128A)::YFP;lin-15+]*, **ZX846:** *lin-15(n765ts⁻);zxEx429[punc-47::ChR2(C128T)::YFP;lin-15+]*, **ZX847:** *lin-15(n765ts⁻);zxEx430[punc-47::ChR2(C128S)::YFP;lin-15+]*, **ZX848:** *lin-15(n765ts⁻);zxEx431[pglr-1::ChR2(H134R)::YFP;lin-15+]*, **ZX849:** *lin-15(n765ts⁻);zxEx432[pglr-1::ChR2(C128S)::YFP;lin-15+]*, **ZX851:** *lin-15(n765ts⁻);zxEx434[ptrx-1::TRX-1B::ChR2(C128S)::YFP;lin-15+]*, **ZX852:** *N2;zxIs19[ptrx-1::TRX-1B::ChR2(C128S)::YFP;lin-15+]*, **ZX884:** *daf-11(m84);zxIs19[ptrx-1::TRX-1B::ChR2(C128S)::YFP;lin-15+]*, **ZX1033:** *lin-15(n765ts⁻);zxEx448[pmyo-3::TRX-1B::ChR2(C128S)::YFP;lin-15+]*, **ZX1034:** *N2;zxEx450[ptrx-1::TRX-1B;pmyo-2::mCherry]*, **ZX1035:** *daf-11(m84); zxEx450[ptrx-1::TRX-1B;pmyo-2::mCherry]*

Molecular biology

GenBank accession of ChR2 is AF461397. Plasmids pCS54(*Pmyo-3::ChR2(C128A)::YFP*) and pCS56(*Pmyo-3::ChR2(C128T)::YFP*) were obtained by exchanging fragments including mutations from pGEMHE-ChR2(C128A) and pGEMHE-ChR2(C128T) into pAG54(*Pmyo-3::ChR2(H134R)aa1-310::YFP*) [4] via StuI/XhoI. pCS86(*pmyo-3::ChR2(C128S)::YFP*) was generated from pCS54 by site-directed mutagenesis. For expression in cholinergic neurons using *Punc-17*, BglII/StuI fragments were transferred from plasmids pCS54, pCS56 and pCS86 to *Punc-17::ChR2(H134R)::YFP* [5] resulting in pCS55(*Punc-17::ChR2(C128A)::YFP*), pCS57(*Punc-17::ChR2(C128T)::YFP*) and pCS87 (*Punc-17::ChR2(C128S)::YFP*). Likewise, StuI/XhoI fragments were swapped from pCS54, pCS56 and pCS86 into *Punc-47::ChR2(H134R)::YFP* [5], yielding pCS124(*Punc-47::ChR2(C128A)::YFP*), pCS125(*Punc-47::ChR2(C128T)::YFP*) and pCS126(*Punc-47::ChR2(C128S)::YFP*). For expression in command interneurons, a *Pglr-1* fragment was PCR-amplified from genomic DNA (primers oCS209(5′-GTGTCACGTGCCATGATTACGCCAAGCTTGC-3′) and oCS210(5′-CAATCCCGGGGATCCTCTAG-3′)), and subcloned into pAG54 and pCS86 using PmlI/BamHI, yielding pCS103(*Pglr-1::ChR2(H134R)::YFP*) and pCS106(*Pglr-1::ChR2(C128S)::YFP*). The *Ptrx-1::TRX-1B* sequence for expression in ASJ was PCR-amplified from genomic DNA (oCS211(5′-GTGTCACGTGAGAATGGATACCTGATCATT-3′) and oCS224(5′-GTGTGGATCCTTGAGCAGATACGTGCTCC-3′)). A PmlI/BamHI fragment was exchanged in pCS86 yielding pCS121(*Ptrx-1::TRX-1B::ChR2(C128S)::YFP*). A fragment was amplified from pCS121 using primers oCS269(5′-GTGTTCTAGAATGTCTCTCACCCAAGGAG-3′) and oCS270(5′-GAGAATGACCGGTGAGG-3') and subcloned into pCS86 with XbaI and XhoI to result in pCS155(*Pmyo-3::TRX-1B::ChR2(C128S)::YFP*). In pCS121, *ChR2(C128S)::YFP* was excised with BglII and EcoRI and replaced by a PCR fragment from pCS121 (primers oCS271(5′-GGTAATTCGGTAAAACTC-3′) and oCS272(5′-CACAGAATTCTCATTGAGCAGATACGTGCTCC-3′) to generate pCS156(*Ptrx-1::TRX-1B*).

Behavioral experiments

Young adult animals were transferred to 5.5 cm dishes containing 4 ml nematode growth medium (NGM). Using an Axiovert 40 CFL microscope (Zeiss) with $10\times$ magnification, 50 W mercury lamp, and computer-controlled shutter (Sutter Instruments), animals were illuminated with 450–490 nm blue light for ChR2 photoactivation and with 565–595 nm yellow light for ChR2 photoinactivation. Intensity was adjusted using neutral density filters (AHF Analysentechnik). For long-term photoactivation and inactivation, LEDs, blue (470 nm; 0.05 mW/mm^2; Luxeon) or yellow (590 nm; 0.04 mW/mm^2; Rapp Optoelectronic), respectively, were used. For body length measurements, videos were recorded (Powershot G5 or G9 digital cameras, Canon). Frames were extracted and either processed using a custom ImageJ script [32] or analyzed with a custom script for Matlab (The MathWorks) [5]. Unless described differently, animals were kept in complete darkness until execution of experiments to avoid unwanted photoactivation of ChR2. To avoid coiling induced by prolonged depolarization of cholinergic neurons [5], we analyzed effects of ChR2 activation in *unc-49(e407)* mutants, lacking GABA$_A$Rs. Body length was normalized to the last second before illumination. Images yielding incorrect values for body length (e.g. coiling animals) were ignored. To monitor effects on dauer-entry, the following strains were cultivated for at least three days in the dark: *daf-11(m84)*, N2, ZX852, ZX884, and ZX1034. Then, young adults were placed on seeded plates, optionally supplemented with ATR while plates were exposed to continuous illumination of two 18 W neon bulbs for three days (blue light intensity: 0.12 µW/mm^2 at the NGM agar surface). Animals were allowed to lay eggs for 10–12 h, and then removed. The fraction of adults and dauers (grown with or without ATR) was scored. To analyze dauer-exit, the following strains were cultivated on seeded plates with or without ATR for at least two days in the dark (to enlarge the fraction of dauer-animals): *daf-11(m84)*, ZX884, and ZX1035. Dauer animals were then transferred to fresh plates, optionally supplemented with ATR and incubated under constant illumination (two 18 W neon bulbs; 0.12 µW/mm^2 blue light intensity). The fraction of adults was then scored daily.

Fluorescence microscopy and Electrophysiology

Expression of ChR2::YFP was analyzed on an Axiovert 200 microscope (Zeiss) with filterset F41-028 (AHF Analysentechnik) and 100 W mercury lamp. Images were captured with an AxioCam MRm camera (Zeiss). Expression in command interneurons and ASJ was analyzed on a Zeiss LSM 510 confocal microscope. Recordings from BWMs were conducted as previously described [5].

Statistics

Data are given as means±s.e.m. Significance between datasets is given as P-value after two-tailed Student's t-test.

Supporting Information

Figure S1 Expression and activation of slow ChR2 variants in body wall muscle cells evokes body contractions. (**a**) ChR2(H134R)::YFP, ChR2(C128T)::YFP, ChR2(C128A)::YFP, ChR2(C128S)::YFP, and TRX-1B::ChR2(C128S)::YFP were expressed in body wall muscle cells using the *myo-3* promoter. Fluorescence micrographs. Scale bar is 10 µm. (**b**) Relative body length of animals expressing ChR2(C128S) while a low-intensity 1 s blue light stimulus (0.01 mW/mm^2; 450–490 nm) was given at t = 0 s. (**c**) Enlarged diagram from (b) ranging from −1–5 s, comparing full contractions evoked by

ChR2(C128S) to largely reduced contractions evoked by ChR2(H134R). (**d**) Relative body length of worms expressing ChR2(C128S) or TRX-1B::ChR2(C128S) while 1s blue (1.4 mW/mm^2; 450–490 nm) or 1 s yellow (4.4 mW/mm^2; 565–595 nm) light pulses were presented, as indicated. Shown are means, error bars are s.e.m.; n = number of animals.
(TIF)

Figure S2 Photoactivation and -inactivation of ChR2(C128S) in cholinergic motorneurons. Repeated activation and inhibition of ChR2(C128S) in cholinergic neurons, using blue and yellow light pulses, as indicated. The body contractions are shown as readout for postsynaptic muscle activation, induced by photo-triggered release of acetylcholine from motorneurons. Shown are mean relative body length and s.e.m.; n = number of animals.
(TIF)

Figure S3 Prolonged depolarization of GABAergic motorneurons via ChR2(C128S). ChR2(H134R) and ChR2(C128S) were expressed in GABAergic motorneurons using the *unc-47* promoter. Body length and the consequent elongation were measured as readout for presynaptic GABA release. (**a**) Mean relative body length of animals while a 1 s blue light stimulus (2.1 mW/mm^2; 450–490 nm) was given at t = 0. (**b**) mean relative body length of animals while alternating 1 s blue (2.1 mW/mm^2; 450–490 nm) or 1 s yellow (6.1 mW/mm^2; 565–595 nm) light pulses were presented. n = number of animals; error bars are s.e.m.; blue and yellow bars indicate the duration of illumination with the respective color of light.
(TIF)

Figure S4 ChR2(C128S) expression in command interneurons and other neurons, using the *Pglr-1* promoter. ChR2(C128S)::YFP was expressed in command interneurons (AVA, AVB, AVD, AVE, PVC) and other cells (AIB, RMD, RIM, SMD, AVG, PVQ, URY) using the *glr-1*-promoter (Maricq et al., 1995, Nature 378:78–81). Confocal z-projection (left) and bright-field image (right). Scale bar = 30 µm.
(TIF)

Figure S5 TRX-1B::ChR2(C128S) expression in ASJ sensory neurons. Shown is a *daf-11(m84)* dauer larva expressing TRX-1B::ChR2(C128S)::YFP in ASJ sensory neurons using the *trx-1* promoter. Dendrites are indicated by arrows, arrowheads point to axons in the nerve ring. Confocal z-projection (left) and bright-field image (right). Scale bar = 30 µm.
(TIF)

Figure S6 Long-term activity test of ChR2(C128S) and ChR2(H134R) in muscle cells of animals removed from ATR plates. Animals expressing ChR2(H134R) or ChR2(C128S) in muscle cells were cultivated on ATR. At larval stage L4, worms were transferred to fresh plates either with or without ATR. At regular intervals blue light (1.4 mW/mm^2; 450–490 nm) was presented and resulting contractions were measured. Shown are means, error bars are s.e.m.; n = number of animals.
(TIF)

Video S1 Photoactivation and −inactivation of ChR2(C128S) in body wall muscle cells. Photoactivation of ChR2(C128S) in body wall muscle cells with blue light (1 s; 450–490 nm; 0.01 mW/mm^2) caused contraction and was terminated with yellow light (1 s; 565–595 nm; 4.4 mW/mm^2); 15 frames per second.
(MOV)

Video S2 Photoactivation and –inactivation of ChR2(C128S) in cholinergic motorneurons. Photoactivation of ChR2(C128S) in cholinergic motorneurons with blue light (1 s; 450–490 nm; 0.01 mW/mm^2) caused contraction and was terminated with yellow light (1 s; 565–595 nm; 2.5 mW/mm^2); 15 frames per second.
(MOV)

Video S3 Photoactivation and –inactivation of ChR2 (C128S) in command interneurons. Photoactivation of ChR2(C128S) in command interneurons with blue light (450–490 nm; 2.1 mW/mm^2) induced backward movement and is reversed by yellow light (565–595 nm; 6.1 mW/mm^2); 15 frames per second.
(MOV)

Author Contributions

Conceived and designed the experiments: CS JFL AG. Performed the experiments: CS JFL. Analyzed the data: CS JFL AG. Contributed reagents/materials/analysis tools: CS JFL EB GN AG. Wrote the paper: CS JFL AG.

References

1. Nagel G, Szellas T, Huhn W, Kateriya S, Adeishvili N, et al. (2003) Channelrhodopsin-2, a directly light-gated cation-selective membrane channel. Proc Natl Acad Sci U S A 100: 13940–13945.
2. Boyden ES, Zhang F, Bamberg E, Nagel G, Deisseroth K (2005) Millisecond-timescale, genetically targeted optical control of neural activity. Nat Neurosci 8: 1263–1268.
3. Li X, Gutierrez DV, Hanson MG, Han J, Mark MD, et al. (2005) Fast noninvasive activation and inhibition of neural and network activity by vertebrate rhodopsin and green algae channelrhodopsin. Proc Natl Acad Sci U S A 102: 17816–17821.
4. Nagel G, Brauner M, Liewald JF, Adeishvili N, Bamberg E, et al. (2005) Light activation of channelrhodopsin-2 in excitable cells of Caenorhabditis elegans triggers rapid behavioral responses. Curr Biol 15: 2279–2284.
5. Liewald JF, Brauner M, Stephens GJ, Bouhours M, Schultheis C, et al. (2008) Optogenetic analysis of synaptic function. Nat Methods 5: 895–902.
6. Han X, Qian X, Bernstein JG, Zhou HH, Franzesi GT, et al. (2009) Millisecond-timescale optical control of neural dynamics in the nonhuman primate brain. Neuron 62: 191–198.
7. Berndt A, Yizhar O, Gunaydin LA, Hegemann P, Deisseroth K (2009) Bi-stable neural state switches. Nat Neurosci 12: 229–234.
8. Radu I, Bamann C, Nack M, Nagel G, Bamberg E, et al. (2009) Conformational changes of channelrhodopsin-2. J Am Chem Soc 131: 7313–7319.
9. Bamann C, Gueta R, Kleinlogel S, Nagel G, Bamberg E (2010) Structural guidance of the photocycle of channelrhodopsin-2 by an interhelical hydrogen bond. Biochemistry 49: 267–278.
10. White JG, Southgate E, Thomson JN, Brenner S (1986) The Structure of the Nervous System of the Nematode Caenorhabditis elegans. Philos Trans R Soc Lond B Biol Sci 314: 1–340.
11. Chalasani SH, Chronis N, Tsunozaki M, Gray JM, Ramot D, et al. (2007) Dissecting a circuit for olfactory behaviour in Caenorhabditis elegans. Nature 450: 63–70.
12. Byerly L, Cassada RC, Russell RL (1976) The life cycle of the nematode Caenorhabditis elegans. I. Wild-type growth and reproduction. Dev Biol 51: 23–33.
13. Cassada RC, Russell RL (1975) The dauerlarva, a post-embryonic developmental variant of the nematode Caenorhabditis elegans. Dev Biol 46: 326–342.
14. Golden JW, Riddle DL (1982) A pheromone influences larval development in the nematode Caenorhabditis elegans. Science 218: 578–580.
15. Golden JW, Riddle DL (1984) The Caenorhabditis elegans dauer larva: developmental effects of pheromone, food, and temperature. Dev Biol 102: 368–378.
16. Vowels JJ, Thomas JH (1992) Genetic analysis of chemosensory control of dauer formation in Caenorhabditis elegans. Genetics 130: 105–123.
17. Riddle DL, Swanson MM, Albert PS (1981) Interacting genes in nematode dauer larva formation. Nature 290: 668–671.
18. Wadsworth WG, Riddle DL (1989) Developmental regulation of energy metabolism in Caenorhabditis elegans. Dev Biol 132: 167–173.
19. Bargmann CI, Horvitz HR (1991) Control of larval development by chemosensory neurons in Caenorhabditis elegans. Science 251: 1243–1246.
20. Schackwitz WS, Inoue T, Thomas JH (1996) Chemosensory neurons function in parallel to mediate a pheromone response in C. elegans. Neuron 17: 719–728.
21. Zheng Y, Brockie PJ, Mellem JE, Madsen DM, Maricq AV (1999) Neuronal control of locomotion in C. elegans is modified by a dominant mutation in the GLR-1 ionotropic glutamate receptor. Neuron 24: 347–361.
22. Maricq AV, Peckol E, Driscoll M, Bargmann CI (1995) Mechanosensory signalling in C. elegans mediated by the GLR-1 glutamate receptor. Nature 378: 78–81.
23. Vowels JJ, Thomas JH (1994) Multiple chemosensory defects in daf-11 and daf-21 mutants of Caenorhabditis elegans. Genetics 138: 303–316.
24. Birnby DA, Link EM, Vowels JJ, Tian H, Colacurcio PL, et al. (2000) A Transmembrane Guanylyl Cyclase (DAF-11) and Hsp90 (DAF-21) Regulate a Common Set of Chemosensory Behaviors in Caenorhabditis elegans. Genetics 155: 85–104.
25. Zwaal RR, Mendel JE, Sternberg PW, Plasterk RH (1997) Two neuronal G proteins are involved in chemosensation of the Caenorhabditis elegans Dauer-inducing pheromone. Genetics 145: 715–727.
26. Fielenbach N, Antebi A (2008) C. elegans dauer formation and the molecular basis of plasticity. Genes Dev 22: 2149–2165.
27. Miranda-Vizuete A, Fierro Gonzalez JC, Gahmon G, Burghoorn J, Navas P, et al. (2006) Lifespan decrease in a Caenorhabditis elegans mutant lacking TRX-1, a thioredoxin expressed in ASJ sensory neurons. FEBS Lett 580: 484–490.
28. Feldbauer K, Zimmermann D, Pintschovius V, Spitz J, Bamann C, et al. (2009) Channelrhodopsin-2 is a leaky proton pump. Proc Natl Acad Sci U S A 106: 12317–12322.
29. Hallam SJ, Jin Y (1998) lin-14 regulates the timing of synaptic remodelling in Caenorhabditis elegans. Nature 395: 78–82.
30. Tomioka M, Adachi T, Suzuki H, Kunitomo H, Schafer WR, et al. (2006) The insulin/PI 3-kinase pathway regulates salt chemotaxis learning in Caenorhabditis elegans. Neuron 51: 613–625.
31. Brenner S (1974) The genetics of Caenorhabditis elegans. Genetics 77: 71–94.
32. Abramoff MD, Magelhaes PJ, Ram SJ (2004) Image Processing with ImageJ. Biophotonics International 11: 36–42.
33. Kim K, Sato K, Shibuya M, Zeiger DM, Butcher RA, et al. (2009) Two chemoreceptors mediate developmental effects of dauer pheromone in C. elegans. Science 326: 994–998.

PACα – an optogenetic tool for *in vivo* manipulation of cellular cAMP levels, neurotransmitter release, and behavior in *Caenorhabditis elegans*

Simone Weissenberger,[*,1,2] Christian Schultheis,[*,2] Jana Fiona Liewald,[*,2] Karen Erbguth,[*] Georg Nagel[†] and Alexander Gottschalk[*,‡]

[*]*Department of Biochemistry, Chemistry, and Pharmacy, Institute of Biochemistry, Goethe-University, Frankfurt, Germany*
[†]*University Wuerzburg, Botanik I, Wuerzburg, Germany*
[‡]*Frankfurt Institute for Molecular Life Sciences (FMLS), Goethe-University, Frankfurt, Germany*

Abstract

Photoactivated adenylyl cyclase α (PACα) was originally isolated from the flagellate *Euglena gracilis*. Following stimulation by blue light it causes a rapid increase in cAMP levels. In the present study, we expressed PACα in cholinergic neurons of *Caenorhabditis elegans.* Photoactivation led to a rise in swimming frequency, speed of locomotion, and a decrease in the number of backward locomotion episodes. The extent of the light-induced behavioral effects was dependent on the amount of PACα that was expressed. Furthermore, electrophysiological recordings from body wall muscle cells revealed an increase in miniature post-synaptic currents during light stimulation. We conclude that the observed effects were caused by cAMP synthesis because of photoactivation of pre-synaptic PACα which subsequently triggered acetylcholine release at the neuromuscular junction. Our results demonstrate that PACα can be used as an optogenetic tool in *C. elegans* for straightforward *in vivo* manipulation of intracellular cAMP levels by light, with good temporal control and high cell specificity. Thus, using PACα allows manipulation of neurotransmitter release and behavior by directly affecting intracellular signaling.

Keywords: cAMP, electrophysiology, optogenetics, photoactivated adenylyl cyclase, synaptic transmission.

J. Neurochem. (2011) **116**, 616–625.

cAMP is a ubiquitous second messenger in intracellular signal transduction and involved in many cellular events and complex biological processes, including hormone signaling (Beavo and Brunton 2002), immune function (Torgersen *et al.* 2002), modulation of synaptic transmission (Kidokoro *et al.* 2004), and memory consolidation (Kandel 2001; Morozov *et al.* 2003). Synthesis of cAMP is accomplished by adenylyl cyclases, soluble or integral membrane proteins that convert ATP to cAMP. Because of the various functions of cAMP and its use in many different organisms, an extensive family of adenylyl cyclases has evolved. Usually, the enzyme activity is regulated by G-proteins. However, a photoactivated adenylyl cyclase (PAC) was isolated from the photosensory organelle of the freshwater flagellate *Euglena gracilis* (Iseki *et al.* 2002; Ntefidou *et al.* 2003). In this unicellular organism, PAC serves as an important photoreceptor that mediates cAMP-dependent phototaxis.

Photoactivated adenylyl cyclase is a blue-light receptor that is composed of four flavoprotein subunits: two PACα and two PACβ subunits. Each subunit consists of two BLUF (sensors of blue-light using FAD) domains binding FAD for photoreception (Anderson *et al.* 2005; Gauden *et al.* 2006) and two cyclase domains to catalyze the conversion of ATP

to cAMP (Iseki *et al.* 2002). PACα and PACβ are independent in their catalytic function, and their ability to form cAMP can strongly and repeatedly be increased by blue light (Yoshikawa *et al.* 2005; Looser *et al.* 2009). However, the specific activity of PACα is about 100-fold higher than that of PACβ (Schroder-Lang *et al.* 2007).

To date, it has been shown that photoactivation of PACα can increase cAMP levels in HEK293 cells (Schroder-Lang *et al.* 2007) and led to a large increase in plasma membrane conductance of *Xenopus* oocytes when the blue-light receptor was coexpressed together with a PKA (cAMP-dependent protein kinase)-activated Cl^- channel (cystic fibrosis transmembrane conductance regulator – CFTR). In the sea slug *Aplysia*, injection of PACα into sensory neurons furthermore facilitated light-activated changes in spike width and amplitude (Nagahama *et al.* 2007). In adult *Drosophila*, stimulation of PACα in neurons modulates behavior by inducing bouts of hyperactivity, unusual freezing as well as a decline in grooming activity (Schroder-Lang *et al.* 2007).

The nematode *Caenorhabditis elegans* has proven to be a powerful *in vivo* model for neurobiological studies. Its elementary, yet versatile nervous system of exactly 302 neurons has been mapped down to the individual synapse, and numerous studies showed that basic protein machineries and neurotransmitters involved in mammalian neurotransmission are conserved (White *et al.* 1986; Miller *et al.* 1996; Bargmann 1998; Richmond 2007). However, compared to rodent models *C. elegans* is easily genetically tractable and most mutants with severe neurotransmission defects are viable.

In *C. elegans*, pre-synaptic cAMP plays a critical role in the regulation of locomotion. At least three Gα-signaling pathways ($G\alpha_{o/i}$, $G\alpha_q$, $G\alpha_s$) appear to be involved in regulating different aspects of synaptic vesicle (SV) release and synaptic signalling. While $G\alpha_{o/i}$ acts inhibitory, the $G\alpha_q$ and $G\alpha_s$ pathways are involved in controlling the release of neurotransmitters and in driving locomotion (Reynolds *et al.* 2005; Schade *et al.* 2005; Charlie *et al.* 2006). The $G\alpha_q$ pathway exerts its effects on locomotion by activating phospholipase Cβ and producing diacyl-glycerol as a pre-synaptic second messenger. Ultimately, this increases release of the excitatory neurotransmitter acetylcholine (ACh) at neuromuscular junctions (Lackner *et al.* 1999; Miller *et al.* 2000). Another major effector important for the $G\alpha_q$ pathway is the RhoGEF (Guanine nucleotide exchange factor) Trio which activates RhoA and also drives locomotion (Williams *et al.* 2007). Neuronal $G\alpha_s$ and $G\alpha_q$ pathways converge to regulate synaptic activity, and the $G\alpha_s$ pathway depends on the $G\alpha_q$ pathway to exert its effects on locomotion. It is believed that in the cholinergic system of *C. elegans* an increase in the intracellular cAMP concentration ($[cAMP]_i$) causes increased ACh release and can subsequently stimulate downstream muscle cells and neurons. Accordingly, gain-of-function mutations in the $G\alpha_s$ pathway, as well as gain-of-

function mutations in the adenylyl cyclase ACY-1, result in increased neurotransmitter release and hyperactive, though highly coordinated locomotion (Schade *et al.* 2005). Yet, many questions regarding pre-synaptic functions of cAMP and the Gα pathway remain unresolved.

Manipulation of cellular signaling in live animals with the help of genetically encoded light-sensitive proteins, such as Channelrhodopsin-2 (ChR2) and Halorhodopsin, has become a highly studied and applied topic in recent years (Nagel *et al.* 2005; Schroll *et al.* 2006; Zhang *et al.* 2006, 2007; Liewald *et al.* 2008; Cardin *et al.* 2010). Among these 'optogenetic' tools, PAC is rather new. Previous attempts to influence intracellular cAMP levels in *C. elegans* by using membrane-permeable cAMP analogs were unsuccessful in inducing hyperactive locomotion, suggesting that the location and/or timing of cAMP increase are critical (Schade *et al.* 2005). In the present study, we used PACα in *C. elegans* for manipulation of intracellular cAMP levels of cholinergic neurons simply by illumination with blue light. Photoactivation led to behavioral changes, i.e. elevated swimming frequency and speed of locomotion, as well as a reduced number of backward locomotion episodes. Concomitantly, miniature post-synaptic current (mPSC) frequency at the neuromuscular junction was increased. Compared to the use of cAMP analogs, this optogenetic tool allows the *in vivo* manipulation of $[cAMP]_i$ in selected cells only and with high spatial and temporal control.

Materials and methods

Genetics

Caenorhabditis elegans strains were cultivated using standard methods on nematode growth medium (NGM) and fed *E. coli* strain OP50-1 (Brenner 1974). Transgenic strains were generated following standard procedures (Fire 1986). Strains used or generated: N2 (wild type), KG1180: *lite-1(ce314)*, ZX784: *lite-1(ce314);zxEx512[punc-17::GFP::PACα; pelt-2::mCherry]* – 'Line 1', ZX785: *lite-1(ce314);zxEx513[punc-17::GFP::PACa; pelt-2::mCherry]* – 'Line 2', KG524: *gsa-1(ce94)*, KG518: *acy-1(ce2)*.

Molecular biology

Photoactivated adenylyl cyclase α cDNA (http://www.ncbi.nlm.nih.gov/protein/BAB85619.1) was kindly provided by Masakatsu Watanabe (Iseki *et al.* 2002). The *punc-17::GFP::PACα* construct was generated as follows: A DNA-fragment of green fluorescent protein (GFP) was PCR amplified from pAG48 (*pacr-13::acr-13::GFP* (Gottschalk *et al.* 2005); primers oSW24 (5′-GCCAGTGCTAGCATGAGTAAAGGAGAAGAACTTTTC-3′) and oSW28 (5′-GCCAGTGGTACCAGTCTGATCATTTGTATAG-TTCATCCATGCCATGTGT-3′)) and subcloned into the punc-17-vector RM#348p (a gift from J. Rand) using *Nhe*I and *Kpn*I to yield the *punc-17::GFP* intermediate plasmid. PACα cDNA was synthesized *in vitro* using the T7 cap scribe kit (Ambion, Austin, TX, USA) from the plasmid AB031225 and subcloned into pGEMR2 (a modified version of pGEM3z; Promega, Madison, WI, USA) to

generate pGEMHE::PACα (Schroll *et al.* 2006). Thereafter, PACα cDNA was cloned from pGEMHE::PACα [primers oSW29 (5′-GACGTGATCATACATCCTTGTTTGGAAAGAAGG-3′) and oSW27 (5′-GCCAGTGGTACCTTAATGTTCATATTTGTGCGAA-CC-3′)] into the *punc-17::GFP* intermediate plasmid using *Bcl*I and *Kpn*I to generate *punc-17::GFP::PACα*. A resulting in-frame stop codon between GFP and PACα from the *Bcl*I restriction site (5′-TGATCA-3′) was then mutated to a *Not*I restriction site (5′-GCGGCCGC-3′) by assembled PCR with primers A (5′-CCGG-GCAATTGGCGATGGCCCTGTCC-3′), B (5′-GCGGCCCACA-CTCATGGGTTCAGGGGC-3′), C (5′-ACAAAGCGGCCGCGTA-CATCCTTGTTTGGAAAGAAGGCC-3′), and D (5′-CTTTCCA-AACAAGGATGTACGCGGCCGCTTTGTATAGTTCATCCATG-CC-3′), adding a nucleotide to restore the reading frame.

Generation of transgenic animals

Transgenic *C. elegans* were obtained by microinjection of 20 ng/μL of the *punc-17::GFP::PACα* plasmid and 20 ng/μL of the co-transformation marker *pelt-2::mCherry*, as well as 60 ng/μL pUC19, into the gonads of *lite-1(ce314)* nematodes by standard procedures. Extrachromosomal arrays were generated to yield the following strains: ZX784: *lite-1(ce314); zxEx512[punc-17::GFP::PACα; pelt-2::mCherry]* – 'Line 1', and ZX785: *lite-1(ce314); zxEx513[punc-17::GFP::PACα; pelt-2::mCherry]* – 'Line 2'.

Fluorescence analysis

Several animals of the same strain were immobilized on an agar pad containing 20 mM NaN_3 in M9 buffer. Images were recorded under 100× magnification on an Axiovert 200 inverse fluorescence microscope (Zeiss, Göttingen, Germany), equipped with an HBO 100 lamp and a GFP filter set. Afterwards fluorescence intensity was analyzed using ImageJ software (Wayne Rasband, National Institutes of Health, USA, http://rsb.info.nih.gov/ij/). A line was drawn for each image spanning the ventral nerve cord from the nerve ring in the head to the worm's tail and fluorescence intensity (8-bit gray-scale) along this line was determined. After background subtraction, individual line scans were averaged, and also the mean intensity for each line was calculated for the whole worm length.

Behavioral assays

To determine locomotion parameters on solid substrate, young adults were filmed on plain NGM plates on a worm tracker platform (Zaber Technologies, Vancouver, BC, Canada) under 10× magnification for 15 s in darkness, 25 s under DPSS laser illumination (Pusch OptoTech, Baden-Baden, Germany; 473 nm, 25.6 mW/mm^2), and 20-s post-illumination, using a DinoLite digital microscope. Their position at each time point was determined using the coordinates of the stage, as obtained from single-worm tracking software (Wormtracker v2.0.3.1, kindly provided by the Schafer lab, MRC-LMB, Cambridge, UK), which detects the animal in a digital image, follows it by steering an x,y-translational stage, and records its coordinates. From this data, the animals' velocity was deduced, and from the resulting videos, the body length was calculated.

As an alternative approach to measure animal velocity, we used a custom developed tracking software, written in LabView, that also controls an x,y-translational stage, films the animal and projects light of a chosen color via an LCD projector onto the animal (Stirman *et al.*, accepted, *Nature Methods*). This system was utilized

in control experiments using lower light power (Figure S2), and thus only 2 mW/mm^2 (450–490 nm) was applied.

For analysis of reversals and bending angles animals were recorded with a Canon Powershot G9 digital camera for 2 min. After 30 s, a 25-s blue light pulse (2 mW/mm^2; 450–490 nm) was applied. Subsequently, single frames were extracted from the videos, and a custom written script for ImageJ software was used to find worm medians (details available upon request). Medians were further divided into nine segments of equal length to calculate angles between the latter ones. Long and short reversals were counted by eye.

For analyzing behavior in liquid, thrashing assays of young adult hermaphrodites were performed in 96-well microtiter plates, containing 80 μL of NGM and 80 μL of M9 saline per well. To stimulate PACα activity, animals were illuminated with an HBO 50 lamp (Zeiss; 450–490 nm, 0.2 mW/mm^2) under 2.5× magnification. Duration of illumination was defined by a computer-controlled shutter (Sutter Instruments, Novato, CA, USA). Assays were recorded with a Powershot G9 camera (Canon, Krefeld, Germany) and swimming cycles (the worm's body bends forth and back per each cycle) were counted for defined time bouts before, during, and after blue light illumination.

In all experiments, light power was measured by placing the detector of a powermeter (Thorlabs, Newton, NY, USA) at the focal plane and position in which animals would be present during experiments.

Electrophysiology

Recordings from dissected body wall muscle cells were conducted as described previously (Liewald *et al.* 2008). Light activation was performed using an LED lamp (KSL-70, Rapp OptoElectronic, Hamburg, Germany; 470 nm, 8 mW/mm^2) and controlled by the HEKA amplifier software. mPSC analysis was done by Mini Analysis software (Synaptosoft, Decatur, GA, USA, version 6.0.7).

Statistics

Data are given as means ± SEM. Significance between data sets after two-tailed Student's *t*-test or after ANOVA is given as *p*-value.

ARRIVE guidelines

The ARRIVE guidelines have been followed.

Results

PACα can be expressed in cholinergic neurons of *C. elegans*

We heterologously expressed PACα, N-terminally fused with GFP, from extrachromosomal arrays. The fusion protein was expressed from the *unc-17* promoter to facilitate expression in cholinergic neurons (Alfonso *et al.* 1993). Since *C. elegans* generally avoids intense light (particularly blue – UV) in a photophobic response mediated by the putative light-unresponsive-1 (LITE-1) photosensor (Edwards *et al.* 2008; Liu *et al.* 2010), we used a *lite-1(ce314)* mutant background for generation of transgenic PACα strains. This null mutation in the *lite-1* gene strongly reduces photophobic reactions to blue light.

Fluorescence microscopy confirmed expression of the GFP::PACα fusion protein in cholinergic motor neurons and

their processes along the ventral nerve cord (Fig. 1a–c; arrows) as well as in cholinergic neurons in the head (Fig. 1a and d). Furthermore, it was detected in commissures connecting the nerve cords (Fig. 1b, arrowhead). Within the neuronal cell bodies the protein was evenly distributed in cytosol and nucleus.

In order to examine whether there is any dependency between potential PACα mediated effects and the amount of PACα expressed, we selected and subsequently worked with two different transgenic lines exhibiting different expression levels (Figs 1d,e and S1): Line 2 (ZX785) had only
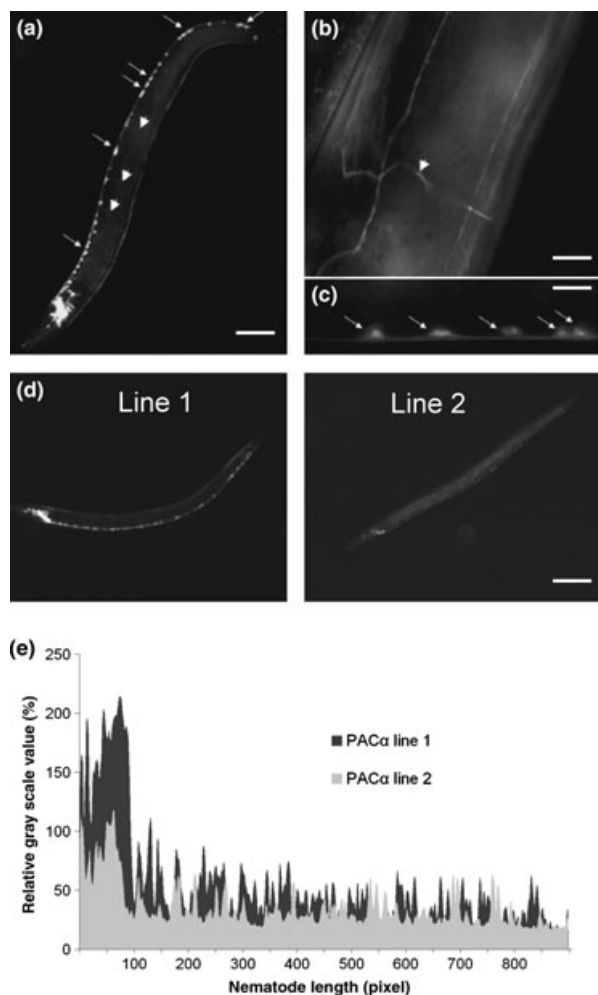
Fig. 1 Expression of PACα in cholinergic neurons of *C. elegans*. (a–c) Expression of GFP::PACα in cholinergic neurons is shown by fluorescence. Arrows point to neuronal cell bodies within the nerve cord. Scale bars: 50 (a) and 10 μm (b, c). Expression was also found in commissures (b; see arrowhead) which connect the nerve cords. (d) Fluorescence intensity was higher in PACα line 1 than in line 2. Scale bar: 150 μm. (e) Comparison of fluorescence intensity between transgenic lines 1 and 2. Relative fluorescence intensity is shown along the length of the animal (1 pixel corresponds to 1.25 μm). Values are displayed as means (*n* = 10).

$64 \pm 11\%$ relative fluorescence intensity (and thus PACα expression) of line 1 (ZX784).

## Photoactivation of PACα causes an increase in swimming frequency

Next, we analyzed whether photoactivation of PACα in cholinergic neurons has any effects on the behavior of the animals. Studies on *C. elegans* motility frequently employ the thrashing assay which is performed in liquid medium by counting lateral swimming cycles (body thrashes). Before illumination the thrashing frequency was highest in control animals (0.69 Hz; Fig. 2a) and PACα line 2 (low expression; 0.61 Hz), while line 1 (high expression) had a reduced frequency (0.32 Hz). Upon photoactivation with blue light ($\lambda = 450$–490 nm) the thrashing frequency immediately increased up to 255% and 164% for lines 1 and 2, respectively, and remained elevated for a few seconds after the end of the light stimulus (Fig. 2a and b; Video S1). In contrast, thrashing frequency in control animals stayed unaltered during the entire period of photostimulation.

The results demonstrate that PACα was functionally expressed and that the elevation of intracellular $[cAMP]_i$ in cholinergic neurons by photoactivation of PACα was sufficient to activate targets of cAMP. According to the current state of knowledge an increase in $[cAMP]_i$ in cholinergic neurons promotes release of the excitatory neurotransmitter ACh (Reynolds *et al.* 2005; Schade *et al.* 2005; Charlie *et al.* 2006). Thus, the effects on motility we observed were presumably triggered by a cAMP-dependent release of ACh at neuromuscular junctions (NMJs) which in turn can stimulate downstream muscle cells and neurons. The relative increase in body thrashes was significantly larger in line 1 than in line 2 suggesting a direct correlation between the amount of cAMP synthesized and increase in the thrashing frequency (Fig. 2b).

Photoactivation of PACα causes an increase in crawling velocity

The locomotion on solid substrate was analyzed quantitatively with a computerized single-worm tracking system (Wormtracker v2.0.3.1). In absence of blue light, both PACα-expressing lines moved more slowly than control animals. However, when transgenic animals were illuminated for 25 s (473 nm; 25.6 mW/mm^2), the light stimulus clearly affected their locomotion (Fig. 3a and b). Within a few seconds of illumination they showed a significant increase in velocity which persisted throughout the light stimulus, likely because of increased cAMP levels. A maximal acceleration to $145 \pm 11\%$ (line 1) and $150 \pm 8\%$ (line 2) of the initial velocity was reached about 18 s after light onset. After the stimulus ended, the velocity decreased, most likely reflecting cellular phosphodiesterase activity. The light-induced increases in velocities of both transgenic lines were similar despite different PACα expression levels, and were both
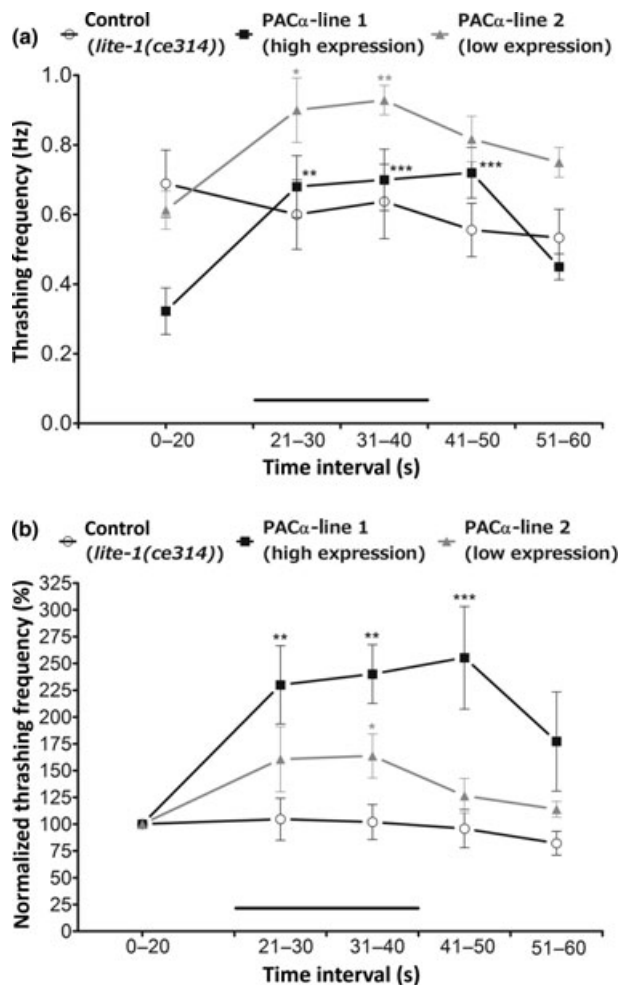
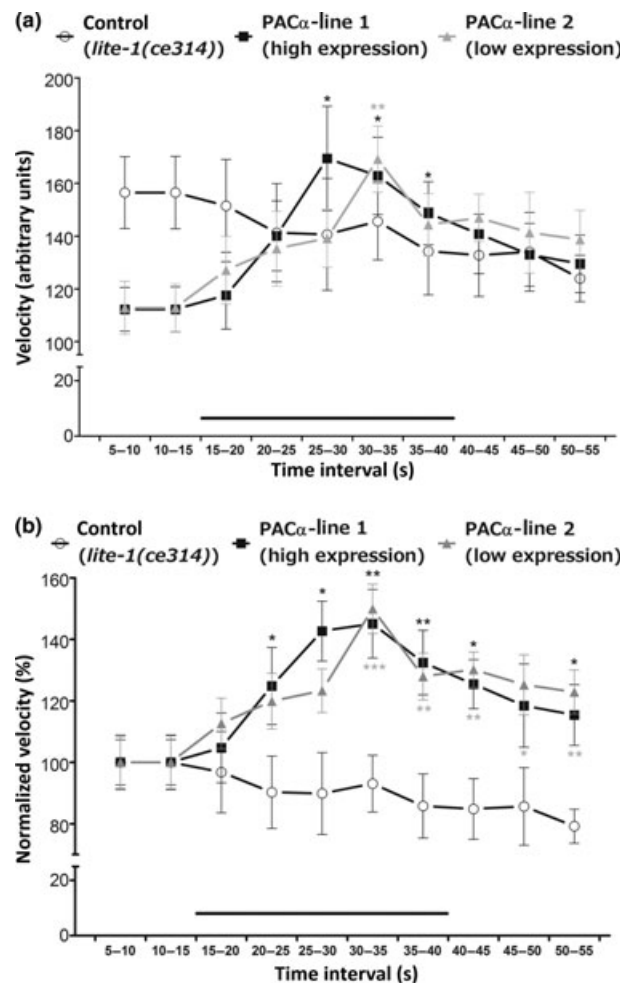**Fig. 2** Photoactivation increases swimming frequency in *C. elegans* expressing PACα in cholinergic neurons. (a) The thrashing frequency is displayed for *lite-1(ce314)* controls, PACα-expressing line 1 (high expression), and PACα-expressing line 2 (low expression). Swimming cycles were determined for 20- and 10-s intervals. Statistically significant differences are related towards the initial velocity of each line before illumination. (b) Relative thrashing frequency with statistical values being relative towards the control animals (*lite-1(ce314)*). In both graphs, illumination over a period of 20 s is indicated by a black bar. Values are displayed as means ± SEM ($n = 10$). $*p < 0.05$, $**p < 0.01$, and $***p < 0.001$.

Fig. 3 Effects of photoactivation of PACα on the velocity of *C. elegans* on solid substrate. Displayed are *lite-1(ce314)* controls as well as PACα-expressing line 1 (high expression) and line 2 (low expression). (a) Velocity during photostimulation is given in arbitrary units. Statistically significant differences are related towards the initial velocity of each line before illumination. (b) Relative velocity with values of each line being normalized towards the velocity at the start of the experiment. Statistically significant differences of PACα-expressing line 1 and line 2 are related towards controls. The period of the light stimulus (25 s) is highlighted by a black bar. Values are displayed as means ± SEM ($n = 26$–35). $*p < 0.05$, $**p < 0.01$, and $***p < 0.001$.

significantly higher than the *lite-1(ce314)* controls, which did not alter their velocity in response to light. We also used a lower stimulation light intensity (2 mW/mm²), obtaining qualitatively similar results (Figure S2), although the extent of the velocity increase was lower (20–30% increase vs. 50% obtained at 25.6 mw/mm²). This indicates that 2 mW/mm² does not fully saturate PACα effects.

The locomotion of PACα-expressing animals was normal and highly coordinated. For example, we analyzed mean bending angles of the animals during locomotion and did not observe any light-dependent alterations (Figure S3). This

behavior is in accordance with studies on gain-of-function mutants in the Gαs pathway which are expected to have constitutively elevated cAMP levels and show hyperactive but highly coordinated locomotion (Schade *et al.* 2005). Interestingly, gain-of-function (g.o.f.) mutants in the adenylyl cyclase ACY-1 (allele *ce2*) moved with increased velocity when compared to the wild type: the fractional increase resembled the velocity increase of both PACα lines during photostimulation (Figure S2). Similarly elevated velocity was measured for *gsa-1(ce94)* Gαs g.o.f. mutants (data not shown).

Stimulation of PACα influences mPSCs in body wall muscle cells

To directly examine the effects of PACα stimulation on synaptic transmission and neurotransmitter release we carried out electrophysiological recordings on whole-cell patch-clamped body wall muscle cells. We analyzed mPSCs (excitatory) that represent neurotransmitter release at the NMJ by spontaneous fusion of one or few SVs. mPSCs were compared between *lite-1(ce314)* controls and PACα-expressing line 1 (high expression).

In animals expressing PACα, blue light stimulation for 45 s changed the dynamics of spontaneous transmitter release. Illumination led to a slight increase in the amplitude of mPSCs from 26.6 ± 3.2 pA to 32.2 ± 3.3 pA (Fig. 4a and c). Importantly, we also observed a significant increase of the event frequency from 29.5 ± 5.4 Hz to 39.8 ± 5.6 Hz (Fig. 4a–c). The increase in mPSC frequency was observed

within 750 ms after the onset of irradiation and this fast effect demonstrates the feasibility of influencing the cAMP level with good temporal control. The increase persisted for a few seconds after the light stimulus was turned off.

Based on the fact that photoactivation of PACα leads to an increased cAMP synthesis in cholinergic motor neurons this should subsequently stimulate neurotransmitter (ACh) release at the pre-synapse and lead to the detected increase in the number of mPSCs (Reynolds *et al.* 2005; Schade *et al.* 2005). This verifies that the behavioral effects we observed previously were caused by an increase in the ACh release rate. The altered mPSC frequency suggests that the release probability of SVs was elevated. The increase in mPSC frequency also tended to cause more simultaneous SV fusions which may have resulted in mPSCs of increased amplitude, especially just after the stimulus onset.
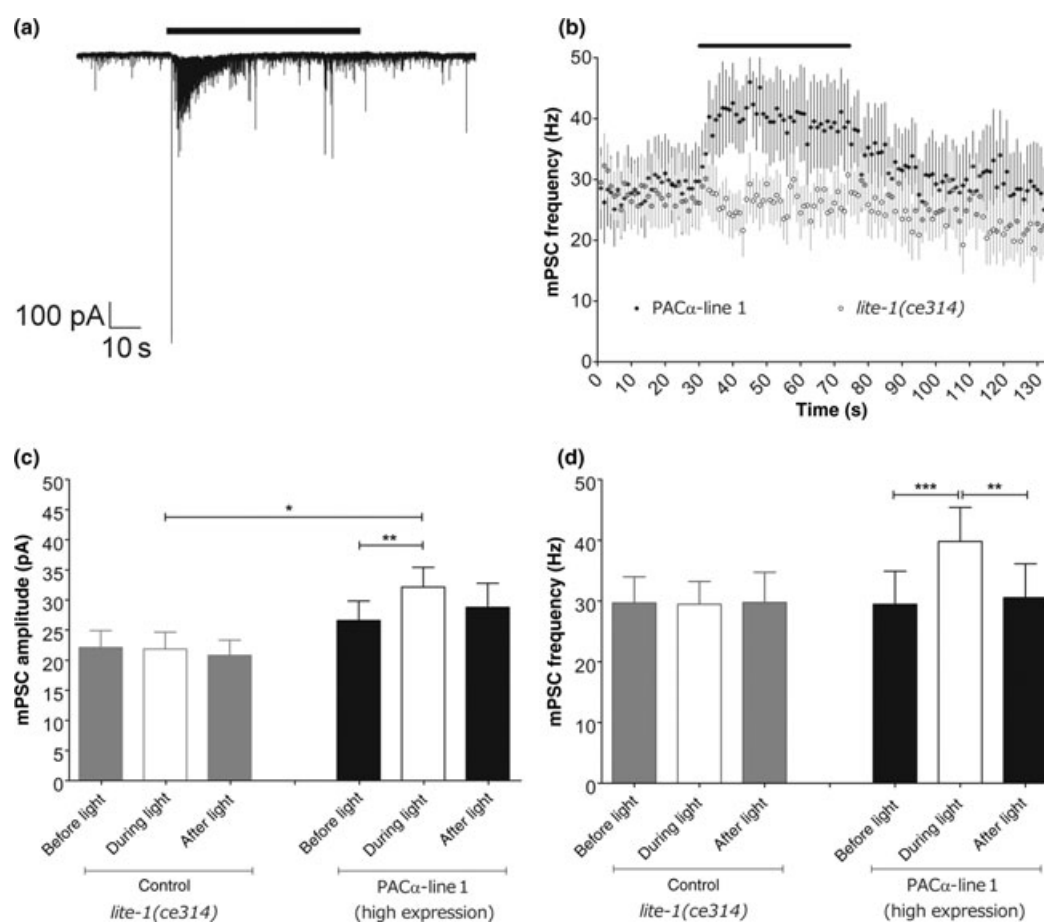
Fig. 4 Photoactivation of PACα increases the frequency of miniature post-synaptic currents (mPSCs) in patch-clamped body wall muscle cells of *C. elegans*. (a) Original trace showing photo-stimulated currents in a transgenic animal expressing PACα in cholinergic neurons (line 1; high expression). Illumination over a period of 45 s is indicated by a black bar. (b) Changes in mPSC frequency in control animals (*lite-1(ce314)*) and PACα line 1 (high expression). Illumination over a period of 45 s is indicated by a black bar. Recorded values were analyzed in 1000 ms intervals. (c) mPSC amplitude in PACα line 1 (high expression) is increased during photoactivation compared to *lite-1(ce314)* controls. (d) mPSC frequency in PACα line 1 (high expression) is increased during photoactivation compared to control animals (*lite-1(ce314)*). Values are displayed as means ± SEM (n = 8 for *lite-1(ce314)*; n = 10 for PACα line 1). *p < 0.05, **p < 0.01, and ***p < 0.001.

A significant increase in ACh release at the NMJ might cause muscle contractions and marked changes in body length – similar to what is observed in light-stimulated animals expressing ChR2 in cholinergic neurons (Liewald *et al.* 2008). Thus, we monitored whether light-stimulation affects the body length of PACα transgenic animals. However, we could not observe any changes in length when blue light was applied (Figure S4).

Photoactivation of PACα causes a decrease in the frequency of long reversals

The locomotion of *C. elegans* is a useful measure in studies of neurobiological signaling pathways as it is a complex behavior. It mainly consists of a sinusoidal forward movement, however, the crawling is regularly interrupted by discrete motor activities such as reversals (temporary backward crawling) and omega turns (a reversal followed by an almost 180° turn; the worm's body resembles the Greek letter Ω). Directional changes allow the animal to explore its environment. The frequency of reversals is influenced by environmental conditions such as availability of food or mechanical stimulation (Zhao *et al.* 2003) – factors which are detected by sensory neurons, and communicated via command interneurons (Fig. 5b) to motor neurons (Gray *et al.* 2005).

Before illumination, the number of long reversals (= pull-back length more than half the length of the head) was larger in PACα line 1 than in control animals. However, during photostimulation animals expressing PACα showed a strong decrease in the number of long reversals (Fig. 5a). For PACα line 1 (high expression) the number of long reversals decreased from 1.6 ± 0.4 to 0.1 ± 0.1 reversals/min, while for PACα line 2 (low expression) the number decreased from 1.0 ± 0.3 to 0.2 ± 0.2 reversals/min. Likewise, g.o.f. mutants in the $G\alpha_s$ pathway, i.e. *gsa-1(ce94)* and *acy-1(ce2)* (Schade *et al.* 2005), showed similar characteristics. These animals performed almost no long reversals at all and like photoactivated PACα animals, they moved mainly forward (data not shown). In contrast, control animals did show an increase in the number of long reversals from 0.8 ± 0.3 to 1.5 ± 0.4 reversals/min. In the PACα line with high expression level, we also found a light-dependent rise in body bends with particularly strong bending angle, such that head and tail directly contacted each other (Figure S5; not equivalent to the previously described omega turns, as no reversal was preceding the body bend.) Head/tail contacts increased from 0.6 ± 0.2 to 1.6 ± 0.5 per minute, however, this increase was not significant.

Discussion

In the present study, we showed that PACα can be applied as a useful optogenetic tool in *C. elegans*, *in vivo*, to rapidly and transiently manipulate intracellular cAMP levels in selected cells by simple photoactivation. Following PACα photoactivation in cholinergic neurons, increased cAMP production
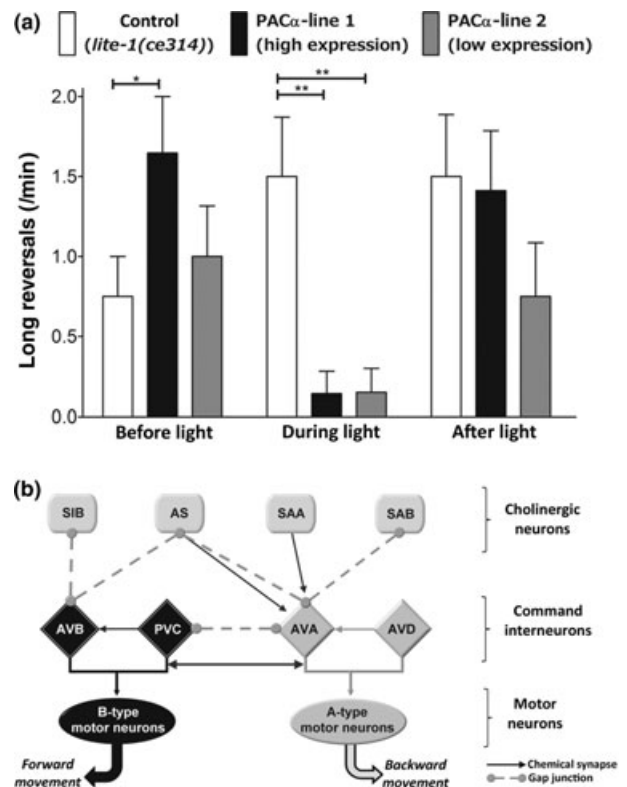
Fig. 5 Photoactivation leads to a decrease in the number of long reversals in PACα-expressing animals. (a) Displayed are values for *lite-1(ce314)* controls, PACα-expressing line 1 (high expression), and PACα-expressing line 2 (low expression). During illumination there was a significant decrease in the number of long reversals in both PACα-expressing lines compared to control animals. Values are displayed as means ± SEM (n = 16–17). (b) Schematic display of connections between cholinergic neurons and command interneurons that could be relevant for influencing long reversals (modified from Goodman 2006). *$p < 0.05$ and **$p < 0.01$.

resulted that was seemingly sufficient to mimic an activation of the cellular $G\alpha_s$ signaling pathway, which together with the $G\alpha_q$ pathway regulates synaptic activity (Reynolds *et al.* 2005). We observed behavioral changes, namely increased swimming frequency and locomotion velocity, presumably triggered by cAMP-dependent release of the excitatory neurotransmitter ACh (Reynolds *et al.* 2005; Schade *et al.* 2005). Subsequently, ACh stimulated downstream neurons and body wall muscle cells.

An increased release of ACh at the NMJ was confirmed by electrophysiological recordings from body wall muscle cells where we found a reversible increase in the frequency and amplitude of mPSCs during photostimulation. The frequency returned to baseline levels within a few seconds after the end of the light stimulus, probably because of the fast activity of endogenous phosphodiesterases degrading cAMP. Similar results were obtained in *Drosophila* larvae by Bucher and Buchner (2009): Following expression in motor neurons,

photoactivation of PACα caused an increased frequency of miniature excitatory junction potentials (mEJPs) at the NMJ. While in *Drosophila* changes in mEJP frequency occurred with a delay of about 1 min after the start of the photoactivation, effects in *C. elegans* occurred within 750 ms. This time frame very much resembles results in *Euglena* where the intracellular cAMP level significantly increased within 1 s after photoactivation (Yoshikawa *et al.* 2005). Our results suggest that the time frame for PACα-dependent stimulation of ACh release in *C. elegans* is rather short.

The naturally occurring PACα provides researchers with a means of increasing [cAMP]$_i$ in *C. elegans* only in genetically defined cells of interest by using cell type-specific promoters. We observed effects within a few seconds of photoactivation; in contrast pharmacological agonists increase intracellular cAMP levels less rapidly and without spatial specificity. Usually, pharmacological substances, such as the adenylyl cyclase agonist forskolin, or the membrane-permeable cAMP analog dibutyryl cAMP, are used to influence [cAMP]$_i$. However, in *Drosophila* these drugs took about 15–30 min to cause increases in the mEJP frequency that were of the same dimension as those observed just shortly after a light pulse in animals expressing PACα in motor neurons (Yoshihara *et al.* 2000; Bucher and Buchner 2009). These factors are of special importance since a previous attempt to use membrane-permeable cAMP analogs to influence locomotion in *C. elegans* was unsuccessful and showed that timing and location of cAMP are crucial (Schade *et al.* 2005).

In our study, we also observed a reduction in the number of long reversals during photostimulation. Some of the cholinergic neurons in which PACα was expressed have established synapses and gap junctions to command interneurons (AVB, PVC, AVA, AVD; Fig. 5b; White *et al.* 1986) which in turn regulate aspects of locomotion. While AVB and PVC can trigger forward movement via B-type motor neurons, AVA and AVD can trigger backward movement via A-type motor neurons (Bhatla 2009). Importantly, each pair of command interneurons also inhibits the opposite type, forming a bi-stable switch that alternates between both directions of movement. A cAMP-dependent release of ACh by cholinergic motor neurons may thus cause a disparity in this network of command interneurons and alter the balance of forward and reverse locomotion.

Importantly, PACα photoactivation appeared to trigger cellular activity not in an 'uncoordinated' manner. Rather, neurons were still able to evoke coordinated network activity and locomotion but simply showed exaggerated output while no alteration in body length was seen. This is in contrast to the strong depolarizing stimulation of the cholinergic motor circuit using ChR2, which induces a simultaneous massive release of neurotransmitter from cholinergic cells, overrides any intrinsic locomotory program and causes strong body contractions and paralysis (Liewald *et al.* 2008). Compared

to other methods and optogenetic tools PACα also is advantageous, as it does not require any additional chromophore, it is not harmful for the cell, and its substrate ATP, as well as its chromophore FAD, are readily available.

However, even before any exposure to light the swimming frequency in PACα-expressing line 1 was reduced. Similarly, the velocity on solid substrate in both transgenic lines only reached about 72% of those of control animals. This can be explained by the basal (dark) activity of PACα (Iseki *et al.* 2002). For *Xenopus* oocytes expressing PACα it was shown that even in the dark [cAMP]$_i$ was increased (Schroder-Lang *et al.* 2007). A chronically elevated cAMP level in cholinergic cells of *C. elegans* might evoke compensatory effects on neurotransmitter release pathways resulting in a down-regulation. In an unstimulated state, they generally may release less ACh and therefore the motility of the transgenic animals may be reduced. In accordance with this assumption, line 1, expressing high PACα levels, showed a stronger down-regulation of the swimming frequency than line 2 (low expression). This is again in line with results obtained on *Xenopus* oocytes where a correlation between PACα expression level and extent of dark activity was observed (Schroder-Lang *et al.* 2007). These effects could hint at mechanisms which may regulate transmitter release in cholinergic neurons and compensate for a chronic increase of [cAMP]$_i$. In contrast, *acy-1* g.o.f. mutants showed a constitutive increase in velocity. However, the *acy-1* and *unc-17* expression patterns are only partially overlapping (i.e. *acy-1* is expressed in many more, if not all neurons, including the locomotion command interneurons; http://www.wormbase.org), which may explain conflicting results. The undesired basal activity exhibited by PACα potentially restricts its application but might be mitigated by using lower expression levels. Thus, one should find a balance between an expression which is low enough to minimize dark activity while being high enough to cause significant effects.

One point to consider is that naturally occurring cAMP signaling is restricted to small domains close to the plasma membrane (Beavo and Brunton 2002) which may well influence the way that this signaling molecule affects downstream pathways. PACα, however, is neither localized to the membrane nor restricted to small domains. Thus, cAMP produced by PACα may have more diverse and possibly unwanted effects. However, future modifications of the protein might help to restrict its subcellular localization.

In the future, PACα can be employed in *C. elegans* to examine in more detail the function of various (neuronal) cells, to better understand the signal transduction within neurons as well as to clarify the specific role of various neurons in complex neural circuits. Furthermore, it can be used to explore the pre-synaptic function of cAMP and the neuronal Gα$_s$ pathway in triggering the release of neurotransmitter and in modulating synaptic transmission. It would also be interesting to further investigate the adaptation of

neurotransmitter release to a chronic [cAMP]$_i$ increase. Such studies will be helpful in further dissecting the large network of proteins involved in regulating neurotransmitter release and behavior. Finally, Ryu *et al.* (2010) and Stierl *et al.* (2010) just recently discovered a bacterial photoactivated adenylyl cyclase, called bPAC or BlaC, in *Beggiatoa sp*. This enzyme is smaller than PACα and has alternative properties. Furthermore, mutations of BlaC were engineered to generate a photoactivated guanylyl cyclase (BlgC) which now allows to manipulate cGMP levels (Ryu *et al.* 2010).

Acknowledgements

Supporting information

Additional Supporting information may be found in the online version of this article:

Figure S1. Comparison of fluorescence intensity in transgenic lines 1 and 2.

Figure S2. Effects of photoactivation of PACα on the velocity of *C. elegans* on solid substrate using low light intensity (2 mW/mm^2), and increase of the velocity by a gain-of-function mutation in the adenylyl cyclase *acy-1*.

Figure S3. Photoactivation of PACα does not affect bending angles.

Figure S4. Photoactivation of PACα does not affect body length.

Figure S5. Photoactivation of PACα affected the frequency of strong body bends, causing a direct contact between head and tail.

Video S1. Photoactivation increases swimming frequency in *C. elegans* expressing PACα in cholinergic neurons.

As a service to our authors and readers, this journal provides supporting information supplied by the authors. Such materials are peer-reviewed and may be re-organized for online delivery, but are not copy-edited or typeset. Technical support issues arising from supporting information (other than missing files) should be addressed to the authors.

References

Alfonso A., Grundahl K., Duerr J. S., Han H. P. and Rand J. B. (1993) The Caenorhabditis elegans unc-17 gene: a putative vesicular acetylcholine transporter. *Science* **261**(5121), 617–619.

Anderson S., Dragnea V., Masuda S., Ybe J., Moffat K. and Bauer C. (2005) Structure of a novel photoreceptor, the BLUF domain of AppA from Rhodobacter sphaeroides. *Biochemistry* **44**(22), 7998–8005.

Bargmann C. I. (1998) Neurobiology of the Caenorhabditis elegans genome. *Science* **282**(5396), 2028–2033.

Beavo J. A. and Brunton L. L. (2002) Cyclic nucleotide research–still expanding after half a century. *Nat. Rev. Mol. Cell Biol.* **3**(9), 710–718.

Bhatla N. (2009) *C. elegans Neural Network*. (http://wormweb.org/neuralnet).

Brenner S. (1974) The genetics of Caenorhabditis elegans. *Genetics* **77**(1), 71–94.

Bucher D. and Buchner E. (2009) Stimulating PACalpha increases miniature excitatory junction potential frequency at the Drosophila neuromuscular junction. *J. Neurogenet.* **23**(1–2), 220–224.

Cardin J. A., Carlen M., Meletis K., Knoblich U., Zhang F., Deisseroth K., Tsai L. H. and Moore C. I. (2010) Targeted optogenetic stimulation and recording of neurons in vivo using cell-type-specific expression of Channelrhodopsin-2. *Nat. Protoc.* **5**(2), 247–254.

Charlie N. K., Thomure A. M., Schade M. A. and Miller K. G. (2006) The Dunce cAMP phosphodiesterase PDE-4 negatively regulates G alpha(s)-dependent and G alpha(s)-independent cAMP pools in the Caenorhabditis elegans synaptic signaling network. *Genetics* **173**(1), 111–130.

Edwards S. L., Charlie N. K., Milfort M. C., Brown B. S., Gravlin C. N., Knecht J. E. and Miller K. G. (2008) A novel molecular solution for ultraviolet light detection in Caenorhabditis elegans. *PLoS Biol.* **6**(8), e198.

Fire A. (1986) Integrative transformation of Caenorhabditis elegans. *EMBO J.* **5**(10), 2673–2680.

Gauden M., van Stokkum I. H., Key J. M., Luhrs D., van Grondelle R., Hegemann P. and Kennis J. T. (2006) Hydrogen-bond switching through a radical pair mechanism in a flavin-binding photoreceptor. *Proc. Natl Acad. Sci. USA* **103**(29), 10895–10900.

Goodman M. B. (2006). Mechanosensation, in *Worm Book* (The *C. elegans* Researcher Community, eds), pp. 1–14. Available at: www.wormbook.org.

Gottschalk A., Almedom R. B., Schedletzky T., Anderson S. D., Yates J. R. and Schafer W. R. (2005) Identification and characterization of novel nicotinic receptor-associated proteins in Caenorhabditis elegans. *EMBO J.* **24**, 2566–2578.

Gray J. M., Hill J. J. and Bargmann C. I. (2005) A circuit for navigation in Caenorhabditis elegans. *Proc. Natl Acad. Sci. USA* **102**(9), 3184–3191.

Iseki M., Matsunaga S., Murakami A., Ohno K., Shiga K., Yoshida K., Sugai M., Takahashi T., Hori T. and Watanabe M. (2002) A blue-light-activated adenylyl cyclase mediates photoavoidance in Euglena gracilis. *Nature* **415**(6875), 1047–1051.

Kandel E. R. (2001) The molecular biology of memory storage: a dialog between genes and synapses. *Biosci. Rep.* **21**(5), 565–611.

Kidokoro Y., Kuromi H., Delgado R., Maureira C., Oliva C. and Labarca P. (2004) Synaptic vesicle pools and plasticity of synaptic transmission at the Drosophila synapse. *Brain Res. Brain Res. Rev.* **47**(1–3), 18–32.

Lackner M. R., Nurrish S. J. and Kaplan J. M. (1999) Facilitation of synaptic transmission by EGL-30 Gqalpha and EGL-8 PLCbeta: DAG binding to UNC-13 is required to stimulate acetylcholine release. *Neuron* **24**(2), 335–346.

Liewald J. F., Brauner M., Stephens G. J., Bouhours M., Schultheis C., Zhen M. and Gottschalk A. (2008) Optogenetic analysis of synaptic function. *Nat. Methods* **5**(10), 895–902.

Liu J., Ward A., Gao J. *et al.* (2010) C. elegans phototransduction requires a G protein-dependent cGMP pathway and a taste receptor homolog. *Nat. Neurosci.* **13**(6), 715–722.

Looser J., Schroder-Lang S., Hegemann P. and Nagel G. (2009) Mechanistic insights in light-induced cAMP production by photoacti-

vated adenylyl cyclase alpha (PACalpha). *Biol. Chem.* **390**(11), 1105–1111.

Miller K. G., Alfonso A., Nguyen M., Crowell J. A., Johnson C. D. and Rand J. B. (1996) A genetic selection for Caenorhabditis elegans synaptic transmission mutants. *Proc. Natl Acad. Sci. USA* **93**(22), 12593–12598.

Miller K. G., Emerson M. D., McManus J. R. and Rand J. B. (2000) RIC-8 (Synembryn): a novel conserved protein that is required for G(q)alpha signaling in the C. elegans nervous system. *Neuron* **27**(2), 289–299.

Morozov A., Muzzio I. A., Bourtchouladze R., Van-Strien N., Lapidus K., Yin D., Winder D. G., Adams J. P., Sweatt J. D. and Kandel E. R. (2003) Rap1 couples cAMP signaling to a distinct pool of p42/44MAPK regulating excitability, synaptic plasticity, learning, and memory. *Neuron* **39**(2), 309–325.

Nagahama T., Suzuki T., Yoshikawa S. and Iseki M. (2007) Functional transplant of photoactivated adenylyl cyclase (PAC) into Aplysia sensory neurons. *Neurosci. Res.* **59**(1), 81–88.

Nagel G., Brauner M., Liewald J. F., Adeishvili N., Bamberg E. and Gottschalk A. (2005) Light activation of channelrhodopsin-2 in excitable cells of Caenorhabditis elegans triggers rapid behavioral responses. *Curr. Biol.* **15**(24), 2279–2284.

Ntefidou M., Iseki M., Watanabe M., Lebert M. and Hader D. P. (2003) Photoactivated adenylyl cyclase controls phototaxis in the flagellate Euglena gracilis. *Plant Physiol.* **133**(4), 1517–1521.

Reynolds N. K., Schade M. A. and Miller K. G. (2005) Convergent, RIC-8-dependent Galpha signaling pathways in the Caenorhabditis elegans synaptic signaling network. *Genetics* **169**(2), 651–670.

Richmond J. E. (2007). Synaptic function. *WormBook* (ed. The C. elegans Research Community), doi: 10.1895/wormbook.1.69.1, http://www.wormbook.org.

Ryu M. H., Moskvin O. V., Siltberg-Liberles J. and Gomelsky M. (2010) Natural and engineered photoactivated nucleotidyl cyclases for optogenetic applications. *J. Biol. Chem.* **285**, 41501–41508.

Schade M. A., Reynolds N. K., Dollins C. M. and Miller K. G. (2005) Mutations that rescue the paralysis of Caenorhabditis elegans ric-8 (synembryn) mutants activate the G alpha(s) pathway and define a third major branch of the synaptic signaling network. *Genetics* **169**(2), 631–649.

Schroder-Lang S., Schwarzel M., Seifert R., Strunker T., Kateriya S., Looser J., Watanabe M., Kaupp U. B., Hegemann P. and Nagel G. (2007) Fast manipulation of cellular cAMP level by light in vivo. *Nat. Methods* **4**(1), 39–42.

Schroll C., Riemensperger T., Bucher D. *et al.* (2006) Light-induced activation of distinct modulatory neurons triggers appetitive or aversive learning in Drosophila larvae. *Curr. Biol.* **16**(17), 1741–1747.

Stierl M., Stumpf P., Udwari D. *et al.* (2010) Light-modulation of cellular cAMP by a small bacterial photoactivated adenylyl cyclase, bPAC, of the soil bacterium beggiatoa. *J. Biol. Chem.* Epub ahead of print on October 28, 2010, doi: 10.1074/jbc.M110.185496.

Torgersen K. M., Vang T., Abrahamsen H., Yaqub S. and Tasken K. (2002) Molecular mechanisms for protein kinase A-mediated modulation of immune function. *Cell. Signal.* **14**(1), 1–9.

White J. G., Southgate E., Thomson J. N. and Brenner S. (1986) The structure of the nervous system of the nematode Caenorhabditis elegans. *Philos. Trans. R Soc. Lond. B Biol. Sci.* **314**(1165), 1–340.

Williams S. L., Lutz S., Charlie N. K., Vettel C., Ailion M., Coco C., Tesmer J. J., Jorgensen E. M., Wieland T. and Miller K. G. (2007) Trio's Rho-specific GEF domain is the missing Galpha q effector in C. elegans. *Genes Dev.* **21**(21), 2731–2746.

Yoshihara M., Suzuki K. and Kidokoro Y. (2000) Two independent pathways mediated by cAMP and protein kinase A enhance spontaneous transmitter release at Drosophila neuromuscular junctions. *J. Neurosci.* **20**(22), 8315–8322.

Yoshikawa S., Suzuki T., Watanabe M. and Iseki M. (2005) Kinetic analysis of the activation of photoactivated adenylyl cyclase (PAC), a blue-light receptor for photomovements of Euglena. *Photochem. Photobiol. Sci.* **4**(9), 727–731.

Zhang F., Wang L. P., Boyden E. S. and Deisseroth K. (2006) Channelrhodopsin-2 and optical control of excitable cells. *Nat. Methods* **3**(10), 785–792.

Zhang F., Wang L. P., Brauner M. *et al.* (2007) Multimodal fast optical interrogation of neural circuitry. *Nature* **446**(7136), 633–639.

Zhao B., Khare P., Feldman L. and Dent J. A. (2003) Reversal frequency in Caenorhabditis elegans represents an integrated response to the state of the animal and its environment. *J. Neurosci.* **23**(12), 5319–5328.

11.3. <u>CD-ROM</u>

Contents of the enclosed CD-ROM:

- Dissertation as PDF file

- Publications arising from the thesis including supplemental information

12. <u>Curriculum Vitae</u>

Personal Details

Name	Christian Schultheis
Date of Birth	27th of January 1982
Place of Birth	Offenbach am Main, Germany

Education

since 11/2007

PhD thesis on "Development and Application of Optogenetic Methods to Functionally Characterize Synaptic Transmission and Neural Circuits in the Nematode *Caenorhabditis elegans*", Goethe-University, Frankfurt am Main, Germany, Institute of Biochemistry, Group of Prof. Dr. Gottschalk

01/2007-09/2007

Diploma thesis on "Enhancing cell specificity and surface expression of Channelrhodopsin-2 and Halorhodopsin in excitable cells of *Caenorhabditis elegans*", Goethe-University, Frankfurt am Main, Germany, Institute of Biochemistry, Group of Prof. Dr. Gottschalk

10/2002-09/2007

Study of *Biochemistry* at the Goethe-University, Frankfurt am Main, Germany (mark 1,0; passed with distinction)

07/2001

Abitur at the Friedrich-Ebert-Gymnasium, Mühlheim am Main, Germany (mark 1,0)

Work Experience

01/2008-05/2008	Scientific stay at the Samuel Lunenfeld Research Institute, Mt Sinai Hospital, Toronto, Canada, Group of Prof. Dr. Zhen
04/2006-05/2006	Internship at the Max-Planck-Institute for Biophysics, Frankfurt am Main, Germany, Group of Prof. Dr. Schwarz
07/2005-10/2005	Internship at the Max-Planck-Institute for Biochemistry, Munich, Germany, Group of Prof. Dr. Stemmann
04/2004-05/2004	Internship at the Goethe-University, Frankfurt am Main, Germany, Institute of Biochemistry, Group of Prof. Dr. Gottschalk
06/2002-09/2002	Internship at Foster Chemicals, Jüchen, Germany, Dr. Piehl

Awards and Scholarships

06/2010	Scholarship of the *Integrated Research Training Group* (TRAM) for the „Neuronal Development, Synaptic Function & Behavior *C. elegans* Topic Meeting", Madison, USA
06/2009	Scholarship of the Hermann-Willkomm-Stiftung for the „17th International *C. elegans* Meeting 2009", Los Angeles, USA
01/2008-05/2008	Scholarship of the Boehringer Ingelheim Foundation for a scientific stay at Samuel Lunenfeld Research Institute, Mt Sinai Hospital, Toronto, Canada, Group of Prof. Dr. Zhen
10/2007	"Diplom-Förderpreis" Award of Procter & Gamble
05/2007-11/2011	e-Fellows scholarship

Publications

*: equal contribution

2011 *„Real-time multimodal optical control of neurons and muscles in freely behaving Caenorhabditis elegans"*; Jeffrey N Stirman, Matthew M Crane, Steven J Husson, Sebastian Wabnig, <u>Christian Schultheis</u>, Alexander Gottschalk, Hang Lu; Nature Methods, Volume 8(2)

„PACα – an optogenetic tool for in-vivo manipulation of cellular cAMP levels, neurotransmitter release, and behavior in Caenorhabditis elegans"; Simone Weissenberger*, <u>Christian Schultheis</u>*, Jana F Liewald*, Karen Erbguth, Georg Nagel, Alexander Gottschalk; Journal of Neurochemistry, Volume 116(4)

„Optogenetic analysis of GABA$_B$ receptor signaling in Caenorhabditis elegans motor neurons"; <u>Christian Schultheis</u>*, Martin Brauner*, Jana F Liewald, Alexander Gottschalk; Journal of Neurophysiology, Volume 106(2)

„Optogenetic long-term manipulation of behavior and animal development"; <u>Christian Schultheis</u>, Jana F Liewald, Ernst Bamberg, Georg Nagel, Alexander Gottschalk; PLoS One, Volume 6(4)

"Optogenetic analysis of synaptic vesicle recycling by high-pressure freeze electron microscopy in Caenorhabditis elegans"; Jan Hegermann, Martin Brauner*, Jana F Liewald*, <u>Christian Schultheis</u>*, Maike Kittelmann, Alexander Gottschalk, Stefan Eimer; in preparation

2009 *„An ER-resident membrane protein complex regulates nicotinic acetylcholine receptor subunit composition at the synapse"*; Ruta B Almedom*, Jana F Liewald*, Guillermina Hernando, <u>Christian Schultheis</u>, Diego Rayes, Jie Pan, Thorsten Schedletzky, Harald Hutter, Cecilia Bouzat, Alexander Gottschalk; EMBO Journal, Volume 28(17)

2008 *„Optogenetic analysis of synaptic function"*; Jana F Liewald*, Martin Brauner*, Greg J Stephens, Magali Bouhours, <u>Christian Schultheis</u>, Mei Zhen, Alexander Gottschalk; Nature Methods, Volume 5(10)

Conference Contributions (Talks)

08/2011   *SFB 807 – Transport and Communication across Biological Membranes – Retreat 2011*, Frauenchiemsee, Germany: "Long-term cell activation to alter behavior and animal development – and improvements beyond"

08/2010   *International Summerschool of Biochemistry*, Woffelsbach, Germany: "Step Function Opsins: novel tools that allow *in-vivo* long-term cell-activation"

06/2010   *Neuronal Development, Synaptic Function & Behavior C. elegans Topic Meeting*, Madison, USA: "Using Channelrhodopsin-2 Step Function Opsins to complement the optogenetics toolbox"

05/2010   *International Conference on Channelrhodopsin and light-gated enzymes*, Hiddensee, Germany: „ChR2 slow mutants - expanding the optogenetics toolbox"

03/2010   *SFB 807 – Transport and Communication across Biological Membranes – Retreat 2010*, Naurod, Germany: "Step Function Opsins – A ChR2 mutation allows long-term depolarization"

08/2009   *International Summerschool of Biochemistry*, Burg Hoheneck, Germany: "WDFY-2: A new player in synaptic transmission"

03/2009   *SFB 807 – Transport and Communication across Biological Membranes – Retreat 2010*, Hirschegg, Austria: "Application and improvement of optogenetic methods in *Caenorhabditis elegans*"

10/2007   *Akademische Feier der Goethe-Universität Frankfurt 2007*, Frankfurt am Main, Germany: "Lichtgesteuerte, spezifische Stimulation von erregbaren Zellen in *Caenorhabditis elegans*"

Conference Contributions (Posters)

11/2010   *1st Rhine-Main Neuroscience Network Conference*, Oberwesel, Germany: „Optogenetic long-term manipulation of behavior and animal development"

06/2010   *Neuronal Development, Synaptic Function & Behavior C. elegans Topic Meeting*, Madison, USA: "Optogenetic analysis of GABA$_B$ receptor signaling in *Caenorhabditis elegans* motor neurons"

09/2009   *European Conference on Nematode Neurobiology 2009*, Cambridge, England: "Improving optogenetic methods in *Caenorhabditis elegans*"

06/2009   *17th International C. elegans Meeting 2009*, Los Angeles, USA: „Improving optogenetic methods in *Caenorhabditis elegans*"

08/2008   *International Summerschool of Biochemistry*, Plankstetten, Germany: "Optogenetics in *Caenorhabditis elegans*"

05/2008   *International Conference on Channelrhodopsin and light-gated enzymes*, Frauenchiemsee, Germany: „Specific expression of ChR2 in *Caenorhabditis elegans*"

Additional Qualifications

-      Concession for buying, using and marketing of chemical substances according to the "Chemikalien-Verbotsverordnung"